

1
2
3
4
5
6
7
8
9
10
11
12
13
14
15
16
17
18
19
20
21
22

The beauty of numbers

From neurons to perception

PhD thesis

Written by

Yuxuan Cai

Promotor: prof. dr. S. O. Dumoulin

Copromotor: dr. S. Hofstetter

Funding:

The work presented in this thesis was supported in part by the following grants:

- China Scholarship Council (CSC) scholarship [201706750008] (Y. C.)
- Netherlands Wetenschaps Organisatie (NWO)-VICI grant 016.Vici.185.050 (S. O. D)

23

24

Contents

25

26 **Chapter 1** General introducton **3**

27 **Chapter 2** Topographic numerosity maps cover subitizing and estimation ranges **12**

28 **Chapter 3** Attention drives numerosity selective responses **37**

29 **Chapter 4** Are numerosity maps involved in symbolic numeral processing. **60**

30 **Chapter 5** Comparing numerosity maps at 3T and 7T MRI **79**

31 **Chapter 6** General discussion **101**

32 **Appendix A** Supplementary materials for Chapter 2 **109**

33 **Appendix B** Supplementary materials for Chapter 3 **114**

34 **Appendix C** Supplementary materials for Chapter 4 **117**

35 **Appendix D** Supplementary materials for Chapter 5 **120**

36 **References** **127**

37 **Summary in Dutch** **142**

38 **Curriculum Vitae** **143**

39 **List of publications** **144**

40 **Acknowledgements** **146**

41

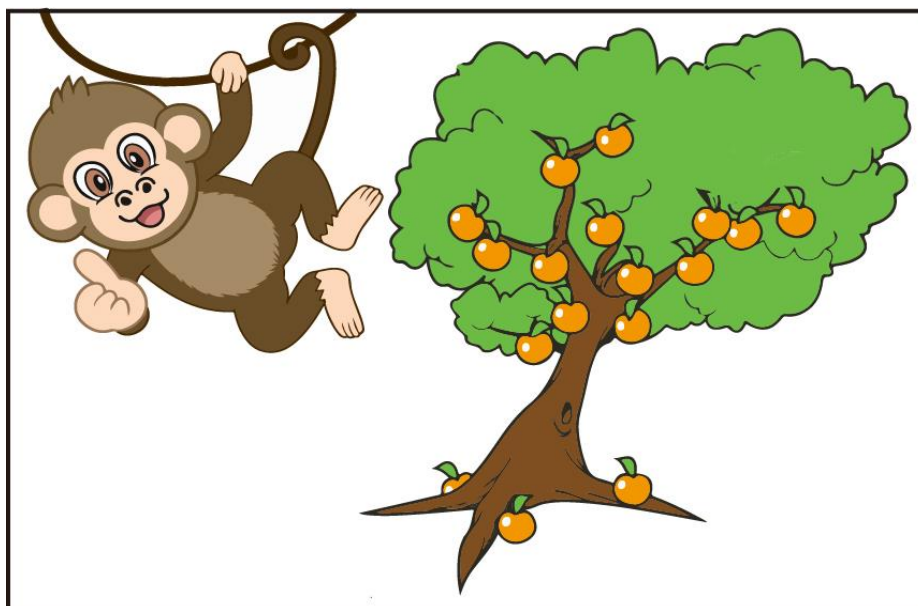
42
43
44
45
46
47
48
49
50
51
52
53
54
55
56
57
58
59
60
61
62
63
64
65
66
67
68
69
70
71
72

Chapter 1

General introduction

73 **The “number sense”**

74 Number, like color and movement, is a basic element of the environment. The cognition of
75 number, including **non-symbolic** and **symbolic number processing**, is therefore ubiquitous
76 and necessary in daily life. Human and animals share the ability to process non-symbolic
77 number information, namely, **numerosity** (i.e., the set size of a group of items). This ability is
78 present in pre-lingual infants (Hyde & Spelke, 2011; Izard, Sann, Spelke, & Streri, 2009), birds
79 (Emmerton, Lohmann, & Niemann, 1997), fishes (Agrillo, Dadda, Serena, & Bisazza, 2008)
80 and insects (Dacke & Srinivasan, 2008) and helps to guide humans and animals’ behavior and
81 decisions. Thus, numerosity perception is believed to be a ‘number sense’, an intuitive
82 understanding of countable quantities across species (D. C. Burr, Anobile, & Arrighi, 2018a;
83 S. Dehaene, 2001; Andreas Nieder, 2021). Numerosity perception is critical for navigating the
84 world, exploiting food sources and avoiding predation (e.g., a monkey processes numerosity
85 and chooses the tree branch with most fruit, as showed in Figure 1.1). Therefore, the neural
86 mechanism of numerosity perception is of great interest to psychologist and neuroscientists
87 and has been studied with various techniques, including electrophysiology (Andreas Nieder,
88 Freedman, & Miller, 2002a; Sawamura, Shima, & Tanji, 2002), neuroimaging (Eger, Sterzer,
89 Russ, Giraud, & Kleinschmidt, 2003; Fornaciai, Brannon, Woldorff, & Park, 2017; Piazza,
90 Izard, Pinel, Le Bihan, & Dehaene, 2004), computational modelling (S. Dehaene & Changeux,
91 1993; B. M. Harvey, Klein, Petridou, & Dumoulin, 2013) and more recently, deep learning
92 algorithms ((Kim, Jang, Baek, Song, & Paik, 2021; Nasr, Viswanathan, & Nieder, 2019;
93 Stoianov & Zorzi, 2012; Zorzi & Testolin, 2018).



95 **Figure 1.1 A cartoon example of a monkey processes the number of fruits on a tree.**
96 Numerosity perception is critical to guide human and animals' behavior and decision in daily
97 life.

98

99 **Neural mechanism of numerosity perception**

100 *Evidence from single-cell recordings*

101 By recording spike rates in single neurons of non-human primates, electrophysiological studies
102 have found neurons tuned to numerosity in the intraparietal areas (A. Nieder & Miller, 2004;
103 Andreas Nieder et al., 2002a; Sawamura et al., 2002). The response curves of these neurons
104 show a 'bell-shaped' coding scheme, peaking at a specific numerosity (their **preferred**
105 **numerosity**), regardless of the physical appearances of the items (Andreas Nieder & Dehaene,
106 2009). These neurons respond maximally to their preferred numerosities and decrease their
107 responses as the distance increases from this numerosity. Later studies found numerosity-
108 selective neurons also in crows (Ditz & Nieder, 2015) and humans (neurosurgical patients)
109 (Kutter, Bostroem, Elger, Mormann, & Nieder, 2018).

110

111 *Evidence from neuroimaging studies*

112 With the development of functional magnetic resonance imaging (fMRI), we are able to non-
113 invasively explore the neural mechanism of numerosity perception in healthy participants.
114 Combining fMRI and adaptation paradigms, Piazza and colleagues (2004) have demonstrated
115 a compressed coding for numerosity in the human intraparietal sulcus, alike to the tuning
116 curves observed in single neurons. Later on, Eger and colleagues (2009) deciphered distinct
117 patterns for symbolic and non-symbolic number formats from human brain activity and the
118 patterns evoked by numerosity changed in a gradual fashion as a function of numerical distance,
119 suggesting an orderly layout of numerosity representations. Moreover, discriminability of
120 numerosity-evoked fMRI activity patterns in the human intraparietal cortex was found to be
121 associated with behavioral enumerations (Lasne, Piazza, Dehaene, Kleinschmidt, & Eger,
122 2019).

123

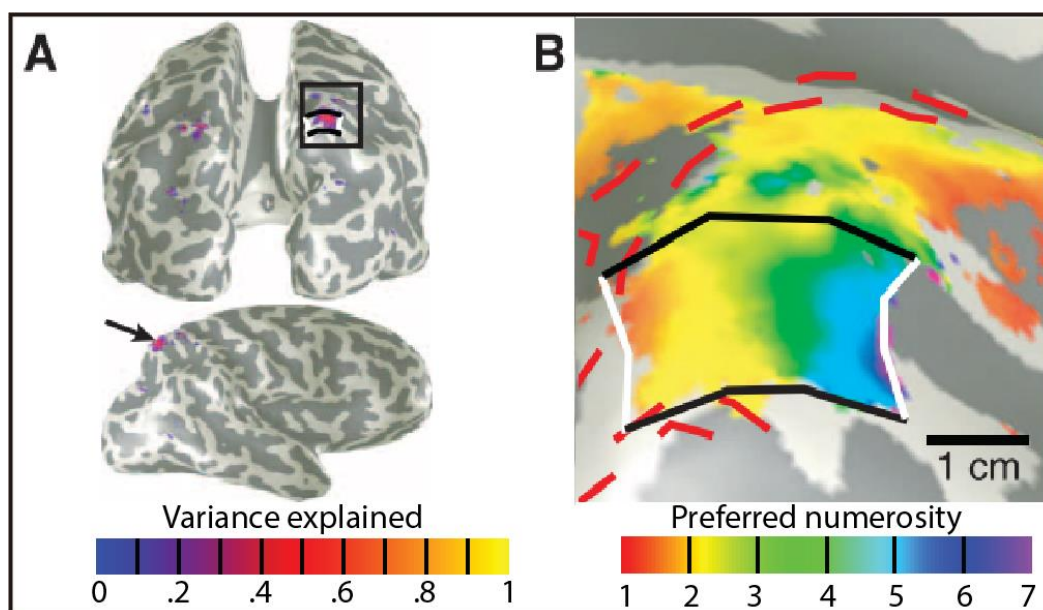
124 *Evidence from computational modelling and deep learning*

125 Based on the evidence from neurophysiology and neuroimaging, our colleagues have since
126 used **population receptive field** (pRF) modelling (Dumoulin & Wandell, 2008) and **ultra-**
127 **high field** (UHF) fMRI (i.e. 7 Tesla) to explore numerosity representations in the human brain
128 (B. M. Harvey et al., 2013). A Gaussian function defined by a set of parameters was utilized

129 as a neural model to describe the tuning curve of numerosity-selective neural populations. More
130 specifically, preferred numerosity is indicated by the peak of the tuning function and the **tuning**
131 **width** is indicated by the full-width at half maximum of the Gaussian. In that study, our
132 colleagues initially found that numerosity-selective neural populations are organized in the
133 human parietal cortex in a **topographic map** where preferred numerosity changes gradually
134 and orderly across the cortical surface (Figure 1.2). Such topographic organization was later
135 found throughout the human brain, at the temporal-occipital cortex (NTO), the parietal-
136 occipital cortex (NPO), the parietal cortex (NPC1 – NPC3), and the frontal cortex (NF),
137 forming a network of numerosity maps (Ben M. Harvey & Dumoulin, 2017a). In this thesis,
138 we refer to these maps as NTO (numerosity maps at the temporal-occipital cortex) and so forth,
139 as defined in previous studies (Ben M. Harvey & Dumoulin, 2017a; Hofstetter, Cai, Harvey,
140 & Dumoulin, 2021; Tsouli, Cai, et al., 2021) and following naming conventions of newly
141 discovered visual field maps in human cortex (Wandell, Dumoulin, & Brewer, 2007).

142 More recently, with the popularity and wide applications of deep learning algorithms,
143 computational research using artificial deep neural networks models have shown numerosity-
144 tuned responses (Nasr & Nieder, 2021; Nasr et al., 2019; Zorzi & Testolin, 2018), even in
145 networks with no training (Kim et al., 2021).

146 Thus, converging evidence demonstrated a specialized neural system for processing
147 numerosity and that numerosity-tuned neurons are the core of this network. In this thesis, we
148 used pRF modelling approach and UHF fMRI to explore the neural mechanism of numerosity,
149 assess the properties of the numerosity-tuned neural populations along the topographic maps,
150 and establish links between neural tuning and behavioral perception of numerosity.



151

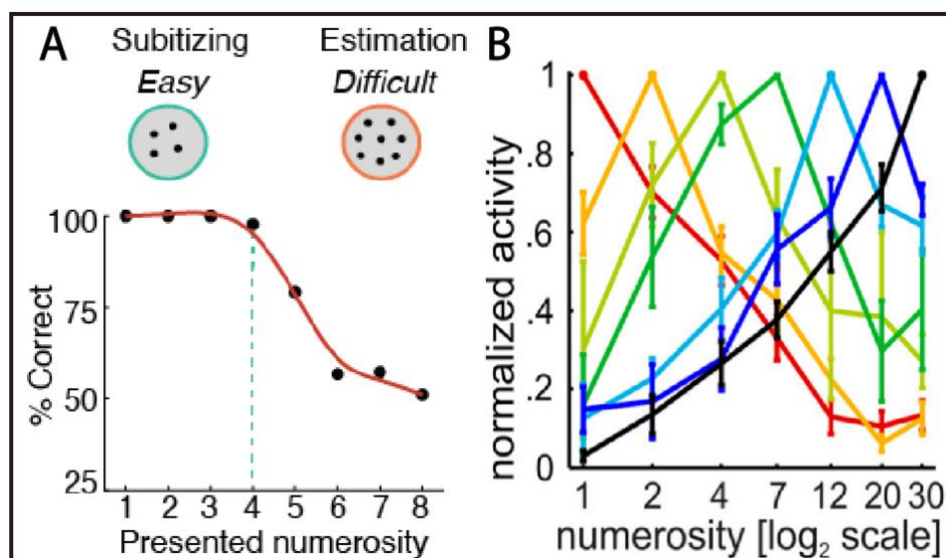
152 **Figure 1.2 Topographic numerosity map in the human parietal cortex.** (A) The variance
 153 explained by the model highlighted a region in the right parietal cortex where the neural
 154 populations demonstrated numerosity tuning. The black square is enlarged in B. (B) Preferred
 155 numerosities of the neural populations increased from medial to lateral ends (white lines) of
 156 the region of interest (black and white lines). Adapted from (B. M. Harvey et al., 2013).

157

158 **Distinct behavioral performances on small and large numerosities**

159 It is well-documented that discrimination on a small number of items, typically less than four
 160 items (known as **subitizing**), is fast and error-free (Kaufman & Lord, 1949). This is distinct
 161 from the behavioral performance on large numerosities (known as **estimation**), which is more
 162 time-consuming and error-prone as numerosities increase (Trick & Pylyshyn, 1994) (Figure
 163 1.3A). Thus, small and large numerosities are thought to be processed under two separate
 164 systems (Feigenson, Dehaene, & Spelke, 2004; Revkin, Piazza, Izard, Cohen, & Dehaene, 2008;
 165 Xu, 2003). However, this theory is not universally accepted. Neurophysiological evidence
 166 suggests that a single mechanism underlies small and large numerosities, given that the tuning
 167 curves of neurons preferring small and large numerosities are encoded in logarithmic scale in
 168 the same way (Figure 1.3B) (Ditz & Nieder, 2016b; A. Nieder & Merten, 2007). Thus, an
 169 alternative theory suggests that an **approximate number system** (ANS) represents all
 170 numerosities (Ditz & Nieder, 2016a; Merten & Nieder, 2009; Andreas Nieder & Miller, 2004b).
 171 To test these two hypotheses, we investigated the representation of small and large
 172 numerosities in the human brain in Chapter 2. We speculated that the discrepancy between the
 173 subitizing and estimation ranges may reflect neural tuning properties of numerosity
 174 representation.

175



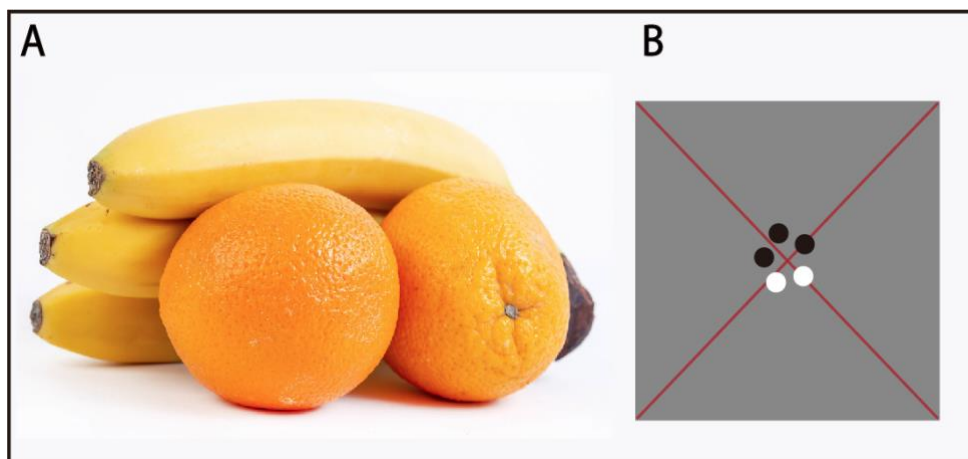
176 **Figure 1.3 Two theories of neural mechanisms underlying small and large numerosities.**
177 (A) Enumeration of up to four items (subitizing) is error free, while enumeration of larger
178 numerosities (estimation) is error prone. Based on this distinct behavioral performance, two
179 systems are thought to process small and large numerosities. Adapted from (Tsouli, Harvey, et
180 al., 2021). (B) Single-cell recordings show similar tuning curves for small and large
181 numerosities, suggesting a single mechanism underlying small and large numerosities
182 representations. Adapted from (Ditz & Nieder, 2016a).

183

184 **The role of attention in numerosity perception**

185 Another argument derived from the discrete performances in the subitizing and estimation
186 ranges is whether attention is required in numerosity perception. Due to the quick and accurate
187 judgements, subitizing has been assumed to be pre-attentive (Trick & Pylyshyn, 1993, 1994),
188 that is, we perceive the numerosity even when attentional focus is not directed to the
189 numerosity feature (i.e., **feature attention**) (Castaldi, Piazza, Dehaene, Vignaud, & Eger,
190 2019), or to where the stimulus is presented (i.e., **spatial attention**) (Hesse, Schmitt,
191 Klingenhoefer, & Bremmer, 2017). Nevertheless, recent psychological studies suggested that
192 numerosities in subitizing but not estimation range require attentional resources (Anobile, Turi,
193 Cicchini, & Burr, 2012; D. C. Burr, Turi, & Anobile, 2010) and that attention affects
194 enumeration of both small and large numerosities (Vetter, Butterworth, & Bahrami, 2008).
195 Some studies used explicit numerosity tasks that require participants' attention to numerosity,
196 for example by discriminating two numerosities (Pomè, Anobile, Cicchini, Scabia, & Burr,
197 2019). Whereas some studies did not require numerosity judgements but require participants
198 to perform tasks based on other aspects of the stimuli, for example detecting color changes of
199 the presented dots (B. M. Harvey et al., 2013; Viswanathan & Nieder, 2013). Whether
200 participants were involved in a numerosity task or not, they were exposed to the stimulus and
201 attended to some features of the stimulus. We refer to such attentional control that humans use
202 cognitive information (e.g., cues) to direct attention to relevant objects (targets) in a visual
203 scene as **endogenous attention**, which can be considered as a **top-down processing**.
204 Alternatively, participants could also have little or no control over their attention during
205 perceptual processing. For example, our attention is easily and involuntarily drawn to 'oddball'
206 stimuli that are very different from the background (e.g., a deviant numerosity within a
207 sequence of equal stimuli) (Hesse et al., 2017). We refer to this stimulus-driven attention as
208 **exogenous attention**, which can be considered as a **bottom-up processing** (Corbetta &
209 Shulman, 2002).

210 We live in a complex world in which a single scene may have multiple objects with
211 different numerosities. For example, a monkey may be asked to choose from a pile of fruits,
212 e.g., three bananas and two oranges (Figure 1.4A). How does numerical information of the
213 monkey's interest and attention ('two bananas') is extracted from the visual scene and what are
214 the neural responses to the numerical information that is not attended ('three oranges')? In all
215 the studies mentioned above, only one set of items was used, that is, the dots displayed in the
216 visual scene were perceived as one single set. Thus, attention to the stimulus is inseparable and
217 directed to one numerosity in the visual scene all the time. To mimic the dynamic natural
218 environment and explore the role of attention in numerosity perception, we used complex
219 numerosity stimuli consisting of two dot subsets (Figure 1.4B), and manipulated attentional
220 focus towards either one of the two subsets (Chapter 3). In this experimental design we were
221 able to assess attentional modulation on numerosity responses and explore the neural responses
222 to the unattended subset.



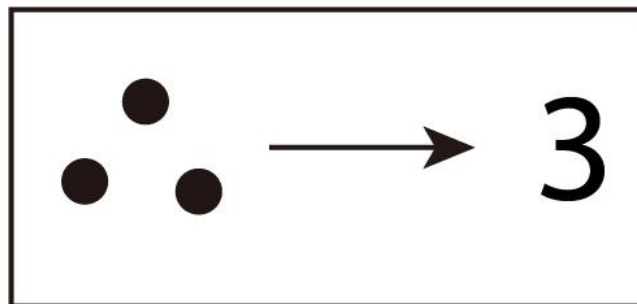
223
224 **Figure 1.4** Examples of complex numerosity stimuli in (A) daily life and in (B) schematic
225 experimental design.

226

227 **Towards symbolic number processing**

228 As discussed above, humans and animals share the ability to process non-symbolic numerosity,
229 while only humans possess the unique ability to process **symbolic numbers** (Figure 1.5). This
230 ability is attained via learning of abstract symbols such as Arabic numbers, number words,
231 math and so forth, which relies on language development and education (Ansari, 2008;
232 Halberda & Feigenson, 2008). Whether non-symbolic numerosity and symbolic number are
233 represented in a common abstract coding scheme is a longstanding debate (Ansari, 2007;
234 Andreas Nieder, 2004). Based on the distinct perceptual consequences, some researchers
235 propose two independent systems: an approximate system for non-symbolic numerosity and

236 an exact system for symbolic number (X. He, Guo, Li, Shen, & Zhou, 2021; Marinova,
237 Sasanguie, & Reynvoet, 2021; Sasanguie, De Smedt, & Reynvoet, 2017). Moreover, recent
238 evidence from single-cell recordings on neurosurgical patients showed distinct neurons tuned
239 to number symbol and numerosity in the medial temporal lobe (Kutter et al., 2018). Yet, an
240 alternative hypothesis suggests that numerosity and symbolic number are interconnected.
241 Specifically, numerosity perception is thought to be the precursor to the development of
242 symbolic numerical cognition (Halberda, Mazocco, & Feigenson, 2008; Andreas Nieder,
243 2020a, 2020b; Piazza, 2010). fMRI adaptation studies have revealed similar number-evoked
244 activation in the intraparietal cortex of both hemispheres, using Arabic numbers (Naccache,
245 Dehaene, Inerm, Hospitalier, & Joliot, 2001) or dot arrays (Piazza et al., 2004) In addition,
246 cross-notation fMRI adaptation has also been observed in the human parietal and prefrontal
247 cortex (Piazza et al., 2007, but see (Cohen Kadosh et al., 2007). As mentioned above,
248 numerosity-tuned neural populations are organized in networks of topographic maps across the
249 human cortex. With the advance of pRF modelling and UHF, in Chapter 4 we investigated
250 whether the numerosity maps are also involved in symbolic number processing.



251
252 **Figure 1.5** Examples of non-symbolic numerosity (e.g., a dot array) and symbolic number
253 stimulus (e.g., an Arabic number 3).

254
255 **Numerosity maps at standard field strength of 3T**

256 The field of cognitive neuroscience is weighing evidence about whether to move from the
257 current standard field strength of 3T to UHF of 7T and above. The MRI systems operating at
258 UHF provide greatly increased signal-to-noise (SNR) and sensitivity to blood oxygenation
259 level dependent (BOLD) contrast (van der Zwaag, Schäfer, Marques, Turner, & Trampel, 2016;
260 Viessmann & Polimeni, 2021; Yacoub et al., 2001), which increases the popularity of UHF at
261 7T and above in cognitive neuroscience. So far, numerosity maps have only been detected at
262 7T (B. M. Harvey et al., 2013; Ben M. Harvey & Dumoulin, 2017a; Hofstetter et al., 2021;
263 Hofstetter & Dumoulin, 2021; Tsouli, Cai, et al., 2021) and whether it is possible to be
264 reconstructed at 3T remains unknown. Thus, in Chapter 5 we investigated whether the

265 numerosity maps could be detected at 3T and to what extent 7T outperforms 3T in terms of the
266 model predictive power. We predicted that more data points would be required to reconstruct
267 robust numerosity maps using 3T data (for example by averaging more functional runs).
268 Though MR physicists and engineers have extensively compared MR systems operating at
269 different fields, this study aim to contribute to the field by providing evidence from the
270 perspective of cognitive neuroscience.

271

272

273

274

275

276

277

278

279

280

281

282

283

284

285

286

287

288

289

290

291

292
293
294
295
296
297
298
299
300
301
302
303
304
305
306
307
308
309
310
311
312
313
314
315
316
317
318
319
320
321
322

Chapter 2

Topographic numerosity maps cover subitizing and estimation ranges

Published as:

Cai, Y., Hofstetter, S., van Dijk, J., Zuiderbaan, W., van der Zwaag, W., Harvey, B. M., & Dumoulin, S. O. (2021). Topographic numerosity maps cover subitizing and estimation ranges. *Nature communications*, 12(1), 1-10.

Acknowledgement of author contributions:

S. O. D. conceived the study. Y. C. and B. M. H. created the stimuli. Y. C., J. van D. and W. van der Z. collected the data. Y. C. analysed the data with some help from W. Z.; Y. C., S. H., B. M. H and S. O. D wrote the paper. All authors commented on the paper. S. O. D. and S. H. provided supervision.

Supplementary materials for this chapter can be found in Appendix A.

323 **Abstract**

324 Numerosity, the set size of a group of items, helps guide behaviour and decisions. Non-
325 symbolic numerosities are represented by the approximate number system. However, distinct
326 behavioural performance suggests that small numerosities, i.e. subitizing range, are
327 implemented differently in the brain than larger numerosities. Prior work has shown that neural
328 populations selectively responding (i.e. hemodynamic responses) to small numerosities are
329 organized into a network of topographical maps. Here, we investigate how neural populations
330 respond to large numerosities, well into the ANS. Using 7T fMRI and biologically-inspired
331 analyses, we found a network of neural populations tuned to both small and large numerosities
332 organized within the same topographic maps. These results demonstrate a continuum of
333 numerosity preferences that progressively cover both the subitizing range and beyond within
334 the same numerosity map, suggesting a single neural mechanism. We hypothesize that
335 differences in map properties, such as cortical magnification and tuning width, underlie known
336 differences in behaviour.

337

338

339

340

341

342

343

344

345

346

347

348

349

350

351

352

353

354

355

356

357 **Introduction**

358 Perception of numerosity (the set size of a group of items) guides human and animal behaviour
359 and decisions(D. Burr & Ross, 2008; S. Dehaene, 2001; Andreas Nieder, 2020b; Andreas
360 Nieder & Dehaene, 2009). Both humans and animals perceive numerosity over a wide
361 numerical range. The approximate number system (ANS) is a core system that is commonly
362 recognized to process non-symbolic number (i.e. numerosity) and relates to symbolic number
363 processing(Gallistel & Gelman, 1992; Meck & Church, 1983). The ANS is thought to produce
364 an intuitive “number sense” across species(Cantlon & Brannon, 2006) and throughout human
365 development(Izard et al., 2009), and represent increasing numerosities with decreasing
366 precision in accord with Weber’s law (Whalen, Gallistel, & Gelman, 1999). Primarily based
367 on the distinct behavioural performances, a separate system termed object tracking system
368 (OTS) (Storm & Pylyshyn, 1988) is thought to process small numerosities, typically up to four,
369 known as subitizing range(Kaufman & Lord, 1949). This system is thought to be distinct from
370 larger numerosities, known as estimation range (Trick & Pylyshyn, 1994). Evidence supporting
371 the distinct systems for numerosity processing comes from the discontinuous behavioural
372 performances, such as reaction time and accuracy, and distinct neural signatures(Anobile,
373 Cicchini, & Burr, 2016; Feigenson et al., 2004). For example, numerosity judgements within
374 the subitizing range yields accurate enumerations, which fails for larger numerosities, and may
375 violate Weber’s law(Revkin et al., 2008).

376 However, the separate numerosity systems are not universally accepted(Chesney &
377 Haladjian, 2011; Cordes, Gelman, Gallistel, & Whalen, 2001; Andreas Nieder & Miller,
378 2004b). Neurophysiological studies on non-human primates found neurons that selectively
379 respond to different numerosities(Andreas Nieder, Freedman, & Miller, 2002b; Sawamura et
380 al., 2002). These numerosity-selective neurons respond to small and large numerosities with
381 similar logarithmic tuning functions as human(Piazza et al., 2004). Single neuron recording
382 studies conducted on monkeys and crows found no sudden change in the behavioural
383 performance and no distinct neural responses between small and large numerosities(Ditz &
384 Nieder, 2016a; Andreas Nieder & Miller, 2004a). Moreover, numerosity discrimination
385 follows Weber’s law in both small and large numerosities(Ditz & Nieder, 2016b; A. Nieder &
386 Merten, 2007). Thus, these studies suggest that there is no need to assume separate systems for
387 small and large numerosities.

388 Here we investigate the neural mechanisms underlying the representation of small and
389 large numerosities in the human brain. We refer to the numerosity ranges as small and large,
390 because subitizing range varies between participants and we did not tailor our experiment for

391 individual participants(Mandler & Shebo, 1982). We measured BOLD responses of
392 numerosity-selective neural populations within functional magnetic resonance imaging (fMRI)
393 recording sites(B. M. Harvey et al., 2013). We have previously shown these populations to
394 respond maximally to numerosities in a small range (i.e. 1 to 7) and to be arranged in orderly
395 topographic maps(Ben M. Harvey & Dumoulin, 2017a). Here we measure their responses to a
396 wider range of numerosities, well into the ANS (i.e. 1 to 64).

397 Based on prior knowledge about topographic maps(Deyoe et al., 1996; Wandell et al.,
398 2007) and numerosity processing(S. Dehaene, 2003; Andreas Nieder, 2016), we will evaluate
399 two hypotheses. First, small and large numerosities may be processed in distinct cortical
400 regions. We have previously described neural populations responding maximally to small
401 numerosities in an extensive network of topographically organized brain areas(B. M. Harvey
402 et al., 2013; Ben M. Harvey & Dumoulin, 2017a). As perception of larger numerosities shows
403 some different properties, such as more time-consuming and error-prone, larger numerosities
404 may produce responses in distinct neural populations in a distinct set of areas. Second, neurons
405 responding maximally to large numerosities could be placed in the same topographic map, i.e.
406 along the systematic topographic progression including both the small and large ranges. This
407 would be akin to stimulating greater eccentricities in the same visual field map(Wandell et al.,
408 2007). Even if small and large numerosities are represented at the same topographic map, there
409 may still be perceptual differences between small and large numerosities. For example, central
410 versus peripheral vision are processed in the same topographic visual field map, but their
411 perception differs considerably(Wandell et al., 2007). Following this hypothesis, neural
412 populations responding to large numerosities may display distinct properties, such as broader
413 tuning, thus leading to different perceptual properties.

414 We investigate these hypotheses using ultra-high field (7 Tesla) fMRI and population
415 receptive field (pRF) modelling(Dumoulin & Wandell, 2008). We measured BOLD response
416 of neural populations that tuned to small and large numerosities and compared estimated neural
417 numerosity preferences to investigate how different numerosity ranges are represented in the
418 brain. We find that both numerosity ranges are represented in the same topographic maps, and
419 we suggest that differences in neural response selectivity and topographic map properties, such
420 as tuning width and cortical magnification respectively, underlie the different perceptual and
421 behavioural properties of small and larger numerosities.

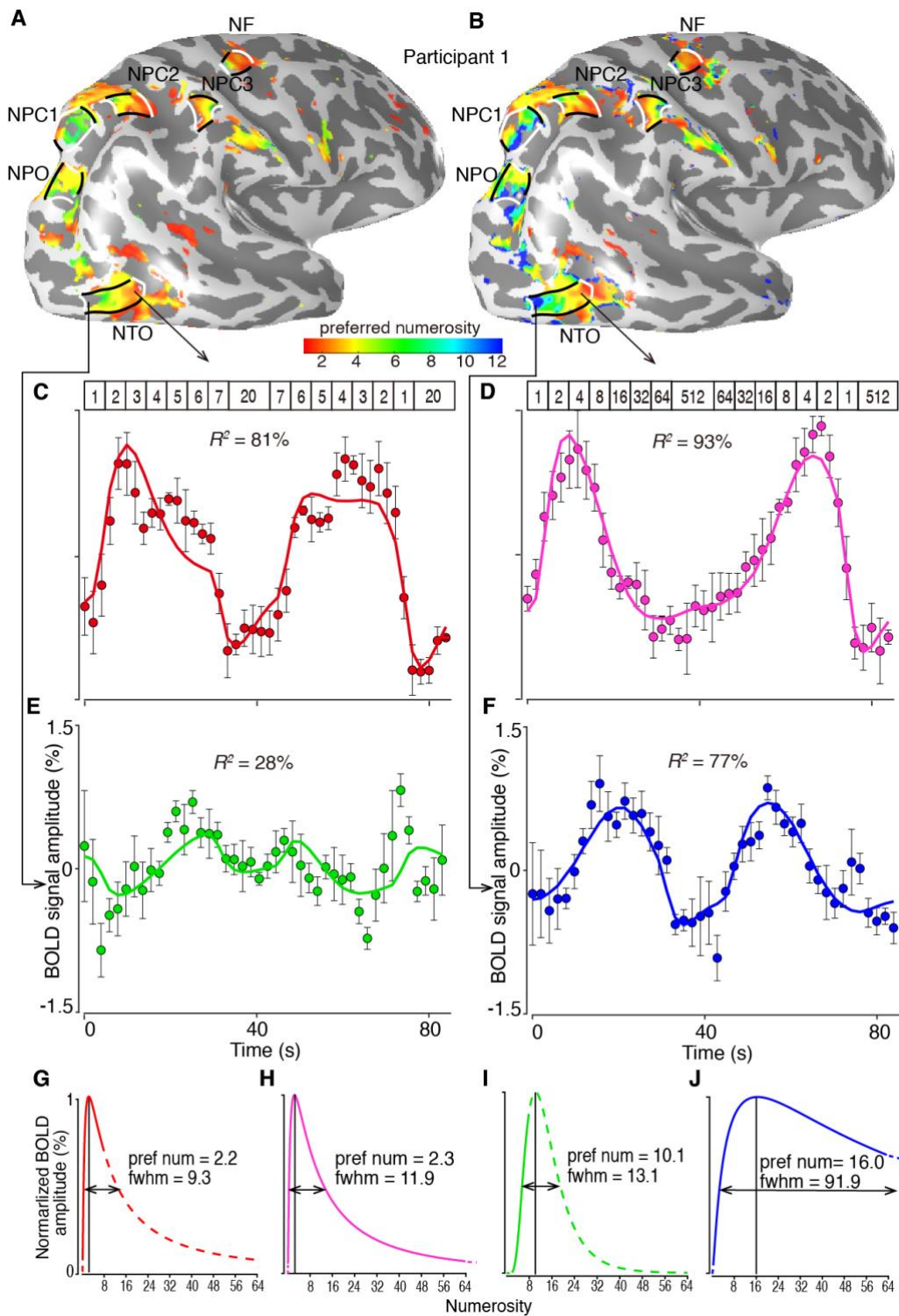
422

423 **Results**

424 *Neural populations in the same cortical regions respond to small and large numerosities*

425 When participants viewed the small numerosity range, i.e. 1 to 7, we found neural populations
426 tuned to these small numerosities. These neural populations were organized in a network of
427 topographic numerosity maps in line with our previous observations (B. M. Harvey et al., 2013;
428 Ben M. Harvey & Dumoulin, 2017a). This network consisted of six numerosity maps, in the
429 temporo-occipital cortex (NTO), parieto-occipital cortex (NPO), parietal cortex (NPC1-3), and
430 in the superior frontal cortex (NF) (Figure 2.1A & B). Within each map, the numerosity-
431 selective neural populations changed gradually along the cortical surface in their preferred
432 numerosity (the numerosity producing the largest response in each population). For example,
433 in NTO (Figure 2.1A), neural populations preferring smaller numerosities clustered at the
434 inferior temporal gyrus while numerosity preferences increased posteriorly along the map
435 (white lines). When participants viewed the large numerosity range, i.e. 1 to 64, we found a
436 similar network of topographic numerosity maps as the one derived from viewing the small
437 range (Figure 2.1B). Similar networks of topographic numerosity maps were also found in all
438 other participants (Supplementary Figure 2.1B).

439 To illustrate the tuned responses, we extracted the response time courses of two
440 example recording sites (voxels) elicited by viewing the small (Figure 2.1A, C & E) and large
441 (Figure 2.1B, D & F) numerosity ranges. These example sites are located in the anterior and
442 posterior regions of the NTO map (Figure 2.1A & B). For the anterior recording site, the neural
443 response models captured more than 80% of the response variance in both conditions (Figure
444 2.1C & D). This site had similar preferred numerosities in both conditions, i.e. 2.2 and 2.3
445 respectively (Figure 2.1G & H). When viewing the small numerosity range, the posterior
446 recording site's response increased monotonically over the presented range, reflecting a
447 preferred numerosity above 7 (Figure 2.1I). However, this preferred numerosity could not be
448 determined accurately as this response reached a maximum beyond the presented range (Figure
449 2.1E). When viewing the large numerosity range, the maximum response occurred at the
450 presentation of larger numerosities (above 7) (Figure 2.1F). As this maximum was within the
451 large stimulus range, this allowed us to determine the preferred numerosity at 16 (Figure 2.1J).
452 This demonstrates that neural populations with larger preferred numerosities are found near
453 those with the small preferred numerosities at the same cortical area.



454

455 **Figure 2.1. Neural population responses to small and large numerosities.** A & B Cortical
 456 surface rendering of the right hemisphere shows a similar network of numerosity maps in both
 457 presented ranges. Preferred numerosities of cortical recording sites, estimated from responses
 458 to the small range (A) and the large range (B) for recording sites with over 30% of variance
 459 explained by the neural response model. Black lines outline the lateral borders of individual
 460 numerosity maps. The borders denoting the lowest and the highest preferred numerosities in

461 each map are marked by white lines. **C & D** An example fMRI recording site in anterior NTO
462 shows different fMRI time courses (dots) for small (**C**) and large (**D**) numerosity ranges. Both
463 time courses are similarly well captured by the predictions (coloured lines) of similar neural
464 response models. Dots represent mean response amplitudes; error bars represent the standard
465 errors over repeated measurements ($n = 4$). The presented numerosities are indicated at the top
466 of the graph. **E & F** An example fMRI recording site in posterior NTO shows a higher preferred
467 numerosity. This response does not reach a maximum in the small numerosity range (**E**). Dots
468 represent mean response amplitudes; error bars represent the standard errors over repeated
469 measurements ($n = 4$). **G & H** For both numerosity ranges, the anterior NTO site's response is
470 predicted by similar neural response models. **I & J** For the large numerosity range, posterior
471 NTO site's response is well predicted by a neural response model (**J**). However, this sites'
472 preferred numerosity is above the small numerosity range, so it could not be determined
473 accurately (**I**), produces only low-amplitude responses and yields poorer model fits (**E**) with
474 this range. Preferred numerosity is indicated by the highest response amplitude in the neural
475 model, and tuning width is indicated by the full width at half maximum (FWHM). The neural
476 response model within the presented range is shown with solid lines, outside the range with
477 dashed lines.

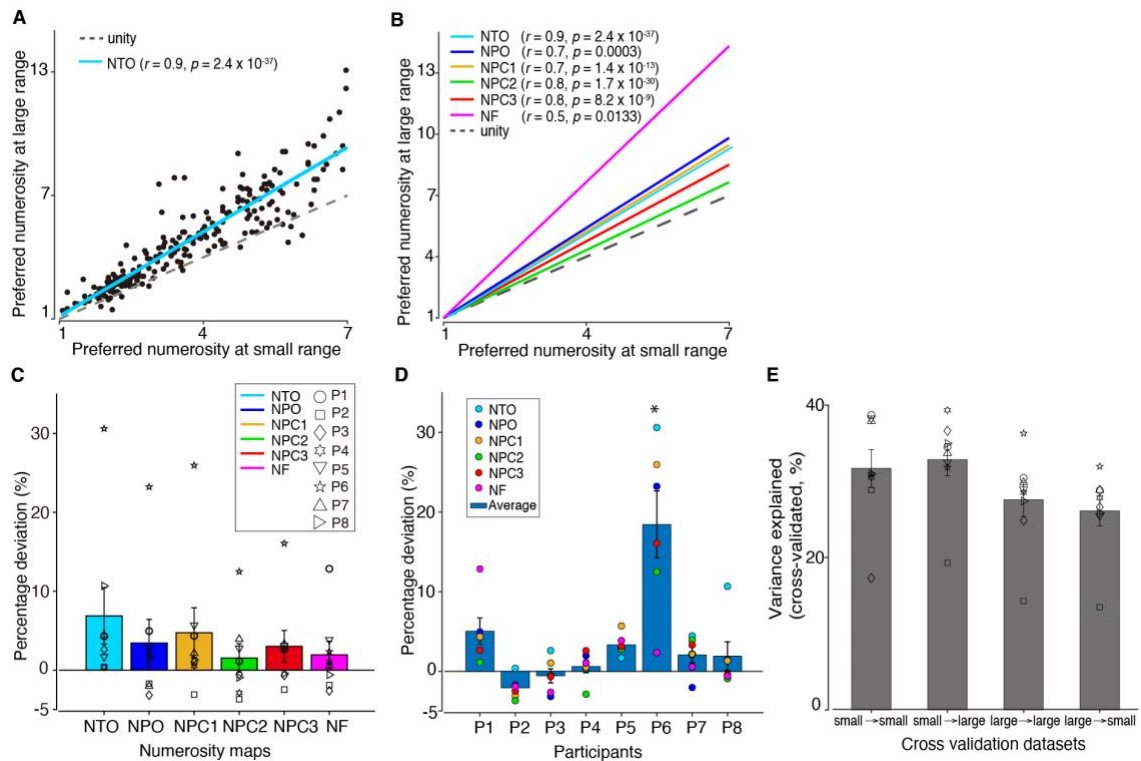
478

479 *Selectivity of neural populations remains stable*

480 We found strong correlations between the preferred numerosities estimated from the two
481 numerosity ranges, especially for the overlapping portion (Figure 2.2A & B), in all maps and
482 all participants (Supplementary Figure 2.2). We selected these preferred numerosities estimates
483 based on two criteria: variance explained exceeded 30% and the preferred tuning fell within
484 the presented ranges (i.e. 1-7 and 1-64 for the small and large ranges, respectively). This
485 indicates a similar spatial organization of numerosity preferences between the two conditions,
486 though it does not test how similar these preferences are. To quantify their similarity, we
487 computed the extent to which the distribution of preferred numerosities estimated from the
488 small and large ranges deviated from the unity line (where the two estimates are identical), i.e.
489 the percentage deviation, for each map in each participant (see Methods). Zero percentage
490 deviation indicates identical preferred numerosity estimates between conditions. A Wilcoxon's
491 signed rank test showed that the percentage deviations of all the maps across participants were
492 significantly above zero (two-sided, $p = 0.0006$, $z = 3.4$, $df = 47$) (Figure 2.2C). This
493 demonstrated that preferred numerosities were significantly larger when estimated from the
494 large numerosity range. However, the median percentage deviation was only around 3.59%,

495 far smaller than the change in mean presented numerosities (454%), so, though significant, the
496 effect size is small. ANOVA analyses of the percentage deviations in all the maps and
497 participants demonstrated a significant effect of participant, but no effect of map and no
498 interaction. Post-hoc analysis showed that only one participant had a significantly different
499 percentage deviation from other participants (two-way ANOVA; $F_{(7,47)} = 13.36$, $p = 3.0 \times 10^{-8}$,
500 followed by post hoc analysis, Bonferroni corrected for multiple comparisons) (Figure 2.2D).

501 Furthermore, we performed a cross validation analysis (see Methods). To estimate the
502 model's predictability and reliability, we fit pRF estimates on one half split dataset to the
503 response elicited by the other half split dataset and computed the cross-validated variance
504 explained (i.e. cvR^2) of the two conditions, respectively (within-condition cross validation).
505 Next, we fit pRF estimates on small numerosity to the response elicited by large numerosity
506 and computed the cvR^2 , and vice versa (cross-condition cross validation). We use the format
507 of "pRF predictor \rightarrow test data" (e.g., "large \rightarrow small") to indicate using data from large
508 numerosity range to predict data acquired while viewing small numerosity ranges. We
509 averaged the cvR^2 from all the possible iterations: "small \rightarrow small", "small \rightarrow large", "large
510 \rightarrow large" and "large \rightarrow small" cross validations, respectively. We then performed a within-
511 subject two-way ANOVA analysis to compare the cvR^2 between within- and cross-condition
512 validations. There were no significant differences ($p > 0.025$, two-sided, Bonferroni corrected
513 for multiple comparisons). As Figure 2.2E shows, all of the half-split datasets show
514 considerably high predictive power, suggesting that the pRF estimates are similar across
515 conditions. The results of cross validation analyses also show strong correlations between
516 preferred numerosity estimated from the two ranges and a slight increase of numerosity
517 preference at the large range. (Supplementary Figure 2.5A-B).



518

519 **Figure 2.2. Relationship between numerosity preferences estimated from small and large**
 520 **ranges indicates similar numerosity selectivity and topographic progressions. (A)**

521 Participant 1's NTO (see the maps in Figure 2.1A & B) numerosity preferences estimated from
 522 the two ranges were strongly correlated (see legend of the Pearson correlation coefficients and
 523 statistical significance). Dots show the estimates from individual recording sites (variance
 524 explained > 30%), the blue line shows the linear fit between the two estimates, the dashed line
 525 shows unity (i.e. identical preferences). (B) Linear fits from all six of this participant's maps.

526 These also reflect strong correlations in each map (see legends), indicating a similar spatial
 527 organization of estimated numerosity preferences, and are consistently above the unity line.

528 (C) Bars show averaged percentage deviation quantifying the difference between the slopes of
 529 the linear fits (in B) and the unity line for each map. Error bars show the standard errors of the
 530 mean over participants (n = 8). A two-sided Wilcoxon signed rank test shows the percentage
 531 deviation of all these maps were above zero (z = 3.4, p = 0.0006, df = 47), suggesting a slight

532 increase of preferred numerosity estimates at the large range. (D) Bars show averaged
 533 percentage deviation (same as in C) for each participant. Error bars show the standard errors
 534 of the mean (n = 6). Post hoc analysis shows significant difference between participant 6 and
 535 other participants (Bonferroni corrected for multiple comparisons; * indicates p = 3.0 x 10⁻⁸).

536 (E) Bars represent averaged cross-validated variance explained of the within- and cross-
 537 condition cross validation datasets. Error bars indicate standard errors of the mean over

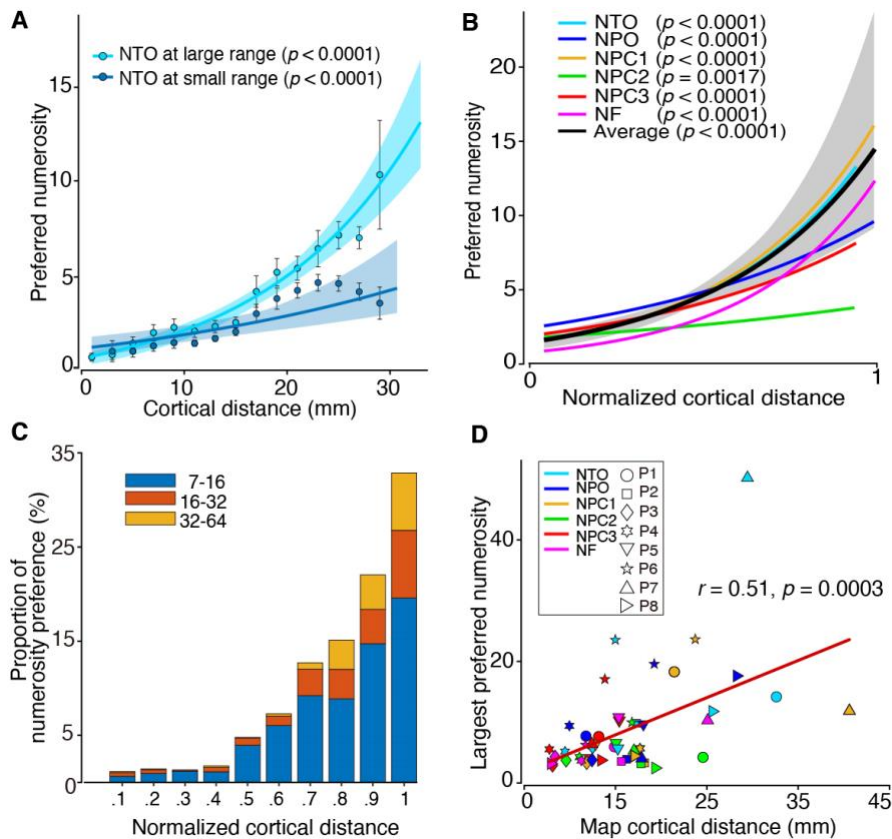
538 participants ($n = 8$). Within-subject two way ANOVA analysis shows no significant differences
539 between the cross validation datasets ($p > 0.025$, two-sided, Bonferroni corrected for multiple
540 comparisons). Source data are provided as a source data file.

541

542 *More cortical area devoted to smaller numerosities*

543 The change of numerosity preferences along each map was quantified by measuring the
544 distance of each data point from the borders of the map with the highest and the lowest
545 numerosity preferences (white lines in Figure 2.1A & B, see Methods). The numerosity
546 preference progressed systematically along the cortical surface (Fig. 3a). Consistent with
547 previous studies (B. M. Harvey et al., 2013; Ben M. Harvey & Dumoulin, 2017a), we found a
548 cortical magnification effect, with less cortical surface responding to larger numerosities, in all
549 the maps of all the participants (Figure 2.3B, Supplementary Figure 2.3).

550 To visualize the location of populations with large numerosity preferences (above 7),
551 we calculated the proportion of large numerosity preferences in each 10% cortical distance
552 interval. As shown in Figure 2.3C, neural populations tuned to large numerosities are located
553 towards the end of the maps. This suggests that numerosity preferences progressed from small
554 to large continuously along the same topographic map. Last, we found a significant correlation
555 between the size of the maps (cortical distance) and the largest preferred numerosity in these
556 maps ($r = 0.51$, $p = 0.0003$; Figure 2.3D). This suggests that tuned responses to larger
557 numerosities are more detectable in larger maps. Using cross validation datasets, similar
558 systematic progressions were found across all maps and all participants (Supplementary Figure
559 2.5C).



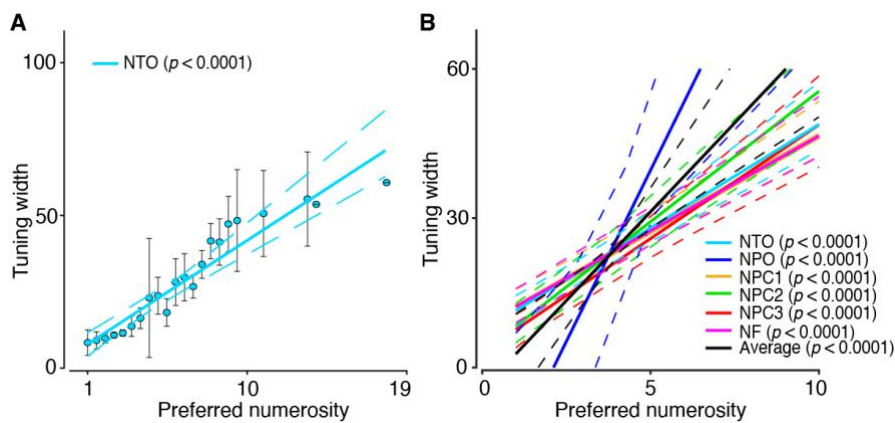
560

561 **Figure 2.3. Visualization of the large numerosity preference locations.** (A) Cortical
 562 progression of small (dark blue) and large (light blue) preferred numerosities with the cortical
 563 distance (between the white lines in Figure 2.1A & B) across participant 1's NTO map. The
 564 preferred numerosity increased systematically for both conditions. Points represent the mean
 565 preferred numerosity in each distance bin (every 2 mm); error bars showing standard errors of
 566 the mean over data points within each bin. Coloured lines show the best logarithmic fits. (B)
 567 Progression of numerosity preferences estimated from the large range as a function of
 568 normalized cortical distance in all the numerosity maps of participant 1. The black line shows
 569 the best logarithmic fit that bins the data points from all the maps across normalized cortical
 570 distance. Shade area shows the 95% confidence interval determined by bootstrapping fits ($n =$
 571 1,000) to the binned points and p-values indicate the probability of the observed change from
 572 permutation analysis ($n = 10,000$), in both panel A & B. (C) Proportion of tuned responses to
 573 large preferred numerosities (above 7) for each 10% interval of normalized cortical distance in
 574 all maps of all participants. Coloured bars represent the proportion of preferred numerosities
 575 ranging from 7-16, 16-32 and 32-64. (D) Map size (cortical distance) correlates with the largest
 576 preferred numerosities in the maps, i.e., large maps typically contain larger numerosity
 577 preferences. Source data are provided as a source data file.

578

579 *Tuning width increases with preferred numerosity*

580 To illustrate the change of tuning width with preferred numerosity, we plotted tuning width
581 against preferred numerosity estimated by viewing the large numerosity range (Figure 2.4).
582 Population tuning widths increase with preferred numerosities systematically across all
583 numerosity maps of all the participants (Supplementary Figure 2.4), in line with the observation
584 at the small numerosity range (B. M. Harvey et al., 2013). The cross validated datasets show
585 similar changes of tuning width increase with preferred numerosity (Supplementary Figure
586 2.5D-E).



587

588 **Figure 2.4. Tuning width changes with preferred numerosity.** (A) Tuning width increases
589 with preferred numerosity in participant 1's NTO map elicited by the large range. Recording
590 points are binned based on preferred numerosity. Points represent the mean tuning width within
591 each bin, error bars represent the standard errors of the mean over all the data points within
592 each bin. Solid line is the linear fit to the bins, weighted by the inverse of the standard error of
593 each bin. (B) Linear fits of tuning width against preferred numerosity of all the numerosity
594 maps averaged across participants (solid coloured lines) and across maps (solid black line). In
595 both panel a & b: dashed lines represent 95% confidence intervals determined by bootstrapping
596 fits to the binned points ($n = 1,000$). The statistical significance of the slopes was determined
597 with permutation analysis ($n = 10,000$), indicating the probability of observed tuning width
598 change by chance.

599

600 **Discussion**

601 We found a network of neural populations tuned to small and large numerosities organized as
602 topographic maps in the same cortical regions. These neural populations exhibit stable
603 numerosity selectivity regardless of presented numerosity range. When the participants were
604 viewing the large range, i.e. 1 to 64, we found populations with larger numerosity preferences
605 (above 7) located at the end of the maps (near higher preferences within the small range). These

606 numerosity maps exhibit features akin to maps for primary sensory organs (retinotopic maps,
607 tonotopic maps and somatotopic maps), such as a larger extent of cortical surface devoted to
608 smaller numerosities, i.e. cortical magnification (Ben M. Harvey & Dumoulin, 2011; Sereno et
609 al., 1995). These results demonstrate a continuum of small and large numerosity preferences
610 within the same numerosity map. We therefore propose a single neural mechanism for the ANS
611 up to numerosities of 64. We suggest that small and large numerosities are encoded in the same
612 neural tuning, nevertheless, small and large numerosities differ in their cortical representations.
613 We speculate that the differences of the map properties, such as cortical magnification and
614 tuning width, may underlie the different behavioural and perceptual qualities of small and large
615 numerosities.

616 For the overlapping numerosities between the small and large ranges, i.e. 1 to 7, the
617 numerosity maps were similar. When stimulating with larger numerosities (above 7), the
618 numerosity maps extended in the direction of the higher preferences within the small range
619 condition in a continuous fashion. This is akin to visual field maps, when stimulating with a
620 greater eccentricity a larger proportion of the map is revealed (Wandell et al., 2007). Likewise,
621 a wider numerosity range reveals a larger proportion of the numerosity map.

622 We propose that there are two main theories to explain the results. On one hand, we
623 speculate that the numerosity tuning remains stable but that the stimulus range influences the
624 numerosity responses. A single recording site ($1.75 \times 1.75 \times 1.75 \text{ mm}^3$) will have about 250,000
625 neurons (Braitenberg, 1998). In line with this notion, the tuning width of the total population
626 within a single recording site is quite large: neural populations tuned to 2 have a tuning width
627 of about 10 (see for example in Figure 2.1G & H). Therefore, we assume that at a single neuron
628 level, different preferred tunings are present in the same fMRI recording site, i.e. the population
629 consists of neurons with different preferred numerosities. In other words, the heterogeneity of
630 the neural population alters the overall numerosity preference depending on the presented
631 range. More specifically, the overall numerosity preference of a recording site is an average of
632 the preferred numerosities of the neural populations within this recording site. For example, at
633 the same recording site, the averaged population tuning would be higher for the large
634 numerosity range because the neurons sensitive to larger numerosities in the recording site will
635 contribute more to the population responses when the larger numerosities are presented, and
636 less when smaller numerosities are presented. We found only a slight increase of preferred
637 numerosity at the same recording site (i.e. the slope is slightly above the unity line) when
638 stimulated with the large range, even in the lower portion of the range (i.e. 1-7). However, the
639 overall deviation is small (around 3.59%). This suggests that the majority of neurons within a

640 recording site tend to have similar preferred numerosities. Furthermore, neural tuning
641 estimated from the large range predicts a large signal variation of the responses derived from
642 the small range, and vice versa (Figure 2.2E). Therefore, we suggest that the numerosity
643 preference of single neurons is likely stable, but the heterogeneity of the neural population may
644 give rise to different preferred numerosity estimations when the stimulus changes.

645 On the other hand, another possible explanation is that the tuning of neural population
646 depends on the presented stimuli and the numerosity maps are dynamic remapping of the tuning
647 properties. Previous studies have demonstrated that numerosity is susceptible to adaptation
648 akin to primary sensory perceptions (D. C. Burr, Anobile, & Arrighi, 2018b; D. Burr & Ross,
649 2008; Piazza et al., 2004). Recently, Tsouli et al. (Tsouli, Cai, et al., 2021) found that
650 numerosity adaptation altered the preferred numerosity within the numerosity map, resulting a
651 predominantly attractive biases towards the numerosity of the adaptor. Moreover, the
652 adaptation effect increases as the numerical distance between the unadapted preferred
653 numerosity and the adaptor increases. Let us assume that the neural population at a recording
654 site responded selectively to the numerosity 4. When stimulated repeatedly and sequentially
655 with larger numerosities (e.g. 8-64), the preferred numerosity of the neural population could
656 shift to a higher number, due to the attractive bias of adaptation towards the larger numerosities.
657 Thus, the numerosity maps would show some systematic changes in numerosity preference
658 depending on the numerosity range, i.e. dynamic remapping of the neural population tuning
659 properties. As we note in the Methods, our stimulus sequence presented the numerosities
660 changed systematically in both ascending and descending directions and the small and large
661 ranges were interleaved during scanning. By doing so, we aim to balance opposing effects of
662 preceding lower and higher numerosities and habituation effects of the small or large range.
663 Furthermore, as Supplementary Figure 2.1 shows, stimulating with only large numerosities
664 (>7) resulted in poor estimates of the maps and only elicited responses at the maps consisting
665 of neural populations tuned to larger numerosities. This suggests that the neural population
666 tuning is less likely to change dynamically to follow the presented stimulus. Thus, though we
667 cannot exclude context-dependent remapping, we are not convinced of this theory given the
668 possibility of range-dependent differences in the contributions of different parts of a
669 heterogeneous neural population (the first theory). Therefore, we favour the interpretation that
670 under our stimulus design the numerosity tuning remains predominantly stable.

671 In line with our findings, the stability of numerosity selectivity is also evident at a
672 temporal scale. At a single neuron level, neurophysiological recordings on non-human primates
673 demonstrated that numerosity-selective neurons maintain reliable tunings after the numerosity

674 stimulations disappear(Andreas Nieder et al., 2002b; Andreas Nieder & Miller, 2003).
675 Similarly, stable numerosity selectivity is also found in corvid birds when retaining information
676 of numerosity in working memory and the neuronal activity during the delay period could
677 predict behavioural performance(Ditz & Nieder, 2015). These findings suggest that tuned
678 responses of numerosity-selective neurons are stable across time, at least they hold information
679 of the pre-presented numerosity in working memory. This enables a reliable neural system to
680 maintain information temporally to deal with the task demand. Together with our findings, we
681 suggest that numerosity tunings are stable, providing a reliable neural system for numerosity
682 perception at the cortical representation and temporal processing scales.

683 The largest preferred numerosities detected in the numerosity maps were smaller than
684 the largest presented numerosity (i.e. 64), and these neural populations are found located at the
685 end of the map. In addition, stimulating with only larger numerosities (i.e. above 7) does not
686 reveal the complete maps, or a clear topographic progression, but mainly produces responses
687 at the sites where the maps have neural populations tuned to large numerosities (Supplementary
688 Figure 2.1C). There were few responses to larger numerosities beyond 12. This could be
689 interpreted as evidence that the cortical encoding is different for larger numerosities than
690 smaller ones. However, fewer responses to large numerosities does not necessarily mean there
691 are no neurons responding to these large numerosities. Evidence from single neuron recordings
692 demonstrate neurons selective for large numerosities(A. Nieder & Merten, 2007). In our study,
693 neurons with tuning to very large numerosities may be hidden in the overall neural populational
694 response dominated by neurons tuned to smaller numerosities. Therefore, we suggest that small
695 and large numerosities are represented similarly in terms of their neural tunings.

696 Furthermore, based on our observations, less cortical area is devoted to representing
697 larger numerosities. We assume that the largest numerosity we can measure is constrained by
698 the surface area of the numerosity map. For example, the largest preferred numerosity of a
699 given recording site (voxel) is derived by averaging the preferred numerosities of the neural
700 populations within this site. In such a way, the representative preferred numerosity of a given
701 recording site will always be smaller after averaging values from the subpopulations. This
702 could also explain why the size of numerosity map correlates with the potential largest
703 preferred numerosity within the map (Figure 2.3D). If the map is small in size (fewer voxels),
704 we cannot resolve individual populations preferring larger numerosities as they are mixed with
705 those preferring smaller numerosities at the same recording sites. If the maps are larger in size
706 however, we could distinguish the neural populations tuned to larger numerosities and those
707 tuned to smaller numerosities in separated voxels.

708 Furthermore, we propose that the cortical magnification explains why stimulating with
709 only larger numerosities (i.e. above 7) does not reveal the complete maps or topographic
710 progression. We speculate that the cortical magnification factor, i.e. fewer cortical surface area
711 is devoted to larger numerosities, accounts for the fact that fewer representations for larger
712 numerosities (e.g. 16 - 64) were detected. In visual cortex, there is a smaller fraction of cortical
713 surface for representing larger eccentricities(Daniel, Whitteridge, Hospital, & London, 1961;
714 Wandell et al., 2007), likewise, there are evidences point at a similar decline in surface area for
715 representing larger numerosities(B. M. Harvey et al., 2013; Ben M. Harvey & Dumoulin,
716 2017a). Thus, it seems likely that the detection of the largest numerosity was also constrained
717 by the cortical magnification effect of the numerosity map representation. In support of this
718 assumption, Cheyette et al.(Cheyette & Piantadosi, 2020) suggested that the limited amount of
719 information processing capability of the underlying neural circuits leads to the inaccurate
720 perception of large numerosity, while a single system represents small and large numerosity.

721 The continuum of cortical representation of small and large numerosities argues for a
722 single numerosity neural representation mechanism, in line with the single enumeration system
723 of the ANS. However, numerosity estimation is fast and accurate for the subitizing range,
724 where some studies report a clear violation of Weber's law(Revkin et al., 2008; Xu, 2003).
725 Enumeration suddenly becomes slow and error-prone beyond this range, showing an increase
726 in reaction time and a decrease in precision(Balakrishnan & Ashby, 1991; Pomè, Anobile,
727 Cicchini, & Burr, 2019). Therefore, this dissociation is held to reflect two separate systems in
728 enumerations at different set sizes(Feigenson et al., 2004). However, reported differences in
729 the dependence for small versus large numbers do not necessary imply the existence of two
730 separate systems. Because for small numerosities the imprecision of the numerosity
731 representation remains below one item while for larger numerosities to achieve the same
732 discrimination precision more numerical distance is required, which results in more overlap
733 and a ratio-dependent effect(Andreas Nieder, 2020a, 2020b).

734 Although we suggest that a common neural mechanism underlies numerosity
735 representation across a wide range, it may nevertheless have distinct perceptual and
736 behavioural consequences between the subitizing and estimation ranges. The fast and accurate
737 perception on small numerosities is because more cortical area of the numerosity maps are
738 devoted to smaller numerosities(B. M. Harvey et al., 2013; Ben M. Harvey & Dumoulin,
739 2017a). This is consistent with the observation in macaque prefrontal cortex that single neurons
740 with smaller numerosity preferences occurred more frequent, with a progressive decrease in
741 frequency toward higher numerosity preferences(A. Nieder & Merten, 2007). This cortical

742 representation of small and large numerosities resembles the logarithmic coding of
743 numerosity(Kutter et al., 2018; Andreas Nieder & Miller, 2003; Piazza et al., 2004).
744 Neurophysiological studies in macaque and corvids show logarithmically numerosity encoding
745 in single neurons(Ditz & Nieder, 2015; Andreas Nieder, 2016). Logarithmic coding allows a
746 wide range of numerosities to be encoded, thus increasing the scope of neural representation
747 and perception of numerosity(Dayan & Abbott, 2001). The cortical magnification of
748 numerosity maps provides the neural circuits for such a logarithmic coding space. Perception
749 on large numerosities gets inaccurate and takes more time as the tuning width increases with
750 the preferred numerosity. Thus, we speculate that the properties of numerosity representation,
751 such as cortical magnification and tuning width, give rise to distinct perceptual performance
752 on small and large numerosities.

753 Despite much evidence for a number sense in humans, there have been arguments about
754 whether numerosity is sensed directly or derived indirectly from other non-numerical
755 information in the stimulus, such as dot size and density(S. C. Dakin, Tibber, Greenwood,
756 Kingdom, & Morgan, 2011; Gebuis & Reynvoet, 2012). One reason why the argument is
757 particularly compelling is that numerosity is intrinsically correlated with many other physical
758 features. For example, we have shown a correlation between the neural tuning of object size
759 and numerosity, with largely overlapping topographic maps. However, object size and
760 numerosity tuning result from distinct mechanisms, indicated by their distinct tuning properties
761 and map organizations(Ben M. Harvey, Fracasso, Petridou, & Dumoulin, 2015). Previous
762 studies from other labs have demonstrated separate mechanisms for perception of numerosity
763 and density(Anobile, Cicchini, & Burr, 2014; Anobile, Cicchini, et al., 2016) that a regime of
764 texture mechanism represents densely packed items that cannot be individuated as separate
765 items. Note that in previous studies(B. M. Harvey et al., 2013; Ben M. Harvey & Dumoulin,
766 2017a), we used various stimulus conditions, such as constant area, constant dot size, constant
767 circumference, high density and various shapes. In these studies, we consistently found
768 topographic numerosity maps in all the stimulus configurations, which suggests that the
769 topographic maps depend on numerosity rather than other stimulus information. We have also
770 demonstrated that responses in these maps cannot be explained by neural tuning for these non-
771 numerical features(Ben M. Harvey & Dumoulin, 2017b). In the current study, we used a
772 stimulus configurations total surface area held constant across numerosity, ensuring equal
773 luminance in all the numerosity displays. The stimuli were presented in a larger central visual
774 field of 4° than the original setting of 1.5°, as this configuration allows larger numerosity

775 stimuli to have enough space to individuate each item. But in this stimulus configuration
776 density increases with numerosity and total item perimeter decreases, for example. We believe
777 the response we observe reflect numerosity because this has been conclusively demonstrated
778 in the same maps in our previous studies(B. M. Harvey et al., 2013; Ben M. Harvey &
779 Dumoulin, 2017a; Ben M. Harvey et al., 2015), although it was not possible to design the
780 experiment to conclusively demonstrate this in the current data with the large numerosity range.

781 Based on these results, we suggest that differences in neural properties within the same
782 topographic map underlie the different cognitive behaviours of numerosity perception. This is
783 commonly seen in visual field maps with perceptual differences between central (foveal) and
784 peripheral vision. Visual field maps show changes in cortical magnification and receptive field
785 size with eccentricity. Specifically, more of the cortical area is devoted to central vision with
786 smaller receptive fields. Such differences in cortical magnification and receptive field size may
787 reflect different perceptual processing requirements(Wandell et al., 2007). Therefore, like
788 visual cortex, we suggest that, not only are topographic maps a core principle of brain
789 organization, but the differential features of cognitive topographic maps underlie differences
790 in cognition.

791

792 **Methods**

793 *Participants*

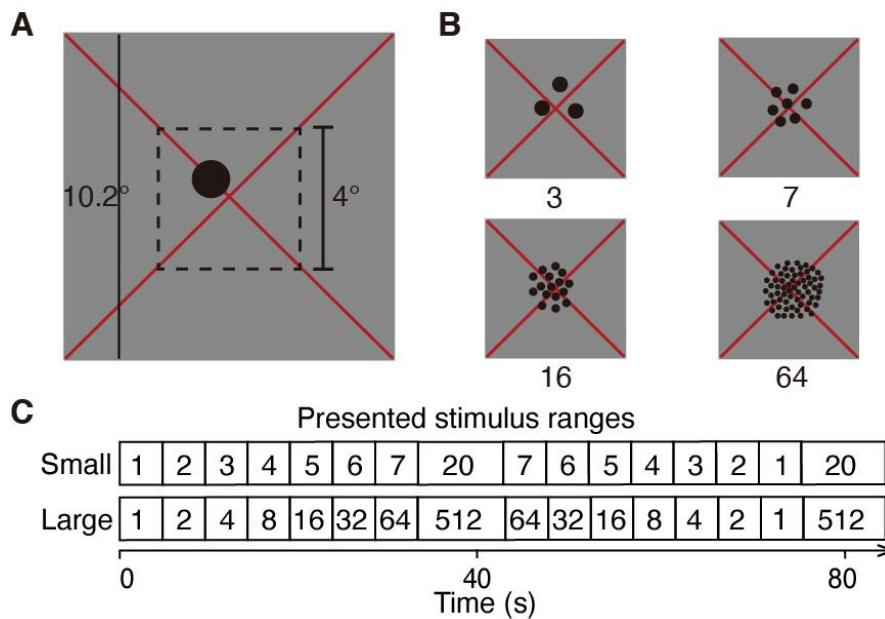
794 We present data from eight participants (one female, age range 25 – 45 years). All the
795 participants had normal or correct-to-normal visual acuity. All were well educated, with good
796 mathematical abilities. Written informed consent was obtained before every MRI session. All
797 experimental procedures were approved by the ethics committee of University Medical Centre
798 Utrecht.

799

800 *Stimuli and experiment design*

801 Visual stimuli were presented on a 69.84 x 39.29 cm LCD screen (Cambridge Research
802 Systems) behind the MRI bore. Participant was required to lie still and view the display through
803 a mirror attached to the head coil. The total distance from the attached mirror to the display
804 screen was 220 cm. The display resolution was 1920 x 1080 pixels. Visual stimuli were
805 generated in Matlab using PsychToolbox(Brainard, 1997; Denis G Pelli, 1997). A large
806 diagonal cross composed of thin red lines was displayed consistently across the entire screen,
807 which allows accurate fixation. Participants were asked to fixate the intersection of the cross.
808 Stimuli consisted of a group of dots with a constant total surface area presented in the central

809 4° (diameter) of the visual field. Dots were randomly positioned at each presentation so that
810 each dot fell entirely within this area, to distribute contrast energy equally across the stimulus
811 area for all numerosities (Figure 2.5). Each numerosity presentation that contained the same
812 number of dots was placed in a new, random position, so no specific visual position was
813 associated with any numerosity. To prevent perceptual grouping, individual items were
814 distributed roughly homogeneously across the stimulus area. All of the numerosity
815 presentations were displayed as black or white dots on a grey background. Dot patterns were
816 presented briefly (300ms) to ensure participants did not have time to count. A new random
817 pattern was presented every 650ms, with 350ms presentation of a uniform grey background
818 between dot pattern presentations. This was repeated six times, over 3900ms, corresponding to
819 two fMRI volume acquisitions (TRs), before the numerosity changed. On 10% of numerosity
820 presentations, the dots were shown in white instead of black. Participants were instructed to
821 press a button when white dots were shown to ensure they were paying attention to the stimulus
822 during the fMRI acquisition and responded to 90-100% of white dot presentations within each
823 functional run. No numerosity judgements were required. Main stimuli in the small numerosity
824 range consisted of 1 to 7 dots, with 20 dots as the baseline, while large numerosities consisted
825 of 1 to 64 dots and a baseline of 512 dots. To test neural populations responses to larger
826 numerosities, a third numerosity range consisted of only large numerosities from 8 to 64 dots
827 and a baseline line of 512 dots was introduced, namely, the large-control range (Supplementary
828 Fig. 1a). The main numerosity stimuli were first presented in ascending order, followed by a
829 longer period (15.6 seconds) where presented with the baseline stimuli (20 or 512 dots in the
830 small or large range respectively), then followed by the main numerosities in descending order,
831 followed by another identical baseline period. This sequence was repeated four times (4 cycles)
832 for each functional run. The long baseline period had a similar function to the blank periods
833 used in visual field mapping stimuli in population receptive field experiments (Dumoulin &
834 Wandell, 2008). During this period, little neural response was expected from numerosity-
835 selective neurons preferring the main numerosities of interest, as such a relatively large
836 numerosity should be well outside of the numerosity range that elicits strong responses. This
837 long period also allows hemodynamic responses to return to baseline between blocks of
838 changing numerosity.



839

840 **Figure 2.5. Illustration of stimuli and experimental design.** (A) A full example stimulus as
 841 seen by the participants in the scanner. The dot pattern covered the central 4° (visual angle)
 842 diameter within an 10.2° diameter mean-luminance (grey) field. A large, thin, red fixation cross
 843 passes diagonally through the center of the display, and through the center of the dot pattern.
 844 Participants fixated at the intersection of the cross. (B) Example numerosity stimuli, where the
 845 total surface area of the dot pattern is constant across numerosities. c The sequence of the
 846 numerosity stimuli presented to the participants at the small and large ranges, respectively.

847

848 *MRI acquisition and preprocessing*

849 Anatomical MRI data were acquired from a Philips 7T scanner (Philips Medical Systems, Best,
 850 NL). MP2RAGE T1 anatomical MRI data were acquired at the spatial resolution of 0.64 x 0.64
 851 x 0.64 mm³ (resampled to 1 x 1 x 1 mm³ for the follow-up processing), repetition time (TR)
 852 was 6.2 ms, echo time (TE) was 3 ms, and flip angle was 5/7 degrees. Functional T2*-weighted
 853 multi-band (factor=2) 2D echo planar images (EPI) were acquired on a Philips 7T scanner
 854 using a 32 channel head coil (Philips Nova Medical) at a resolution of 1.75 x 1.75 x 1.75 mm³,
 855 with a full-brain-coverage field of view (FOV=106 x 112 x 236) covering 64 slices. TR was
 856 1950ms, TE was 25ms, and flip angle was 70 degrees. Functional runs were each 182 time
 857 frames (354.9 seconds) in duration, of which the first six time frames (11.7 seconds) were
 858 discarded to ensure the signal was at a steady state. Within each session eight functional runs
 859 were acquired with the small and large numerosity ranges interleaved to avoid adaptation. Each
 860 participant was scanned for two sessions on separate days. In addition, we collected eight
 861 functional runs on seven of our participants with the large-control range.

862 T1 anatomical scans were automatically segmented using CBS tools (www.nitrc.org)
863 and then manually edited to minimize segmentation errors using ITK-SNAP(Yushkevich et al.,
864 2006) (www.itksnap.org). This provides a highly accurate description of the cortical surface,
865 an anatomical segmentation space used for analysis of cortical organization. The cortical
866 surface was reconstructed at the grey-white matter border and rendered as a smoothed 3D
867 surface. Head movement and motion artefacts between and within functional scans were
868 measured and corrected for in AFNI(Cox, 1996). Motion-corrected functional data were then
869 averaged and the resulting mean image was co-registered to the segmented anatomy. Individual
870 functional images were then co-registered to the same anatomical space using the same
871 transformation.

872

873 *fMRI data analysis*

874 Functional data analysis was performed in mrVista, which is freely available at
875 (<https://github.com/vistalab/vistasoft>). First, data from separate sessions was imported into the
876 same anatomical space for each participant. Functional runs (n = 8) collected for the same
877 condition (small or large range) were averaged to produce a dataset with strong signal strength.
878 Second, the averaged functional dataset was collapsed onto the nearest point on the cortical
879 surface across depth to further increase on signal strength, which generated a (folded) 2D grey
880 matter surface. Then we performed the canonical numerosity modelling developed to estimate
881 the tuning properties of numerosity-selective neural populations(Dumoulin & Wandell, 2008;
882 B. M. Harvey et al., 2013). Briefly, a one-dimensional neural model defined as a Gaussian
883 function in logarithmic space was adopted. The Gaussian function characterized by a set of
884 parameters: preferred numerosity (mean) and tuning width (standard deviation). The model
885 predicts neural responses by taking the presented numerosity at each time point and evaluating
886 the Gaussian function's amplitude at this numerosity. Then convolving these predicted neural
887 response time course with a hemodynamic response function (HRF) to generate predicted fMRI
888 time courses. The predicted fMRI time course with the minimum sum of squared errors (R^2)
889 residuals to the recorded signal was chosen, and the Gaussian function parameters that
890 generated this prediction were used to summarize the recording site's response. The goodness
891 of model fit (R^2 , i.e. variance explained) was thresholded at 30% to select recording sites with
892 clear numerosity selective responses: recording sites with lower variance explained were
893 excluded from further analysis. The modelling procedure allows preferred numerosity
894 estimates outside the range of the presented stimuli, ensuring estimates within the stimulus
895 range are not just the best of a limited set. We excluded from analysis any recording sites where

896 the preferred numerosity was outside the presented range accordingly. Finally, the preferred
897 numerosity data was projected onto the smoothed cortical surface.

898

899 *Definition of region of interest*

900 We defined regions of interest (ROI) where the numerosity-selective neural populations are
901 organized topographically similar to previously reported numerosity maps (Ben M. Harvey &
902 Dumoulin, 2017a). In total, six ROIs were drawn for the right hemisphere in the temporo-
903 occipital cortex, parieto-occipital cortex, parietal cortex, and superior frontal cortex,
904 corresponding to six numerosity maps: NTO, NPO, NPC1, NPC2, NPC3, NF. In each ROI, we
905 defined map borders on the lowest and highest preferred numerosities (white lines) and the
906 map edges around the local increase in model goodness of fit (black lines) (Figure 2.1A-B &
907 Supplementary Figure 2.1B).

908

909 *Correlation analysis between numerosity preferences*

910 Pearson correlation analysis was performed between numerosity preference estimated from the
911 small and large ranges. This included the recording sites that had variance explained above
912 30% in both conditions. Taking into account the functional resolution of the recording sites,
913 the total number of data points (n) used to calculate correlation's probability was reduced by
914 the factor by which functional voxels were up-sampled onto the 2D cortical surface.

915 To quantify the similarity between the numerosity preferences estimated from the two
916 ranges, we calculated the percentage deviation. We calculated the difference of the slopes
917 between the linear fit line of the numerosity preference correlation and the unity line ($y = x$).
918 The percentage deviation of the unity line was set to 0, indicating that the estimates of small
919 and large numerosity preference are equal. The largest possible deviation is indicated by the
920 best fit function of $y = 10.5x - 9.5$, where the estimate of the largest numerosity at small range
921 (i.e. 7) corresponds to the estimate of the largest numerosity at the large range (i.e. 64). The
922 percentage deviation of this best possible fit was set to 1. Thus, for each map, the percentage
923 deviation = $(p-1)/9.5$, where p is the slope of the best fit of the correlation. We performed a
924 Wilcoxon signed rank test (two-tailed) to the percentage deviations of all maps in all
925 participants. A two-way ANOVA was performed to test the statistical difference in the
926 percentage deviations between maps and participants, followed by post hoc analysis with
927 Bonferroni correction for multiple comparisons.

928

929 *Analysis of change of numerosity preferences along maps*

930 For each ROI, we calculated the distance of each recording site to the nearest points on the
931 borders of the map with the lowest and highest numerosity preferences. The ratio between the
932 distances to each border was computed, which gives a normalized distance along the ROI in
933 the primary direction of preferred numerosity change. Then we multiplied this normalized
934 distance by the mean length of the ROI in this direction, which gives a measure of the distance
935 along the ROI for each recording site.

936 We binned the data points within every 2 mm distance interval along each ROI. The
937 mean and standard error of the preferred numerosity of the points within the bin was calculated.
938 We fitted logarithmic functions to bootstrapped samples of the bin means. From these
939 bootstrapped fits we took the median slope and intercept as the best fitting numerosity
940 progression. We determined 95% confidence intervals by plotting all lines generated during
941 bootstrapping iterations and finding the 2.5 and 97.5 percentiles values for these fits. The
942 statistical significance of the slopes was determined with a permutation analysis, where the
943 order of distance bins was randomized (10,000 times). The slopes were fitted at each
944 permutation, and the probability of finding the observed slope by chance was calculated as the
945 number of times where the slope in the randomized permutation was equal to or greater than
946 the observed slope.

947 We normalized the cortical distance of each ROI to visualize the progression of
948 numerosity preference in a similar way. We binned the recording sites within every 10%
949 interval of the normalized cortical distance along each ROI. To visualize the location of neural
950 populations selectively responding to larger numerosities (above 7), we sorted neural
951 populations preferred large numerosities into three subranges (i.e. 7-16; 16-32; 32-64) at each
952 bin. We calculated the proportion of these recording sites among all the selected recording sites
953 in the same bin. The proportions of each subrange at each bin of all maps in all participants
954 were averaged and stacked. Last, we extracted the largest preferred numerosity of each map
955 estimated from the large range and calculated the correlation between these preferred
956 numerosities and the cortical distance of the maps.

957

958 *Analysis of change of tuning width with numerosity preference*

959 In each ROI, we binned data based on preferred numerosities at each range, with numerosity
960 increments of 0.25 between bins. The mean and standard error of each bin were calculated. We
961 fitted linear functions to bootstrapped samples of the bin means. We determined 95%
962 confidence intervals by plotting all lines generated during bootstrapping iterations and finding
963 the 2.5 and 97.5 percentiles values for these fits. Similar permutation analysis, as described

964 above, was used to calculate the probability of finding the observed tuning width change by
965 chance. Unstable fits are common seen in some ROIs where there are little information in the
966 data set to distinguish tuning widths.

967

968 *Cross validation analysis*

969 We cross validated the results by splitting the data into two halves for each condition, based on
970 odd versus even runs, resulting in four half cross validation datasets (i.e. small-odd, small-
971 even, large-odd and large-even). Two types of cross validations were done: within-condition
972 and cross-condition. We selected the recording points from each cross validation datasets based
973 on the criterion that the preferred tuning from 1 to 7, which present at both the small and the
974 large ranges.

975 For the within-condition validation, we extracted the model prediction of the selected
976 voxels from one dataset (e.g. large-odd) and fitted that to the other dataset (e.g. large-even) of
977 the same condition and vice versa, namely the “small → small” and “large → large”
978 validations. This resulted in two iterations of each condition and we calculated the cross-
979 validated variance explained (cvR^2) of each iteration. For the cross-condition validation, we
980 extracted the model prediction from one cross validation dataset (e.g. small-odd) and fitted that
981 to the two datasets of a different condition (e.g. large-odd & large-even), namely the “small →
982 large” and “large → small” validations. This resulted in eight iterations of cross validation by
983 taking the model prediction from each dataset in turn. We then calculated the averaged within-
984 condition and cross-condition cvR^2 across all iterations and across maps and participants. A
985 within-subject repeated measures two-way ANOVA analysis was performed using JASP to
986 compare within- and cross-condition validations (Fig. 2e)(JASP Team, 2020).

987 To validate the results of the large range data, we selected the voxels with the criteria
988 that the preferred tuning fell at the large range and with the cvR^2 larger than 30%. We replicated
989 the main analyses using the cross validation datasets (see Supplementary Fig. 5).

990

991 **Acknowledgments**

992 This research was supported by a China Scholarship Council (CSC) scholarship
993 [201706750008] (Y.C.), a Ammodo KNAW Award (S.O.D), an NWO-VICI grant
994 016.Vici.185.050 (S.O.D) and an NWO-VIDI grant 452-17-012 (B.M.H).

995

996 **Competing interests**

997 The authors declare no competing interests.

998
999
1000
1001
1002
1003
1004
1005
1006
1007
1008
1009
1010
1011
1012
1013
1014
1015
1016
1017
1018
1019
1020
1021
1022
1023
1024
1025
1026
1027
1028
1029
1030
1031

Data availability

The data sets generated during the current study are available from the corresponding author upon reasonable request. Source data of presented figures are provided with this paper.

Code availability

The code that supports the findings of this study is available from the corresponding author upon reasonable request.

1032
1033
1034
1035
1036

1037
1038
1039
1040
1041
1042
1043
1044
1045
1046
1047
1048
1049
1050
1051
1052
1053
1054
1055
1056
1057
1058
1059
1060
1061
1062
1063
1064

Chapter 3

Attention drives human numerosity selective responses

Under review

Acknowledgement of author contributions:

Conceptualization: Y.C., S.H., S.O.D.; Study Design: Y.C., B.M.H, S.O.D.; Data Collection and Analysis: Y.C.; Writing - Original draft: Y.C.; Review & Editing: Y.C., S.H., S.O.D, B.M.H; Supervision: S.H., S.O.D.; Funding Acquisition: Y.C., S.O.D. All authors approved the final version of the manuscript for submission.

Supplementary figures of this chapter can be found in Appendix B.

1065 **Abstract**

1066 Numerosity, the set size of a group of items, helps guide behaviour and decisions. Previous
1067 studies have shown that neural populations respond selectively to numerosities. How
1068 numerosity is extracted from the visual scene is a longstanding debate, often contrasting low-
1069 level visual with high-level cognitive processes. Here, we investigate how attention influences
1070 numerosity selective responses. The stimuli consisted of black and white dots within the same
1071 display. Participants' attention was focused on either black or white dots, while we
1072 systematically changed the numerosity of black, white and total dots. Using 7T fMRI, we show
1073 that the numerosity-tuned neural populations respond only when attention is focused on their
1074 preferred numerosity, irrespective of the unattended or total numerosities. Without attention,
1075 responses to preferred numerosity were inhibited. Unlike traditional effects of attention in the
1076 visual cortex where attention enhances already existing responses, these results suggest that
1077 attention is required to drive numerosity selective responses.

1078

1079

1080 **Keywords**

1081 numerosity-selective response, inhibition, feature-based attention, feature-similarity, attention
1082 field model

1083

1084

1085

1086

1087

1088

1089

1090

1091

1092

1093

1094

1095

1096

1097

1098

1099 **Introduction**

1100 Perception of numerosity, i.e. the set size of a group of items, guides human and animals'
1101 behaviour and decisions (Brannon & Terrace, 1998; S. Dehaene, 2001; Andreas Nieder, 2020a;
1102 Andreas Nieder & Dehaene, 2009). Behaviour often requires numerosity perception, for
1103 example choosing the bag or tree with the most fruits when shopping or foraging.
1104 Neurophysiological experiments have described neurons tuned to numerosity, responding
1105 maximally when a specific numerosity is displayed, with responses decreasing with distance
1106 increases from this preferred numerosity, in non-human primates (A. Nieder & Merten, 2007;
1107 Andreas Nieder et al., 2002a), crows (Ditz & Nieder, 2015, 2016a) and humans (Kutter et al.,
1108 2018). Functional magnetic resonance imaging (fMRI) experiments also revealed responses to
1109 numerosity comparison tasks (A. S. Dehaene et al., 2016) and later to specific numerosities
1110 (Eger et al., 2009; Piazza et al., 2004). We have since used population receptive field (pRF)
1111 modelling (Dumoulin & Wandell, 2008) to show these responses to specific numerosities
1112 reflect neural populations tuning for different numerosities in each fMRI recording site (B. M.
1113 Harvey et al., 2013). These neural populations are organized in topographic maps where
1114 preferred numerosity changes gradually across the cortical surface. A network of topographic
1115 numerosity maps is found throughout the human brain (Cai, Hofstetter, van Dijk, et al., 2021a;
1116 Ben M. Harvey & Dumoulin, 2017a; Hofstetter et al., 2021; Tsouli, Cai, et al., 2021).

1117 There is a longstanding debate on how numerosity is extracted from the visual scene.
1118 While some have proposed that numerosity perception follows non-numerical image features
1119 such as area and density that are often correlated with numerosity (Steven C. Dakin, Tibber,
1120 Greenwood, Kingdom, & Morgan, 2011; Durgin, 2008; Gebuis, Gevers, & Cohen Kadosh,
1121 2014), growing convergent research indicates numerosity itself is perceived directly by humans
1122 and represented in the brain akin to other visual features such as colour and motion (D. Burr &
1123 Ross, 2008). This evidence is provided from psychophysical (Cicchini, Anobile, & Burr, 2016;
1124 DeWind, Adams, Platt, & Brannon, 2015), neuroimaging (DeWind, Park, Woldorff, &
1125 Brannon, 2019; Ben M. Harvey & Dumoulin, 2017b, 2018; Park, Dewind, Woldorff, &
1126 Brannon, 2016) and computational (Kim et al., 2021; Stoianov & Zorzi, 2012; Zorzi & Testolin,
1127 2018) approaches. Numerosity may be estimated from early visual representations, such as
1128 spatial frequency domain image representations (Steven C. Dakin et al., 2011; Paul, van
1129 Ackooij, ten Cate, & Harvey, 2021). Such estimation of numerosity may also underlie the
1130 similarity of numerosity to low-level visual properties like position, orientation and spatial
1131 frequency in aspects of its perception (e.g., adaptation (D. Burr & Ross, 2008)) and neural
1132 representation (e.g., neural tuning and topographic mapping (Tsouli, Harvey, et al., 2021)).

1133 Despite the potentially low-level estimation of numerosity by the visual system, higher-level
1134 processes are clearly involved in numerosity perception, such as for example grouping
1135 (Maldonado Moscoso, Castaldi, Burr, Arrighi, & Anobile, 2020; Pan, Yang, Li, Zhang, & Cui,
1136 2021), connectedness (L. He, Zhou, Zhou, He, & Chen, 2015; Kirjakovski & Matsumoto,
1137 2016), multisensory integration (Anobile, Arrighi, Togoli, & Burr, 2016a; Andreas Nieder,
1138 2012) and attention (Anobile, Stievano, & Burr, 2013; Ansari, Lyons, Van Eimeren, & Xu,
1139 2007; D. C. Burr et al., 2010).

1140 Behavioural studies investigating the role attention plays in numerosity processing have
1141 provided mixed results, and whether and to what extent attention modulates neural responses
1142 to numerosity remain unknown. Numerosity perception has been argued to be pre-attentive, i.e.
1143 numerosity is perceived spontaneously even when participants are not involved in a numerosity
1144 task and when their focus of attention is not directed towards the stimulus (Hesse et al., 2017).
1145 On one hand, enumerating small number of objects up to 4 items, i.e. subitizing, shows fast
1146 and error-free behavioural results, and has therefore traditionally been assumed to be pre-
1147 attentive (Trick & Pylyshyn, 1993, 1994). On the other hand, attention is needed in numerosity
1148 processing, even in the subitizing range. It has been demonstrated that subitizing required
1149 attentional processes by using an inattentional blindness paradigm (Railo, Koivisto, Revonsuo,
1150 & Hannula, 2008). This view was supported by recent studies using cross-sensory dual tasks
1151 and documented that subitizing and mapping numerosity onto space are attentional-demanding
1152 (Anobile, Cicchini, & Burr, 2012; Anobile, Turi, et al., 2012). Even more attentional resources
1153 are needed for subitizing than in the estimation range, i.e. for a smaller than a larger number of
1154 items (D. C. Burr et al., 2010; Pomè, Anobile, Cicchini, Scabia, et al., 2019).

1155 Here we ask how neural responses, specifically in neural populations tuned to
1156 numerosity, are affected by attention. In the visual cortex, neural responses reflect both
1157 stimulus-driven responses and attentional modulation (Carrasco, 2011; Reynolds & Chelazzi,
1158 2004; Ungerleider, 2000). Typically, the attentional modulation is conceptualized as a gain
1159 factor that modulates neural responses (Maunsell & Treue, 2006; McAdams & Maunsell,
1160 1999a; Reynolds & Heeger, 2009). In neural mechanisms of numerosity perception, the
1161 balance between stimulus-driven responses and attentional modulation is unclear. Some studies
1162 have explicitly used tasks (e.g. a delayed match-to-numerosity task) manipulating attention
1163 towards the numerosity of presented stimulus (Ditz & Nieder, 2016b; A. Nieder & Merten,
1164 2007; Andreas Nieder et al., 2002a). Others observed similar responses in the absence of an
1165 explicit numerosity task (e.g. a color discrimination task), and speculatively, in the absence of
1166 attention to the numerosity per se (Cai, Hofstetter, van Dijk, et al., 2021a; B. M. Harvey et al.,

1167 2013; Ben M. Harvey & Dumoulin, 2017a; Hofstetter et al., 2021; Hofstetter & Dumoulin,
1168 2021; Tsouli, Cai, et al., 2021; Viswanathan & Nieder, 2013). However, all of these studies
1169 displayed only one set of items, and so do not require attention to be focused on some items
1170 but not others.

1171 Here we determined how established numerosity selective responses change when the
1172 participant pays attention to different subsets of items within the display. We recorded blood
1173 oxygen level dependent (BOLD) signals using ultra-high field (i.e. 7 Tesla) fMRI (Cai,
1174 Hofstetter, van der Zwaag, Zuiderbaan, & Dumoulin, 2021) in three consecutive experiments
1175 and analysed these responses using neural model-based analyses (Dumoulin & Wandell, 2008).

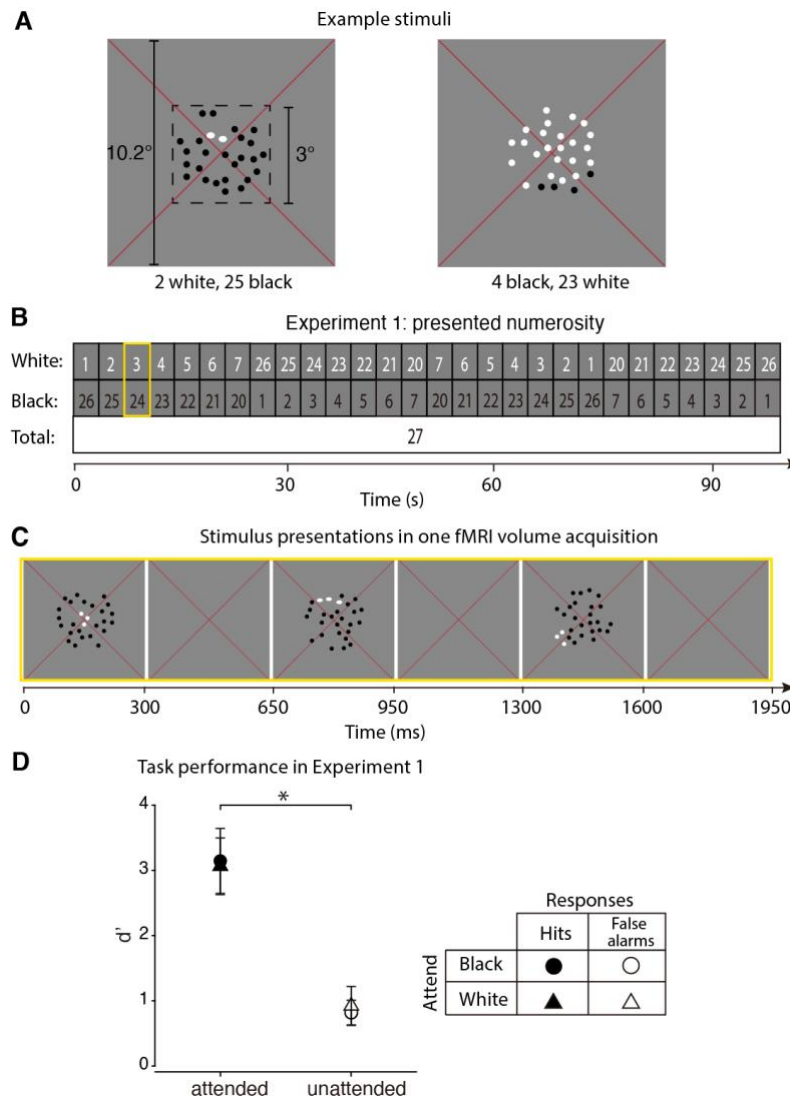
1176

1177 **Results**

1178 *Behavioural tasks modulate attention*

1179 In Experiment 1, we presented a stimulus consisting of black and white dots of a fixed total
1180 numerosity (Figure 3.1A) while systematically varying the ratio of the two subsets (Figure
1181 3.1B,C), and instructed participants to pay attention to (the shape of) one or the other subset.
1182 No numerosity judgements on either dot subset were required (Figure 3.1A,C), and the same
1183 stimulus was presented regardless of which subset was attended. Participants were told which
1184 dot subset they should attend and perform the shape detection task on with a verbal instruction
1185 ('attend black' or 'attend white') through the scanner's intercom. The participants responded
1186 with a button press when the attended dot subset changed from circular to oval. The aspect
1187 ratio of the ovals was adjusted so that difficulty was equated between participants
1188 (Supplementary Table 3.1).

1189 To evaluate the task performance, we computed the discriminability index (d') (Figure
1190 3.1D). We found significantly higher d' values for the attended than the unattended dot subset
1191 in both the 'attend black' and 'attend white' conditions in Experiment 1 (Paired t -test, $t_{ab} =$
1192 22.6 , $p_{ab} = 8.2 \times 10^{-21}$; $t_{aw} = 19.3$, $p_{aw} = 8.5 \times 10^{-19}$). Based on participant reports, we assume the
1193 d' above zero for the unattended dot subset is primarily driven by accidental hits when
1194 responding to the attended dot subset, namely false alarms. These results show that participants
1195 were paying attention to the cued dot subset during scanning (see Supplementary Table 3.1 for
1196 task performance of individual participants).



1197

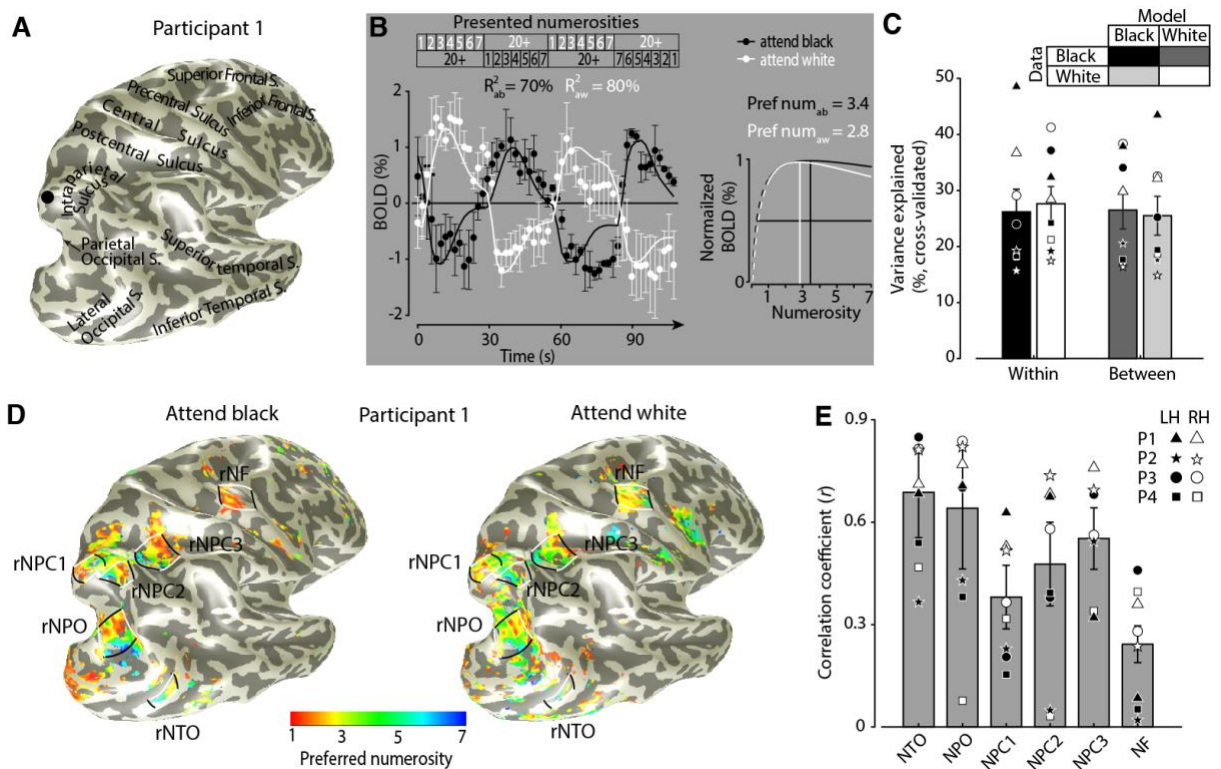
1198 **Figure 3.1. Stimuli, study design and task performance in Experiment 1.** (A) Two example
 1199 stimuli. A large, thin red fixation cross passed diagonally through the centre of the display. The
 1200 dot pattern consisting of a black dot subset and a white dot subset covered the central 3°
 1201 (diameter) of the visual field on a grey screen with 10.2° vertical extent. In 20% (each dot
 1202 subset accounts for 10%) of the stimulus presentations the dots were shown as ovals instead of
 1203 circles, like the white dots in the left panel. (B) Numerosity stimulus sequence: while the white
 1204 dot subset systematically increased from 1 to 7, the black dot subset systematically decreased
 1205 from 26 to 20. So the overall numerosity presented was always 27. This sequence repeated
 1206 with colour switched and then continued with the smaller subset decreasing and the larger
 1207 subset increasing. (C) Presentations of an example numerosity stimulus (yellow box in B)
 1208 within one fMRI volume acquisition (TR = 1950 ms). Participants were verbally instructed to
 1209 attend either the black or white dot subset and perform the shape detection task on the attended
 1210 subset. (D) Behavioural performance evaluated as discriminability indices (d') in the ‘attend

1211 black' (circles) and 'attend white' (triangles) conditions. Filled markers denote detection
 1212 performance on the attended subset, i.e. hits, and open markers on the unattended subset, i.e.
 1213 false alarms. *, $p < 0.00001$ by paired t -test.

1214

1215 *Numerosity responses follow the numerosity of the attended set*

1216 To illustrate the attentional modulation of numerosity-tuned responses, we extracted the fMRI
 1217 response time courses elicited by the 'attend black' and 'attend white' condition of an example
 1218 recording site in the superior parietal lobule at the right hemisphere of one participant (Figure
 1219 3.2A, black point). In Experiment 1, 27 dots were constantly displayed. However, we found
 1220 these two time courses (Figure 3.2B, left panel) show opposite neural response patterns, with
 1221 the peak response occurring after the presentation of low numerosities in the attended set in
 1222 each condition. The difference in response indicates the underlying neural populations are
 1223 modulated by the attentional task which requires focus on a specific subset of dots presented
 1224 on the screen. The numerosity pRF model was fit using only the numerosity of the attended set,
 1225 and its predictions captured most of the response variance ($R^2 > 70\%$) in these time courses
 1226 (Figure 3.2B, left panel). The pRF models give similar preferred numerosity estimates in both
 1227 conditions (Figure 3.2B, right panel). This result suggests that numerosity responses follow the
 1228 numerosity of the attended set.



1229

1230 **Figure 3.2. Modulation of numerosity selective neural responses by attention.** (A)
1231 Anatomical rendering of the right cerebral cortex of one participant. Black point indicates the
1232 cortical location in the superior parietal lobule from which we selected an example recording
1233 site. (B) Two fMRI response time courses from this recording site, elicited by the ‘attend black’
1234 and ‘attend white’ conditions, respectively. Left panel: the time courses show very different
1235 response patterns to the identical stimulus presentations (top). The responses follow the
1236 numerosity of the attended set. Points represent mean response amplitudes over repeated
1237 measurements. The pRF models tuned to the attended set’s numerosity predict these responses
1238 well (black and white lines, R^2 denotes variance explained). Right panel: neural tuning models
1239 that best predict these time courses. This recording site preferred similar numerosities (Pref
1240 num), irrespective of the attention condition. (C) Cross-validated variance explained by the
1241 models in the numerosity maps, evaluated within and between attention conditions. Bars show
1242 the mean variance explained across hemispheres, shapes indicate each individual participant
1243 and hemisphere. (D) A similar network of numerosity maps at both hemispheres derived from
1244 the two attention conditions. Maps show numerosity preferences estimated from responses to
1245 numerosities of the attended set at those recording sites with $R^2 > 30\%$. White lines denote
1246 maps borders following the lowest and highest preferred numerosities seen in each map. Black
1247 lines outline the other borders of each map. (E) Preferred numerosity estimates derived from
1248 the two conditions were well correlated. Bars show mean Pearson correlation coefficients
1249 across participants. In all panels, error bars represent standard errors of the mean.

1250

1251 We split the data into two halves and performed cross validation analyses using within-
1252 and between-condition validations. The model parameters determined from one data half
1253 closely predicted the responses to the attended numerosity in the other half well, regardless of
1254 which dot subset was attended (Figure 3.2C). Repeated measures ANOVA analysis shows no
1255 significant difference in model fits among all the cross validation combinations ($p > 0.025$,
1256 two-sided, Bonferroni corrected for multiple comparisons). Therefore numerosity-tuned
1257 responses followed the numerosity of the attended set similarly, and did not depend which dot
1258 subset was attended.

1259 As previously shown (Cai, Hofstetter, van Dijk, et al., 2021a; B. M. Harvey et al., 2013;
1260 Ben M. Harvey & Dumoulin, 2017a; Hofstetter et al., 2021; Tsouli, Cai, et al., 2021), we found
1261 the numerosity-tuned neural populations were organized in a network of topographic
1262 numerosity maps (Figure 3.2D, Supplementary Figure 3.1). Within each map, the neural
1263 preferred numerosity varied gradually across the cortical surface. For example, in a map in the

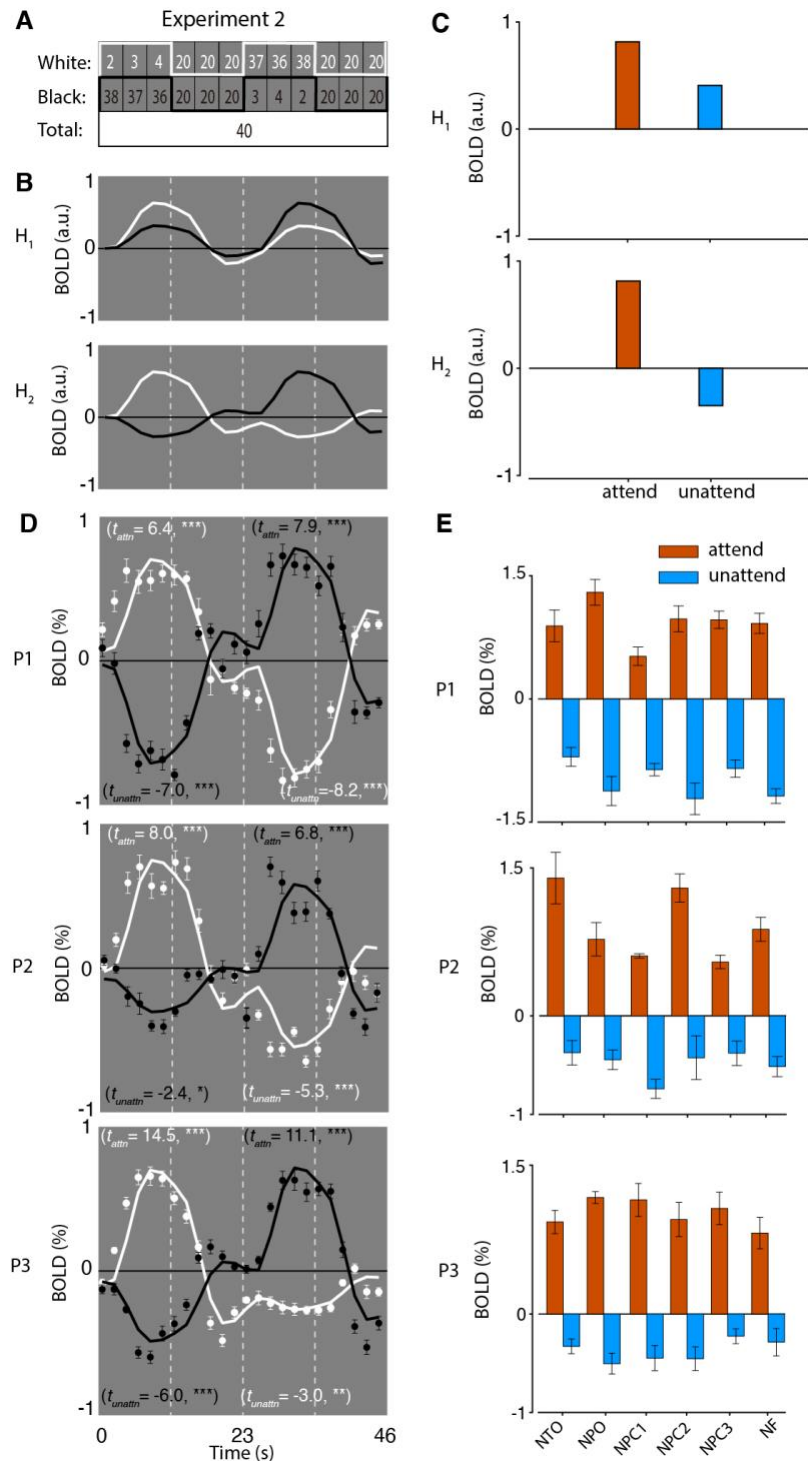
1264 superior parietal cortex (NPC1), numerosity preference increased systematically from medial
1265 to lateral (white lines in Figure 3.2D). The numerosity maps derived from the two attention
1266 conditions were very similar, indicating the preferred numerosities of the neural populations
1267 they contain were independent of which dot subset was attended. To quantify the similarity
1268 between the pRF estimates derived from the two attention conditions, we performed a Pearson
1269 correlation analysis. The preferred numerosity estimates within the maps from the two
1270 conditions were repeatably positively correlated (two-sided Wilcoxon signed rank test of
1271 correlation coefficients, $z = 5.97$, $p = 2.4 \times 10^{-9}$, $df = 47$), indicating a similar spatial distribution
1272 numerosity preferences of the neural populations on the cortical surface (Figure 3.2E).

1273

1274 *No stimulus-driven response of the preferred but unattended numerosities*

1275 In Experiment 1, we established that neural responses are dominated by the numerosity in the
1276 attended set. However, Experiment 1 does not reveal what the neural responses to the
1277 unattended set are. For example, the unattended set may elicit smaller responses, no response,
1278 or may even suppress the response. Thus, in Experiments 2, we used a 2 x 2 block design to
1279 establish the response amplitude to the preferred, but unattended numerosities.

1280 In Experiment 2, we focussed on neural populations preferring the numerosities of 2 to
1281 4 in the numerosity maps (see ROI definition in the Methods section). The dot subset with the
1282 preferred numerosities consisting of 2/3/4 dots were presented at the 1st block and 3rd block,
1283 while being attended and unattended (Figure 3.3A). The total numerosity was fixed at 40. We
1284 predicted the response time courses (Figure 3.3B) and response amplitudes (Figure 3.3C)
1285 according to two hypotheses. In Hypothesis 1, the neural populations respond to the preferred
1286 but unattended numerosities, but to a smaller degree than to the preferred and attended
1287 numerosities. In other words, the neural responses follow the preferred numerosity. This
1288 hypothesis follows visual cortical responses where attention boosts responses, but without
1289 attention there is still a stimulus-driven response (O'Craven, Rosen, Kwong, Treisman, &
1290 Savoy, 1997). In Hypothesis 2, there is no response to the preferred numerosities in the absence
1291 of attention, namely the neural responses follow the attended numerosity. Note that Hypothesis
1292 2 predicts a decrease in response amplitude during the block of the preferred but unattended
1293 numerosities. This decrease is driven by the higher numerosities in the attended set (36/37/38)
1294 which are further away from the preferred numerosities (2/3/4) than the baseline numerosity
1295 (20) is.



1296

1297 **Figure 3.3. Study design, hypotheses and responses in Experiment 2.** (A) Experimental
 1298 design. Stimuli consisted of a subset of 2/3/4 dots in one color and another subset of 38/37/36
 1299 dots in the opposite color, or two equal subsets of 20 black and 20 white dots, presented
 1300 simultaneously. The preferred numerosities of 2 to 4 were either in the attended or unattended
 1301 set of black or white dots. (B) Hypothesized numerosity responses under attentional
 1302 modulation in the two conditions. Hypothesis 1 (H_1) is that neural responses follow preferred
 1303 numerosities. Stronger responses occur when preferred numerosities (2/3/4) are in the attended

1304 set than when they are in the unattended set in a given condition. Hypothesis 2 (H₂) is that
1305 neural responses follow the attended numerosity only. Increased responses occur when
1306 preferred numerosities are in the attended set, while no response or decreased responses occur
1307 when they are in the unattended set. Black and white lines indicate the ‘attend black’ and
1308 ‘attend white’ conditions, respectively. (C) Predicted response amplitudes of preferred
1309 numerosities in the attended set (red) and unattended set (blue) following H₁ (top) and H₂
1310 (lower). (D) Measured response time courses and general linear model (GLM) predictions.
1311 Compared to the baseline of 20 dots in both subsets, increased responses occurred when
1312 preferred numerosities were in the attended set, while decreased responses occurred when they
1313 were in the unattended set. Points represent mean response amplitudes over repeated
1314 measurements. Solid lines show the GLM predictions. *T* values demonstrate statistically
1315 significant difference in response amplitudes between conditions where preferred numerosities
1316 were in the attended (t_{attn}) or unattended set (t_{unattn}), compared to the baseline, in a given
1317 condition. *, $p < 0.05$; **, $p < 0.01$; ***, $p < 0.0001$. (E) Averaged response amplitudes when
1318 the preferred numerosities were in the attended (red) and unattended (blue) sets across both
1319 conditions at individual maps. In all panels error bars represent standard error of the mean.

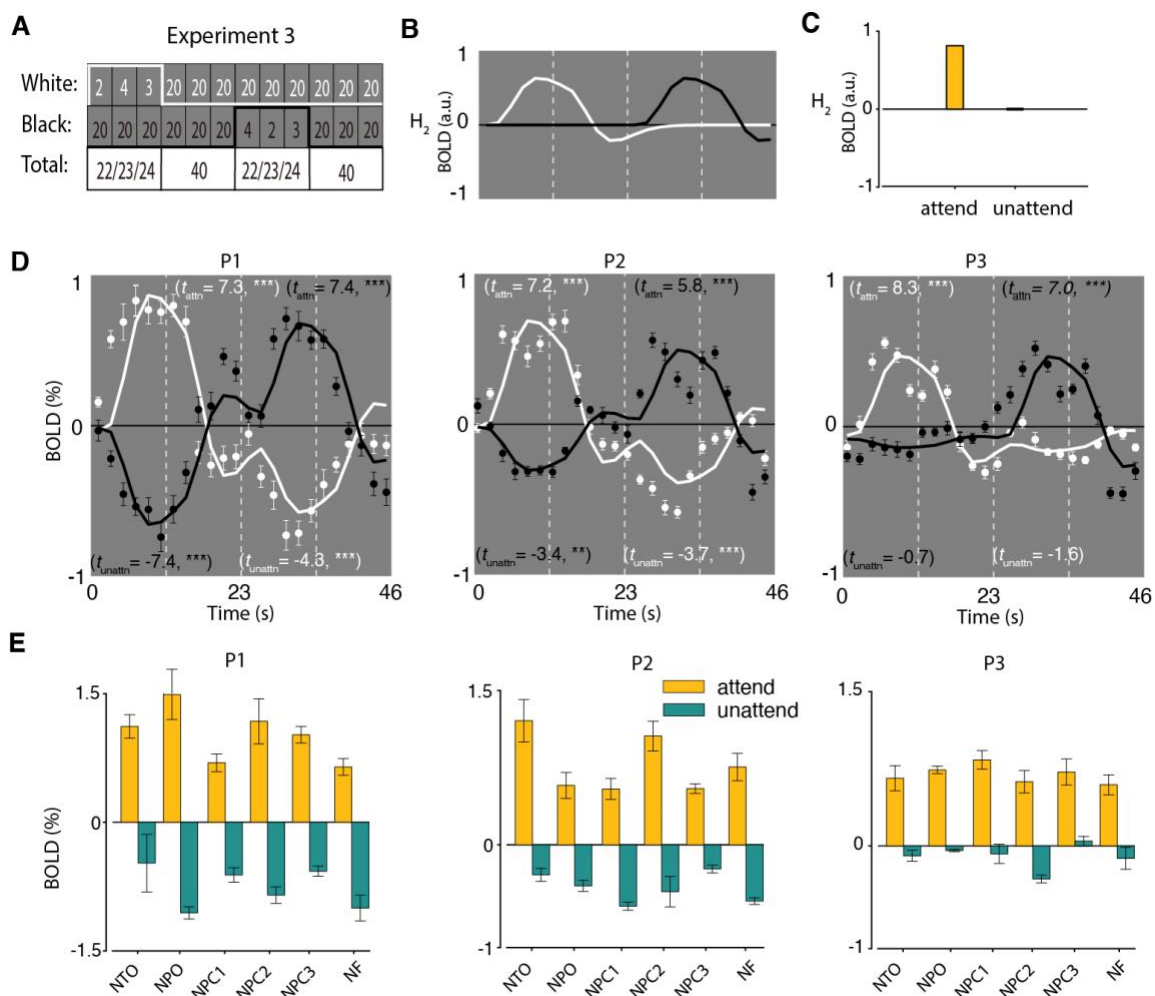
1320

1321 We extracted and averaged the time courses of the voxels within all the numerosity
1322 maps that had the preferred numerosities of 2 to 4 (defined from Experiment 1). General linear
1323 models (GLM) were fitted to these time courses (Figure 3.3D). *T*-tests demonstrated significant
1324 different responses between the conditions where the preferred numerosities were in the
1325 attended or unattended sets (compared to the baseline of 20 dots in both subsets) (Figure 3.3D).
1326 Response amplitudes of preferred numerosities in the attended set and unattended set were
1327 computed for individual maps (Figure 3.3E). In line with the ROI definition, increased response
1328 amplitudes were seen when participants attended the dot subsets with the preferred
1329 numerosities. Furthermore, in line with Hypothesis 2, decreased response amplitudes were seen
1330 when the preferred numerosities (2/3/4) were in the unattended set. We then performed a
1331 repeated measures ANOVA analysis on the response amplitudes, followed by post hoc
1332 analyses with Bonferroni correction for multiple comparisons. The main effect for attention
1333 was statistically significant ($F_{(1, 2)} = 81.577, p = 0.012$), while the main effect for maps ($F_{(5, 10)}$
1334 $= 1.140, p = 0.400$) and the interaction between attention and maps ($F_{(5, 10)} = 0.877, p = 0.530$)
1335 did not reach a significant level. Therefore, there appears to be no stimulus-driven response to
1336 the preferred but unattended numerosities.

1337

1338 *Suppression of preferred but unattended numerosities*

1339 In Experiment 2 the overall numerosities were kept constant while the non-preferred
 1340 numerosity varied. Therefore, it is not clear to what extent the decreased responses were
 1341 induced by the non-preferred numerosities (38/37/36) in the attended set, or by the preferred
 1342 numerosities (2/3/4) in the unattended set. Decrease in response may be explained by the
 1343 numerosities of the attended set alone: a lower response would be expected because 36/37/38
 1344 is further away from the preferred numerosity than 20 is. Alternatively, the decrease in response
 1345 could be due to the presentation of the preferred, but unattended numerosities. Therefore, in
 1346 Experiment 3 only one non-preferred numerosity was shown, and as a result the total
 1347 numerosity varied while the non-preferred numerosity in the attended set was fixed at 20
 1348 (Figure 3.4A). Following Hypothesis 2, which suggests neural responses follow the
 1349 numerosity of the attended set, we predict no increased response when the preferred
 1350 numerosities are in the unattended set in Experiment 3 (Figure 3.4B, C).



1351
 1352 **Figure 3.4. Suppressive neural population responses modulated by preferred but**
 1353 **unattended numerosities.** (A) Study design of Experiment 3. A subset of 2/3/4 dots was either

1354 attended or unattended while keeping the non-preferred numerosity constantly at 20 dots in
1355 another subset, regardless of attended or unattended. (B) Predicted responses following
1356 Hypothesis 2: neural responses follow the numerosity in the attended set, thus no response to
1357 the preferred but unattended numerosity is expected. (C) Predicted response amplitudes when
1358 the preferred numerosities are in the attended set (yellow) and unattended (green) set. (D)
1359 Measured response time courses and GLM predictions. Compared to the baseline of 20 dots in
1360 both subsets, increased responses occurred when preferred numerosities are in the attended set,
1361 while decreased responses occurred when they are in the unattended set. Black and white
1362 symbols indicate the ‘attend black’ and ‘attend white’ conditions, respectively. Points represent
1363 mean response amplitudes over repeated measurements. Solid lines represent the GLM
1364 predictions. *T* values demonstrate statistical difference in response amplitudes between
1365 conditions where preferred numerosities were in the attended (t_{attn}) or unattended set (t_{unattn}),
1366 compared to the baseline, in a given condition. *, $p < 0.05$; **, $p < 0.01$; ***, $p < 0.0001$. (E)
1367 Averaged response amplitudes when the preferred numerosities were in the attended set
1368 (yellow) and unattended (green) set across both conditions at individual maps. In all panels
1369 error bars represent standard error of the mean.

1370

1371 In line with the definition of the ROI and Experiment 2, the neural population showed
1372 increased responses when the preferred numerosities were in the attended set. However, they
1373 still revealed decreased responses when the preferred numerosities were in the unattended set,
1374 compared to the baseline. This result is not only visible in the response time series (Figure
1375 3.4D) but also in statistical comparisons of response amplitudes in individual maps (Figure
1376 3.4E). Repeated measures ANOVA analysis was performed on the response amplitudes,
1377 followed by post hoc analyses with Bonferroni correction for multiple comparisons. Analogous
1378 to the results of Experiment 2, the main effect for attention was statistically significant ($F_{(1, 2)}$
1379 $= 19.311$, $p = 0.048$), while the main effect for maps ($F_{(5, 10)} = 1.662$, $p = 0.231$) and the
1380 interaction between attention and maps ($F_{(5, 10)} = 1.065$, $p = 0.434$) did not reach a significant
1381 level. This result does not support Hypothesis 2’s prediction that the neural response only
1382 follows the attended set’s numerosity, and will therefore remain at baseline during the
1383 unattended blocks. The decreased responses induced when the preferred numerosities were in
1384 the unattended set suggest that, in the absence of attention, the preferred numerosities actively
1385 suppress the neural population responses.

1386

1387 **Discussion**

1388 Here we studied how attention affects numerosity-tuned neural responses. In three experiments
1389 we changed the numerosity of black and white dot subsets within the same display, while
1390 participants performed an attention-demanding, non-numerical task on either the black or white
1391 dot subset. In Experiment 1, we analysed responses to these stimuli using pRF models tuned
1392 to the numerosity of the attended set, and found that numerosity-tuned neural responses
1393 followed the numerosity of the attended set. In Experiments 2 and 3 we investigated the
1394 responses to the unattended set. We did not observe any stimulus-driven response without
1395 attention and even observed suppression of responses by the preferred numerosities when
1396 unattended. Therefore, we propose that attention drives numerosity selective responses even
1397 when non-numerical features are attended, with the non-attended sets producing inhibitory
1398 responses in neural populations that would otherwise prefer the numerosities of the non-
1399 attended sets.

1400 Our results suggest that attention drives numerosity responses. Importantly, attention
1401 was directed to one subset of the dot pattern using a shape-task and no numerosity judgement
1402 was required. In line with these observations, in animals, neural responses to numerosity are
1403 typically measured while animals are performing numerosity comparison tasks that they have
1404 been thoroughly trained in (Ditz & Nieder, 2015; A. Nieder & Merten, 2007; Andreas Nieder
1405 et al., 2002a). These tasks require attention to both the dot set and its numerosity. Similar
1406 responses were observed in untrained animals that paid attention to the dot color but paid
1407 attention to the dot pattern nevertheless (Viswanathan & Nieder, 2013). Likewise, our previous
1408 studies directed attention towards the stimulus using a dot-color task (Cai, Hofstetter, van Dijk,
1409 et al., 2021a; B. M. Harvey et al., 2013; Ben M. Harvey & Dumoulin, 2017a; Hofstetter et al.,
1410 2021; Hofstetter & Dumoulin, 2021; Tsouli, Cai, et al., 2021). Thus, in both human and animal
1411 studies that do not require numerosity judgements, the participant pays attention to the dot set
1412 itself. Therefore, it seems that attention to some feature of the stimuli is always involved to
1413 some degree. Our study shows that this focus of attention is essential to numerosity processing.

1414 In the visual cortex, attention enhances stimulus-driven responses of neurons preferring
1415 the attended location or feature (Corbetta, Miezin, Dobmeyer, Shulman, & Petersen, 1990;
1416 Treue & Maunsell, 1996). For example, spatial attention increases responses of neurons with
1417 receptive fields at the attended location (Connor, Preddie, Gallant, & Van Essen, 1997; Moran
1418 & Desimone, 1985); attention to a specific orientation increases the responses of V4 neurons
1419 preferring this orientation (McAdams & Maunsell, 1999a, 1999b); attention to a specific
1420 motion direction increases the responses of MT neurons preferring that direction (Treue &
1421 Martínez Trujillo, 1999). Even which feature within a complex display is attended affects

1422 response amplitudes: in a display with both stationary and moving dots, attention to the moving
1423 dots produces larger response than attention to the stationary dots in the motion-responsive
1424 area MT. Yet, even with attention diverted away, stimulus-driven motion alone still elicits
1425 neural responses albeit to a smaller degree (O'Craven et al., 1997). This appears different from
1426 numerosity responses. Attention appears required for numerosity-selective neural responses,
1427 driving or gating the responses. Thus, unlike responses in the early visual cortex, which happen
1428 whenever the preferred stimulus is shown, both bottom-up and top-down mechanisms appear
1429 necessary to drive numerosity responses. We speculate that this may be because numerosity-
1430 tuned responses emerge at later stages of visual processing, while previously-studied
1431 orientation tuned (McAdams & Maunsell, 1999b, 1999a), motion direction tuned (Treue &
1432 Martínez Trujillo, 1999; Treue & Maunsell, 1996), and spatially tuned (Connor et al., 1997;
1433 Martínez-Trujillo & Treue, 2004) responses are present in the primary visual cortex.

1434 More recent findings further demonstrate that the facilitation of responses when the
1435 attended feature matches the neuron's response preference is accompanied by an inhibition of
1436 responses in neurons with tuning preferences far from the attended feature (Martinez-Trujillo
1437 & Treue, 2004). Martinez-Trujillo and Treue recorded the responses of direction-selective
1438 neurons in macaque area MT while systematically changing the attended direction in a task
1439 outside the neuron's receptive field. Changing from a neuron's preferred to its anti-preferred
1440 direction caused a systematic change of the attentional modulation from an enhancement to a
1441 suppression. This is in line with a feature similarity gain model of attention (Maunsell & Treue,
1442 2006; Treue & Martínez Trujillo, 1999). In the current experiments, we recorded responses in
1443 the neural populations preferring small numerosities (2/3/4) and neural responses were highest
1444 when the numerosity of the attended set also had a small numerosity. When the attended set
1445 had a large numerosity (20/36/37/38), the decreased responses we observed could be attributed
1446 to the dissimilarity between the attended numerosity and the preferred numerosity of the
1447 underlying neural populations. Alternatively, our results might be explained within the
1448 framework of a normalization model of attention (Reynolds & Heeger, 2009), which
1449 incorporates three basic components: the stimulation field, the normalization field and the
1450 attention field. The attention field acts as a gain field and is also suggested to have an inhibitory
1451 surround (Puckett & Deyoe, 2015). If the normalization field operates in the feature space of
1452 numerosity the model is similar to the feature similarity gain model of attention. In both cases,
1453 our results suggest that the attention field has both a facilitatory and an inhibitory component.

1454

1455 Can these results be explained by other features of our stimulus or task, such as attention to a
1456 specific spatial location or shape changes? In our stimulus design, the smaller dot subset with
1457 the preferred numerosities (of the neural populations of interest) was always grouped together,
1458 so this likely to be grouped based on spatial proximity (Anobile, Castaldi, Moscoso, Burr, &
1459 Arrighi, 2020; Maldonado Moscoso et al., 2020; Zhao & Yu, 2016). Numerosity response
1460 seems likely to be enhanced by spatial attention at this location, given that numerosity must
1461 ultimately be derived from early visual image representations (Steven C. Dakin et al., 2011;
1462 Paul et al., 2021). However, we believe the spatial distribution of the two dot subsets is not
1463 sufficient to account for the effect of attention we observed. First, the dot subset with a
1464 preferred numerosity was displayed simultaneously with the other dot subset with a non-
1465 preferred numerosity. Second, the position of the other dot subset was randomized on each
1466 display so no location was associated with any particular numerosity. Finally, the shape of the
1467 dots was changed homogenously within the same dot subset, thus there was no grouping effect
1468 within each dot subset.

1469 To summarize, here we have shown that attention to a group of items strongly
1470 modulates neural responses to its numerosity, even though numerosity itself is not task-relevant
1471 or endogenously attended. We propose that both lower-level and higher-level processes are
1472 required in numerosity perception. On one hand, numerosity is perceived spontaneously even
1473 without an explicit numerical task, including the current study (Cai, Hofstetter, van Dijk, et al.,
1474 2021a; B. M. Harvey et al., 2013; Ben M. Harvey & Dumoulin, 2017a; Hofstetter et al., 2021;
1475 Tsouli, Cai, et al., 2021; Viswanathan & Nieder, 2013). On the other hand, higher-level
1476 cognitive control, such as attention, also plays an important role in processing numerical
1477 information. We live in a complex world in which a single scene may have many different
1478 types of objects with different numerosities. Representing the numerosity of task-relevant
1479 objects while ignoring the numerosity of other objects may therefore be vital to the effective
1480 numerosity perception in natural scenes.

1481

1482 **Methods**

1483 *Participants*

1484 We present data from four participants in three different consecutive experiments (two females,
1485 age range 27 – 32 years). Each experiment replicates and builds on the previous experiment,
1486 thus this study focuses on internal replication and number of trials per participant rather than
1487 number of participants with limited trials (Baker et al., 2020). All the participants had normal
1488 or corrected-to-normal visual acuity. All were well educated, with good mathematical abilities.

1489 Written informed consent was obtained before every MRI session. All experimental procedures
1490 were approved by the ethics committee of VU University Amsterdam.

1491

1492 *Stimuli and experimental design*

1493 Visual stimuli were presented on a 69.84 x 39.29 cm LCD screen (Cambridge Research
1494 Systems) behind the MRI bore. Participants were required to lie still and view the display
1495 through a mirror attached to the head coil. The total distance from the attached mirror to the
1496 display screen was 220 cm. The display resolution was 1920 x 1080 pixels. A button box
1497 recorded behavioural responses. Visual stimuli were generated in Matlab using PsychToolbox
1498 (Kleiner, Brainard, & Pelli, 2007). In all the experiments, a large diagonal cross composed of
1499 thin red lines was displayed consistently across the entire screen, serving as a fixation marker.
1500 The numerosity stimuli consisted of black and white dots presented simultaneously in the
1501 central 3° (diameter) of the visual field. In 10% of the total stimuli presentations, black dots
1502 were shown in ovals instead of circles, and in another 10% of the stimulus presentations, white
1503 dots were shown as ovals. The aspect ratio of the ovals was adjusted in practice runs prior to
1504 scanning so that difficulty was equated between participants (for aspect ratios for each
1505 participant see Supplementary Table 3.1). At the start of each scan run, participants were
1506 verbally instructed which group they should pay attention to through the scanner's intercom
1507 system, using the instructions 'attend black' or 'attend white'. The order of these two
1508 conditions alternated every two runs in each session, and was counterbalanced between
1509 sessions in the same participant. Participants fixated the red cross throughout the experiments,
1510 and pressed a button when they detected a subtle shape change (from circular to oval) of the
1511 group they were instructed to pay attention to. No numerosity judgement was required. Task
1512 performance was quantified using the discriminability index (d') of the signal detection theory,
1513 which denotes participants' sensitivity to the difference between the signal present and signal
1514 absent distributions (Green & Swets, 1966). We determined a response as a hit if it occurred
1515 within 2 seconds after a signal presentation, otherwise it was classified as a false alarm.

1516

1517 *Experiment 1*

1518 In previous studies, the stimulus systematically varied total numerosity (Cai, Hofstetter, van
1519 Dijk, et al., 2021a; B. M. Harvey et al., 2013; Ben M. Harvey & Dumoulin, 2017a; Hofstetter
1520 et al., 2021; Hofstetter & Dumoulin, 2021; Tsouli, Cai, et al., 2021). In Experiment 1, we fixed
1521 the total numerosity (i.e. 27 dots) and systematically varied the ratio of black and white dots.
1522 Specifically, the numerosity stimulus consists of a subset of black dots and another subset of

1523 white dots in the same display. The numerosities of these two sets systematically increased and
1524 decreased to map responses to their numerosities, but the changes of the two subsets were
1525 coordinated so the total numerosity of the whole display remained constant at 27. The dots
1526 were randomly positioned at each presentation so that each dot fell entirely within the stimulus
1527 area and no specific visual position was associated with any numerosity. Individual dots were
1528 distributed roughly homogeneously to avoid perceptual grouping. Dots in the subset with a
1529 smaller set size were presented next to each other (Figure 3.1A).

1530 We used a similar design as was previously used to uncover numerosity maps (Cai,
1531 Hofstetter, van Dijk, et al., 2021a; B. M. Harvey et al., 2013; Ben M. Harvey & Dumoulin,
1532 2017a; Hofstetter et al., 2021; Hofstetter & Dumoulin, 2021; Tsouli, Cai, et al., 2021).
1533 Specifically, the numerosity of the white dot subset increased from 1 to 7, while the black dot
1534 subset decreased from 26 to 20 (Figure 3.1B). Then, the black dot subset increased from 1 to
1535 7, while the white dot subset decreased from 26 to 20. Then, the white dot subset decreased
1536 from 7 to 1, while the black dot subset increased from 20 to 26. Finally, the black dot subset
1537 decreased from 7 to 1, while the white dot subset increased from 20 to 26. This sequence was
1538 repeated three times at each functional run. Participants 1 and 3 were shown with this
1539 presentation sequence, while the other participants were shown with the same sequence but in
1540 the opposite dots color (i.e. first the black dot subset increased from 1 to 7, while the white dot
1541 subset decreased from 26 to 20 accordingly). We analysed the responses to the stimuli focusing
1542 the numerosity of the attended set. For example, when participants attended the white dot
1543 subset (‘attend white’ condition), the numerosity of the attended set first increased from 1 to
1544 7, then decreased from 26 to 20, then decreased from 7 to 1, then increased from 20 to 26. We
1545 have previously shown that most numerosity-tuned neural populations have a numerosity
1546 preference below seven (Cai, Hofstetter, van Dijk, et al., 2021a). When the numerosity of the
1547 attended set was in the 1-7 range, we therefore expected a large response from these neural
1548 populations and a large modulation of the response by the changes in numerosity. When the
1549 numerosity of the attended set was in the 20-26 range, we expected little response from these
1550 neural populations and little modulation of the response as well. Thus, a long period of
1551 attending a dot subset with a large numerosity serves as a baseline period, allowing the
1552 haemodynamic responses to return to baseline.

1553 Each numerosity dot pattern was presented briefly (300 ms) to ensure participants did
1554 not have time to count (Figure 3.1C). A new random pattern was presented every 650 ms, with
1555 a 350 ms presentation of a uniform grey background between dot pattern presentations. This
1556 was repeated three times, over 1950 ms, corresponding to one fMRI volume acquisition (i.e.,

1557 TR). Each numerosity was presented six times, corresponding to 2 TRs, before moving to next
1558 numerosity in the stimulus sequence.

1559

1560 *Experiment 2*

1561 In order to investigate the extent to which numerosity responses were modulated by numerosity
1562 preference and attentional state, we applied a 2 (preferred numerosity vs. non-preferred
1563 numerosity) x 2 (attended vs. unattended) block-design experiment (Fig. 3A). We focused on
1564 the neural populations that had preferred numerosities of 2 to 4, determined from Experiment
1565 1, given that the large proportions of neural populations tuned to these numerosities (Cai,
1566 Hofstetter, van Dijk, et al., 2021a; A. Nieder & Merten, 2007). To maintain a constant total
1567 numerosity of 40 in the stimulus displays, the stimuli consisted of a small subset of 2/3/4 dots
1568 and a large subset of 38/37/36 dots in the opposite color, or two equal-sized subsets of 20 black
1569 dots and 20 white dots.

1570 Each dot pattern was presented similarly to Experiment 1 with 300 ms presentation of
1571 a dot pattern followed by 350 ms presentation of a grey background. This was repeated six
1572 times for each numerosity when the stimuli consisted of variable-sized dot subsets
1573 (presentations of 2+38, 3+37 or 4+36 dots) and 18 times when the stimuli consisted of two
1574 equal-sized subsets (presentations of 20+20 dots). The presentations of the numerosities of
1575 2/3/4 were randomized within the block, yet keeping the total numerosity to 40 dots. The total
1576 surface area of each dot pattern remained constant.

1577 The stimuli were presented in four blocks, each block lasted 11.7 seconds. As in
1578 Experiment 1, participants were informed to which dot subset they should perform a shape
1579 change detection task on by verbal instructions at the start of each scan run. This block-design
1580 stimulus sequence was repeated seven times at each run. This block structure produces robust
1581 BOLD responses, ensuring a sufficient blank period for the hemodynamic responses to return
1582 to baseline between blocks.

1583

1584 *Experiment 3*

1585 In Experiment 2 the non-preferred numerosities varied to match the preferred numerosity so as
1586 to remain the total numerosity constant at 40. Thereby the non-preferred numerosities in the
1587 attended or unattended set also varied. To further understand numerosity responses to preferred
1588 numerosities in the unattended set, in Experiment 3 we fixed the non-preferred numerosity at
1589 20, both in the attended or unattended set. Specifically, we used stimuli that consisted of a
1590 subset of 2/3/4 dots in one color and another subset of 20 dots in the opposite color, or two

1591 equal subsets of 20 black dots and 20 white dots (Fig. 4A). In other words, the non-preferred
1592 numerosity was constant but the total numerosity varied. Stimulus presentations were identical
1593 to Experiment 2.

1594

1595 *MRI acquisition and preprocessing*

1596 MRI data were acquired from a Philips 7 Tesla scanner (Philips Medical Systems, Best,
1597 Netherlands). T1 anatomical data were acquired with an MP2RAGE sequence (Marques et al.,
1598 2010) at the spatial resolution of 0.7 mm³, repetition time (TR) was 6.2 ms, echo time (TE)
1599 was 2.5 ms, and flip angle (FA) was 5 degrees. Functional T2*-weighted two-dimensional echo
1600 planar images (EPI) were acquired using a 32-channel head coil (Philips Nova Medical) with
1601 the following parameters: isotropic resolution of 1.75 mm³, full-brain-coverage field of view
1602 (FOV = 234 x 112 x 184 mm) covering 64 slices, TR/TE = 1950/25 ms, and FA = 70°, multi-
1603 band factor = 2. Each functional run had 174 TRs and lasted 339.3 seconds. Top-up scans that
1604 included the opposite phase-encoding direction were acquired following each functional run.
1605 Each scanning session included eight functional runs. Experiment 1 included two scanning
1606 sessions that were collected on separate days, resulting in eight runs for the ‘attend black’ and
1607 ‘attend white’ conditions, respectively. Three of the participants were scanned for Experiments
1608 2 and 3 on separate days. Each experiment had one session including eight runs. The order of
1609 the two attention conditions was randomised between sessions and participants. One functional
1610 run of the ‘attend black’ condition in Experiment 1 of Participant 3 was excluded due to signal
1611 dropout in the image data.

1612 T1 anatomical scans were resampled to an isotropic resolution of 0.6 mm³ and
1613 preprocessed and automatically segmented grey and white matter using cbs-tools
1614 (<https://www.cbs.mpg.de/institute/software/cbs-hrt>). Segmentation errors were manually
1615 edited using ITK-SNAP (Yushkevich et al., 2006). The cortical surface was reconstructed at
1616 the grey-white matter border and rendered as a smoothed 3D surface. Functional runs were
1617 corrected for head movement and motion using AFNI (Cox, 1996). Image distortions in the
1618 gradient encoding direction were corrected for using the top-up scans (Andersson, Skare, &
1619 Ashburner, 2003). The first six TRs of each functional run were discarded to ensure steady-
1620 state magnetization. Functional runs were registered to the anatomical images using vistasoft
1621 (<https://github.com/vistasoft/wiki>). Functional data were interpolated to the anatomical
1622 segmentation space using trilinear interpolation. Functional runs from separate sessions were
1623 imported to the same T1-weighted anatomical space. The time-series data were then aligned to
1624 the anatomical space and then averaged based on the attention conditions in each experiment,

1625 respectively. Data from all recording sites (voxels) were collapsed and averaged onto the
1626 nearest point on the cortical surface, which generated a (folded) two-dimensional
1627 representation of the grey matter nodes and increased signal strength. The fMRI data were
1628 analysed at this space with pRF modelling (Experiment 1) and GLM analyses (Experiments 2
1629 and 3). No spatial or temporal smoothing was applied to the functional data.

1630

1631 *pRF modelling*

1632 pRF modelling was applied to the fMRI data collected in Experiment 1 in order to characterize
1633 the numerosity tuning of each recording site in the attention conditions (Dumoulin & Wandell,
1634 2008). Briefly, to characterize numerosity tuning, the pRF model describes the averaged tuning
1635 of the underlying neural populations using a one-dimensional logarithmic Gaussian function
1636 (B. M. Harvey et al., 2013). The Gaussian function is characterized by preferred numerosity
1637 (mean of the Gaussian) and tuning width (standard deviation of the Gaussian).

1638 The pRF model is estimated based on the fMRI data and the time course of the
1639 presented numerosities. In Experiment 1 the total presented numerosity was constant (i.e. 27
1640 dots) throughout the time course and so predicts a constant response and explains no response
1641 variance. However, the numerosity of the attended set changed, so the pRF model was fitted to
1642 the attended set's numerosity rather than the total numerosity. For a large group of candidate
1643 preferred numerosities and tuning widths, a predicted neural response time course is calculated
1644 by taking the attended set's numerosity at each time point and evaluating the candidate
1645 Gaussian function's amplitude at each numerosity in the stimulus time course. Each candidate
1646 predicted neural response time course is then convolved with a canonical hemodynamic
1647 response function (HRF) to create a candidate predicted fMRI time course. The predicted fMRI
1648 time course that brings the best agreement to the measured fMRI time course at this recording
1649 site was chosen. Participant-specific HRF parameters were estimated over the whole fMRI
1650 volume and applied to refit the pRF (Ben M. Harvey & Dumoulin, 2011). The Gaussian
1651 function's parameters that generated the best fit fMRI time course were used to characterize
1652 the response at this recording site. The pRF fitting procedure allows preferred numerosity
1653 estimates outside the range of the numerosities in the attended set, ensuring estimates within
1654 the stimulus range are not just the best of a limited set.

1655

1656 *Definition of region of interest*

1657 We rendered the preferred numerosities of the response model from the average of both
1658 attention conditions in Experiment 1 onto the cortical surface. We excluded recording sites

1659 where the preferred numerosity was outside the main attended numerosity range (i.e. 1-7) or
1660 the variance explained by the pRF model was lower than 30% from further analysis. Six ROIs
1661 were drawn on each hemisphere corresponding to the six numerosity maps described in
1662 previous studies (Cai, Hofstetter, van Dijk, et al., 2021a; Ben M. Harvey & Dumoulin, 2017a;
1663 Hofstetter et al., 2021; Tsouli, Cai, et al., 2021): NTO at the temporo-occipital cortex, NPO at
1664 the parietal-occipital cortex, NPC1-3 around the postcentral sulcus of the parietal cortex, and
1665 NF in superior frontal cortex. In each map, we manually defined lines on the lowest and highest
1666 points of preferred numerosity (“end” borders). The edges of the map (“side” borders) were
1667 defined around local regions showing good fits of numerosity-tuned response models.

1668 We extracted voxels within these numerosity maps that had the preferred numerosities
1669 of 2 to 4 and had more than 30% variance explained by the pRF models in both conditions
1670 from Experiment 1, resulting in a new ROI. This ROI was then used for further analysis in
1671 Experiments 2 and 3.

1672

1673 *GLM analysis*

1674 We performed GLM analyses on the fMRI data recorded in Experiments 2 and 3. The timing
1675 of presentations of the preferred numerosities in the attended set and in the unattended set
1676 served as two predictors in the GLM. This was convolved with a two-gamma HRF to account
1677 for the delayed and dispersed blood flow responses (Glover, 1999). Paired *t*-test was performed
1678 to demonstrate the different responses between conditions where preferred numerosities were
1679 in the attended set or in the unattended set, compared to the baseline condition, in a given
1680 condition. Response amplitudes (betas, denoted as percentage BOLD signal change) of
1681 individual maps were computed across hemispheres for individual participants. Repeated
1682 measures ANOVA analysis was performed on the response amplitudes of all participants, with
1683 the factors of attentional states and individual maps. Post-hoc analyse was performed
1684 afterwards with Bonferroni correction for multiple comparisons.

1685

1686 *Correlations of pRF estimates derived from two attention conditions*

1687 Pearson correlation analysis was performed between numerosity preferences estimated from
1688 the ‘attend black’ and ‘attend white’ conditions in Experiment 1. Taking into account the
1689 functional resolution of the recording sites, the total number of data points (n) used was reduced
1690 by the factor that functional voxels were up-sampled onto the 2D cortical surface to calculate
1691 the correlation’s probability. The correlation coefficients were transformed into z-scores using

1692 Fisher z -transformation before averaging the correlation coefficients across maps and
1693 participants.

1694

1695 *Cross validations*

1696 We cross validated the numerosity tuning response model fits between the ‘attend black’ and
1697 ‘attend white’ conditions. Specifically, we split the data of each condition into two halves based
1698 on odd or even runs and cross-validated the pRF estimates within- and between-condition.
1699 Specifically, we fitted the numerosity pRF model on one half dataset and used this to predict
1700 the responses from the other half. We fitted that model to another dataset of the same condition
1701 or the opposite condition, giving the cross-validated variance explained (cvR^2) in each case.
1702 We averaged the cvR^2 from all the iterations of the cross validation combinations. A repeated
1703 measures two-way ANOVA analysis was performed in JASP (JASP Team, 2020) to compare
1704 the cvR^2 of the within- and cross-condition validations.

1705

1706 **Data availability**

1707 The data sets generated during the current study are available from the corresponding authors
1708 upon reasonable request.

1709

1710 **Code availability**

1711 The code that supports the findings of this study is available in the Vistasoft repository
1712 (<https://github.com/vistalab/vistasoft>). Additional code is available from the corresponding
1713 authors upon reasonable request.

1714

1715 **Acknowledgment**

1716 This research was supported by a China Scholarship Council (CSC) scholarship
1717 [201706750008] (Y. C.), an NWO-VICI grant 016.Vici.185.050 (S. O. D.) and an NWO-VIDI
1718 grant 452-117-012 (B. M. H.).

1719

1720

1721

1722

1723

1724

1725

1726
1727
1728
1729
1730
1731
1732

Chapter 4

1733
1734
1735
1736

1737 Numerosity maps at the human temporal-occipital lobe involved in
1738 symbolic number processing

1739
1740
1741
1742
1743
1744
1745
1746 (*under review*)

1747
1748
1749

1750 *Acknowledgement of author contributions:*

1751 Conceptualization: Y.C., S.H., S.O.D.; Data Collection and Analysis: Y.C.; Writing - Original
1752 draft: Y. C.; Review & Editing: Y.C., S.H., S.O.D; Supervision: S.H., S.O.D.; Funding
1753 Acquisition: Y. C., S. O. D. All authors approved the final version of the manuscript for
1754 submission.

1755

1756 Supplementary figures of this chapter can be found in Appendix C.

1757

1758 **Abstract**

1759 Numerosity, the set size of a group of items, helps guide human and animals' behavior and
1760 decisions. Numerosity perception is thought to be a precursor of symbolic numerical cognition.
1761 Previously, we uncovered neural populations selectively tuned to numerosities organized in a
1762 network of topographic maps. Here we investigate whether these numerosity maps are also
1763 involved in the processing of symbolic numbers, using ultra-high field fMRI at 7 Tesla and a
1764 number-detection task. We found that the numerosity map at the temporal-occipital cortex
1765 (NTO) also respond to symbolic numbers. Furthermore, we found that the numerosity-tuned
1766 neuronal populations at the NTO map in the left hemisphere are tuned to symbolic numbers.
1767 These results reveal different functions of the numerosity maps and, in particular, support the
1768 role of the ventral temporal-occipital cortex in linking non-symbolic numerosity and symbolic
1769 numerical processing.

1770

1771 **Keywords: 5-7**

1772 Numerosity map, symbolic number, ventral temporal cortex, number form area, ultra-high field
1773 fMRI

1774

1775

1776

1777

1778

1779

1780

1781

1782

1783

1784

1785

1786

1787

1788

1789

1790

1791

1792 **Introduction**

1793 Numerosity, i.e., the set size of a group of items, helps guide humans and animals' behavior
1794 and decisions (S. Dehaene, 2001; Andreas Nieder, 2020b, 2021). Humans share the ability to
1795 perceive numerosity with many animal species, including non-human primates (Brannon &
1796 Terrace, 1998; Cantlon & Brannon, 2006; Sawamura et al., 2002), birds (Ditz & Nieder, 2015;
1797 Emmerton et al., 1997), fish (Agrillo et al., 2008), and insects (Cantlon, Platt, & Brannon, 2009;
1798 Giurfa, 2019). Newborn babies and preverbal infants are also able to perceive non-symbolic
1799 numerosity (Feigenson et al., 2004; Izard et al., 2009; Strauss & Curtis, 1981). However, only
1800 human adults possess a unique numerical competence, i.e. symbolic numerical cognition, that
1801 involves the learning of abstract symbols such as Arabic numerals, number words, math and
1802 so forth (Ansari, 2008; Andreas Nieder & Dehaene, 2009).

1803 Whether non-symbolic numerosity and symbolic numbers are represented in a common
1804 abstract coding scheme is a longstanding debate (Ansari et al., 2007; Cohen Kadosh et al., 2007;
1805 S. Dehaene, 1992; Andreas Nieder, 2004; Piazza et al., 2007). Two competing hypotheses have
1806 been proposed. Based on behavioral observations, some researchers propose the existence of
1807 two independent numerical systems: one for approximate non-symbolic numerosities and
1808 another for exact symbolic numbers (X. He et al., 2021; Marinova et al., 2021; Sasanguie et
1809 al., 2017). In agreement with this view, neuroimaging evidence has shown distinct neural
1810 activation patterns evoked by non-symbolic and symbolic number formats (J. Bulthé, De Smedt,
1811 & Op de Beeck, 2014; Eger et al., 2009). More recently, single-cell recordings in the medial
1812 temporal lobe of neurosurgical patients revealed distinct neurons selectively tuned to non-
1813 symbolic and symbolic numbers (Kutter et al., 2018).

1814 Alternatively, another view suggests that non-symbolic numerosity and symbolic
1815 numbers are interconnected. The approximate number system (ANS) shared by human adults,
1816 infants and animals, is believed to be the precursor to the development of symbolic numbers
1817 (Ansari, 2008; S. Dehaene, 2001; Feigenson et al., 2004; Andreas Nieder, 2020a; Piazza, 2010).
1818 It has often been assumed that number symbols acquire their meaning by being mapped onto
1819 the pre-existing non-symbolic representations of numerical magnitude, i.e., the 'mental number
1820 line' (Verguts & Fias, 2004). The ANS is characterized by two behavioral characteristics: the
1821 'numerical distance effect' and 'numerical size effect' (S. Dehaene, Dehaene-Lambertz, &
1822 Cohen, 1998). Psychophysics studies have demonstrated that both non-symbolic (Buckley &
1823 Gillman, 1974) and symbolic (Moyer & Landauer, 1967) numerical magnitudes are subject to
1824 these two effects (Defever, Sasanguie, Gebuis, & Reynvoet, 2011). Moreover, and crucially,
1825 performance with non-symbolic numerical tasks predicted children's mathematics performance

1826 (Gilmore, McCarthy, & Spelke, 2010; Halberda et al., 2008), and training on non-symbolic
1827 arithmetic skills improved symbolic math performance (Park, Bermudez, Roberts, & Brannon,
1828 2016). Brain imaging studies identified regions primarily in the parietal and frontal lobes as
1829 key areas of both non-symbolic and symbolic number processing (Arsalidou & Taylor, 2011;
1830 Piazza et al., 2007; Sokolowski, Fias, Mousa, & Ansari, 2017). Examination on brain-damaged
1831 patients associated deficits at key regions responsible for numerosity processing with
1832 dyscalculia and acalculia, a learning disability in comprehending and manipulating numbers
1833 (S. Dehaene, Molko, Cohen, & Wilson, 2004).

1834 In the last decades, evidence from single-cell recording in non-human primates (Andreas
1835 Nieder et al., 2002b), crows (Ditz & Nieder, 2015), and human (Kutter et al., 2018) have shown
1836 neurons tuned to numerosity, responding maximally when a specific numerosity is displayed,
1837 with responses decreasing as distance from this preferred numerosity increases. Similar
1838 numerosity-tuned responses were shown using an fMRI adaptation paradigm (Piazza et al.,
1839 2004). We have since used population receptive field (pRF) modelling (Dumoulin & Wandell,
1840 2008) to show that these neural population responding to specific numerosities are organized
1841 in topographic maps where preferred numerosity changes gradually across the cortical surface
1842 (B. M. Harvey et al., 2013). A network of these numerosity maps were found throughout the
1843 human cortex, specifically in the temporal-occipital lobe (NTO), parietal-occipital lobe (NPO),
1844 parietal lobe (NPC1-3) and frontal lobe (NF) (Cai, Hofstetter, van Dijk, et al., 2021b; Ben M.
1845 Harvey & Dumoulin, 2017a; Hofstetter et al., 2021; Tsouli, Cai, et al., 2021). However, the
1846 role these maps play in numerosity perception and symbolic numerical cognition is still
1847 unknown (Tsouli, Harvey, et al., 2021).

1848 Here we ask whether numerosity-selective neural populations within the established
1849 network of numerosity maps are also involved in the processing of symbolic numbers. In our
1850 former study (Harvey et al., 2013), we did not find evidence to support the involvement of a
1851 map in the right superior parietal lobe (NPC1) in symbolic number processing. Here, we revisit
1852 this question with two conceptual advances. First, we evaluate the entire network of
1853 topographic maps and we speculate that functional specialization of the maps differ (Tsouli,
1854 Harvey, et al., 2021). We hypothesize that the function of the topographic maps may differ
1855 (Tsouli, Harvey, et al., 2021), in particular for symbolic number processing. Second, we
1856 redesigned the stimulus and task. Specifically, we suspect that the lack of response to the
1857 presentation of numbers might have been due to the failure of perceiving the semantic meaning
1858 of the presented number symbols, i.e. the number concepts. In the Harvey et al. (2013) study,
1859 participants judged the color of the stimuli but no number judgements were required. The

1860 magnitude information of non-symbolic numerosity (e.g., a dot pattern of “●●”) spontaneously
1861 emerges with a stimulus presentation in the visual format (D. Burr & Ross, 2008; Cicchini et
1862 al., 2016). However, this might not be the case for symbolic numbers (e.g., “2” or “two”), of
1863 which the physical appearance of a symbol bears no numerical information. Furthermore,
1864 attention appears necessary to numerosity perception (Anobile, Cicchini, et al., 2012; D. C.
1865 Burr et al., 2010; Pomè, Anobile, Cicchini, Scabia, et al., 2019). Thus, having a task that
1866 involves judgment of symbolic numbers will both focus attention on the number and force
1867 participants to process its magnitude information.

1868 Using ultra-high field fMRI at 7 Tesla (Cai, Hofstetter, van der Zwaag, et al., 2021), we
1869 recorded blood oxygen level dependent (BOLD) signals while participants were engaged in a
1870 symbolic number experiment with a number-detection task. We analysed the neural responses
1871 to symbolic numbers using a general linear model (GLM) analysis throughout the cortex, and
1872 within the participant’s numerosity maps. We applied a neural model-based analysis, i.e. pRF
1873 modelling (Dumoulin & Wandell, 2008) to investigate whether numerosity-tuned neural
1874 populations at the numerosity maps are also tuned to symbolic numbers.

1875

1876 **Methods**

1877 *Participants*

1878 We present data from seven participants (three females, age range 24 – 48 years, two left-
1879 handed). All the participants had normal or corrected-to-normal visual acuity. All were well
1880 educated, with good mathematical abilities. Written informed consent was obtained before
1881 every MRI session. All experimental procedures were approved by the ethics committee of VU
1882 University Amsterdam (Netherlands).

1883

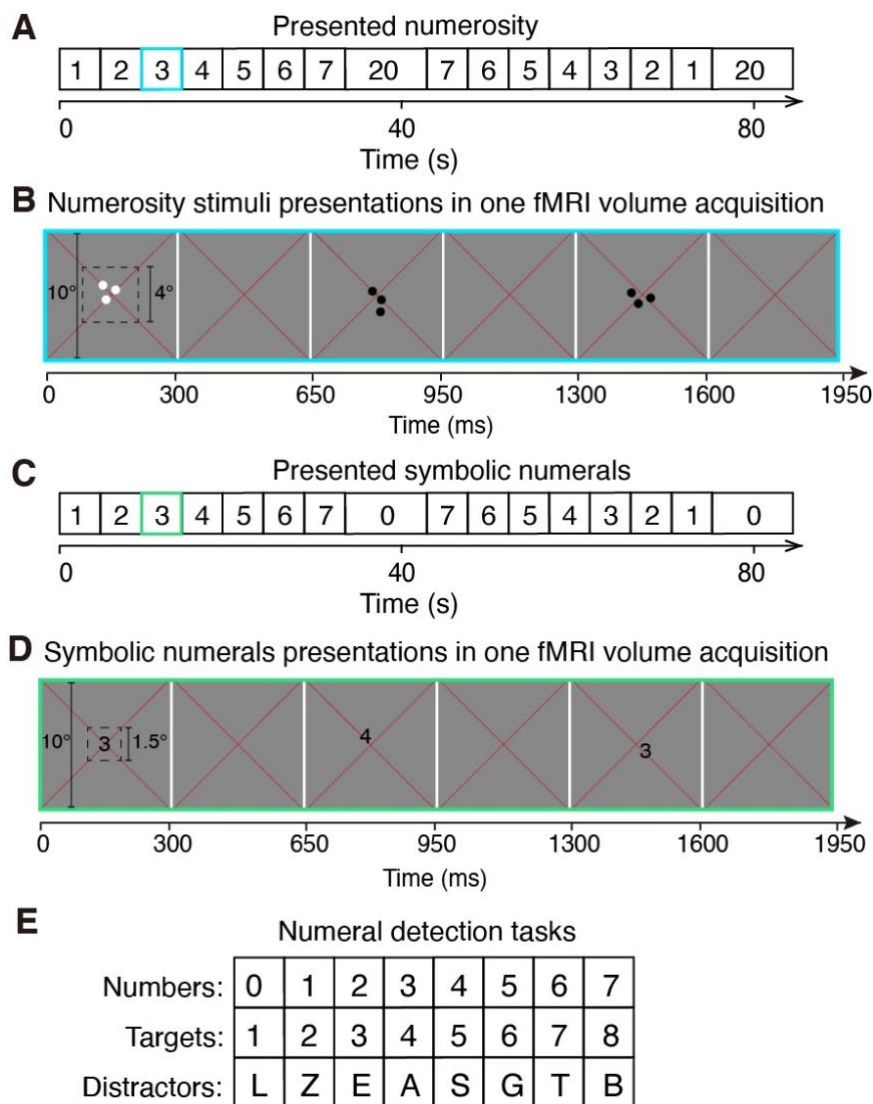
1884 *Stimuli and experimental Design*

1885 Visual stimuli were presented on a 69.84 x 39.29 cm LCD screen (Cambridge Research
1886 Systems) behind the MRI bore. Participants were required to lie still and view the display
1887 through a mirror attached to the head coil. The total distance from the attached mirror to the
1888 display screen was 220 cm. The display resolution was 1920 x 1080 pixels. A button box
1889 recorded behavioural responses. Visual stimuli were generated in Matlab using PsychToolbox
1890 (Kleiner et al., 2007). A large diagonal cross composed of thin red lines was displayed
1891 consistently across the entire screen, serving as a fixation marker.

1892

1893 *Localizing non-symbolic numerosity maps*

1894 We first ran a localizer experiment to identify the numerosity maps of our participants. We
 1895 used the same study design as was previously used (Cai, Hofstetter, van Dijk, et al., 2021b; B.
 1896 M. Harvey et al., 2013; Ben M. Harvey & Dumoulin, 2017a; Hofstetter et al., 2021; Tsouli,
 1897 Cai, et al., 2021). Specifically, a sequence of numerosity stimuli consisting of 1 to 7 dots were
 1898 first presented in ascending order, followed by a long period (15.6 seconds) where presented
 1899 with the baseline numerosity of 20 dots, then followed by the same sequence in descending
 1900 order and another identical baseline period (Figure 4.1A). This sequence was repeated four
 1901 times for each fMRI scan run.



1902
 1903 **Figure 4.1. Illustration of experimental design and stimulus presentations.** (A) The
 1904 sequence of the presented non-symbolic numerosity used to localize the numerosity maps. (B)
 1905 Schematic representation of an example stimulus presentation in the numerosity maps localizer
 1906 experiment (blue frame in A) within one fMRI volume acquisition (i.e. one TR). Each dot
 1907 pattern was presented briefly (300 ms) at the central 4° of the visual field, followed by a 350

1908 ms presentation of a gray background before a new random positioned dot pattern presentation.
1909 Each pattern of the same numerosity was repeatedly presented six times, corresponding to two
1910 TRs, before the numerosity changed. Participants fixated the red cross at the centre and pressed
1911 a button when dots were shown in white rather than black. (C) The sequence of presented
1912 symbolic numbers. (D) Schematic representation of an example trial of symbolic number '3'
1913 in the symbolic experiment (green frame in C) within one TR. Each symbol was presented
1914 briefly (300 ms) at the central 1.5° of the visual field, with an inter-stimulus-interval of 350 ms
1915 of a gray background. Each number was presented six times before moving to the next number.
1916 Participants fixated at the red cross and responded when the presented number increased in
1917 magnitude by one as compared to the previous presented number. (E) Letters, similar in
1918 morphology to the target numbers, were used as distractors.

1919

1920 Numerosity stimuli consisted of a group of dots with a constant total surface area presented
1921 in the central 4° (diameter) of the visual field. Dots were randomly positioned at each
1922 presentation so that each dot fell entirely within this area, to distribute contrast energy equally
1923 across the stimulus area for all numerosities. Each numerosity presentation that contained the
1924 same number of dots was placed in a new, random position, so no specific visual position was
1925 associated with any numerosity. To prevent perceptual grouping, individual items were
1926 distributed roughly homogeneously across the stimulus area. All of the numerosity stimuli were
1927 displayed as black or white dots on a gray background. Dot patterns were presented briefly
1928 (300 ms) to ensure participants did not have time to count. A new random pattern was presented
1929 every 650 ms, with 350 ms presentation of a uniform gray background between dot pattern
1930 presentations. This was repeated six times, over 3900 ms, corresponding to two fMRI volume
1931 acquisitions (TR), before the numerosity changed (Figure 4.1B). On 10% of numerosity
1932 presentations, the dots were shown in white instead of black. Participants were asked to fixate
1933 at the red cross in the center and press a button when whites dots were shown to ensure they
1934 were paying attention to the stimulus during fMRI acquisition. Participants responded to 90-
1935 100% of the white dots presentations within each run. No numerosity judgements were required.

1936

1937 *Symbolic number experiment*

1938 We used a similar sequence as the numerosity stimulus sequence, but instead of dots we
1939 showed Arabic numbers from 1 to 7, and a baseline period using the number '0' (zero). The
1940 number '0' was used instead of '20' in order to keep all the stimuli as single-digit numbers
1941 (Figure 4.1C) as '20' may be interpreted as containing two items (Jessica Bulthé, De Smedt, &

1942 Op de Beeck, 2015). This stimulus sequence was presented in ascending (1 - 7), then
1943 descending order (7 - 1) followed by a baseline period, respectively. This sequence also
1944 repeated four times (cycles) for each functional run.

1945 Symbolic number stimuli were randomly presented in the central 1.5° (diameter) of the
1946 visual field. Each number was presented briefly (300 ms) with an inter-stimulus-interval of 350
1947 ms of a uniform gray background between stimulus presentations. Each number was repeated
1948 six times, over 2 TRs before the number changed. Participants fixated the red cross and pressed
1949 a button when the number increased in magnitude by one as compared to the previous presented
1950 number. A list of capitalized letters that were morphologically similar to the symbolic numbers
1951 from 1 to 8 were used as distractors: ‘L’, ‘Z’, ‘E’, ‘A’, ‘S’, ‘G’, ‘T’, ‘B’ (Figure 4.1E). All the
1952 numbers and letters were displayed in the font of ‘Arial Unicode MS’ with the font size of 27.
1953 When the stimulus sequence was presented in an ascending order, there were always seven
1954 regular stimulus changes in symbolic number in one cycle that would require a response
1955 (‘embedded trials’, e.g. when the stimulus changed from 1 to 2, 2 to 3, etc.). In addition to the
1956 embedded trials, at random points along the sequence the stimuli presented was a number
1957 increased by one as compared to the previous number (‘catch trials’), or a letter that was
1958 morphologically similar to the target number (‘distract trials’) (Figure 4.1E). The ‘catch trials’
1959 and ‘distract trials’ correspond to 20% of the total number of stimulus presentation trials.
1960 Percentage of correct responses were calculated for the ‘embedded trials’ and ‘catch trials’,
1961 respectively. Responses to the distractor letters or any trials other than the ‘embedded trials’
1962 and ‘catch trials’ were counted as false alarms. Task performance was quantified using the
1963 discriminability index (d') of the signal detection theory, which denotes participants’
1964 sensitivity to the targets (Green & Swets, 1966). We determined a response as a hit if it occurred
1965 within 2 seconds after a signal presentation, otherwise it was classified as a false alarm.

1966

1967 *MRI acquisition and preprocessing*

1968 All MRI data were acquired using a Philips 7T scanner (Philips Medical Systems, Best, NL).
1969 MP2RAGE (Marques et al., 2010) T1 anatomical MRI data were acquired at the spatial
1970 resolution of $0.64 \times 0.64 \times 0.64 \text{ mm}^3$ (resampled to $0.6 \times 0.6 \times 0.6 \text{ mm}^3$ for following
1971 processing). Repetition time (TR) = 6.2 ms, echo time (TE) = 3 ms, and flip angle (FA) = 5°.
1972 Functional T2*-weighted multi-band (factor = 2) 2-dimensional echo planar images (EPI) were
1973 acquired using a 32 channel head coil (Philip Nova Medical) at a resolution of $1.75 \times 1.75 \times$
1974 1.75 mm^3 . A full-brain-coverage field of view (FOV = $106 \times 112 \times 236$) covering 64 slices

1975 was used. TR = 1950 ms, TE = 25 ms, FA = 70°. Each functional scan run has 182 TRs (354.9
1976 seconds in duration), of which the first six TRs were discarded to ensure the signal was at a
1977 steady state. Participants were scanned for eight functional runs in one session to localize the
1978 numerosity maps, except for participant 4 who had nine runs. For the symbolic number
1979 experiment, each participant was scanned for two sessions on separate days, resulting in fifteen
1980 to seventeen functional runs in total.

1981 T1 anatomical images were automatically segmented using cbs-tools
1982 (<https://www.nitrc.org/projects/cbs-tools/>) and then manually edited to minimize segmentation
1983 errors using ITK-SNAP (Yushkevich et al., 2006). This provides a highly accurate description
1984 of the cortical surface, an anatomical segmentation space used for analysis of cortical
1985 organization. The cortical surface was rendered as a smoothed 3D surface. Head movement
1986 and motion artefacts between and within functional images were measured and corrected for
1987 in AFNI (Cox & Hyde, 1997). Using Vistasoft (<https://github.com/vistalab/vistasoft/wiki>), the
1988 motion-corrected functional images were co-registered to the same anatomical space using the
1989 same transformation. The time-series data were aligned to the anatomy and then averaged. Data
1990 were imported to the anatomical segmentation space using trilinear interpolation. To increase
1991 signal strength, data from all recording sites (voxels) were collapsed onto the nearest point on
1992 the cortical surface layer. This formed a (folded) 2D representation of the gray matter nodes.
1993 pRF modelling and subsequent statistical analyses were performed at this space.

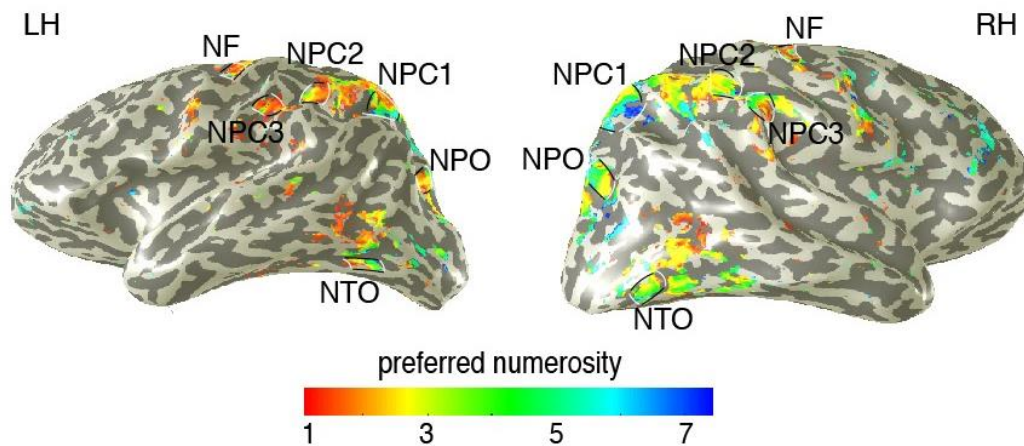
1994

1995 *pRF modelling of responses to non-symbolic numerosity*

1996 pRF modelling was applied to estimate numerosity responses (Dumoulin & Wandell, 2008; B.
1997 M. Harvey et al., 2013). Briefly, a one-dimensional logarithmic model was used to predict
1998 numerosity responses. This model describes tuning in logarithmic numerosity space using a
1999 Gaussian function characterized by preferred numerosity (mean of the Gaussian) and tuning
2000 width (standard deviation of the Gaussian).

2001 At each gray matter voxel, the pRF model is estimated based on the recorded signal and
2002 the predicted time course. A prediction of the neural response time course was produced by
2003 overlapping the stimulus (numerosity) at each time point with the Gaussian tuning function.
2004 By convolving this prediction with a hemodynamic response function (HRF), a predicted
2005 response time course was generated. The pRF parameters for each voxel were chosen by those
2006 predicted fMRI time courses that bring the best agreement to the recorded signal, denoted as
2007 variance explained (R^2). Last, participant-specific HRF parameters were estimated over the
2008 whole fMRI volume and these parameters were used to refit the pRF.

2009 The pRF fitting procedure allows preferred numerosity estimates outside the range of the
2010 presented stimuli, ensuring estimates within the stimulus range are not just the best of a limited
2011 set. We excluded from analysis any recording sites where the preferred numerosity was outside
2012 our presented range and the variance explained was lower than 30%. We then projected the
2013 preferred numerosity of these recording sites on the smoothed cortical surface (Figure 4.2 &
2014 Supplementary Figure 4.1).



2015
2016 **Figure 4.2. Topographic numerosity maps in the human cortex.** An example of preferred
2017 numerosity estimates in one participant for the left and right hemispheres. Black lines outline
2018 the edge borders of individual numerosity maps and white lines denote the lowest and highest
2019 preferred numerosities in each map. The map of preferred numerosity estimates is thresholded
2020 at a variance explained of 30%. LH, left hemisphere. RH, right hemisphere. See Supplementary
2021 Figure 4.1 for maps of all other participants.

2022
2023 *Definition of regions of interest*

2024 We defined regions of interest (ROI) where the numerosity-selective neural populations are
2025 organized topographically similar to previously reported numerosity maps (Figure 4.2) (Cai,
2026 Hofstetter, van Dijk, et al., 2021b; Ben M. Harvey & Dumoulin, 2017a; Hofstetter et al., 2021;
2027 Tsouli, Cai, et al., 2021). In general, a network of six numerosity maps were defined on the left
2028 and right hemispheres, respectively. These maps lay in the temporal-occipital cortex (NTO),
2029 parietal-occipital cortex (NPO), parietal cortex (NPC1, NPC2, NPC3) and superior frontal
2030 cortex (NF). Within each ROI, we manually defined map borders on the lowest and highest
2031 preferred numerosities (white lines) and the map edges around the local regions with increase
2032 in model goodness of fit (black lines).

2033
2034 *Analysis of neural responses to symbolic numbers*

2035 First, we performed GLM analyses on the averaged functional data of the symbolic number
2036 experiment. The GLM analyses included the presentation of the main numbers (i.e., “1-7”) as
2037 a predictor. We projected the t -values at the recording sites where the GLM model explained
2038 more than 30% of the variance at the site onto the cortical surface. We then tested the neural
2039 responses to symbolic numbers within the numerosity maps. We averaged the time-series
2040 across voxels within each map and fitted the averaged time-series with the GLM model to
2041 attain the t -values representing the overall responses at individual maps. We performed a
2042 repeated two-way ANOVA analysis on the t -values of individual maps in both hemispheres of
2043 all the participants, followed by a post-hoc analysis for multiple comparisons (JASP Team,
2044 2020). Then, a one sample t -test was performed on the t -values at each map across participants
2045 to test whether the overall responses at individual maps in each hemisphere are significantly
2046 higher than zero.

2047 Next, to explore whether the neural responses in the NTO maps are also tuned to symbolic
2048 numbers, we fitted pRF models to the data. In contrast to the numerosity model, we fitted a
2049 Gaussian tuning function in linear numerical space as symbolic numbers are more precisely
2050 and linearly represented (Verguts & Fias, 2004). We then averaged the variance explained by
2051 the pRF models across voxels within bilateral NTO maps, respectively.

2052 We cross-validated the results by splitting the data into two halves, based on odd and even
2053 runs. We fitted both the GLM model and pRF model on each half dataset. The variance
2054 explained of the pRF prediction from one half dataset was evaluated on the time series of the
2055 other half dataset, yielding new variance explained at the recording sites. Cross-validated
2056 variance explained by the GLM model or pRF model were then calculated by averaging the
2057 resulting variance explained over the two halves datasets, respectively. We then quantified the
2058 proportion of recording sites where neural activity is better explained by tuning models rather
2059 than the GLM at bilateral NTO maps, respectively. Differences between the (cross-validated)
2060 variance explained of the pRF model and (cross-validated) variance explained of the GLM
2061 were calculated. We performed a pair t -test to compare the degree of the difference in the
2062 variance explained of the pRF model and GLM model. A Wilcoxon’s sign rank test was
2063 performed on the degree of difference to investigate whether the difference is significantly
2064 higher than zero.

2065 Finally, we performed a Pearson correlation analysis between the preferred numerosity
2066 estimates and the preferred number estimates at the recording sites responding to both
2067 numerosity and symbolic numbers in the NTO map. Taking into account the functional
2068 resolution of the recording sites, the total number of data points (n) used to calculate

2069 correlation's probability was reduced by the factor by which functional voxels were up-
2070 sampled onto the 2D cortical surface.

2071

2072 *Conversion to MNI coordinates*

2073 Our analyses were in individual participant space. To identify the location of the NTO map on
2074 an average brain, we converted these to MNI x , y , z coordinates. We first located at each
2075 individual participants' map centres on the cortical surface. We then transformed each
2076 participant's anatomical MRI data, together with these map centre locations, into MNI
2077 averaged template space using MINC toolkit (Collins, Neelin, Peters, & Evans, 1994)
2078 (<http://packages.bic.mni.mcgill.ca>) and rigid alignment and linear scaling. We took the mean
2079 and standard deviation of the resulting MNI coordinates of the NTO map across participants.

2080

2081 **Results**

2082 *Participants engaged in the task*

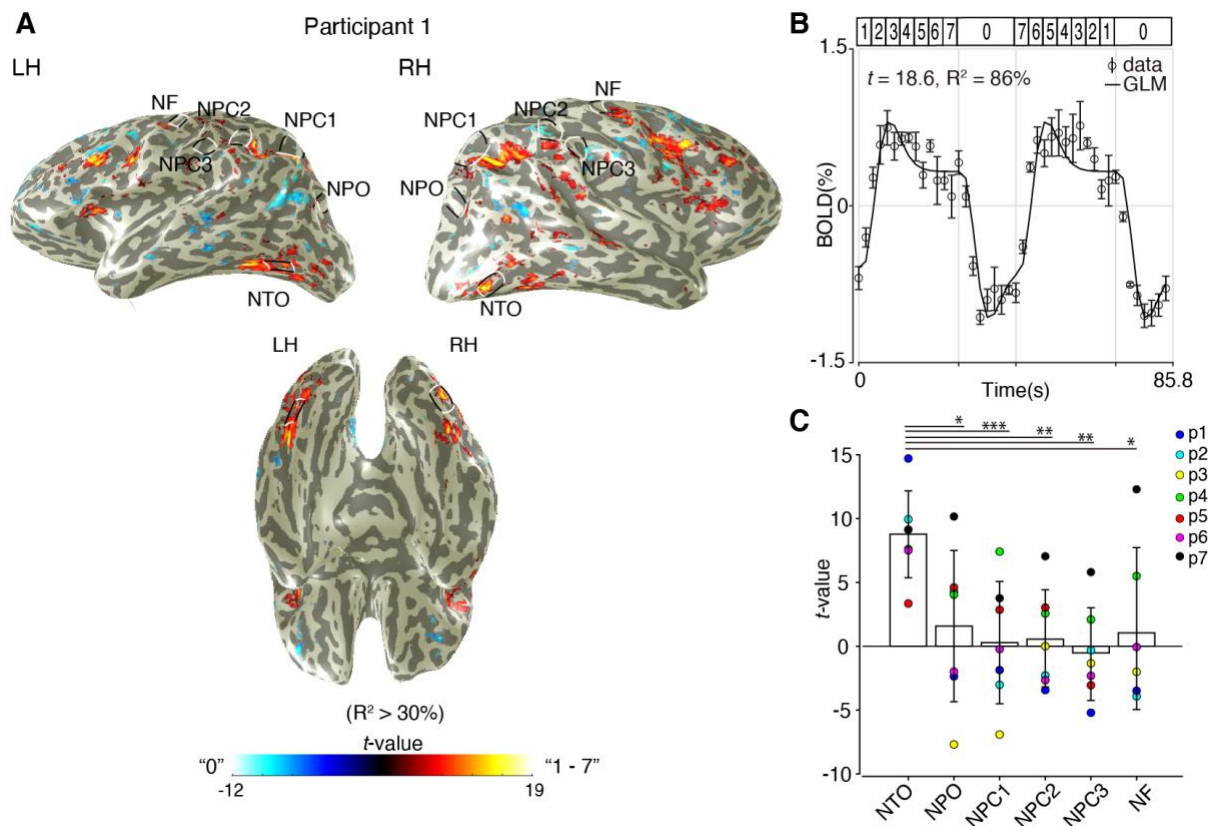
2083 All the participants performed the task with a high percentage of correct responses, both of
2084 detecting changes in symbolic numbers as part of the stimulus sequence ('embedded trials',
2085 mean \pm SD: 93.6% \pm 3.4%, $d' = 4.1 \pm 0.4$) and random changes ('catch trials', 83.3% \pm 9.6%,
2086 $d' = 3.7 \pm 0.4$). The percentage correct and d' suggest that participants were engaged in the
2087 task and processing the semantic meaning of the presented numbers (see Supplementary Table
2088 4.1 for the performance of individual participants).

2089

2090 *Numerosity map NTO responds to symbolic numbers but not the other maps*

2091 Figure 4.3A shows the results of the GLM analysis of the main testing numbers of "1-7" (red)
2092 and the baseline number of "0" (blue). Most brain regions responding to symbolic numbers did
2093 not overlap with the location of the numerosity maps, except for NTO maps in the ventral
2094 stream of the bilateral temporal occipital cortices (Figure 4.3A lower panel, see also
2095 Supplementary Figure 4.2 for the results of all other participants). To illustrate the responses
2096 to symbolic numbers, we extracted a time-series from an example recording site at the NTO
2097 map of participant 1 (Figure 4.3B). Responses were observed at the presentation of the main
2098 symbolic numbers ($t = 18.6$), and the GLM prediction captured most of the variance in the
2099 signal ($R^2 = 86\%$). Repeated two-way ANOVA analysis with the factors of hemispheres and
2100 maps (see Methods) showed a significant effect of maps ($F_{(5,78)} = 7.28$, $p < 0.001$), but no
2101 significant effect of laterality ($F_{(1,78)} = 0.142$, $p = 0.726$) and no interaction effect ($F_{(5,78)} = 1.124$,
2102 $p = 0.379$). Based on these results, we averaged t -values of individual maps across hemispheres

2103 for individual participants (Figure 4.3C, but see results for left and right hemispheres separately,
 2104 in Supplementary Figure 4.3). Post-hoc analysis showed that the NTO map exhibited
 2105 significantly higher responses to symbolic numbers than other maps (Bonferroni corrected for
 2106 multiple comparisons, Figure 4.3C). Furthermore, one-sample *t*-test performed on the *t*-values
 2107 of each individual map across participants showed that only the NTO map exhibited responses
 2108 significantly higher than zero ($t = 6.12 \times 10^{-7}$, $p = 0.0005$). These results indicate that neural
 2109 populations at the NTO map not only respond to non-symbolic numerosity but also to symbolic
 2110 numbers.



2111
 2112 **Figure 4.3. Stimulus-driven responses to symbolic numbers at numerosity maps.** (A) The
 2113 result of an example participant of the GLM analysis which contrasted the responses to the
 2114 number of “0” (blue colors) and “1-7” (yellow-red colors). Lower panel shows the ventral view
 2115 of the cortical surface where the responses to symbolic numbers overlap with the NTO map.
 2116 Only recording sites (i.e. voxels) where the variance explained (R^2) by the GLM exceeding 30%
 2117 were projected on the cortical surface. (B) Response time-series to symbolic numbers at an
 2118 example recording site extracted from the NTO map. The GLM prediction (solid line) captured
 2119 86% of the variance at this recording site with a corresponding *t*-value of 18.6. Dots represent
 2120 the averaged response amplitude and error bars represent standard errors of the mean over
 2121 repeated measures. (C) Averaged *t*-values at individual maps across hemispheres and

2122 participants. Repeated two-way ANOVA analysis (followed by post-hoc analysis for multiple
2123 comparison) shows that responses at NTO are significantly higher than responses at the other
2124 maps. Bars represent the mean and error bars represent the standard deviations of the mean. *,
2125 $p = 0.005$; **, $p = 0.002$; ***, $p < 0.001$.

2126

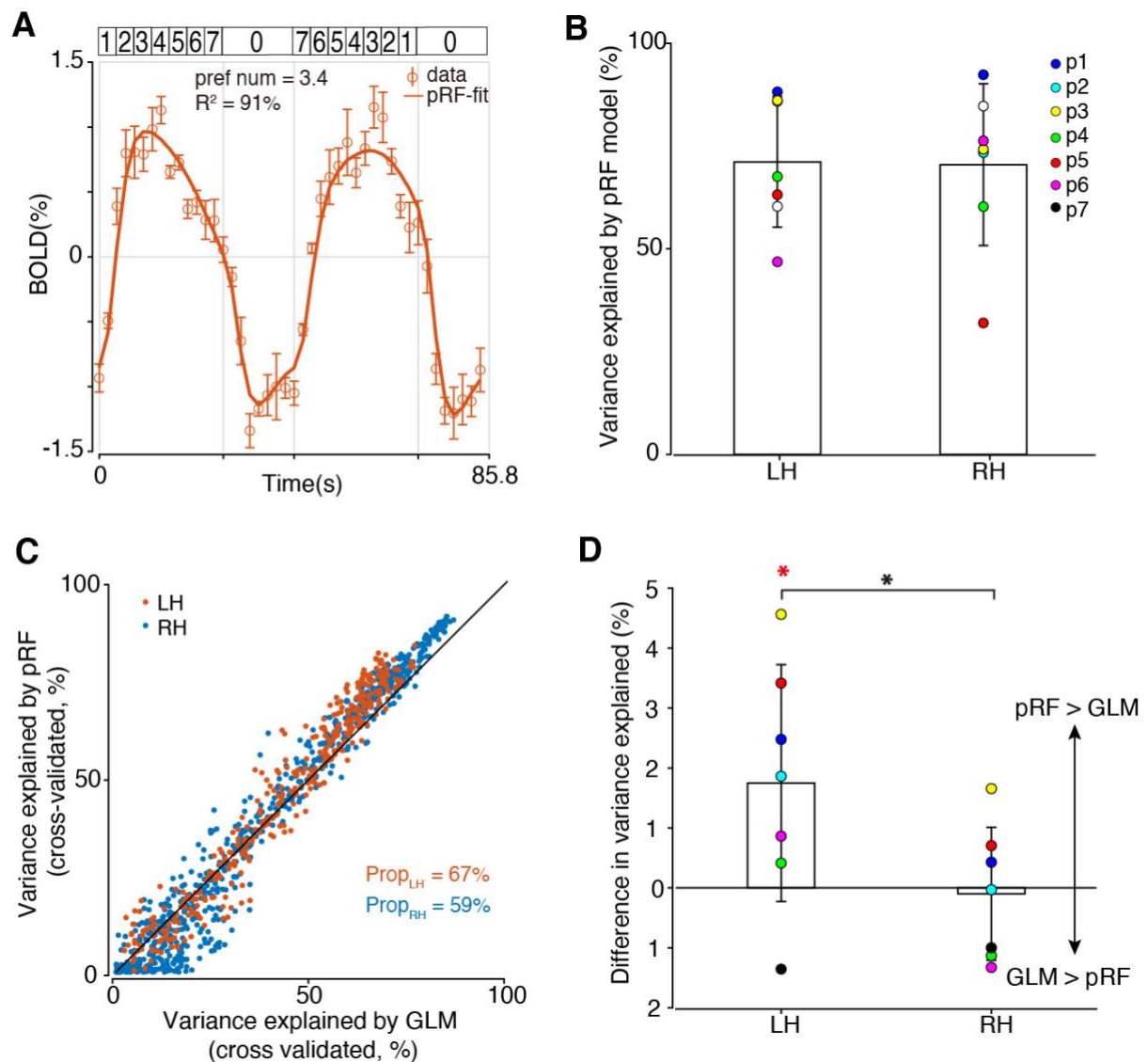
2127 *Are responses at the NTO map also tuned to symbolic numbers?*

2128 Next we asked whether the responses to symbolic numbers at the NTO maps also show tuning
2129 characteristics which underlies perception (Tsouli, Harvey, et al., 2021), rather than untuned
2130 stimulus-driven responses. We found that the pRF models explained the data well and captured
2131 most of the response variance. Figure 4.4A shows a time-series of an example recording site at
2132 the NTO map of participant 1 (open circles). The pRF model explained about 90% of the
2133 variance at this site (solid line), and indicated that this recording site prefers the symbolic
2134 number of about 3.4. Overall, the pRF models achieved considerable variance explained at
2135 bilateral NTO maps across all the participants (mean \pm SD: $R^2 = 71 \pm 16\%$ in the left NTO map
2136 and $70\% \pm 20\%$ in the right NTO map) (Figure 4.4B).

2137 We quantified the proportion of the recording sites where the tuning model explained
2138 more variance in the neural responses than the GLM (Figure 4.4C-D). Overall, more than half
2139 of the recording sites at the NTO maps across participants and hemispheres showed higher
2140 variance explained by the tuning model (mean \pm SD: $56 \pm 14\%$ in the left NTO map and 52%
2141 $\pm 11\%$ in the right NTO map). However, only the responses at the left NTO maps were
2142 significantly higher than zero (Wilcoxon sign rank test, $p = 0.0391$). Paired t -test showed that
2143 the left NTO maps had a significantly higher variance explained by the tuning model than the
2144 right NTO maps ($t = 4.53$, $p = 0.004$). These results suggest that numerosity-tuned neural
2145 populations at the left NTO map are also tuned to symbolic numbers.

2146 We compared the preferred numerosity estimates and preferred number estimates of
2147 the neural populations in the left NTO map that responded to both stimuli. We did not find a
2148 significant correlation between these estimates (Pearson correlation coefficient, mean \pm SD: r
2149 $= 0.10 \pm 0.2$) (Supplementary Figure 4.4). These results suggest that the neural populations
2150 tuned to symbolic numbers in the left NTO map were distinct from the neural populations tuned
2151 to non-symbolic numerosity.

2152



2153

2154 **Figure 4.4. Numerosity-tuned neural populations at the left NTO map are tuned to**

2155 **symbolic numbers.** (A) Response time-series of an example recording site at the NTO map of

2156 participant 1 and the pRF model prediction. Dots represent the mean response amplitude and

2157 error bars represent standard error of the mean over repeated measures. The best fit neural

2158 model (solid line) captured more than 90% of the variance at this site. (B) Averaged variance

2159 explained at bilateral NTO maps across participants of the pRF models fitted with the averaged

2160 time series across recording sites within the map. (C) Cross-validated variance explained by

2161 pRF model and GLM at all the recording sites within the NTO map of participant 1. Black line

2162 indicates an equal variance explained by the GLM and pRF model. Texts indicate the

2163 proportion of recording sites where the pRF model fit the data better than the GLM. (D)

2164 Difference in variance explained at bilateral NTO maps derived by pRF and GLM models,

2165 averaged across participants. The NTO map in the left hemisphere shows significantly higher

2166 variance explained than zero (indicated by the red *, $p = 0.0391$), and significantly different

2167 from the variance explained of the right NTO map (indicated by the black *, $p = 0.004$). LH,
 2168 left hemisphere. RH, right hemisphere.

2169

2170 Last we investigated the NTO map in the context of other regions implicated in functional
 2171 specializations in the ventral cortex, in particular the number form area (NFA). To identify the
 2172 coordinates of the NTO map, we transformed the hemispheres of each participant into Montreal
 2173 Neurological Institute (MNI) space and averaged the coordinates across participants. Table 1
 2174 shows the averaged coordinates (values are given as mean (SD), see Supplementary Table 4.2
 2175 for the coordinates of individual participants) at the centre of the NTO map in the current study
 2176 and in our previous study (Ben M. Harvey & Dumoulin, 2017a). We then compared with the
 2177 coordinates of the NFA previously reported in the inferior temporal gyrus and suggested to be
 2178 specialized for Arabic numeral processing. Though we refrain from statistical analyses on these
 2179 coordinates given all the differences in methods, we propose that NTO is close but distinct
 2180 from the NFA.

2181

Table 1. The MNI coordinates of the NTO map and the NFA

Cortical regions	Reported studies	Left hemisphere			Right hemisphere		
		x	y	z	x	y	z
NTO map	current study (n = 7)	-40(4)	-67(8)	-8(4)	40(3)	-74(4)	-7(4)
	Harvey et al., 2017 (n = 5)	-42(3)	-77(3)	3(8)	44(7)	-75(1)	-4(3)
NFA	Shum et al., 2013 (n = 5)	-	-	-	51	-54	-24
	Abboud et al., 2015 (n = 9)	-	-	-	54	-45	-17
	Hermes et al., 2017 (n = 10)	-	-	-	57	-51	-17
	Yeo et al., 2017 (meta-analysis)	-	-	-	51	-49	-15
	Grotheer et al., 2016 (n = 24)	-60	-57	-17	61	-45	-17

2182 (n: number of participants; -: no data)

2183

2184 **Discussion**

2185 Here we studied whether numerosity-tuned neural populations within a network of topographic
2186 maps respond to symbolic numbers. We used a number-detection task that requires participants'
2187 attention and forced processing of the semantic meaning of the presented Arabic numbers.
2188 Behavioral measures indicate that the participants indeed processed the semantic meaning of
2189 the numbers. We found that neural populations in the ventral temporal occipital cortex (NTO),
2190 but not the other numerosity maps, respond to symbolic numbers. The neural populations
2191 within the left NTO map were also found to be tuned to the presented numbers.

2192 Previously, our colleagues explored neural responses to symbolic numbers (B. M.
2193 Harvey et al., 2013). In that study, however, the focus was only on the superior parietal cortex
2194 (NPC1) and with a task that did not require participants to attend or process the semantic
2195 meaning of the numbers. Here, we revisit this question exploring the established network of
2196 numerosity maps throughout the brain covering the temporal, parietal and frontal cortices (Cai,
2197 Hofstetter, van Dijk, et al., 2021b; Ben M. Harvey & Dumoulin, 2017a; Hofstetter et al., 2021;
2198 Tsouli, Cai, et al., 2021), together with a number-detection task requiring the participants to
2199 process the semantic meaning of numbers. In the human visual cortex, multiple visual field
2200 maps are specialized for specific functions (Wandell et al., 2007). Analogous to the visual field
2201 maps, we suspect that different numerosity maps are also specialized for different functions
2202 (Tsouli, Harvey, et al., 2021). In line with our previous findings, we did not observe responses
2203 to symbolic numbers in the NPC1 map on the parietal cortex. We did find responses to
2204 symbolic numbers in the NTO map at the ventral stream of the occipitotemporal region (VOT).

2205 We not only found that NTO map responds to symbolic numbers, we also found that
2206 neuronal populations in the left NTO are tuned to symbolic numbers, i.e. preferentially respond
2207 to a specific number. Tuning to symbolic number was uncorrelated to tuning to numerosity
2208 suggests that these are distinct but overlapping populations (Ben M. Harvey, Dumoulin,
2209 Fracasso, & Paul, 2020; Hofstetter et al., 2021). We found tuning to numbers in the left NTO,
2210 which is in line with the observation that single neurons are tuned to symbolic numbers in
2211 human medial temporal lobe (Kutter et al., 2018). We did not find evidence for tuning to
2212 symbolic numbers in right NTO, which may be a genuine hemispheric difference, but can also
2213 be attributed to methodological issues, such as the size of the map (Cai, Hofstetter, van Dijk,
2214 et al., 2021b) or larger (scatter) of tuning preferences of individual neurons thereby blurring
2215 the tuning properties at the population level.

2216 The human VOT region contains functional areas that exhibit strong selectivity for
2217 categories such as faces, bodies, word forms, visual objects and scenes (Op de Beeck, Pillet, &
2218 Ritchie, 2019) and, in addition, visual number symbols (S. Dehaene & Cohen, 1995). Previous

2219 studies have revealed a reproducibly localized NFA in the inferior temporal gyri (Abboud,
2220 Maidenbaum, Dehaene, & Amedi, 2015; Grotheer, Herrmann, & Kovács, 2016; Hannagan,
2221 Amedi, Cohen, Dehaene-Lambertz, & Dehaene, 2015; Hermes et al., 2017; Shum et al., 2013;
2222 Yeo, Wilkey, & Price, 2017). In line with the functional specialization in ventral occipital
2223 cortex, our findings suggest that the numerosity-selective neural populations at the NTO map
2224 also respond to symbolic numbers, indicating that numerosity-tuned neural populations in the
2225 VOT region also play a critical role in symbolic number processing.

2226 Representations of numerosity in parietal and frontal brain regions are well investigated
2227 in both humans and nonhuman primates (S. Dehaene, 2003; B. M. Harvey et al., 2013; Andreas
2228 Nieder & Dehaene, 2009). Studies have demonstrated increased functional connectivity
2229 between ventral temporal regions with parietal and frontal regions during calculation (Park,
2230 Hebrank, Polk, & Park, 2012), and even in the blind (Abboud et al., 2015). Our results show
2231 that the NTO map in the VOT region is involved in symbolic number processing. However,
2232 we did observe responses in other brain regions but not in the remainder of network of
2233 numerosity maps.

2234 Representation of symbolic numbers is suggested to evolve from non-symbolic
2235 numerosity representations (S. Dehaene & Cohen, 2007; Piazza et al., 2007). The high-level
2236 human numerical ability of processing numbers are believed to be linked to evolutionarily
2237 conserved numerosity representation during cognitive development (Halberda et al., 2008;
2238 Szklarek & Brannon, 2017). The finding of human number neurons also support the
2239 hypothesis that symbolic number cognition is rooted in biologically determined mechanisms
2240 (Kutter et al., 2018). In line with these findings, our results that the neural populations in the
2241 NTO map at the ventral temporal-occipital lobe respond to numerosity and number symbols,
2242 support a link between non-symbolic and symbolic numerical processing.

2243

2244 **Conclusions**

2245 To conclude, we found neural populations in the NTO map at the human temporal-occipital
2246 cortex responding to numerosity and number stimuli, while the neural populations in the left
2247 NTO map are also tuned to symbolic numbers. These results support the hypothesis that
2248 numerosity perception is the precursor of the human-unique numerical abilities of processing
2249 number symbols.

2250

2251 **Acknowledgement**

2252 This research was supported by a China Scholarship Council (CSC) scholarship
2253 [201706750008] (Y. C.) and an NWO-VICI grant 016.Vici.185.050 (S. O. D.).

2254

2255 **Competing interests**

2256 The authors declare no competing interests.

2257

2258 **Data and Code Availability Statement**

2259 The code generated during this study is available in the Vistasoft repository
2260 (<https://github.com/vistalab/vistasoft>).

2261

2262 The datasets supporting the current study have not yet been deposited in a public repository
2263 because of participants privacy concerns, but are available from the corresponding author on
2264 request.

2265

2266

2267

2268

2269

2270

2271

2272

2273

2274

2275

2276

2277

2278

2279

2280

2281

2282

2283

2284

2285

2286

2287

2288

2289

Chapter 5

2290

2291

2292

2293

2294 Individualized cognitive neuroscience needs 7T: comparing

2295 numerosity maps at 3T and 7T MRI

2296

2297

2298

2299

2300

2301

2302

2303

2304

2305 *Published as:*

2306 Cai, Y., Hofstetter, S., van der Zwaag, W., Zuiderbaan, W., & Dumoulin, S. O. (2021).

2307 Individualized cognitive neuroscience needs 7T: Comparing numerosity maps at 3T and 7T

2308 MRI. *Neuroimage*, 237, 118184.

2309

2310 *Acknowledgement of author contributions:*

2311 S. O. D. conceived the study. W. van der Z. developed the MR sequences. Y. C. collected and

2312 analyzed the data. W.Z. provided help with some of the analyses code. Y. C. wrote the paper.

2313 S. H., W. van der Z. and S. O. D. edited the paper. S. O. D. and S. H. provided supervision.

2314

2315 Supplementary figures of this chapter can be found in Appendix D.

2316

2317 **Abstract**

2318 The field of cognitive neuroscience is weighing evidence about whether to move from the
2319 current standard field strength of 3 Tesla (3T) to ultra-high field (UHF) of 7T and above. The
2320 present study contributes to the evidence by comparing a computational cognitive neuroscience
2321 paradigm at 3T and 7T. The goal was to evaluate the practical effects, i.e. model predictive
2322 power, of field strength on a numerosity task using accessible pre-processing and analysis tools.
2323 Previously, using 7T functional magnetic resonance imaging and biologically-inspired
2324 analyses, i.e. population receptive field modelling, we discovered topographical organization
2325 of numerosity-selective neural populations in human parietal cortex. Here we show that these
2326 topographic maps are also detectable at 3T. However, averaging of many more functional runs
2327 was required at 3T to reliably reconstruct numerosity maps. On average, one 7T run had about
2328 four times the model predictive power of one 3T run. We believe that this amount of scanning
2329 would have made the initial discovery of the numerosity maps on 3T highly infeasible in
2330 practice. Therefore, we suggest that the higher signal-to-noise ratio and signal sensitivity of
2331 UHF MRI is necessary to build mechanistic models of the organization and function of our
2332 cognitive abilities in individual participants.

2333

2334 **Keywords**

2335 Ultra-high field, BOLD, numerosity map, computational model, cognitive neuroscience

2336

2337

2338

2339

2340

2341

2342

2343

2344

2345

2346

2347

2348

2349

2350

2351 **Introduction**

2352 Cognitive neuroimaging studies typically require fast whole brain image acquisitions with high
2353 signal-to-noise ratio (SNR) and maximal sensitivity to small blood oxygenation level
2354 dependent (BOLD) signal changes for reliable detection. This is especially the case for
2355 computational neuroimaging where we go beyond the detection of activation to build
2356 computational models of neural function in individual participants (De Martino et al., 2018;
2357 Dumoulin & Knapen, 2018; Dumoulin & Wandell, 2008; Kay, Naselaris, Prenger, & Gallant,
2358 2008; Naselaris, Kay, Nishimoto, & Gallant, 2011; Wandell, 1999; Wandell & Winawer, 2015).
2359 The use of magnetic resonance imaging (MRI) systems operating at field strengths greater than
2360 3 Tesla (3T), i.e., ultra-high field (UHF) at 7T and above, is becoming popular in cognitive
2361 neuroscience since these systems provide greatly increased SNR and sensitivity to BOLD
2362 contrast.

2363 One of the earliest discoveries using UHF in the field of cognitive neuroscience was
2364 the existence of topographic maps that represent dimensions of numerical cognition (Cai,
2365 Hofstetter, van Dijk, et al., 2021a; B. M. Harvey et al., 2013; Ben M. Harvey & Dumoulin,
2366 2017a). Following studies, extended this finding of cognitive topographic maps and uncovered
2367 maps representing object size (Ben M. Harvey et al., 2015), time duration (Ben M. Harvey et
2368 al., 2020; Protopapa et al., 2019) and haptic numerosity (Hofstetter et al., 2021). These
2369 discoveries suggested that topographic principles common in primary sensory and motor
2370 cortices may also be an organizational principle of cognitive functions in association cortex.
2371 However, all these studies used 7T functional MRI (fMRI), and anecdotal reports suggested
2372 failure to reconstruct these maps at lower field strengths.

2373 Here, we ask whether these cognitive topographic maps can be reconstructed at 3T and
2374 we will use these maps and computational models to quantify the differences between 3T and
2375 7T. We focus on visual topographic numerosity maps. Numerosity, the set size of a group of
2376 items, is critical to guide human and animals' behaviour and decision (D. Burr & Ross, 2008;
2377 Carey, 2001; Andreas Nieder & Dehaene, 2009). Previously, using population receptive field
2378 (pRF) modelling (Dumoulin & Wandell, 2008) at 7T, we have demonstrated that neural
2379 population in fMRI recording sites (voxel) are selectively responding, i.e., tuned, to certain
2380 preferred numerosities and that this numerosity tuning can be captured with a logarithmic
2381 Gaussian model. Furthermore, different cortical locations have different preferred numerosities
2382 and these preferred numerosities increase systematically across the parietal cortex, i.e., forming
2383 a numerosity topographic map (Cai, Hofstetter, van Dijk, et al., 2021a; B. M. Harvey et al.,
2384 2013; Ben M. Harvey & Dumoulin, 2017a; Hofstetter et al., 2021).

2385 In this study, we measure BOLD responses to a range of numerosities at 3T and 7T,
2386 respectively, and use pRF modelling to evaluate the responses of the numerosity-selective
2387 neural populations. We compare the variance explained by the numerosity model to the
2388 measured responses at the two field strengths as a function of the number scan runs. In this
2389 way, we quantify the extent to which 7T outperforms 3T in terms of the model predictive power.
2390 Though there is already an extensive literature on comparisons between field strengths (Duong
2391 et al., 2003; Alexander Geißler et al., 2013; Pohmann, Speck, & Scheffler, 2016; van der Zwaag
2392 et al., 2009), this work directly compares the dependence of model predictive power on field
2393 strength in the field of computational neuroimaging.

2394

2395 **Methods**

2396 *Participants*

2397 We present data from three participants (one female, age range 22 – 45 years). All participants
2398 had normal or correct-to-normal visual acuity. All participants were well educated, with good
2399 mathematical abilities. Written informed consent was obtained before every scanning session.
2400 All experiments were approved by the ethic committee at University Medical Centre Utrecht.

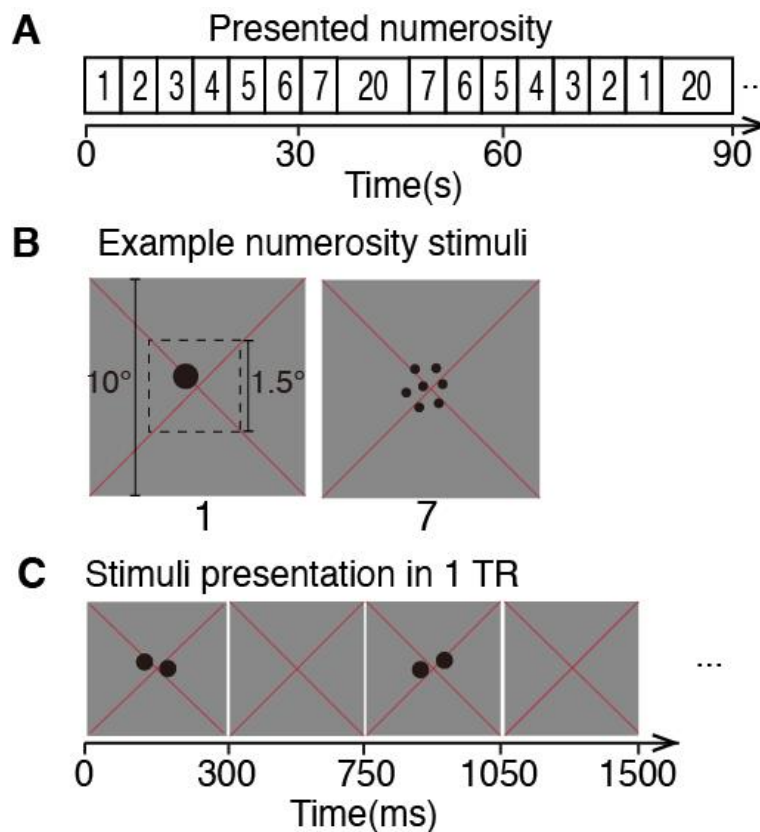
2401

2402 *Stimulus presentation*

2403 Visual stimuli were presented on a 69.84 x 39.29 cm LCD screen (Cambridge Research
2404 Systems) placed behind the 3T and the 7T MRI bores which was viewed through a mirror
2405 mounted on the coil. The distance from the mirror to the display screen was 210 / 220 cm at
2406 the 3T / 7T scanner rooms, respectively. The stimuli were adjusted to have equal visual angle
2407 on the two display screens. The display resolution was 1920 x 1080 pixels.

2408 The visual stimuli were generated in Matlab using PsychToolbox (Brainard, 1997;
2409 Kleiner et al., 2007; D G Pelli, 1997). A large red diagonal cross was displayed continuously
2410 across the entire screen (10.2° diameter), which served as an accurate fixation marker for
2411 participants. Stimuli consisting of various number of dots presented in the central 1.5°
2412 (diameter) of the visual field in a grey background. We used the “constant area” configuration
2413 from the original study (B. M. Harvey et al., 2013), which keeps the total surface area of all
2414 the presented dots combined constant of all the numerosities, ensuring equal luminance across
2415 all the dot arrays. The main numerosity stimuli of 1 to 7 dots were presented sequentially in
2416 ascending order, followed by a longer baseline period (13.5 s) containing 20 dots. Then the
2417 main stimuli were presented in descending order, followed by another baseline period (Figure

2418 5.1A). This sequence was repeated 4 times in each functional run. Before the first cycle
 2419 initialized, there was a pre-scan period (12 s) presenting the baseline numerosity of 20 dots.
 2420 Dots of all the numerosities were positioned randomly and homogeneously to avoid any links
 2421 between numerosity and visual position and grouping effects (Figure 5.1B). Numerosity
 2422 stimuli were presented briefly (300 ms) as black dots to ensure participants did not have time
 2423 to count. This was repeated every 750 ms, each time with a new random dot pattern presented,
 2424 with 450 ms presentation of a uniform grey background between pattern presentations. Each
 2425 pattern of the same numerosity was repeatedly presented six times, over 4500 ms,
 2426 corresponding to 3 fMRI volume acquisitions (repetition time, i.e., TR), before the numerosity
 2427 changed (Figure 5.1C). In 10% of the stimuli presentations, dots were shown in white instead
 2428 of black. Participants were instructed to press a button when they saw white dots to ensure they
 2429 were paying attention to the stimuli during fMRI acquisition. No numerosity judgements were
 2430 required during the experiment. Participants responded correctly on 90-100% of the white dots
 2431 presentations in each run.



2432
 2433 **Figure 5.1. Illustration of the experimental design and stimuli presentation.** (A) Presented
 2434 stimulus sequence in which numerosities consisting of 1 to 7 dots were shown in an ascending
 2435 order followed by a baseline period containing 20 dots, then descended from 7 to 1 followed
 2436 by another baseline period. (B) Two examples of numerosity stimuli presented to the

2437 participant in the scanner. The dot array covered the central 1.5° (visual angle) diameter within
 2438 a 10.2° diameter mean-luminance (grey) screen. A large, thin, red fixation cross passed
 2439 diagonally through the center of the display, and through the center of the dot array. Participants
 2440 were asked to fixate on the intersection of the cross and press a button when dots were shown
 2441 in white. (C) Schematic representation of stimuli presentation in one fMRI volume acquisition
 2442 (TR). Numerosity stimulus was presented briefly (300 ms), followed by a 450 ms presentation
 2443 of a uniform grey background before a new random positioned dot pattern presentation. Each
 2444 pattern of the same numerosity was repeatedly presented six times, over 4500 ms,
 2445 corresponding to 3 TRs, before the numerosity changed.

2446

2447 *MRI acquisition*

2448 Scanning was carried out on two Philips Achieva scanners operating at 3T and 7T. Functional
 2449 data were acquired using 32-channel receive head coils (Philips at 3T and Nova Medical at 7T).
 2450 A multi-slice, single-shot gradient echo (GE) echo planar imaging (EPI) sequence was used at
 2451 both scanners. Acquisition parameters for the EPI are listed in Table 1. At both systems, all
 2452 functional runs had 248 volumes and each session had 8 runs. Three 3T and two 7T sessions
 2453 were acquired for each participant on separate days. Anatomical images of each participant
 2454 were collected at 7T using an MP2RAGE sequence (Marques et al., 2010) in separate sessions.
 2455 The key MR parameters of the T_1 were as follows: matrix size = $273 \times 367 \times 367$, voxel size
 2456 = $0.64 \times 0.64 \times 0.64 \text{ mm}^3$, $TR_{MP2RAGE} = 5.5 \text{ s}$, $TR/TE = 6.2/2.2 \text{ ms}$, $TI_1/TI_2 = 0.8/2.7 \text{ s}$, flip
 2457 angle = $7^\circ/5^\circ$. MP2RAGEs are relatively insensitive to the B_1 -inhomogeneities present at 7T
 2458 and yield good segmentation and co-registration results at high spatial resolution (Haast,
 2459 Ivanov, & Uludağ, 2018; Huntenburg, Steele, & Bazin, 2018).

2460

Table 1. Acquisition parameters for the acquired EPI at 3T and 7T

Field strength (B_0)	TR (ms)	Voxel size (mm^3)	TE (ms)	FA ($^\circ$)	FOV (mm^2)
3T	1500	1.98 x 1.98 x 2.00	28	80	46 x 190 x 190
7T	1500	1.98 x 1.98 x 2.00	25	70	50 x 190 x 190

2461

2462 *Data pre-processing*

2463 Anatomical data pre-processing included skull stripping and resampling to a spatial resolution
 2464 of $0.6 \times 0.6 \times 0.6 \text{ mm}^3$. T_1 images were automatically segmented using cbs-tools (Bazin et al.,
 2465 2014) and then manually edited to minimize auto-segmentation errors using ITK-SNAP

2466 (Yushkevich et al., 2006) (www.itksnap.org/). This provides a highly accurate description of
2467 the cortical surface, an anatomical segmentation space used for analysis of cortical organization.
2468 The cortical surface was reconstructed at the grey-white matter border and rendered as a
2469 smoothed 3D surface. Pre-processing of the functional data was performed using AFNI (Cox,
2470 1996; Cox & Hyde, 1997). The first 8 volumes of each run were discarded to account for signal
2471 equilibrium and participants' adaptation to the immediate environment. Head movement and
2472 motion artefacts between and within the remaining volumes were measured and corrected for.
2473 All functional images collected at the same session were averaged to generate a common mean
2474 EPI image.

2475 Pre-processed functional data were then analysed in mrVista, which is freely available
2476 at (<https://github.com/vistalab/vistasoft>). For each participant, at every session, the mean EPI
2477 image was aligned to the anatomy. Individual functional images were then imported and co-
2478 registered to the same anatomical space using the same transformation. To vary the signal
2479 strength, functional images were averaged with a variable number of runs, e.g., 8, 16 or 24 runs
2480 from the 3T and 8 or 16 runs from the 7T sessions. Subsequently, the averaged datasets were
2481 collapsed onto the nearest point on the cortical surface across depth, which generated a (folded)
2482 2-dimensional grey matter surface. pRF modelling and subsequent statistical analyses were
2483 done at this space, except for the validation analyses using data points across cortical depth
2484 (i.e., un-collapsed data, see below). No spatial or temporal smoothing was applied to the
2485 functional data.

2486

2487 *Numerosity pRF modelling*

2488 We applied pRF modelling to the data using a model that was developed to estimate numerosity
2489 tuning properties in human brains (Dumoulin & Wandell, 2008; B. M. Harvey et al., 2013).
2490 Specifically, a one-dimensional logarithmic model was adopted to predict neuronal responses
2491 at each stimulus time point of the numerosity presentation. The model describes tuning in
2492 logarithmic numerosity space using a Gaussian function characterized by two parameters:
2493 preferred numerosity (central position) and tuning width (standard deviation). A prediction of
2494 the neural response time course was produced by overlapping the stimulus at each time point
2495 with this tuning model. Then by convolving this prediction with a haemodynamic response
2496 function (HRF), a predicted time course was generated. For each voxel on the 2D cortical
2497 surface, the parameters were chosen from the prediction that fits the data most closely by
2498 minimizing the sum of squared errors between the predicted and observed fMRI time series.
2499 The model goodness-of-fit was described by the variance explained (R^2). The neural responses

2500 of each voxel were described by the pRF model with a particular set of parameters. This
2501 modelling procedure was applied to the pre-processed functional data averaged with a variable
2502 number of runs, e.g., 8, 16 or 24 runs from the 3T or 8 and 16 runs from the 7T sessions. Thus,
2503 we reconstructed the numerosity maps at each field strength, for each participant, respectively.

2504

2505 *Definition of region of interest*

2506 We defined region of interest (ROI) on the participants' right hemispheres at the intraparietal
2507 sulcus (IPS), a key brain region for numerosity perception (S. Dehaene, 2001; Feigenson et al.,
2508 2004; Kutter et al., 2018; Andreas Nieder, 2016; Andreas Nieder et al., 2002b), and was the
2509 first location where a topographic map of numerosity was found (B. M. Harvey et al., 2013).
2510 In this study, we refer to this ROI as NPC1 (numerosity map in parietal cortex 1) as defined in
2511 previous studies (Ben M. Harvey & Dumoulin, 2017a) and following naming conventions of
2512 newly discovered visual field maps in human cortex where homologues to non-human primates
2513 are unclear (Wandell et al., 2007). NPC1 lays in the right hemisphere, on the gyrus posterior
2514 to the superior postcentral sulcus, and its center position was found at (22, -61, 60) in Montreal
2515 Neurological Institute (MNI) coordinates (B. M. Harvey et al., 2013; Ben M. Harvey &
2516 Dumoulin, 2017a).

2517

2518 *Model-based analysis*

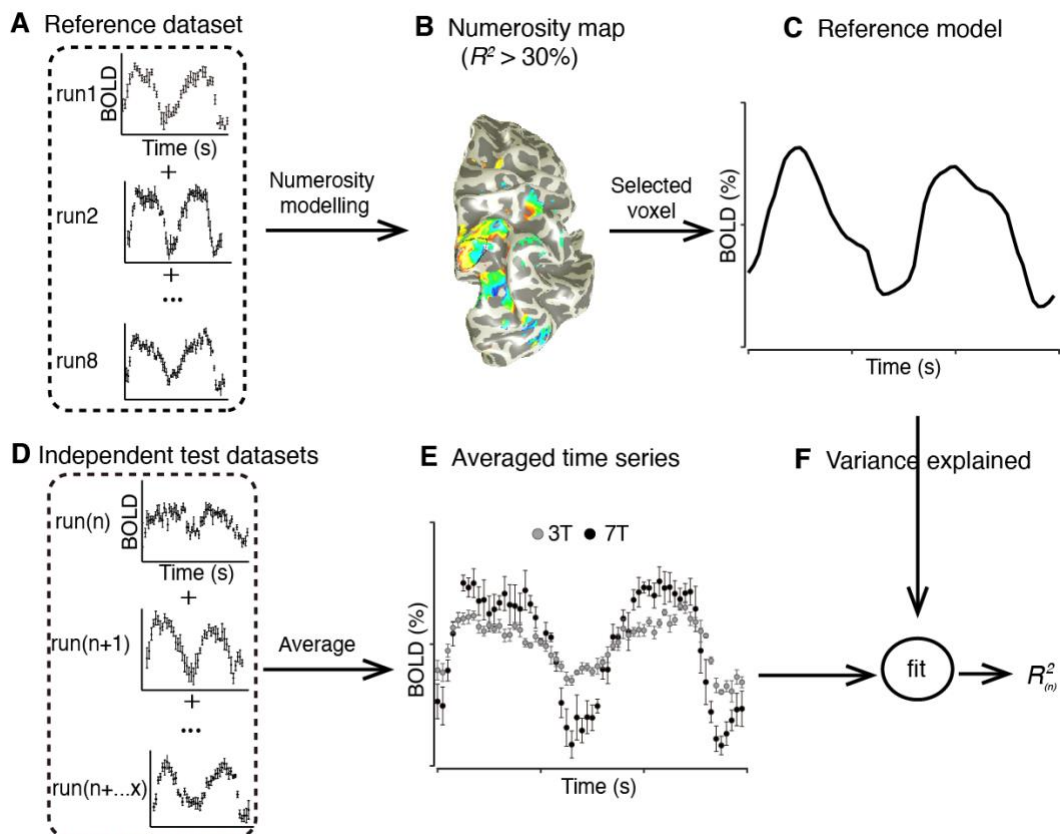
2519 To compare the model predictive power of the two field strengths, without relying on a
2520 predefined model for the functional responses, reference datasets were generated by averaging
2521 8 functional runs from each field strength, respectively (Figure 5.2A). The remaining
2522 individual functional runs were taken as independent test datasets (Figure 5.2D). Every session
2523 was taken as the reference dataset in turn, including all 3T or 7T sessions. Hence, when taking
2524 one 7T session as the reference dataset, the independent test dataset included 8 functional runs
2525 from the other 7T session and 24 runs from the 3T sessions, etc. More comparisons between
2526 reference dataset and independent dataset were made by averaging runs across scanning
2527 sessions. The functional runs of the two 7T sessions were mixed based on odd or even order,
2528 resulting in 4 new reference datasets. Similarly, we created 3 new reference datasets consisting
2529 of eight 3T runs by recruiting every 2 runs from the total 24 3T functional runs. Thus, for each
2530 field strength, six different reference datasets and the remaining runs as test datasets were
2531 generated for further analysis.

2532 We selected voxels from the reference dataset based on two criteria: (1) variance
2533 explained (R^2) exceeded 30% and (2) the preferred tuning fell within the presented numerosity

2534 range (Figure 5.2B). Model predicted time series of the selected voxels in NPC1 were extracted
 2535 as the reference model (Figure 5.2C). For each selected voxel, we extracted the time series of
 2536 each individual run in the independent test datasets (Figure 5.2D). These time series were
 2537 shuffled ($n = 100$) and averaged with increasing number of runs included to produce a new
 2538 time series of the voxel (Figure 5.2E). By fitting the reference model with the averaged time
 2539 series, we obtained the variance explained ($R_{(n)}^2$) of the reference model as a function of
 2540 increasing number of runs (Figure 5.2F).

2541 We iterated this procedure 6 times for each field strength while splitting the data into
 2542 different pairs of reference and test datasets. We averaged the results of each field strength to
 2543 compare the model predictive power between the two field strengths as a function of number
 2544 of runs. We then performed a linear fit of how many 3T runs are required to have the same
 2545 variance explained of one 7T run. This procedure was done for each participant individually.
 2546 Finally, an overall factor between 3T and 7T in terms of number of runs was obtained by
 2547 averaging the linear fits across participants.

2548



2549

2550 **Figure 5.2.** Flowchart of the model-based analysis procedure comparing the predictive power
 2551 between field strengths. (A) Eight functional runs (as one session) of either 3T or 7T were
 2552 averaged and regarded as a reference dataset. (B) Numerosity modelling was performed for

2553 each reference dataset. Voxels with more than 30% of the variance explained (R^2) were selected.
 2554 (C) The ‘reference model’ was extracted from each selected voxel. (D) The remaining
 2555 individual functional runs were taken as independent test datasets, i.e., the 3T and 7T test data.
 2556 (E) The test data was averaged with increasing number of runs to produce averaged time series
 2557 at 3T (grey dots) and 7T (black dots), respectively. (F) By fitting the averaged time series with
 2558 the reference model, we calculated the variance explained of the reference model as a function
 2559 of increasing number of runs ($R_{(n)}^2$). We iterated this procedure 6 times while splitting the data
 2560 into different reference and test datasets.

2561

2562 *Calculation of noise ceiling*

2563 To quantify the maximum explainable variance given the noise in the data, we computed the
 2564 noise ceiling (NC) (Lage-Castellanos, Valente, Formisano, & De Martino, 2019; Machens,
 2565 Wehr, & Zador, 2004; Mante, Frazor, Bonin, Geisler, & Carandini, 2005). Specifically, we
 2566 employed the method described by Machens et al. (2004). Briefly, we calculated the noise
 2567 ceiling as the fraction of variance in the residual noise (σ_η^2) over the variance in the response
 2568 power (σ_s^2):

$$2569 \quad NC = 1 - \frac{\sigma_\eta^2}{\sigma_s^2} \quad (1)$$

2570 This is basically the maximal variance explained given the noise in the data. The response
 2571 power is defined as the average variance over the session (s_t) with $t = 1 \dots M$ time-points:

$$2572 \quad \sigma_s^2 = \left\langle \frac{1}{M} \sum_t s_t^2 \right\rangle \quad (2)$$

2573 the variance in the residual noise is estimated as:

$$2574 \quad \sigma_\eta^2 = \frac{n}{n-1} \left[\left\langle \frac{1}{M} \sum_t s_t^2 \right\rangle - \frac{1}{M} \sum_t \langle s_t \rangle^2 \right] \quad (3)$$

2575 where n indicates the number of sessions, angular brackets denote averaging over sessions.
 2576 Basically, adding up the variance of independent sessions will include the noise in each session,
 2577 while computing the variance after averaging the sessions will remove the noise between
 2578 sessions. Their difference is an estimate of the residual noise. The assumptions behind this
 2579 estimation are minimal: the noise should have zero mean and a non-infinite variance, and
 2580 should be independent between sessions.

2581 As we used one session as a reference dataset in the analysis, we computed the noise
 2582 ceiling across sessions each consisting of 8 runs either at 3T or 7T. Since the number of voxels

2583 selected for further analysis varied based on the reference sessions (see Figure 5.2 of the
2584 analysis flowchart), the noise ceiling was calculated with the voxels selected based on different
2585 reference sessions in turn for each iteration. We averaged the noise ceiling of all the six
2586 iterations to have the noise ceiling of one session (i.e. 8 runs) at each field strength.

2587

2588 *Calculation of tSNR*

2589 Temporal SNR (tSNR) is defined on a voxel-wise manner as the ratio of the mean across time
2590 divided by the standard deviation across time. To avoid bias by large response in active grey
2591 voxels, we calculated tSNR in white matter (WM) in addition to grey matter (GM). A whole-
2592 brain WM mask was defined from the segmented anatomy for each participant. The ROI for
2593 calculating tSNR in GM is confined to the numerosity map NPC1. We calculated tSNR as the
2594 average tSNR across voxels in the WM mask and GM ROI of each individual run at 3T and
2595 7T, respectively. We reported the average tSNR across runs and participants at each field
2596 strength, respectively.

2597

2598 *Comparing preferred numerosity and tuning width estimates at 3T and 7T*

2599 Pearson correlation analysis was performed between numerosity preference and tuning width
2600 estimates derived from the 3T and 7T data. This included the voxels that had variance explained
2601 above 30% in the maps constructed using all the acquired 3T (24 runs) or 7T (16 runs) data,
2602 and the preferred tuning fell within the presented range. Taking into account the functional
2603 resolution of the recording sites, the total number of data points used to calculate correlation's
2604 probability was reduced by the factor by which functional voxels were up-sampled onto the
2605 2D cortical surface. We quantified the similarity between the pRF estimates at 3T and 7T by
2606 dividing the subtraction of two estimates (e.g., X_{7T} and X_{3T}) by their mean, and converted to
2607 percentage: $((X_{7T} - X_{3T}) / ((X_{7T} + X_{3T})/2)) * 100\%$.

2608

2609 *Validation analyses*

2610 In the model-based analysis we used the reference model and compared the variance explained
2611 to the test datasets at 3T and 7T. This analysis depends on the accuracy of the model. In order
2612 to perform a model-free analysis, we extracted the time series of the selected voxels (same
2613 criteria as in the model-based analysis) from the reference datasets as a reference time series.
2614 Analogous to the model-based analysis, the time series of each individual run in the test
2615 datasets (3T or 7T) were averaged with increasing number of runs to produce the averaged time
2616 series for each voxel. Applying with a Pearson correlation analysis, we obtained the correlation

2617 coefficients between the reference time series and the averaged time series from the test
2618 datasets as a function of increasing number of runs ($r_{(n)}$). This procedure is illustrated in
2619 Supplementary Figure 5.1.

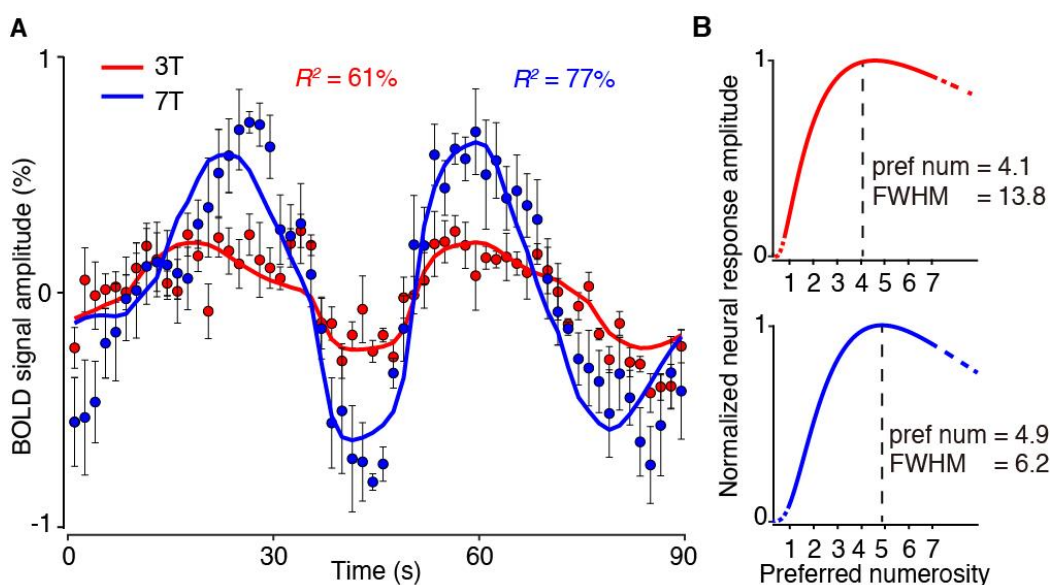
2620 Furthermore, we validated our results by performing both the model-based and model-
2621 free analyses using all data points across the cortical depth (i.e., un-collapsed data), and using
2622 all the data points within the ROI, without any threshold.

2623

2624 3. Results

2625 *BOLD responses of numerosity-selective neural populations at 3T and 7T*

2626 In Figure 5.3A, we show two examples of representative time series and models. The
2627 representative recording site was selected randomly from the 3T data points which has the
2628 averaged variance explained among the selected voxels. We extracted the time series of this
2629 recording site from the datasets that averaging 24 and 16 runs at 3T and 7T, respectively. The
2630 7T time series (blue points) exhibits larger response amplitude than the 3T time series (red
2631 points). The two model predictions explain 61% and 77% of the variance in these time series
2632 recorded at 3T (red line) and 7T (blue line), respectively. The higher percentage BOLD signal
2633 change and variance explained at 7T confirms the higher BOLD signal sensitivity and SNR at
2634 ultra-high field. The pRF models with a particular set of parameters that best fitted to each time
2635 series are shown in Figure 5.3B. The peak response amplitude indicates the preferred
2636 numerosity and the full width half maximum (FWHM) reflects the tuning width of the pRF of
2637 this voxel. At this example recording site, the preferred numerosity was slightly smaller and
2638 the tuning width was larger when estimated at the 3T data (upper panel) than at the 7T data
2639 (lower panel).



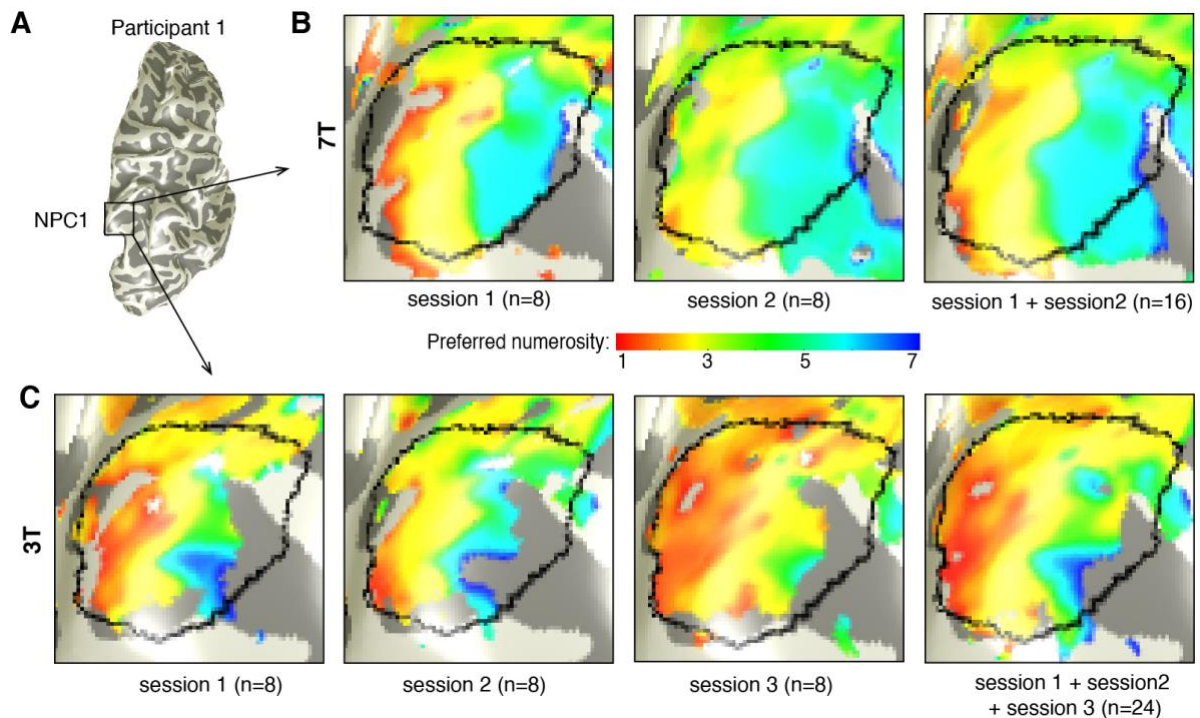
2640

2641 **Figure 5.3. Numerosity-selective neural population responses recorded at 3T and 7T. (A)**
2642 Example fMRI time series extracted from the 3T dataset (average of 24 runs; red points) and
2643 7T dataset (average of 16 runs; blue points), respectively. Points represent mean response
2644 amplitudes and error bars represent standard error across four repeated stimulus cycles.
2645 Coloured lines indicate the model predictions of the 3T (red) and 7T (blue) time series and R^2
2646 denotes the amount of variance explained by the model. **(B)** Profiles of the pRF models that
2647 best fitted the 3T (upper panel) and the 7T (lower panel) time series in **A**. The pRF model is
2648 described by a logarithmic Gaussian tuning function with two parameters: preferred
2649 numerosity (pref num), indicated by the peak response amplitude, and tuning width, defined
2650 by the full width at half maximum (FWHM). Dash lines indicate numerosities outside the
2651 presented stimulus range.

2652

2653 *Numerosity map is more reliably detected at 7T than at 3T*

2654 Figure 5.4 presents the reconstructed numerosity maps of participant 1 using increasing number
2655 of runs acquired at 3T and 7T. Consistent with previous studies (Cai, Hofstetter, van Dijk, et
2656 al., 2021a; B. M. Harvey et al., 2013; Ben M. Harvey & Dumoulin, 2017a), we found
2657 numerosity-selective neural populations in the parietal cortex that are topographically
2658 organized. We found a larger cortical extend above the variance explained threshold of 30% at
2659 the 7T (mean number of voxels \pm SE: 904 ± 56) than the 3T data (695 ± 28). The 3T data were
2660 noisier and therefore could not be adequately captured by the model. At both field strengths,
2661 as the number of runs increased, the noise reduced and the topographic maps became more
2662 robust.



2663

2664

2665

2666

2667

2668

2669

2670

2671

2672

2673

2674

2675

2676

2677

2678

2679

2680

2681

2682

2683

Figure 5.4. The topographic numerosity maps become more robust with increasing numbers of runs, both at 3T and 7T. (A) Anatomical rendering of the right cerebral cortex. Black frame outlines the region of interest (i.e. NPC1) in the intraparietal sulcus at the right hemisphere of participant 1. (B) Topographic maps of numerosity-selective neural populations at NPC1 (black box in A) reconstructed using data of 8 functional runs at the two 7T scanning sessions, and all the runs across sessions (n=16). (C) Topographic maps reconstructed using data of the three 3T scanning sessions, and all the runs across sessions (n=24). Maps show preferred numerosities of cortical recording sites with over 30% of the variance explained. A larger cortical extend above the threshold at the 7T maps than the 3T maps. These maps become more reliable and comparable at 7T and 3T, with increasing number of runs (right panels).

As Figure 5.4 shows, the numerosity maps obtained at 3T were similar to those obtained at 7T. This was also found for the other participants (Supplementary Figure 5.2). We then quantified the similarity between the preferred numerosity and tuning width estimates at the two field strengths by a Pearson correlation analysis. The Pearson correlation analysis indicated that the numerosity preference estimates derived from the two field strengths were highly correlated ($r > 70\%$) (Supplementary Figure 4.3A). However, this was not the case for tuning width (Supplementary Figure 5.3B). Overall, the preferred numerosity estimates at 7T were slightly higher than at 3T, while the tuning width estimates were broader when recorded at 3T (Supplementary Figure 5.3C). We speculate that the smaller tuning width at 7T maybe

2684 mediated by the larger sensitivity to smaller vessels (Duong et al., 2003; Yacoub et al., 2001),
 2685 and the small differences in preferred tuning maybe influenced by the tuning width. However,
 2686 given the sensitivity of tuning width estimates to algorithmic consideration, e.g., the HRF
 2687 estimations (Dumoulin & Wandell, 2008; Lerma-Usabiaga, Benson, Winawer, & Wandell,
 2688 2020) and data quality, we refrain from drawing too strong a conclusion.

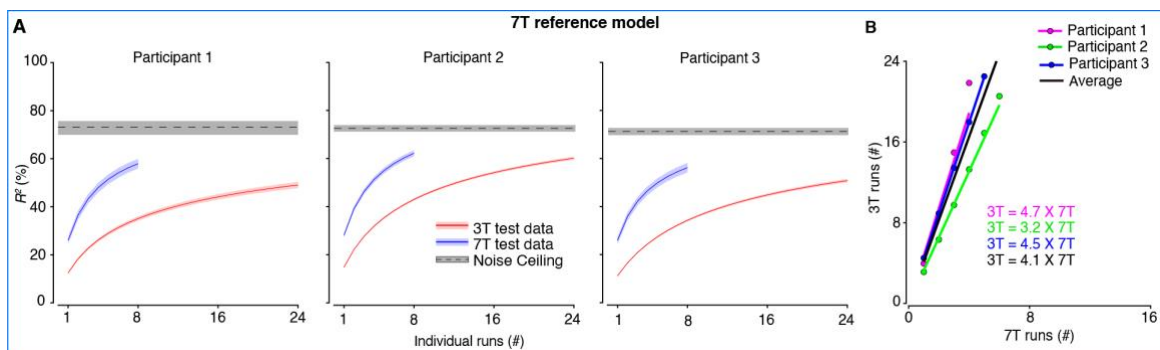
2689

2690 *One 7T run has four times the model predictive power of one 3T run*

2691 Figure 5.5A shows the variance explained by the 7T reference model as a function of increasing
 2692 number of runs of 3T and 7T data, together with the noise ceiling of the 7T data in one session
 2693 (i.e. 8 runs, dashed lines). The variance explained increased as the number of runs increased at
 2694 both field strengths. However, the increase in variance explained was faster at 7T than at 3T.
 2695 In other words, more 3T runs were required to reach the same predictive power at 7T.
 2696 Furthermore, the reference model always captured more variance of the 7T responses, thus the
 2697 resulting variance explained was always higher than that at 3T. For example, averaging 24 3T
 2698 runs ($R^2 = 53\%$) still could not reach the same variance explained of averaging 8 7T runs (R^2
 2699 $= 59\%$) for any of the participants.

2700 The model predictive power is constrained by the noise present in the actual response.
 2701 To quantify the maximum explainable variance (in one session) given the noise in the data, we
 2702 computed the noise ceiling (see Methods). As shown in Figure 5.5A, averaging 24 3T runs or
 2703 averaging 8 7T runs always yielded a lower predictive power than the noise ceiling of one 7T
 2704 session (8 runs).

2705 Next, we then calculated how many 3T runs were required to achieve the same model
 2706 predictive power as a function of the number of 7T runs (Figure 5.5B). On average, one 7T run
 2707 has 4 times the variance explained of one 3T run using the 7T reference model.



2708

2709 **Figure 5.5. Quantification of field strength effects on pRF model predictive power as a**
 2710 **function of number of runs, using the reference model derived from 7T reference datasets.**

2711 (A) The variance explained of the reference model as a function of increasing number of runs

2712 at 3T (red) and 7T (blue). Shaded areas indicate standard errors of the mean over iterations
2713 using different reference datasets ($n=6$). The noise ceiling (dashed line) with 95% confidence
2714 intervals (grey bars) represents the maximum explainable variance (of one 7T session, i.e. 8
2715 runs) given the noise in the data. **(B)** Linear fits of the number of runs required at 3T to have
2716 equivalent model predictive power of one 7T run. Coloured-coded texts indicate the factor
2717 between 3T and 7T runs to achieve the same variance explained for each participant. On
2718 average, one 7T run has 4 times the model predictive power of one 3T run using the 7T
2719 reference model (black).

2720

2721 Similar results were obtained using the reference model derived from 3T reference
2722 datasets (Supplementary Figure 5.4). Averaging the same number of 3T runs ($n = 8$) could not
2723 reach the noise ceiling of one 3T session. However, the predictive power on the 3T and 7T data
2724 increased with increasing number of runs and ultimately outperformed the noise ceiling of 3T
2725 when more than 8 runs were included (Supplementary Figure 5.4A). When using the 3T
2726 reference model, the number of 3T runs to match the 7T data was smaller (Supplementary
2727 Figure 5.4B), likely due to the noisier data quality at 3T as indicated by the lower noise ceiling,
2728 and which likely also resulted in a noisier reference model. Overall, the 7T data had a higher
2729 noise ceiling (mean \pm SD: 72% \pm 2.6%) than the 3T data (55% \pm 3.7%). These results suggest
2730 that 3T data is noisier and the benefits in model predictive power is due to improved data
2731 quality, rather than model accuracy.

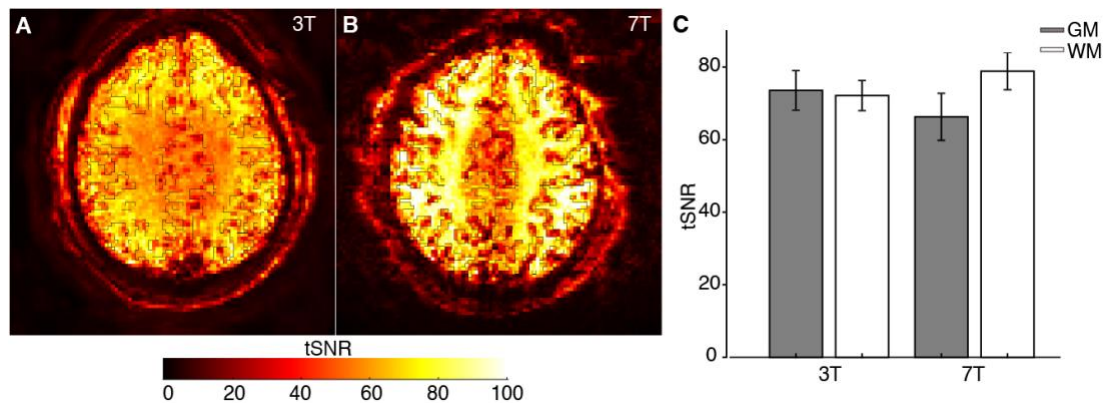
2732 Last, we found similar results using model-free analyses of voxel-wise time series
2733 correlation (Supplementary Figure 5.5), model-based analyses using un-collapsed data points
2734 (Supplementary Figure 5.6) and using all data points within NPC1, i.e. no thresholding
2735 (Supplementary Figure 5.7).

2736

2737 *Comparison of tSNR at 3T and 7T*

2738 Figure 5.6 shows the tSNR maps of one example individual run at 3T (Figure 5.6A) and 7T
2739 (Figure 5.6B), and the averaged tSNR in white matter and grey matter across all runs and
2740 participants at the two field strengths (Figure 5.6C). On average, one 7T run has higher tSNR
2741 in white matter (mean \pm SE: 79 \pm 4) than that at 3T (72 \pm 2). However, at the cortical grey
2742 matter of the numerosity map (NPC1), on average, 3T has higher tSNR (74 \pm 4) than 7T (66 \pm
2743 6) in an individual run. The difference between cortical GM and WM tSNR likely reflects the

2744 increased contributions of stimulus-driven BOLD signal fluctuations and physiological noise
2745 present in cortex at 7T.



2746
2747 **Figure 5.6. Comparison of tSNR at 3T and 7T.** (A, B) Example tSNR maps of one 3T run
2748 (A) and one 7T run (B). Black lines outline the white matter (WM) mask determined from the
2749 segmented anatomy of the same participant. (C) The averaged tSNR of 3T and 7T in grey
2750 matter (GM) at the region of interest of the numerosity map NPC1 (grey bars) and WM (white
2751 bars) in a functional run. Error bars indicate the standard errors of the mean over all the
2752 individual runs of all the participants. Overall, 7T has higher tSNR in WM, while 3T has higher
2753 tSNR in the task-related GM, which likely reflects the increased contributions of stimulus-
2754 driven BOLD signal fluctuations and physiological noise present in the cortex at 7T.

2755

2756 Discussion

2757 We recorded BOLD responses of numerosity-selective neural populations in human parietal
2758 cortex at 3T and 7T, respectively. We used identical numerosity stimuli and tasks and a similar
2759 functional MRI sequence which we optimized for each field strength. We applied identical pre-
2760 processing pipeline and analysed the data using biologically-inspired model-based analyses
2761 (Dumoulin & Wandell, 2008). Subsequently, we quantified the number of runs required to
2762 detect reliable numerosity maps at 3T, compared to 7T, for individual participants. Field
2763 strength effects on the functional data were examined using model predictive power. We were
2764 able to reconstruct the topographic numerosity maps in the intraparietal sulcus at 3T. However,
2765 the topographic maps derived from the 3T data were less reliable and required much more data
2766 than typically acquired in the field. The numerosity maps at both field strengths became more
2767 reliable with increasing number of runs, though the rate of increase was higher at 7T. On
2768 average across participants, one 7T run had about 4 times the model predictive power of one
2769 3T run.

2770 To acquire comparable data at the two different field strengths, we utilized a GE EPI
2771 sequence that we optimized to ensure a good SNR and signal strength at both field strengths.
2772 Specifically, a voxel volume size of $1.98 \times 1.98 \times 2.00 \text{ mm}^3$ was used at both fields. At 7T, the
2773 TE was close to the tissue T_2^* and hence optimum for BOLD contrast, while the TE at 3T (28
2774 ms) was relatively short compared to the grey matter T_2^* (Peters et al., 2007). Such a short TE
2775 is very widely used at 3T to allow acquisition of a higher number of slices in an achievable TR
2776 (Clare, 1997; Volz, Callaghan, Josephs, & Weiskopf, 2019). At both field strengths the FA was
2777 set close to the Ernst angle, and as a result, it was slightly higher at 3T (80°) than at 7T (70°).
2778 Though obviously, these settings influence the results, we do not believe that they bias the
2779 results to favour one field strength over the other.

2780 Previous studies show that imaging at UHF provides a leap forward in both higher SNR
2781 and BOLD signal sensitivity. In the context of fMRI, the static image SNR reflects MRI signal
2782 strength over the noise present in the image in the absence of signal. Pohmann et al., (2016)
2783 demonstrated that the image SNR showed a distinctly supralinear increase with field strength
2784 by a factor of 3.10 ± 0.20 from 3T to 7T, and 1.76 ± 0.13 from 7T to 9.4T over the entire
2785 cerebrum. However, fMRI signals include contributions from thermal noise and correlated
2786 interference due to head motion, scanner instability and non-neuronal physiological noise
2787 arising from cardiac and respiratory fluctuations. As the magnetic field strength increases, the
2788 relative contribution of non-neuronal physiological noise is also increased (Triantafyllou et al.,
2789 2005). If physiological noise contributions dominate over the thermal noise in the imaging
2790 voxel, the SNR is independent of signal strength (Krüger & Glover, 2001), resulting in a
2791 reduced ability to detect activation-induced signal changes. Although the physiological noise
2792 contribution is higher at UHF, the noise effect would be cancelled out when averaging multiple
2793 functional runs as the cardiac and respiratory signals are not task-locked. Thus, we believe that
2794 the data here presented after averaging over runs have only a small contribution from
2795 physiological noise sources.

2796 Furthermore, magnetic field strength increase leads to significant increase of the BOLD
2797 contrast (Gati, Menon, Uffurkil, & Rutt, 1997; Krasnow et al., 2003). The BOLD signal arises
2798 from the field inhomogeneity differences induced by the paramagnetic deoxyhaemoglobin in
2799 the capillaries and venous vessels and the surrounding tissue, which manifests as signal
2800 changes in the order of a few percent (Logothetis, 2002). This BOLD contrast scales
2801 approximately linearly with field strength. A quantitative analysis conducted by van der Zwaag
2802 et al., (2009) found that in brain tissue, the BOLD contrast (approximated by the relaxation

2803 rate change, ΔR_2^*) increases linearly with field strength (0.98 ± 0.08 at 3T and 2.55 ± 0.22 at
2804 7T). Yacoub et al., (2001) found a supralinear field strength dependence of BOLD contrast that
2805 increased by a factor of 2.13 ± 0.23 when going from 4T to 7T. The resulting increase in BOLD
2806 contrast is of great benefit for fMRI studies and can be exploited to reduce the number of
2807 functional runs required to demonstrate robust activation.

2808 In the current study, the BOLD responses recorded at 7T benefit both from the
2809 increased SNR and augmented BOLD contrast, resulting in the factor of 4 times the number of
2810 3T runs required to achieve equivalent model predictive power of one 7T run. The factor of the
2811 number of 3T runs to match the 7T data was smaller using 3T data as reference compared to
2812 using 7T data as reference. We suspect this is due to the noisier data quality of 3T data. Noisier
2813 data results in a pRF model that is less accurate, which in turn limits the amount of variance in
2814 the test data it can explain. The lower noise ceiling of 3T data than 7T data also indicate the
2815 noisier data quality at 3T. Overall, the 7T data is less noisy than the 3T data, yielding the higher
2816 noise ceiling. However, taking into account the noise in the 3T data, the model predictive power
2817 is comparable between different field strength. In other words, relative to the noise ceiling, the
2818 pRF model is applicable and independent to field strengths. Furthermore, the similar results
2819 obtained from the model-free analysis suggest that the benefits of using less 7T runs to obtain
2820 robust numerosity maps is induced by data quality but not model accuracy.

2821 Akin to previous studies we found 7T has higher tSNR than 3T in white matter. The
2822 higher tSNR in white matter at 7T is related to the higher SNR at UHF as tSNR will increase
2823 with increasing image SNR, until a field-strength dependent plateau value is reached (Krüger
2824 & Glover, 2001; Triantafyllou et al., 2005). The tSNR is lower in grey matter (i.e., NPC1) at
2825 7T than 3T. This is likely caused by the larger (stimulus-driven) BOLD responses and higher
2826 physiological noise contributions at 7T. The different behaviour of tSNR in grey and white
2827 matter is more pronounced in this study because of the extra task-induced variance and the
2828 relatively short TE at 3T, e.g., compared to studies that fixed $TE=T_2^*$ in a resting state
2829 acquisition (Triantafyllou et al., 2005). The discrepancy that the grey matter tSNR at 7T is
2830 lower than at 3T while the noise ceiling is higher, is due to the fact that task-induced BOLD
2831 fluctuations are ‘signal’ when calculating the noise ceiling, while they contribute to ‘variance’
2832 in the tSNR calculation.

2833 This finding is in agreement with previous literature. To achieve a significant statistical
2834 power, many runs of a single participant and/or groups of participants are acquired at
2835 conventional field strength scanner (i.e. 3T). In such a way, noise present in fMRI time series

2836 is reduced when multiple runs are averaged together, which leads to a monotonic increase in
2837 statistical significance as increasing number of runs. Using a GO/NOGO task, Torrisi et al.
2838 (2018) compared GLM-based activation analyses and showed significant gains in statistical
2839 power at 7T and fewer subjects were necessary at group level to match the same power at 3T.
2840 Gonzalez-Castillo et al. (2012) acquired 100 functional runs at each of the 3 participants at 3T
2841 and later performed a similar study at 7T (Gonzalez-Castillo et al., 2015), where much less 7T
2842 runs (~25 runs) were required to reach the same percent of grey matter voxels above a statistical
2843 threshold (activated) as 100 3T runs could achieve. This is a similar factor of 4 times
2844 improvement as we suggest here. At UHF scanner (i.e. 7T), higher SNR and tSNR will reduce
2845 the number of runs required from a single participant to detect activation with an expected
2846 statistical power (Murphy, Bodurka, & Bandettini, 2007). We note that this is particularly
2847 relevant for computational neuroimaging, where signals of single voxels differ and are
2848 modelled separately. Furthermore, because the topographic map locations, size and
2849 orientations vary between participants (Dumoulin et al., 2000; B. M. Harvey et al., 2013;
2850 Wandell et al., 2007), averaging of participants in a common space is often not feasible.

2851 This study differs from other studies comparing field strengths dependence on BOLD
2852 signal in three aspects: first, we used a numerosity task that activated brain regions associated
2853 with high level cognition. This experimental design was the same as the paradigm initially used
2854 to uncover the topographic representation of numerosity at UHF (B. M. Harvey et al., 2013).
2855 Previous studies that compared the BOLD signal sensitivity between different field strengths
2856 mainly used simple tasks, e.g., flicker stimulation or finger tapping, to activate the primary
2857 sensory and/or motor cortex (Duong et al., 2003; A. Geißler et al., 2014; Alexander Geißler et
2858 al., 2013; Schäfer et al., 2008). Only a few studies adopted high level cognitive tasks to
2859 compare lower field and UHF. For example, Jerde et al. (2008) compared the task-induced
2860 activation at 4T and 7T (Gourtzelidis et al., 2005) using a mental maze solving paradigm, and
2861 Geißler et al. (2014) compared the language network with a standard overt language fMRI
2862 paradigm between 3T and 7T. Although there have been many studies comparing field
2863 strengths performed by experts in physics and engineering (Alexander Geißler et al., 2013;
2864 Hutton et al., 2011; Li, 2013; Pohmann et al., 2016; Vaughan et al., 2001), additional empirical
2865 evidence using neurocognitive tasks may also aid the cognitive neuroscientist's decision to
2866 execute fMRI experiments at UHF (De Martino et al., 2018; van der Zwaag et al., 2016).
2867 Second, rather than using conventional univariate analysis, such as GLM, we used a custom-
2868 built computational pRF modelling. Though the pRF model is conceptually similar to GLM by
2869 taking the best model fit as the predictor in the design matrix, there are several advantages of

2870 using pRF model to quantify the field strength dependent effect on model predictive power. (i)
2871 The pRF model is an explicit computational model and is expressed in terms of input-referred
2872 parameters (Dumoulin & Wandell, 2008; Wandell & Winawer, 2015) such as locations in the
2873 visual field rather than in terms of a statistic of the fMRI time series. Compared to a GLM, the
2874 pRF model characterizes the responses of neural populations that preferentially tuned to
2875 different stimuli (e.g., numerosities). The response differences to the presented numerosities
2876 could be converted into tuning functions, allowing for a comparison of the tuning parameters
2877 (i.e., preferred numerosity and tuning width), and model predictive performance (i.e., variance
2878 explained) of the fMRI signals. (ii) Our approach was motivated by the anecdotal suggestion
2879 that numerosity maps as discovered by the pRF modelling at 7T could not be reproduced at 3T.
2880 As such, the comparison between 3T and 7T became relevant for the pRF modelling. Though
2881 we show that we can reconstruct the numerosity maps at 3T, this requires much more data than
2882 typically acquired in the field. Last, we used model-based, model-free and other validation
2883 analyses, and these analyses showed similar results.

2884 One of the limitations of the current study is that we only have three participants, but
2885 each participant was scanned for three sessions at 3T and two sessions at 7T. We prefer
2886 scanning multiple sessions on fewer participants than scanning more participants with fewer
2887 sessions for several reasons. First, the aim of the current study is to investigate whether we
2888 could detect numerosity maps at 3T and quantify how many functional runs are required at 3T
2889 to reach equivalent model predictive power at 7T. Thus, for each individual participant, it is
2890 necessary to have more than one 3T session so as to have enough signal strength to compare
2891 to a 7T session. Second, pRF model is commonly used to map functionally specialized brain
2892 regions on individual participant, for example, numerosity maps in the intraparietal sulcus. We
2893 ran the model in the native space of each participant's cortical area thus it is not helpful to
2894 average these individual-specific cognitive maps across participants. Third, having more
2895 sessions on the same participant would help to reduce the confounds of between-subject
2896 variability for comparing different field strengths. To counter-balance the variability of the 3T
2897 data collection on separate days, we also collected two 7T sessions on two days. Each session
2898 was used as the reference dataset in turn to reduce session-specific variability (Viessmann &
2899 Polimeni, 2021). Last, statistical power is a trade-off between number of trials per participant
2900 and number of participants (Baker et al., 2020). Studies with fewer participants but more trials
2901 can have the same statistical power as more participants with fewer trials. Thus, we opt for
2902 collecting more sessions on the same participant rather than having one session on multiple
2903 participants.

2904

2905 **Conclusion**

2906 With the increasing popular application of computational model in neuroimaging, UHF MRI
2907 brings tremendous advantages in advancing our understanding of the brain function, such as
2908 increased sensitivity and greater spatial resolution. This study brings out another benefits of
2909 UHF MRI and demonstrates higher model predictive power at UHF. These results suggest that
2910 future cognitive neuroscience studies may benefit from UHF by collecting less data and
2911 preserving strong statistical power. Thus, UHF functional MRI paves the way for
2912 individualized cognitive neuroscience.

2913 Originally, with all the control experiments involved, it took about 5 hours of scanning
2914 at 7T per individual participant to discover the numerosity maps (B. M. Harvey et al., 2013).
2915 Based on the results we report here, it would have required around 20 hours per participant to
2916 uncover the numerosity maps at 3T, which would have made the initial discovery of numerosity
2917 maps at 3T highly unfeasible in practice. To sum up, UHF benefits cognitive neuroscience with
2918 higher SNR and BOLD sensitivity, and thus reduces the number of runs (trials) required to
2919 achieve reliable activation compared to lower field strength.

2920

2921 **Acknowledgements**

2922 This research was supported by an Ammodo KNAW Award (S. O. D.), an NWO-VICI grant
2923 016.Vici.185.050 (S. O. D.), a KNAW research grant (S. O. D. and W. van der Z.) and a China
2924 Scholarship Council (CSC) scholarship [201706750008] (Y.C.).

2925

2926 **Competing interests**

2927 The authors declare no competing interests.

2928

2929 **Data and Code Availability Statement**

2930 The code generated during this study is available in the Vistasoft repository
2931 (<https://github.com/vistalab/vistasoft>).

2932

2933 The datasets supporting the current study have not yet been deposited in a public repository
2934 because of participants privacy concerns, but are available from the corresponding author on
2935 request.

2936

2937

2938
2939
2940
2941
2942
2943
2944
2945

2946
2947
2948
2949
2950
2951
2952
2953
2954
2955
2956
2957
2958
2959
2960
2961
2962
2963
2964
2965
2966
2967

Chapter 6

General discussion

2968 The present thesis focuses on numerosity perception and its underlying neural mechanisms in
2969 the human brain. We utilized methodological advances in neuroimaging and computational
2970 modelling, such as UHF MRI and pRF modelling, to examine the neural tuning of numerosity
2971 and thereby study several profound questions in the field.

2972 First, in Chapter 2, we tested two competing hypotheses on whether small and large
2973 numerosities are represented under two separate systems or a single mechanism. We
2974 demonstrated that topographic numerosity maps cover both the subitizing and estimation
2975 ranges, suggesting a single neural mechanism underlying small and large numerosities.
2976 Furthermore, as discussed below, these results also support the link between neural tuning and
2977 perception. Second, in Chapter 3, we investigated the role of attention in numerosity perception.
2978 We used three consecutive experiments to show that attention drives numerosity responses and
2979 that the neural populations displayed decreased responses when their preferred numerosities
2980 are shown but not attended (which would otherwise drive maximal response). Third, in Chapter
2981 4, we asked whether numerosity maps are also involved in symbolic number processing. We
2982 found that the numerosity maps at the temporal-occipital cortex also respond to numbers,
2983 supporting a link between numerosity and number symbol processing at the ventral stream.
2984 Last, in Chapter 5, we assessed if the numerosity maps could be reconstructed at the current
2985 standard field strength of 3T MRI. We were able to detect the numerosity maps at 3T, though
2986 averaging more functional runs was required to reconstruct robust maps as compared to those
2987 at 7T. We further quantified that one 7T run had about four times the model predictive power
2988 of one 3T run, which makes the initially uncovering of the numerosity maps infeasible in
2989 practice. Overall, the findings in the current thesis establish links between neural tuning, with
2990 numerosity perception, attention and symbolic number processing, and contribute to the field
2991 in comparing MR systems at different field strengths. Here, we will discuss these results in
2992 more detail, together with a discussion regarding conceptual implications and future directions.

2993

2994 **Neural tuning underlies known numerosity perceptual phenomena**

2995 In Chapter 2 we demonstrated that small and large numerosities are represented continuously
2996 within the same maps, suggesting a single neural mechanism. Furthermore, our results suggest
2997 that the neural tuning properties, such as cortical magnification and tuning width, account for
2998 the known differential perception on subitizing and larger numerosities. Specifically, the quick
2999 and precise numerosity perception at the subitizing range can be explained by more cortical
3000 areas that are devoted to small numerosities and that neurons tuned to small numerosities have
3001 sharper tuning curves.

3002 Neural numerosity tuning can account for other perceptual phenomena, including the
3003 numerical distance and size effects (Tsouli, Harvey, et al., 2021). The tuning curves of neurons
3004 preferring numerically close numerosities (e.g., 8 and 9) overlap more than those preferring
3005 numerically distant numerosities (e.g., 4 and 8), resulting in more similar responses and thereby
3006 more difficult to discriminate (the numerical distance effect). As shown in Chapter 2, the tuning
3007 width increases progressively with increasing numerosity. Therefore, at a given numerical
3008 distance (e.g., a difference of 1), the tuning curves of neurons preferring larger numerosities
3009 (e.g., 8 and 9) overlap more than those preferring smaller numerosities (e.g., 3 and 4), resulting
3010 in less discriminable responses (the numerical size effect).

3011 In addition, neural numerosity tuning can explain perceptual aftereffects of adaptation.
3012 Psychophysical studies have demonstrated that numerosity perception is highly susceptible to
3013 adaptation: adapting to a low numerosity leads to an overestimation of a numerosity
3014 subsequently presented, whereas adapting to a high numerosity leads to an underestimation (D.
3015 C. Burr, Anobile, & Turi, 2011; D. Burr & Ross, 2008; Tsouli, Dumoulin, te Pas, & van der
3016 Smagt, 2019). For example, after adapting to the numerosity of 20, the subsequently presented
3017 numerosity of 10 will be subjectively perceived as the numerosity of 9, i.e., an underestimated
3018 bias. Recently, colleagues and ourselves provided evidence that adaptation to visual
3019 numerosity changes neural numerosity selectivity (Tsouli, Cai, et al., 2021). We speculated
3020 that the neural tuning can explain this phenomenon by viewing the perceptual consequence as
3021 the sum of responding neurons' preferred numerosity states, weighted by those neurons'
3022 response amplitude levels ((Clifford, Wenderoth, & Spehar, 2000; Tsouli, Harvey, et al., 2021).
3023 Repeated stimulation with a specific adapter numerosity (i.e. 20) suppresses the responses of a
3024 population of neurons depending on the amplitude of their responses to the adapter stimulus.
3025 Specifically, the suppressive responses maximize at neurons preferring the adapter numerosity,
3026 and decline at neurons preferring numerosities that are numerically distant to the adapter
3027 numerosity (i.e. <10). Thus, the population responses to numerosities near the adapter will be
3028 biased away from the adapter, accounting for a repulsive shift.

3029 Moreover, neural tuning also underlies interactions between different quantities and
3030 sensory modalities. Previous studies have shown overlapping brain activation evoked by
3031 quantity perception in different sensory modalities (Anobile, Arrighi, Togoli, & Burr, 2016b;
3032 Eger et al., 2003) and also perceptual interactions between quantity dimensions (Arrighi,
3033 Togoli, & Burr, 2014), suggesting a common neural mechanism for different quantities (A.
3034 Nieder, 2012). However, colleagues and ourselves have recently found that while topographic
3035 maps of different quantities, including object size (Ben M. Harvey et al., 2015), timing (Ben

3036 M. Harvey et al., 2020) and haptic numerosity (Hofstetter et al., 2021), spatially overlap in the
3037 cortex, they are all comprised of distinct neural populations (Tsouli, Harvey, et al., 2021). This
3038 finding suggests that observed commonalities in neural and behavioral representation between
3039 quantities are not accounted for by a common neural representational code across quantities,
3040 but by the interaction of spatially intermingled neural populations which are independently
3041 tuned to different quantities and modalities.

3042

3043 **Attention is a necessary ingredient to elicit numerosity selective response**

3044 In the primary sensory cortex, attention usually gains responses by boosting the neural
3045 responses of neurons preferring the attended location or feature, at the expense of neural
3046 responses to other spatial positions or other features (Martinez-Trujillo & Treue, 2004;
3047 McAdams & Maunsell, 1999b; O’Craven et al., 1997). Convergent evidence from
3048 psychophysical (e.g. adaptation) (D. Burr & Ross, 2008), neuroimaging (e.g. topographic maps)
3049 (B. M. Harvey et al., 2013) and computational research (Kim et al., 2021; Nasr et al., 2019;
3050 Stoianov & Zorzi, 2012) indicates that numerosity is a primary attribute, akin to color and
3051 orientation, etc. However, unlike responses in the early visual cortex, which happen whenever
3052 the preferred stimulus is shown, we have found that both bottom-up and top-down processing
3053 appear necessary to drive numerosity responses (Chapter 3). Former studies showed that these
3054 two processes interact in humans to control attention and modulate neural responses to target
3055 stimuli (Carrasco, 2011; Corbetta & Shulman, 2002). Of note, in our study the top-down
3056 attentional control is directed to the stimulus, but not necessarily to the numerosity feature of
3057 the stimulus. Many previous studies have found numerosity-selective responses with tasks that
3058 did not ask for attention directed towards the numerosity feature (B. M. Harvey et al., 2013;
3059 Viswanathan & Nieder, 2013), and even with orthogonal tasks that directed attention away
3060 from numerosity feature (Castaldi et al., 2019). However, in all of these studies, participants
3061 performed some tasks and thereby always attended the stimulus itself. Furthermore, we found
3062 that in the absence of attention, neural populations tuned to the numerosities in the unattended
3063 set displayed suppressive responses. These results suggest that top-down attentional control
3064 gates numerosity responses by selectively modulating sensory processing of numerosity targets
3065 (Hopfinger, Buonocore, & Mangun, 2000).

3066 Our study focuses on how the neural response amplitude is influenced by attentional
3067 modulation, but whether attention alters numerosity selectivity remain unknown. It is up to
3068 future studies to explore whether attentional modulation alter the tuning properties, such as the
3069 selectivity and tuning width, of the neural populations. Previously, our colleagues have

3070 demonstrated that spatial attention attracts pRF to the preferred positions systematically across
3071 the entire visual field, using a model incorporating a stimulus-driven receptive field (represents
3072 neural populational selectivity in the absence of attention) and an attention field (represents
3073 attention's influences and is centered at the attended location) (Klein, Harvey, & Dumoulin,
3074 2014). In consistent with these findings, colleagues and ourselves found adaptation alters
3075 numerosity selectivity (Tsouli, Cai, et al., 2021). Thus, we speculate that attention would
3076 change neural response selectivity of numerosity-tuned neurons throughout the numerosity
3077 maps in a similar manner. It is up to future studies to apply computational models that
3078 conceptualizes attention's influence (i.e., the attention field) and its interactions with the
3079 stimulus-driven neural responses properties.

3080

3081 **Overlap, but distinct neural populations tuned to numerosity and number**

3082 The very first study investigating the functions of the numerosity maps is presented in Chapter
3083 4, where we found that the NTO maps in both hemispheres respond to symbolic numbers, but
3084 that only the one in the left hemisphere also show tuned responses. These findings are in
3085 agreement with previous studies that link numerosity and symbolic number processing
3086 (Libertus, Feigenson, & Halberda, 2011; Andreas Nieder, 2020a; Piazza et al., 2007), and with
3087 laterality biases for number processing in the left side of the human brain (Ansari & Dhital,
3088 2006; Venkatraman, Ansari, & Chee, 2005). However, we did not observe a correlation
3089 between the preferred numerosity and preferred number estimates, suggesting that distinct
3090 neural populations respond to different number formats. This is in line with the recent
3091 observation on single neuron recordings in epilepsy patients (Kutter et al., 2018). Akin to the
3092 observation of the spatially overlapping representations of different quantities and modalities
3093 (Tsouli, Harvey, et al., 2021), as discussed above, we speculate that the neural tuning underlies
3094 the behavioural interactions between numerosity perception and symbolic number processing.
3095 Several reports indicate that numerical education and numerosity perception interact
3096 (Butterworth, 2018). Therefore, numerosity tuning may be influenced by education, and that
3097 neural tuning may undergo further refinement during developmental stages (Ansari, 2008;
3098 Butterworth, 2018; Halberda & Feigenson, 2008).

3099 Moreover, we also found activations elicited by symbolic numbers in the vicinity of the
3100 numerosity maps. As it was out of the scope of this study, we did not perform further analyses
3101 on these parts of the data. It is up to future studies to examine these responses and what is the
3102 organization of number-selective neural populations, i.e. whether number-tuned neural
3103 populations are also organized as topographic maps.

3104

3105 **The BOLD signals and neural population responses**

3106 There are important factors to consider when attempting to translate fMRI finding to
3107 constituent biophysical mechanisms (Logothetis, 2002; Logothetis & Wandell, 2004).
3108 Numerosity selectivity in this thesis was determined by fitting a pRF model to fMRI BOLD
3109 data within a recoding site (i.e. voxel). As such, the numerosity preference is the aggregate of
3110 the receptive fields of all neurons within a fMRI voxel, namely, the averaged preferred
3111 numerosity of a neural population. Therefore, the heterogeneous contribution from different
3112 neurons of the populations at the same voxel may give a different overall response, indicated
3113 by different preferred numerosity estimates depending on the presented numerosity stimuli,
3114 though the neural tuning of single neuron remains stable (Chapter 2).

3115 Another related effect on the preferred numerosity estimates is the voxel size. A larger
3116 voxel will have more heterogeneous neurons, which will result in changes in the overall tuning,
3117 typically to a biased preferred numerosity by averaging more neural populations' tuning
3118 estimates. A novel and recent development in fMRI technique of recording BOLD responses
3119 at very high spatial resolution (i.e. < 1mm) (Ress, Glover, Liu, & Wandell, 2007) might help
3120 to resolve this issue. At such resolution, voxels can also be assigned to different lamina within
3121 the cortical gray matter (Fracasso, Petridou, & Dumoulin, 2016; van Dijk, Fracasso, Petridou,
3122 & Dumoulin, 2020). As feedforward and feedback signals are processed differently across the
3123 lamina, this method could be used to separate feedforward and feedback processing signals of
3124 numerosity responses (van Dijk, Fracasso, Petridou, & Dumoulin, 2021). Although there are
3125 many technical challenges, such as requiring very precise alignment between functional and
3126 anatomical volumes and dealing with tiny neurovascular coupling across the lamina, this
3127 method provides a great promise in the neuroscience fields towards imaging at the human
3128 mesoscopic scale (Dumoulin, Fracasso, van der Zwaag, Siero, & Petridou, 2018). Thus, it is
3129 up to future studies to further explore numerosity neural representation at a finer resolution,
3130 across gray laminar and columnar.

3131 One also needs to be cautious when interpreting the suppressive responses elicited by
3132 the preferred but unattended numerosity as a 'negative' BOLD response (Chapter 3). As the
3133 BOLD responses reflect input and intracortical processing rather than pyramidal cell output
3134 activity (Barbieri, Mazzoni, Logothetis, Panzeri, & Brunel, 2014), it is difficult to infer a
3135 suppressive response from the observed modulation of BOLD activity. In the context of our
3136 findings, negative responses indicate decreased response relative to the baseline response
3137 amplitudes where a zero response was predicted. It is up to future studies to examine this effect

3138 using optimized computational models, such as difference-of-Gaussian model (Zuiderbaan,
3139 Harvey, & Dumoulin, 2012), compress spatial summation (CSS) model (Kay, Winawer, Mezer,
3140 & Wandell, 2013), or normalization model (Aqil, Knapen, & Dumoulin, 2021) that have been
3141 applied in visual field mapping.

3142 Last, in Chapter 5, we compared numerosity maps at 3T and 7T. To compensate for the
3143 data quality at the lower field strength, we used an isotropic resolution of about 2^3 mm, which
3144 is far from the optimal spatial resolution at the UHF (Peters et al., 2007; Triantafyllou et al.,
3145 2005; van der Zwaag et al., 2009). Compared to 7T, the BOLD signals at 3T have lower SNR
3146 and sensitivity, thus much more data points (trials) are required to reconstruct numerosity maps
3147 at 3T (Baker et al., 2021). Moreover, our findings show that the numerosity tuning properties,
3148 e.g., numerosity preference and tuning width, remain stable at different field strengths. This is
3149 in line with our recent study using an alternative fMRI data acquisition technique, i.e. recording
3150 vascular space occupancy (VASO) signals based on changes in cerebral blood volume (CBV),
3151 to reconstruct the visual field maps (Oliveira et al., 2022). These results suggest that the
3152 vascular component of pRF tuning response is not dominating in either VASO-CBV or BOLD
3153 signals, and that pRF model provides a great promise to characterize tuning properties of
3154 numerosity-selective neural populations with variable data measurements.

3155

3156 **Conclusions**

3157 In conclusion, we examined in this thesis the neural mechanism of numerosity perception and
3158 the links between neural tuning and perception by combining ultra-high field fMRI recordings
3159 with biological-inspired modelling analyses. We found that neural populations tuned to small
3160 and large numerosities are ordered in the same topographic maps, suggesting a single
3161 processing mechanism. These results are suggested that numerosity neural tuning properties
3162 can account for the well-documented perceptual differences in the subitizing and estimation
3163 ranges. We demonstrated that attention to the stimulus is essential to drive numerosity selective
3164 responses. By acting as a top-down control mechanism, attentional selection modulates neural
3165 responses to attended information at the expense of information that is not attended.
3166 Specifically, numerosity-tuned neural populations respond maximally to attended stimulus
3167 with their preferred numerosity, and suppress responses when their preferred numerosity was
3168 not attended. We found that numerosity maps at the ventral occipital-temporal cortex also
3169 implant symbolic numbers, indicating links between numerosity perception and symbolic
3170 numerical cognition. Finally, we demonstrated that numerosity maps are detectable using high

3171 field fMRI at 3T, however, much more data is required than at 7T. This result suggests that
3172 ultra-high field MRI systems operating at 7T and above would pave the way for individualized
3173 cognitive neuroscience, such as to map functionally specialized brain regions on individual
3174 participants.

3175

3176

3177

3178

3179

3180

3181

3182

3183

3184

3185

3186

3187

3188

3189

3190

3191

3192

3193

3194

3195

3196

3197

3198

3199

3200

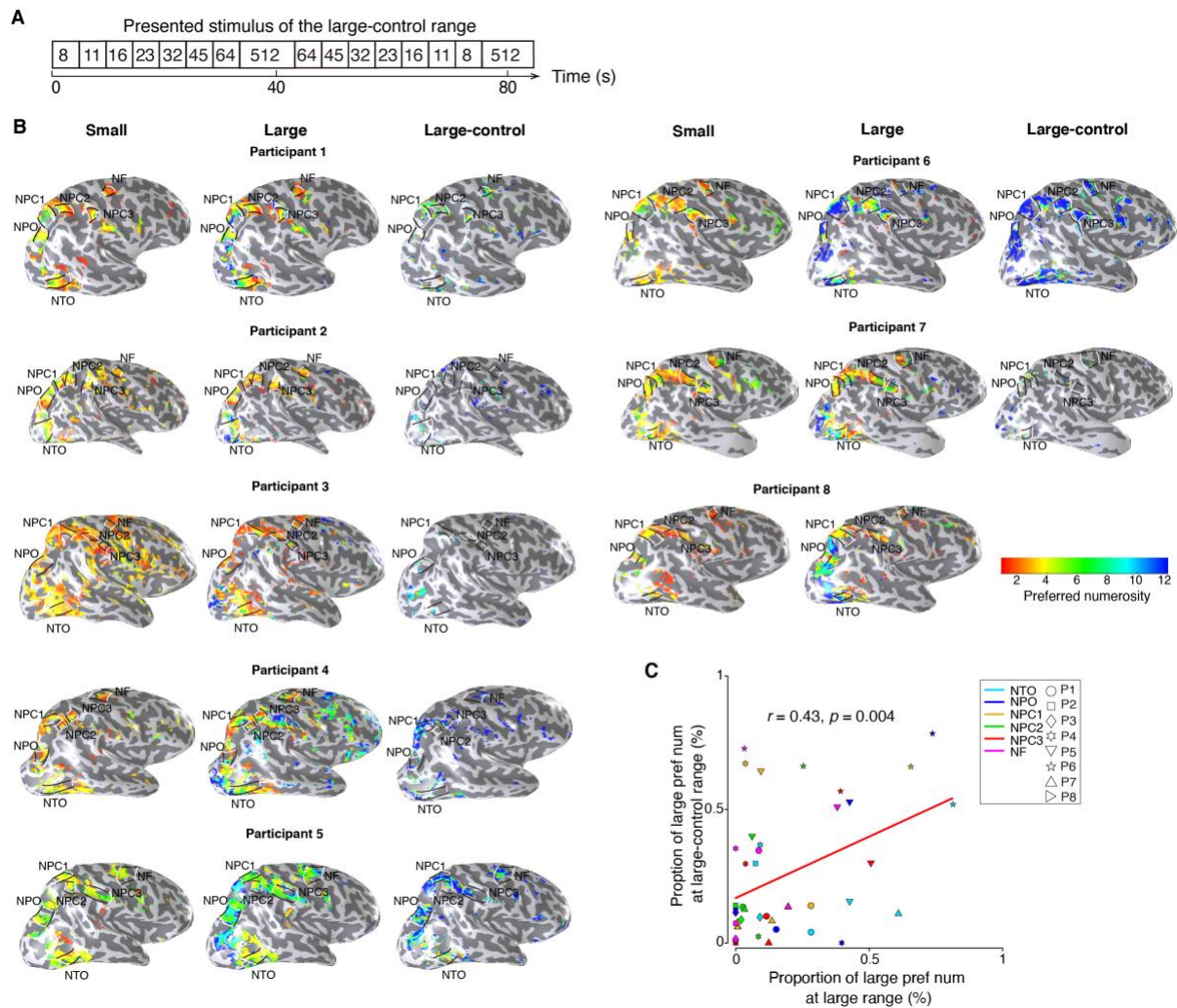
3201

3202

3203
3204
3205

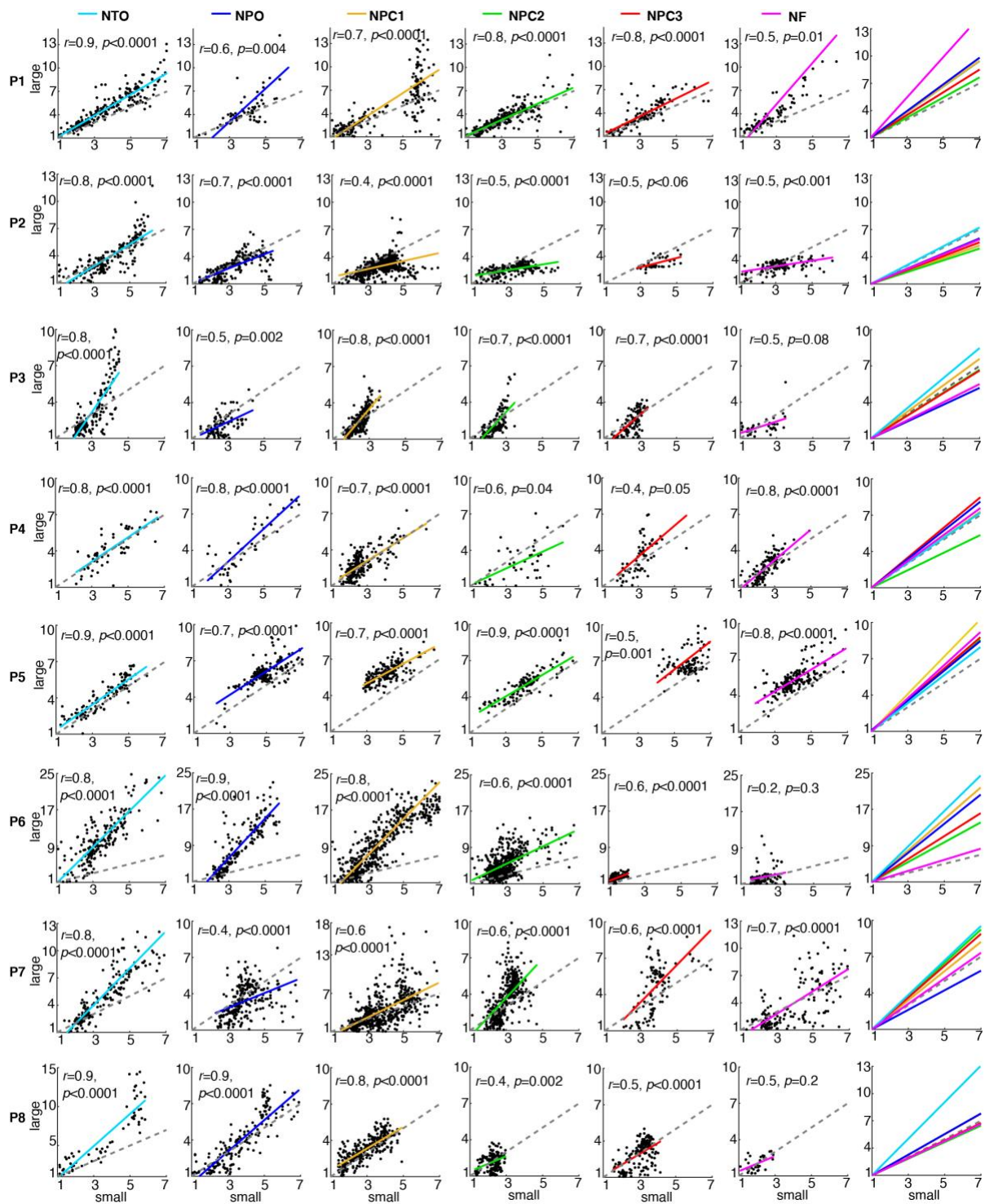
Appendix A

Supplementary materials for Chapter 2



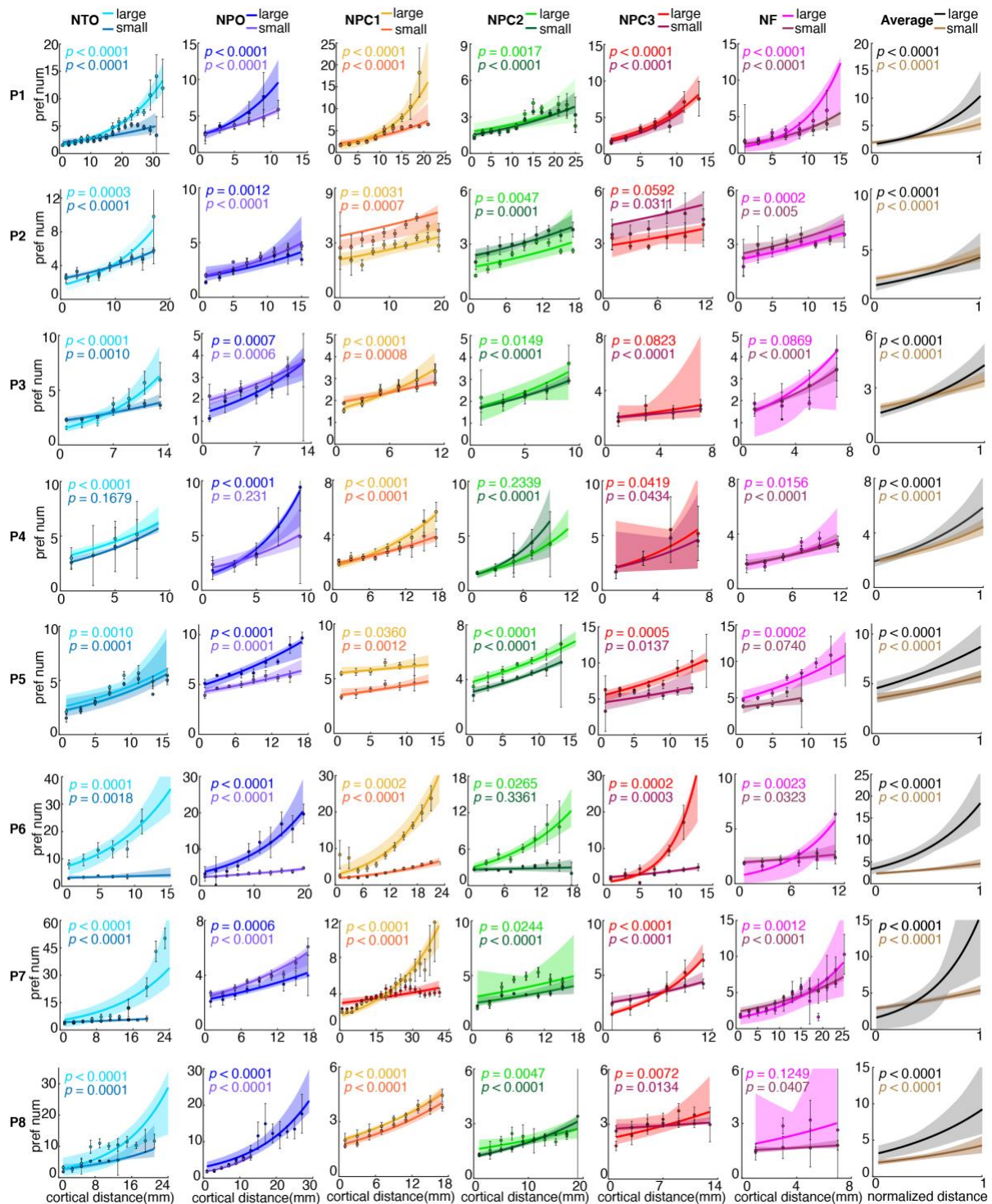
3206
3207
3208
3209
3210
3211
3212
3213
3214
3215
3216
3217
3218
3219

Supplementary Figure 2.1. Visualization of numerosity maps of all participants and relationship of large numerosity preference at the large and large-control ranges. (A) Illustration of the large-control range. **(B)** Visualization of numerosity maps of the small, large and large-control ranges. Cortical surface rendering of the right hemisphere of all the participants show a constant and similar network of numerosity maps at both the small and the large ranges. However, stimulating only with large numerosities (>7, panel a), reveals only part of the maps. Only preferred numerosities are shown where the model explained over 30% of response variance within the recording site. Black lines outline individual numerosity maps. The borders of the lowest to the highest preferred numerosity in each map are marked by white lines. **(C)** Numerosity maps with more neural populations tuned to large numerosities have more responses elicited by the large-control range. Given the cortical magnification, the numerosity maps have few responses to large numerosities, and thus most of the maps show little responses to the large-control range. Source data are provided as a source data file.



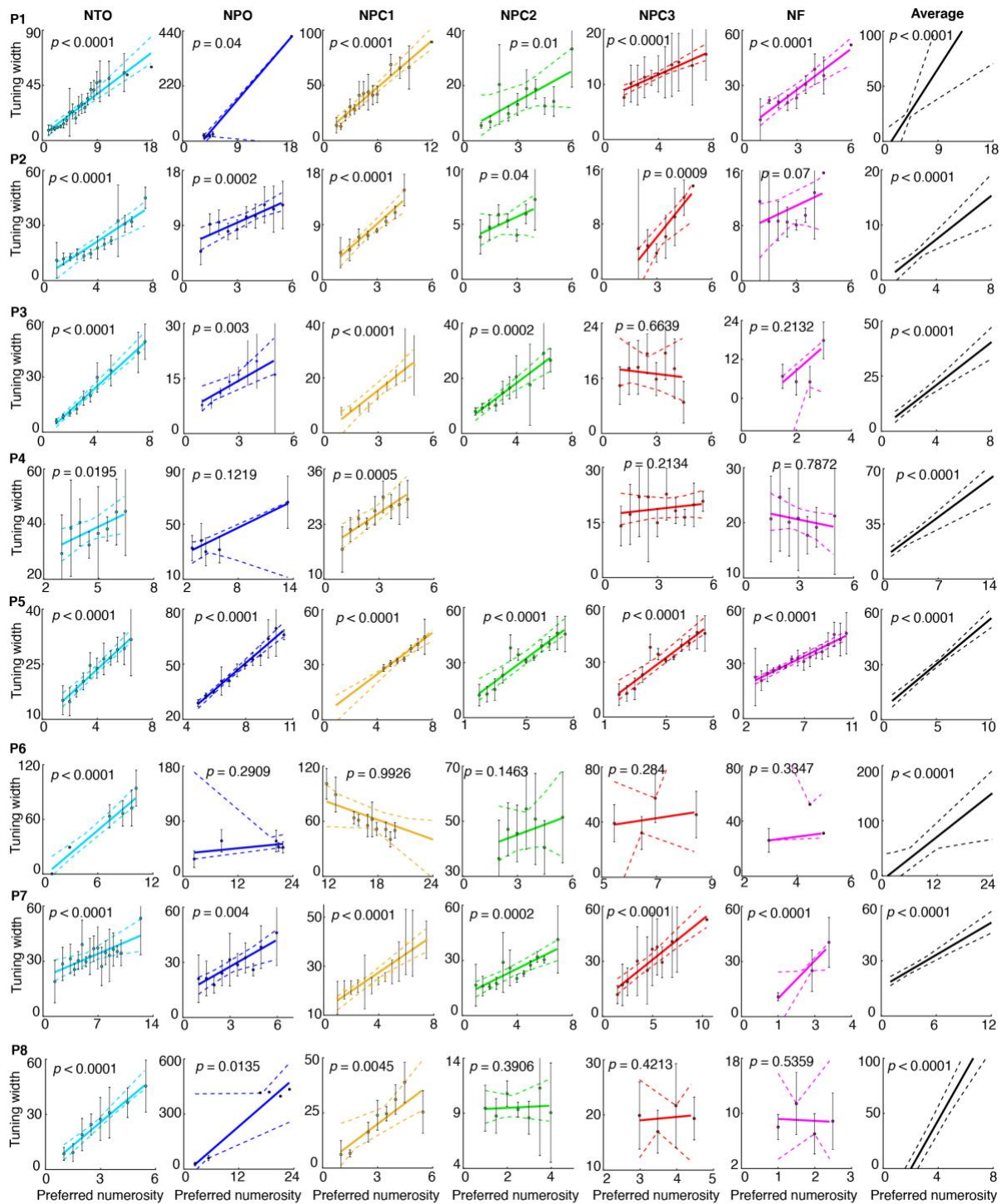
3220

3221 **Supplementary Figure 2.2.** Correlations between numerosity preferences estimated from
 3222 small and large ranges indicate similar numerosity selectivity among individual maps and
 3223 participants (P1–P8). Dots show the estimates from individual recording sites (variance
 3224 explained > 30%), coloured lines indicate the best linear fits between the two estimates, the
 3225 dashed line shows unity (i.e. identical estimates).



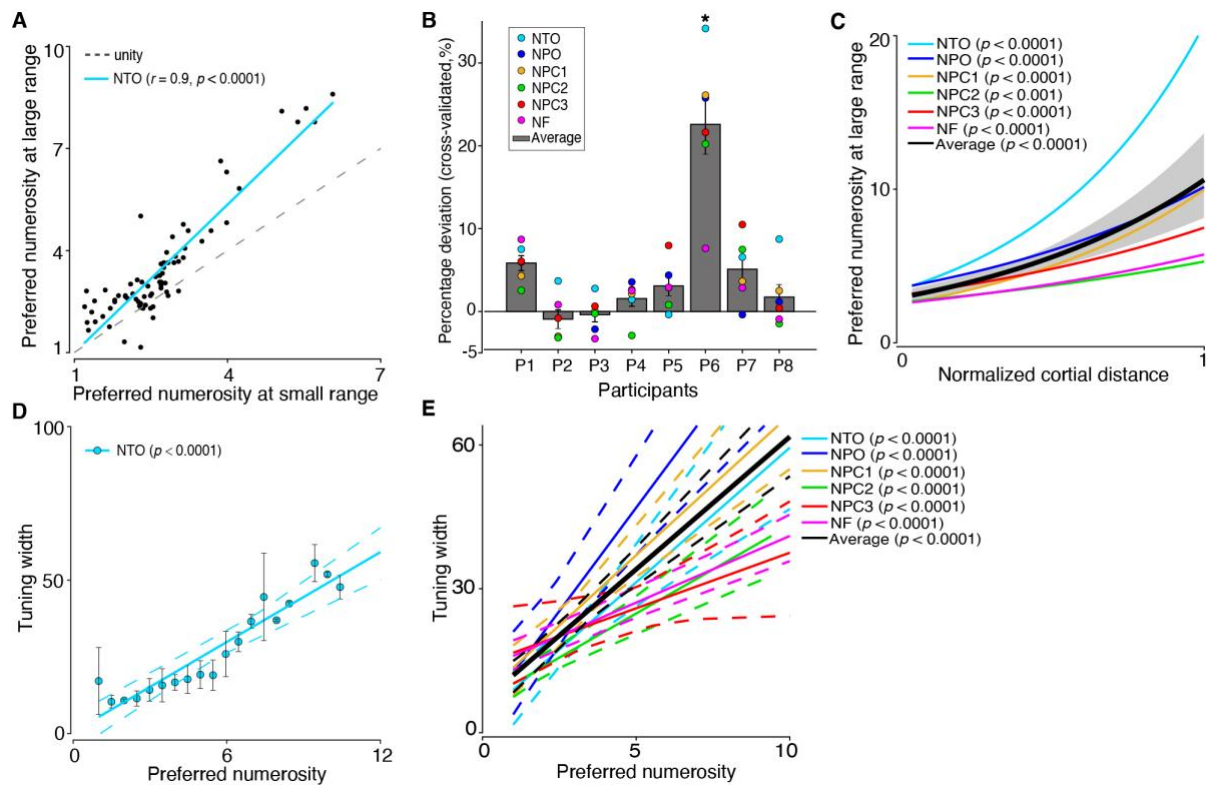
3226

3227 **Supplementary Figure 2.3.** Cortical progression with numerosity preference estimated from
 3228 viewing small and large ranges in individual maps of all participants (P1–P8). Preferred
 3229 numerosities increase systematically for both conditions. Points represent the mean preferred
 3230 numerosity in each distance bin (every 2mm interval), with error bars showing the standard
 3231 errors of the mean over all data points with each bin.



3232

3233 **Supplementary Figure 2.4.** Tuning width progresses with preferred numerosity of all maps
 3234 and all participants. Points represent the mean tuning width in each bin, error bars represent
 3235 the standard error of the mean over all data points in each bin. Solid lines are the linear fit to
 3236 the bins, weighted by the inverse of the standard error of each bin. Dashed lines represent 95%
 3237 confidence intervals determined by bootstrapping fits to the binned points ($n = 1000$). P-values
 3238 give the probability of the observed change from permutation analysis ($n = 10000$).



3239

3240 **Supplementary Figure 2.5. The cross validation datasets show near identical results. (A)**

3241 Participant1's NTO numerosity preferences estimated from an example pair of the cross

3242 validation datasets (e.g. small-odd vs. large-odd) were strongly correlated. Dots show the

3243 estimates from individual recording sites survived from all cross validations iterations ($n = 8$,

3244 variance explained $> 30\%$), the blue line shows the linear fit between the two estimates, the

3245 dashed line shows unity (i.e. identical preferences). **(B)** Bars show the mean cross-validated

3246 percentage deviations for each participant; error bars show the standard errors of the mean over

3247 maps ($n = 6$). Only participant 6 has a significant higher deviation from the unity line than

3248 other participants (two-way ANOVA analysis, followed by post hoc analysis, Bonferroni

3249 corrected for multiple comparison; $F(7,47) = 23.1$, * indicates $p = 2.3 \times 10^{-11}$). **(C)** Progression

3250 of numerosity preferences estimated from the split dataset of the large range as a function of

3251 normalized cortical distance in all numerosity maps, across all participants. The black line

3252 shows the best logarithmic fit that bins the data points from all the maps across normalized

3253 cortical distance. **(D)** Tuning width increases with preferred numerosity in participant1's NTO

3254 map averaged by the two split datasets of the large range. Recording points are bins based on

3255 preferred numerosity. Points represent the average of the mean tuning width within each bin

3256 across the two split datasets, error bars represent the standard errors of the mean over the two

3257 split datasets. Solid line is the linear fit, weighted by the inverse of the standard deviation of

3258 each bin. **(E)** Linear fits of tuning width against preferred numerosity of all the numerosity

3259 maps averaged across the two splits of the large range, across participants (coloured lines) and

3260 across maps (black line). In panel **C - E**: dashed lines represent 95% confidence intervals of

3261 the fits (coloured lines) to the binned points determined by bootstrapping ($n = 1000$). P-value

3262 gives the probability of the observed change from permutation analysis ($n = 10000$). Source

3263 data are provided as a source data file.

3264

Appendix B

Supplementary materials for Chapter 3

3265

3266

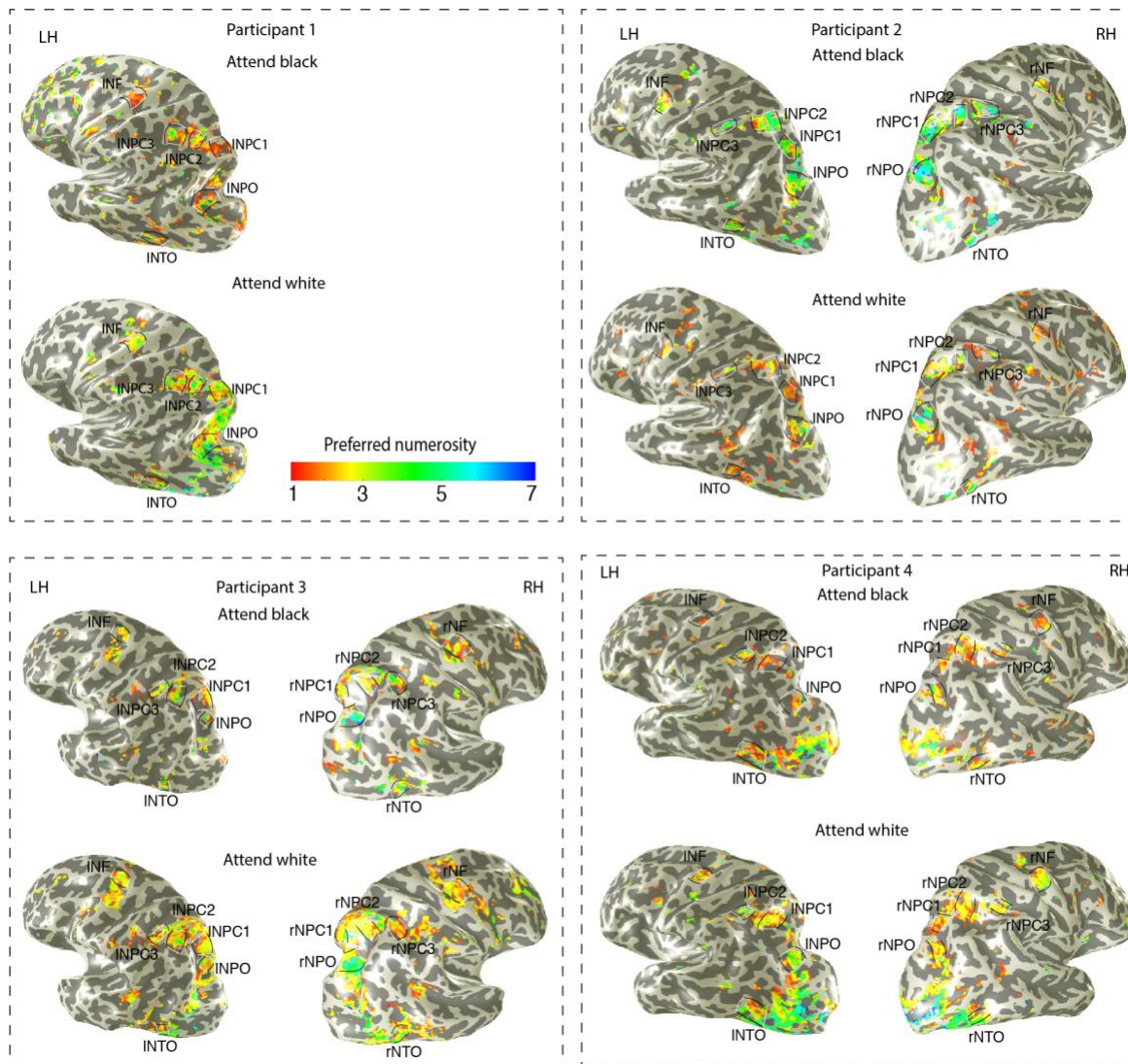
3267

3268 **Supplementary Table 3.1. Task performance of individual participants in Experiment 1**

Participant (#)	Asymmetry level (#)	Attend black: d' (mean \pm std)		Attend white: d' (mean \pm std)	
		attended	unattended	attended	unattended
P1	0.1	3.4 \pm 0.4	0.8 \pm 0.2	3.0 \pm 0.5	1.0 \pm 0.3
P2	0.2	2.8 \pm 0.5	1.0 \pm 0.3	2.9 \pm 0.4	1.0 \pm 0.4
P3	0.2	3.6 \pm 0.4	0.8 \pm 0.1	3.3 \pm 0.4	0.8 \pm 0.2
P4	0.2	3.1 \pm 0.5	0.8 \pm 0.2	3.0 \pm 0.4	0.7 \pm 0.2
Averaged	na	3.2 \pm 0.5*	0.9 \pm 0.2	3.0 \pm 0.5*	0.9 \pm 0.3

3269

3270 Note: Asymmetry level indicates the degree of oval of the dot shape and 0 suggests the dot was
3271 shown in circle. Pair *t*-test was performed to demonstrate the different task performances
3272 between the attended and unattended sets, in a given condition. *, $p < 0.05$.



3273

3274

3275

3276

3277

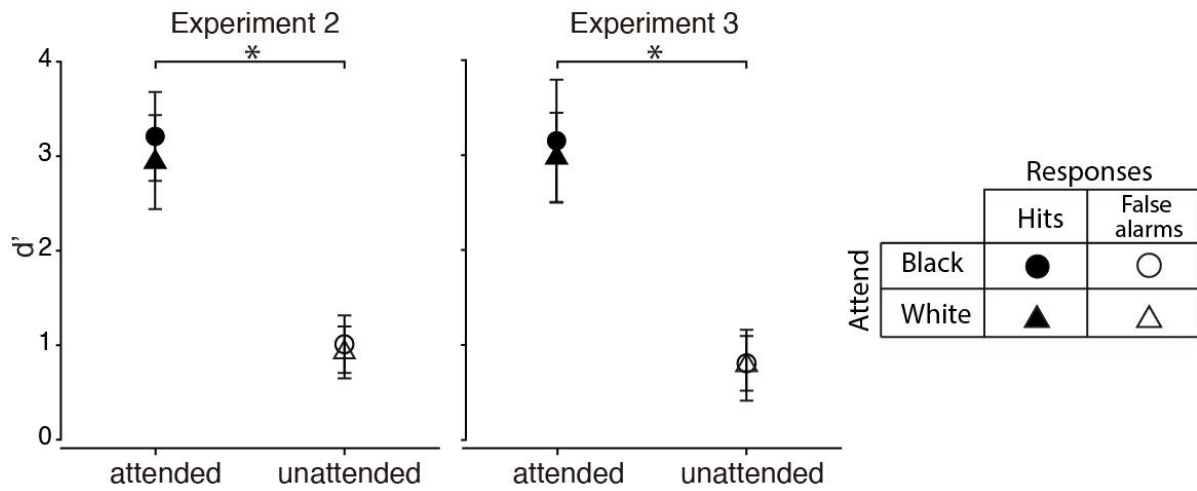
3278

3279

3280

3281

Supplementary Figure 3.1. Visualization of topographic numerosity maps derived from the two attentional conditions of all participants. Cortical surface rendering of both left (LH) and right hemispheres (RH) shows a similar network of numerosity maps. Maps show preferred numerosities of cortical recording sites, estimated from responses to the numerosities in the attended sets (black or white dots), with over 30% of the variance explained by the numerosity pRF model. Black lines outline the lateral borders of individual maps. White lines denote the lowest and the highest preferred numerosities at each map. See Figure 3.2D for maps on the right hemisphere of Participant 1.



3282

3283 **Supplementary Figure 3.2. Behavioural performances of Experiments 2 & 3.** Task

3284 performance was evaluated as discriminability indices (d') in the 'attend black' (circles) and

3285 'attend white' (triangles) conditions. Filled markers denote detection performance on the

3286 attended set, i.e., hits, and open markers on the unattended set, i.e., false alarms. * indicates p

3287 < 0.00001 by paired t -tests (Experiments 2: $t_{ab} = 15.6$, $p_{ab} = 7.6 \times 10^{-9}$; $t_{aw} = 12.7$, $p_{aw} = 6.4 \times 10^{-8}$;

3288 Experiment 3: $t_{ab} = 12.1$, $p_{ab} = 1.0 \times 10^{-7}$; $t_{aw} = 10.5$, $p_{aw} = 4.3 \times 10^{-7}$).

3289

3290

3291

3292

3293

3294

3295

3296

3297

3298

3299

3300

3301

3302

3303

3304

3305

3306

Appendix C

Supplementary materials for Chapter 4

3307

3308

3309

3310 **Supplementary Table 4.1.** Task performance of detecting targeted non-symbolic numerals

Participants (#)	Number of runs (#)	Target detection accuracy (%)		d'
		Catch trials	Embedded trials	
P1	16	70	88	3.7
P2	15	80	92	3.4
P3	17	95	96	4.2
P4	16	88	92	3.7
P5	16	78	96	3.5
P6	16	77	93	3.4
P7	16	95	98	4.3
Average	16	83	94	3.7

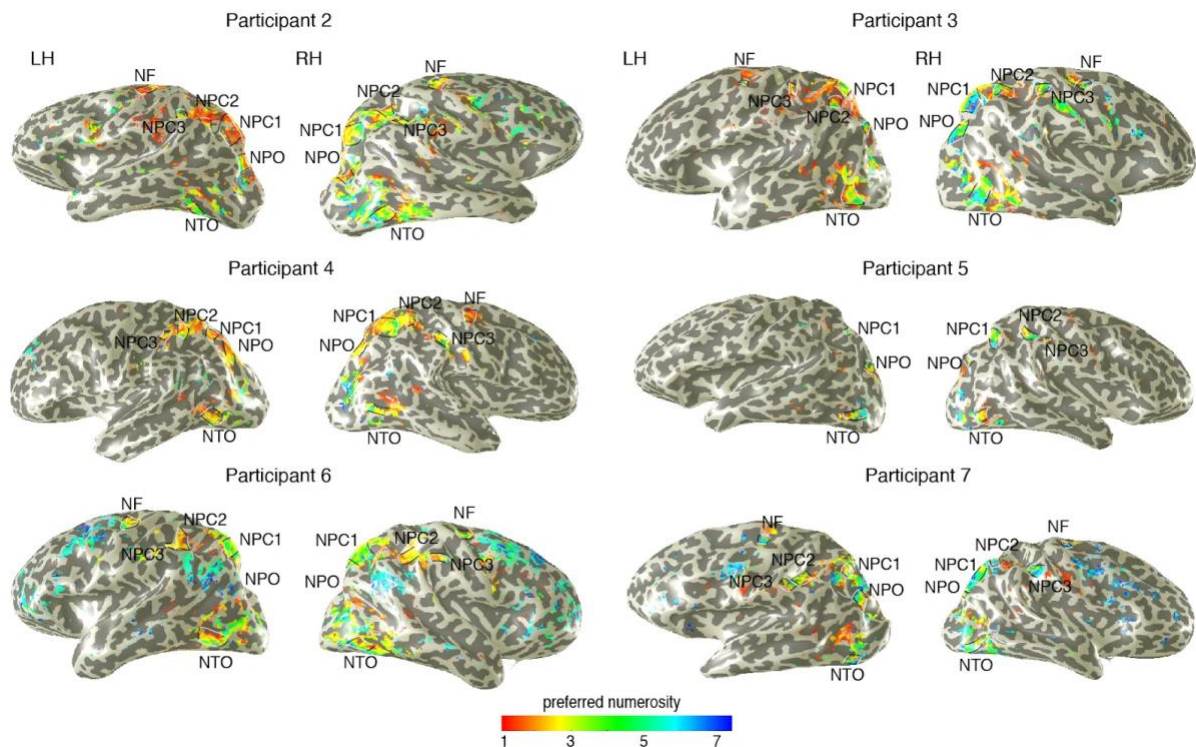
3311

3312

3313 **Supplementary Table 4.2.** MNI coordinates of NTO map of individual participants

Participants (#)	Montreal Neurological Institute coordinates (x, y, z)	
	Left hemisphere	Right hemisphere
P1	(-35, -80, -8)	(35, -72, -8)
P2	(-47, -60, -9)	(42, -71, -11)
P3	(-39, -70, -6)	(44, -71, -5)
P4	(-42, -70, -1)	(40, -74, -5)
P5	(-36, -71, -12)	(40, -81, -7)
P6	(-42, -61, -15)	(41, -73, -14)
P7	(-39, -56, -7)	(36, -77, -2)

3314



3315

3316 **Supplementary Figure 4.1. Cortical rendering of numerosity maps of all individual**

3317 **participants (akin to Figure 4.2).** Black lines outline the edge borders of individual

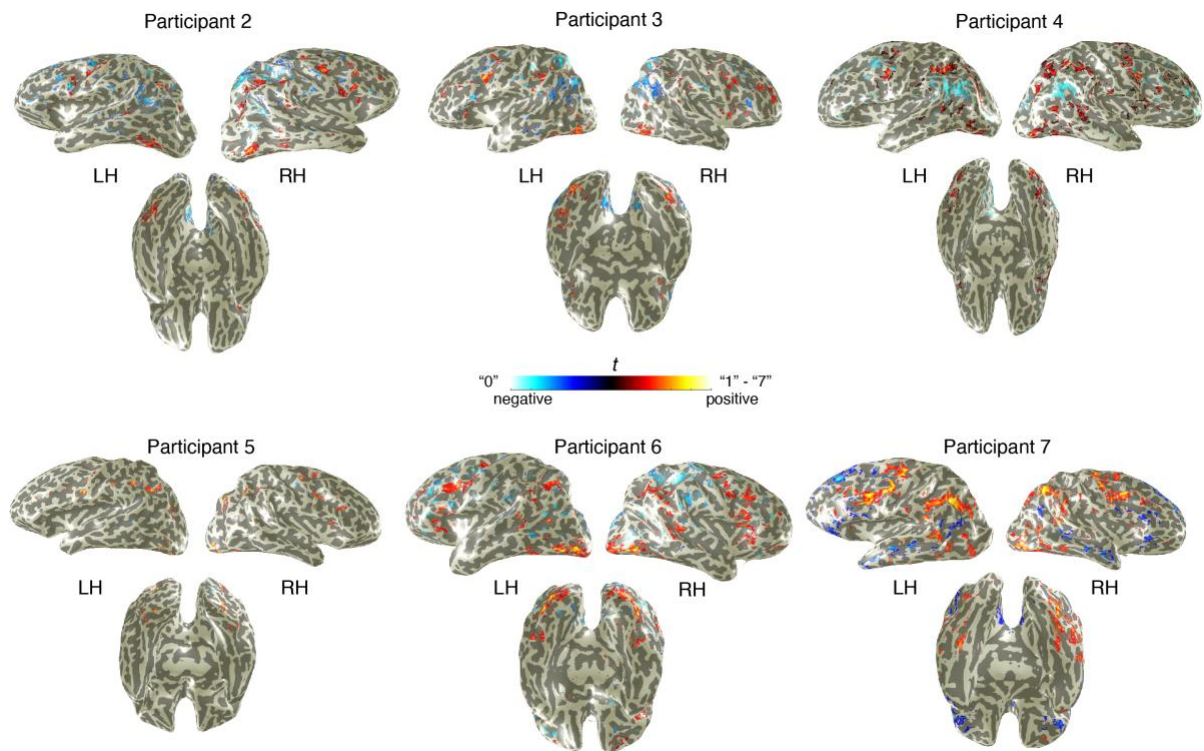
3318 numerosity maps and white lines denote the lowest and highest preferred numerosities in

3319 each map. The map of preferred numerosity estimates is thresholded at a variance explained

3320 of 30%. LH, left hemisphere. RH, right hemisphere.

3321

3322



3323

3324 **Supplementary Figure 4.2. Stimulus-driven responses to symbolic numbers at**
 3325 **numerosity maps for all individual participants (akin to Figure 4.3A).** The result of all
 3326 participants of the GLM analysis which contrasted the responses to the number of “0” (blue
 3327 colors) and “1-7” (yellow-red colors). Lower panel shows the ventral view of the cortical
 3328 surface where the responses to symbolic numbers overlap with the NTO map. Only recording
 3329 sites (i.e. voxels) where the variance explained (R^2) by the GLM exceeding 30% were projected
 3330 on the cortical surface.

3331

3332

3333

3334

3335

3336

3337

3338

3339

3340

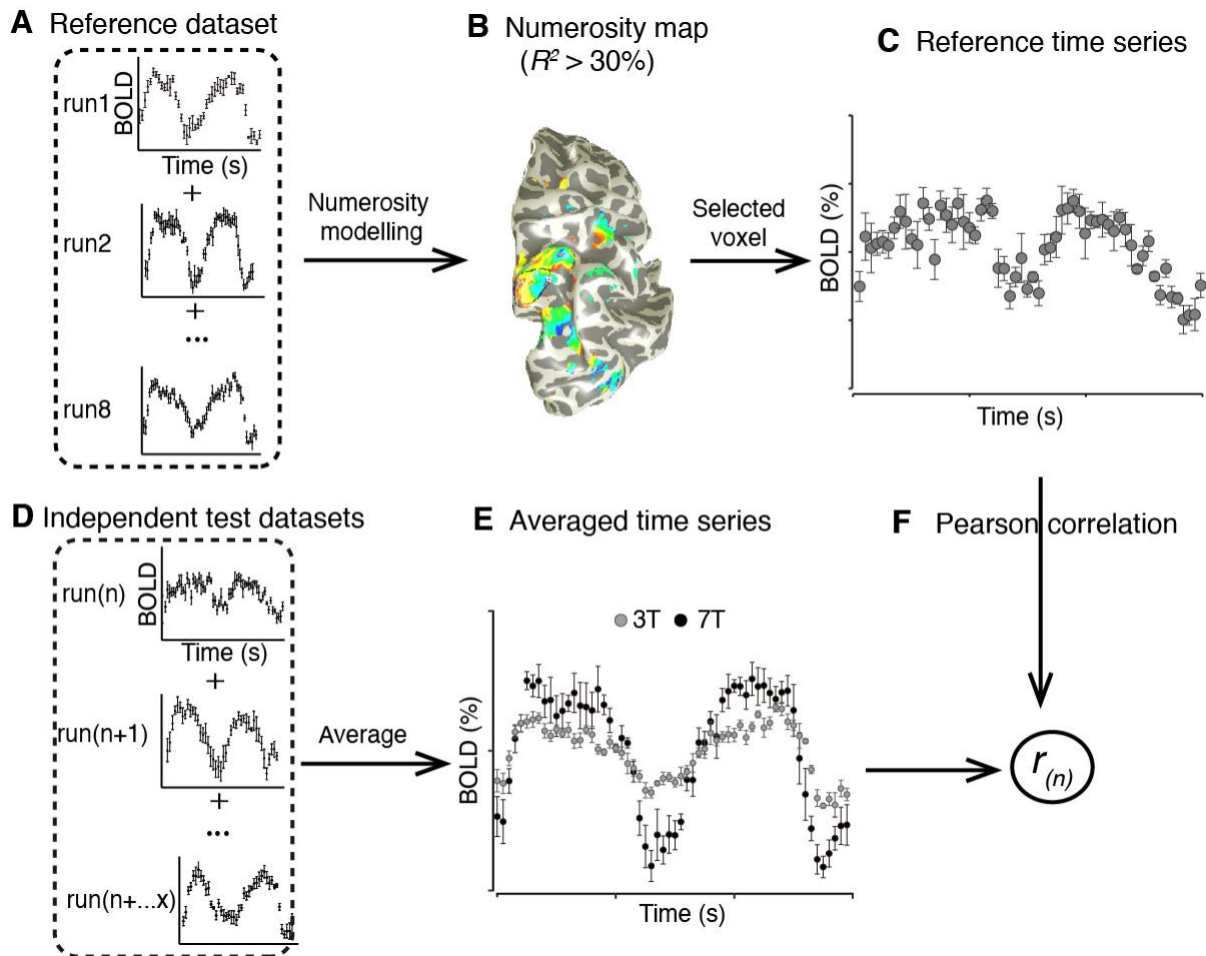
3341

3342

Appendix D

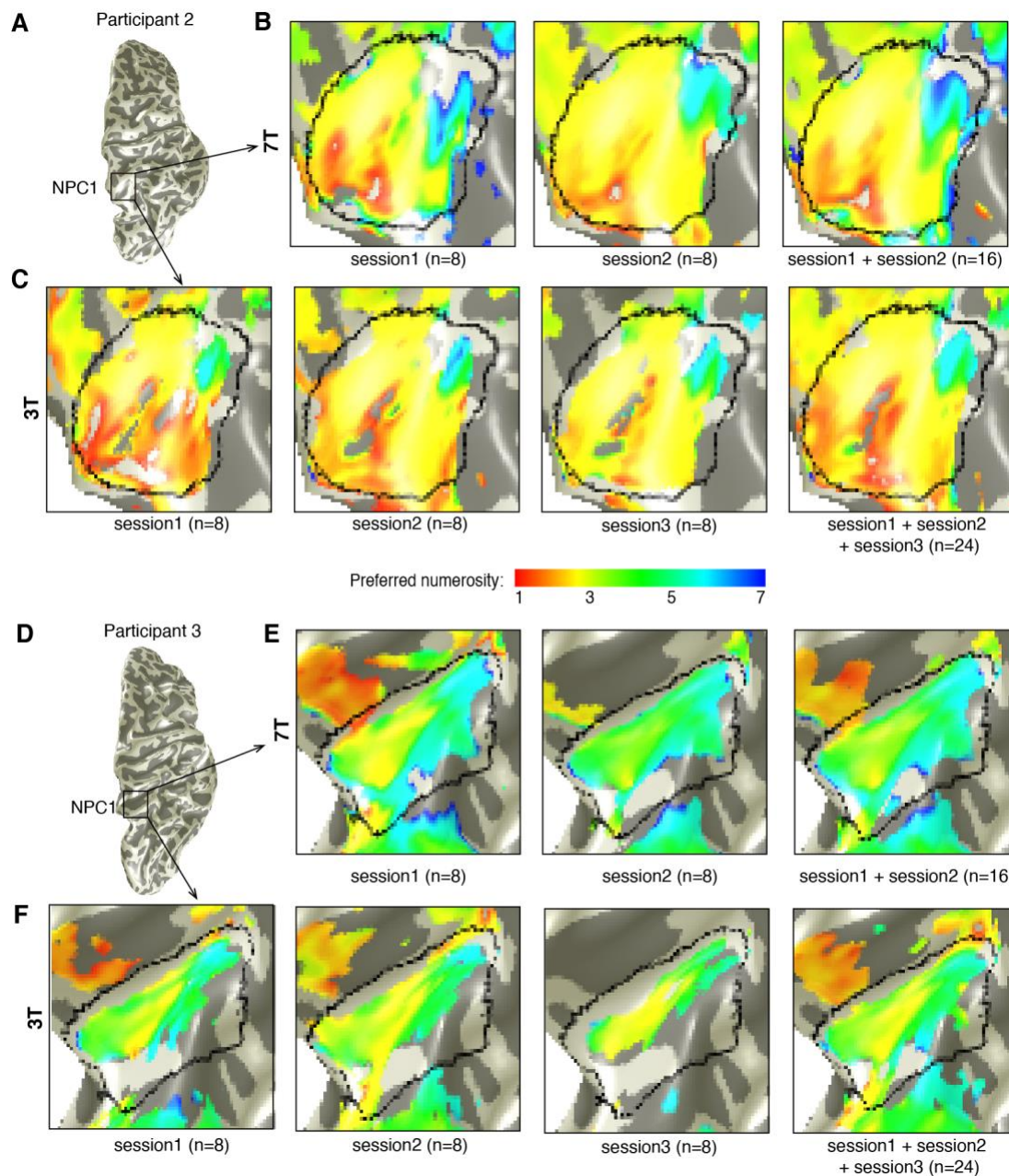
Supplementary materials for Chapter 5

3343
3344
3345



3346

3347 **Supplementary Figure 5.1. Flowchart of the model-free analysis procedure comparing**
3348 **the predictive power between field strengths. (A)** Eight functional runs (as one session) of
3349 either 3T or 7T were averaged and regarded as a reference dataset. **(B)** Numerosity modelling
3350 was performed for each reference dataset. Voxels with more than 30% of the variance
3351 explained (R^2) were selected. **(C)** The ‘reference time series’ was extracted from each selected
3352 voxel. **(D)** The remaining individual functional runs were taken as independent test datasets,
3353 i.e., the 3T and 7T test data. **(E)** The test data was averaged with increasing number of runs to
3354 produce averaged time series at 3T (grey dots) and 7T (black dots), respectively. **(F)** Pearson
3355 correlation coefficients of the ‘reference time series’ and the averaged time series derived from
3356 the test datasets, was calculated as a function of increasing number of runs ($r_{(n)}^2$). We iterated
3357 this procedure 6 times while splitting the data into different pairs of reference and test datasets.



3358

3359

3360

3361

3362

3363

3364

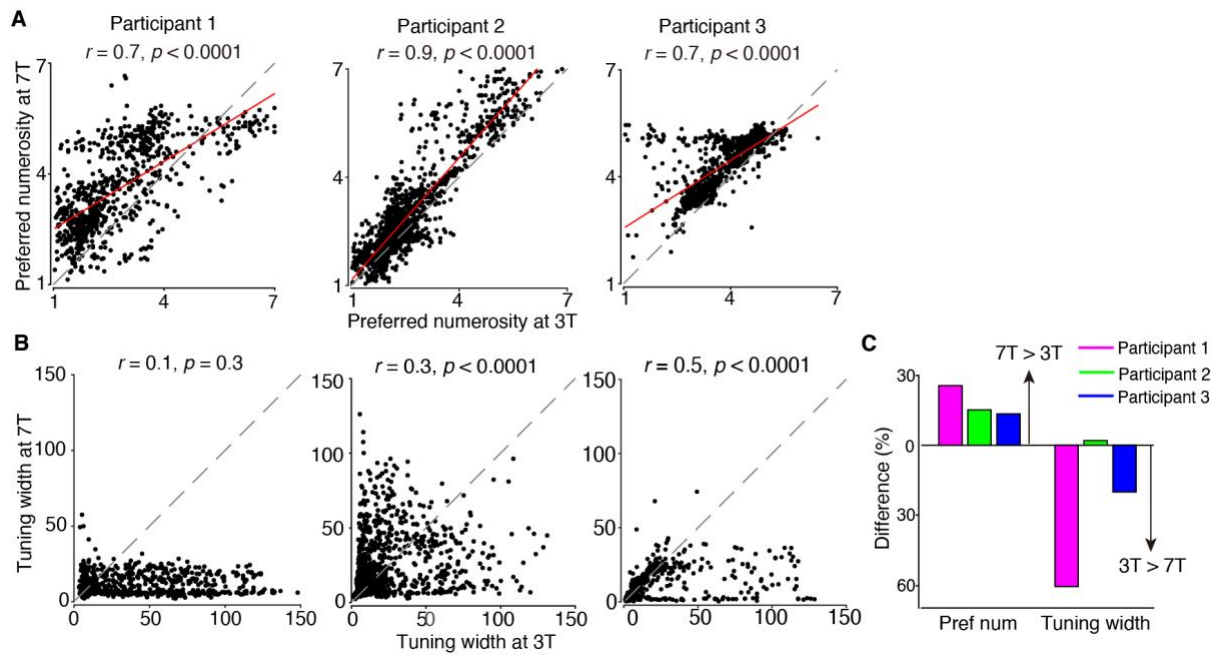
3365

3366

3367

3368

Supplementary Figure 5.2. Topographic numerosity maps of the other two participants at 3T and 7T. (A, D) Anatomical rendering of the right cerebral cortex. Black frames outline the region of interest (NPC1) in the intraparietal sulcus at the right hemisphere of participants 2 and 3, respectively. (B, E) Topographic maps of numerosity-selective neural populations at NPC1 (black box in A/D) reconstructed using data of 8 functional runs at the two 7T scanning sessions, and all the runs across sessions (n=16). (C, F) Topographic maps reconstructed using data of the three 3T scanning sessions, and all the runs across sessions (n=24). Maps show preferred numerosities of cortical recording sites with over 30% of the variance explained. A larger cortical extend above the threshold at the 7T maps than the 3T maps. These maps become more reliable and comparable at 7T and 3T, with increasing number of runs (right panels).



3369

3370 **Supplementary Figure 5.3. The similarity between preferred numerosity and tuning**
 3371 **width estimated at 3T and 7T. (A)** The numerosity preferences estimated at 3T and 7T are
 3372 highly correlated, suggesting the similar numerosity tuning at the two field strengths. **(B)**
 3373 Moderate correlation between tuning widths estimated at the two field strengths. **(C)** Overall,
 3374 the preferred numerosity estimates are slightly higher at 7T, while the tuning width is broader
 3375 at 3T, except for participant 2.

3376

3377

3378

3379

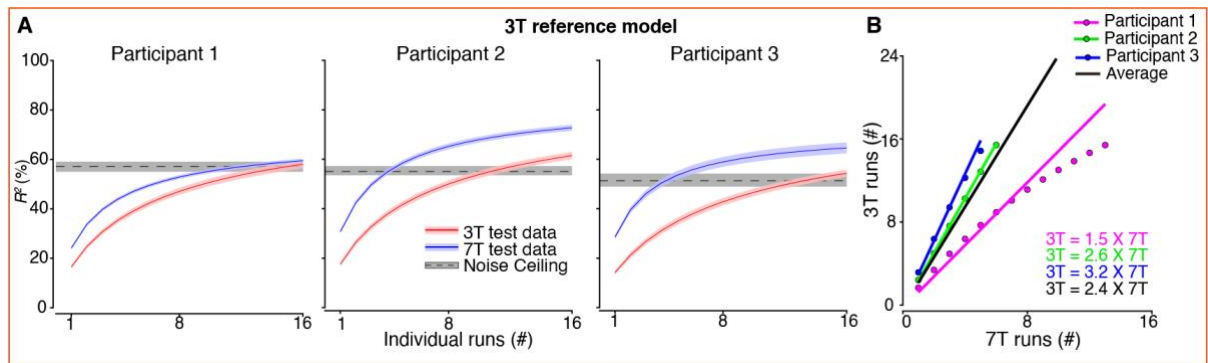
3380

3381

3382

3383

3384



3385

3386 **Supplementary Figure 5.4. Quantification of field strength effects on pRF model**

3387 **predictive power as a function of number of runs, using the reference model derived from**

3388 **3T reference datasets. (A)** The variance explained of the reference model as a function of

3389 increasing number of runs at 3T (red) and 7T (blue). Shaded areas indicate standard errors of

3390 the mean over iterations using different reference datasets (n=6). The noise ceiling (dashed line)

3391 with 95% confidence intervals (grey bars) represents the maximum explainable variance (of

3392 one 3T session, i.e., 8 runs) given the noise in the data. **(B)** Linear fits of the number of runs

3393 required at 3T to have equivalent model predictive power of one 7T run. Coloured-coded texts

3394 indicate the factor between 3T and 7T runs to achieve the same variance explained for each

3395 participant. On average, one 7T run has 2.5 times the model predictive power of one 3T run

3396 using the 3T reference model (black).

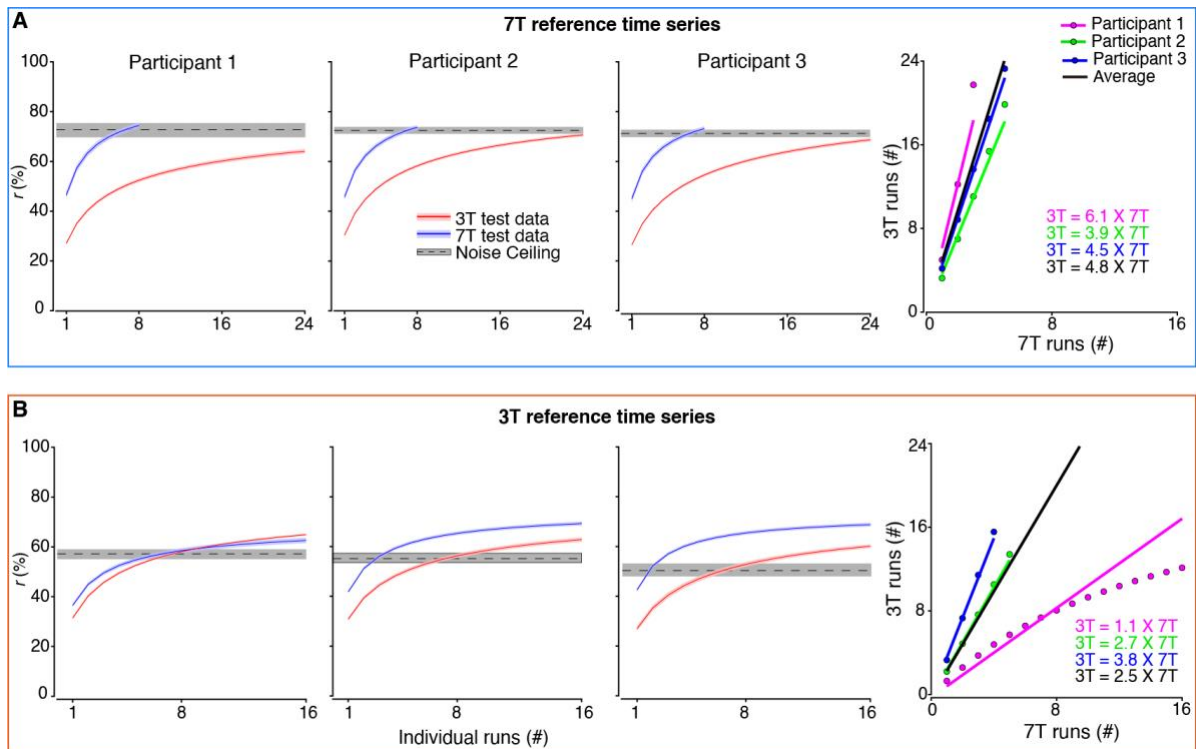
3397

3398

3399

3400

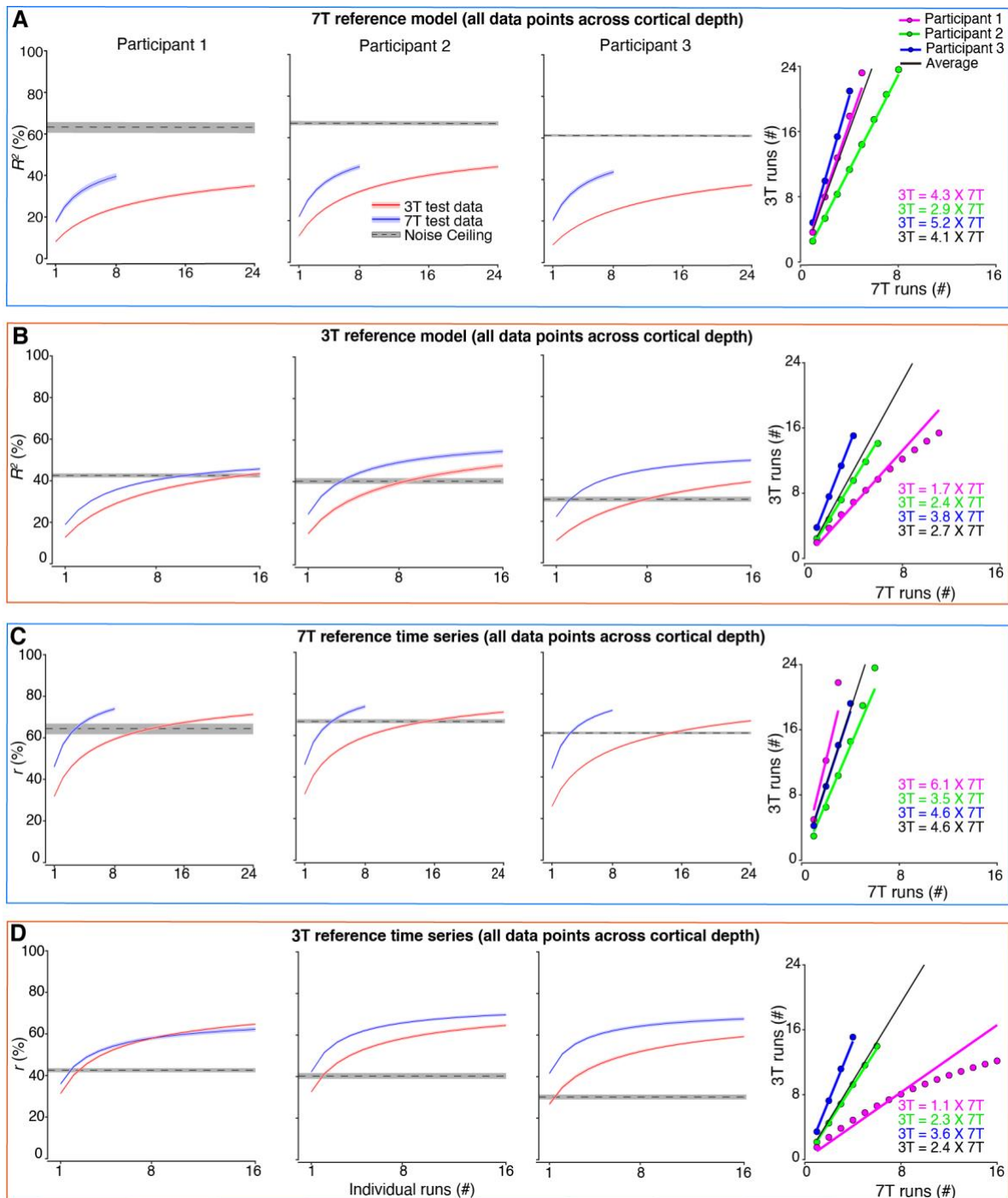
3401



3402

3403 **Supplementary Figure 5.5. Results of the model-free analyses.** (A) Pearson correlations as
 3404 a function of increasing number of runs at 3T (red) and 7T (blue), using 7T reference time
 3405 series. Shaded areas indicate standard errors of the mean over iterations using different
 3406 reference datasets ($n=6$). The noise ceiling (dashed line) with 95% confidence intervals (grey
 3407 bars) represents the maximum explainable variance (of one 7T session, i.e., 8 runs) given the
 3408 noise in the data. Linear fits of the number of runs required at 3T to have equivalent correlation
 3409 coefficient of one 7T run. Coloured-coded lines and texts indicate the factor between 3T and
 3410 7T runs to achieve the same correlation coefficient for each participant, and the black ones
 3411 indicate average across participants. (B) Pearson correlations as a function of increasing
 3412 number of runs at 3T and 7T, using 3T reference time series. The noise ceiling denotes the
 3413 maximum explainable variance (of one 3T session, i.e., 8 runs) given the noise in the data.
 3414 Other symbol representations as denoted in a. These results are in agreement with the results
 3415 of the model-based analyses shown in **Figure 5.5 & Supplementary Figure 5. 4.**

3416



3417

3418 **Supplementary Figure 5.6. Results of the validation analyses using all data points across**

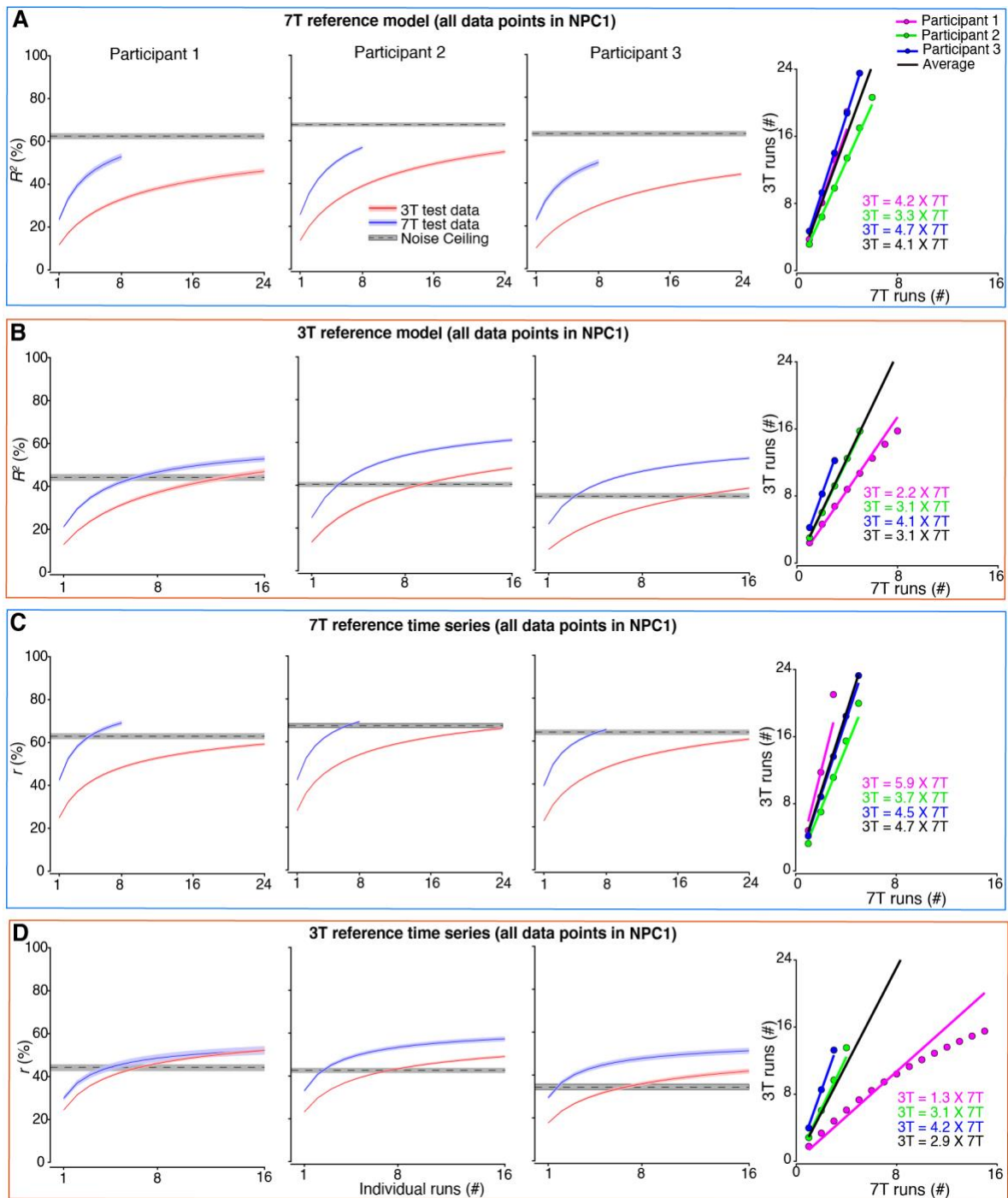
3419 **cortical depth. (A)** Results of the model-based analyses, using 7T reference model derived

3420 from reference datasets. **(B)** Results of the model-based analyses, using 3T reference model.

3421 **(C)** Results of the model-free analyses, using 7T reference time series. **(D)** Results of the

3422 model-free analyses, using 3T reference time series. These results confirm with the main results.

3423



3424

3425 **Supplementary Figure 5.7. Results of the validation analyses using all data points within**

3426 **NPC1, without any thresholding. (A) Results of the model-based analyses, using 7T**

3427 **reference model derived from reference datasets. (B) Results of the model-based analyses,**

3428 **using 3T reference model. (C) Results of the model-free analyses, using 7T reference time**

3429 **series. (D) Results of the model-free analyses, using 3T reference time series. These results**

3430 **confirm with the main results.**

3431

3432

3433 **References**

- 3434 Abboud, S., Maidenbaum, S., Dehaene, S., & Amedi, A. (2015). A number-form area in the
3435 blind. *Nature Communications*, 6. <https://doi.org/10.1038/ncomms7026>
- 3436 Agrillo, C., Dadda, M., Serena, G., & Bisazza, A. (2008). Do fish count? Spontaneous
3437 discrimination of quantity in female mosquitofish. *Animal Cognition*, 11(3), 495–503.
3438 <https://doi.org/10.1007/s10071-008-0140-9>
- 3439 Andersson, J. L. R., Skare, S., & Ashburner, J. (2003). How to correct susceptibility
3440 distortions in spin-echo echo-planar images: Application to diffusion tensor imaging.
3441 *NeuroImage*, 20(2), 870–888. [https://doi.org/10.1016/S1053-8119\(03\)00336-7](https://doi.org/10.1016/S1053-8119(03)00336-7)
- 3442 Anobile, G., Arrighi, R., Togoli, I., & Burr, D. C. (2016a). A shared numerical representation
3443 for action and perception. *ELife*, 5. <https://doi.org/10.7554/eLife.16161>
- 3444 Anobile, G., Arrighi, R., Togoli, I., & Burr, D. C. (2016b). A shared numerical representation
3445 for action and perception. *ELife*, 5, 1–14. <https://doi.org/10.7554/eLife.16161>
- 3446 Anobile, G., Castaldi, E., Moscoso, P. A. M., Burr, D. C., & Arrighi, R. (2020).
3447 “Groupitizing”: a strategy for numerosity estimation. *Scientific Reports*, 10(1), 1–9.
3448 <https://doi.org/10.1038/s41598-020-68111-1>
- 3449 Anobile, G., Cicchini, G. M., & Burr, D. C. (2012). Linear mapping of numbers onto space
3450 requires attention. *Cognition*, 122(3), 454–459.
3451 <https://doi.org/10.1016/j.cognition.2011.11.006>
- 3452 Anobile, G., Cicchini, G. M., & Burr, D. C. (2014). Separate Mechanisms for Perception of
3453 Numerosity and Density. *Psychological Science*, 25(1), 265–270.
3454 <https://doi.org/10.1177/0956797613501520>
- 3455 Anobile, G., Cicchini, G. M., & Burr, D. C. (2016). Number As a Primary Perceptual
3456 Attribute: A Review. *Perception*, 45(1–2), 5–31.
3457 <https://doi.org/10.1177/0301006615602599>
- 3458 Anobile, G., Stievano, P., & Burr, D. C. (2013). Visual sustained attention and numerosity
3459 sensitivity correlate with math achievement in children. *Journal of Experimental Child*
3460 *Psychology*, 116(2), 380–391. <https://doi.org/10.1016/j.jecp.2013.06.006>
- 3461 Anobile, G., Turi, M., Cicchini, G. M., & Burr, D. C. (2012). The effects of cross-sensory
3462 attentional demand on subitizing and on mapping number onto space. *Vision Research*,
3463 74, 102–109. <https://doi.org/10.1016/j.visres.2012.06.005>
- 3464 Ansari, D. (2007). Does the Parietal Cortex Distinguish between “10,” “Ten,” and Ten Dots?
3465 *Neuron*, 53(2), 165–167. <https://doi.org/10.1016/j.neuron.2007.01.001>
- 3466 Ansari, D. (2008). Effects of development and enculturation on number representation in the
3467 brain. *Nature Reviews Neuroscience*, 9(4), 278–291. <https://doi.org/10.1038/nrn2334>
- 3468 Ansari, D., & Dhital, B. (2006). Age-related changes in the activation of the intraparietal
3469 sulcus during nonsymbolic magnitude processing: An event-related functional magnetic
3470 resonance imaging study. *Journal of Cognitive Neuroscience*, 18(11), 1820–1828.
3471 <https://doi.org/10.1162/jocn.2006.18.11.1820>
- 3472 Ansari, D., Lyons, I. M., Van Eimeren, L., & Xu, F. (2007). Linking visual attention and
3473 number processing in the brain: The role of the temporo-parietal junction in small and
3474 large symbolic and nonsymbolic number comparison. *Journal of Cognitive*
3475 *Neuroscience*, 19(11), 1845–1853. <https://doi.org/10.1162/jocn.2007.19.11.1845>
- 3476 Aqil, M., Knapen, T., & Dumoulin, S. O. (2021). Divisive normalization unifies disparate
3477 response signatures throughout the human visual hierarchy. *Proceedings of the National*
3478 *Academy of Sciences of the United States of America*, 118(46).
3479 <https://doi.org/10.1073/pnas.2108713118>
- 3480 Arrighi, R., Togoli, I., & Burr, D. C. (2014). A generalized sense of number. *Proceedings of*
3481 *the Royal Society B: Biological Sciences*, 281(1797), 20141791.
3482 <https://doi.org/10.1098/rspb.2014.1791>

- 3483 Arsalidou, M., & Taylor, M. J. (2011). Is $2+2=4$? Meta-analyses of brain areas needed for
3484 numbers and calculations. *NeuroImage*, *54*(3), 2382–2393.
3485 <https://doi.org/10.1016/j.neuroimage.2010.10.009>
- 3486 Baker, D. H., Vilidaite, G., Lygo, F. A., Smith, A. K., Flack, T. R., Gouws, A. D., &
3487 Andrews, T. J. (2020). Power contours: Optimising sample size and precision in
3488 experimental psychology and human neuroscience. *Psychological Methods*.
3489 <https://doi.org/10.1037/met0000337>
- 3490 Baker, D. H., Vilidaite, G., Lygo, F. A., Smith, A. K., Flack, T. R., Gouws, A. D., &
3491 Andrews, T. J. (2021). Power contours: Optimising sample size and precision in
3492 experimental psychology and human neuroscience. *Psychological Methods*, *26*(3), 295–
3493 314. <https://doi.org/10.1037/met0000337>
- 3494 Balakrishnan, J. D., & Ashby, F. G. (1991). Is subitizing a unique numerical ability?
3495 *Perception & Psychophysics*, *50*(6), 555–564. <https://doi.org/10.3758/BF03207540>
- 3496 Barbieri, F., Mazzoni, A., Logothetis, N. K., Panzeri, S., & Brunel, N. (2014). Stimulus
3497 dependence of local field potential spectra: Experiment versus theory. *Journal of*
3498 *Neuroscience*, *34*(44), 14589–14605. [https://doi.org/10.1523/JNEUROSCI.5365-](https://doi.org/10.1523/JNEUROSCI.5365-13.2014)
3499 [13.2014](https://doi.org/10.1523/JNEUROSCI.5365-13.2014)
- 3500 Bazin, P.-L., Weiss, M., Dinse, J., Schäfer, A., Trampel, R., & Turner, R. (2014). A
3501 computational framework for ultra-high resolution cortical segmentation at 7Tesla.
3502 *NeuroImage*, *93*, 201–209. <https://doi.org/10.1016/j.neuroimage.2013.03.077>
- 3503 Brainard, D. H. (1997). The psychophysics toolbox. *Spatial Vision*, *10*(4), 433–436.
- 3504 Braitenberg, V. (1998). *Cortex: Statistics and Geometry of Neuronal Connectivity*. Berlin:
3505 Springer.
- 3506 Brannon, E. M., & Terrace, H. S. (1998). Ordering of the numerosities 1 to 9 by monkeys.
3507 *Science*, *282*(5389), 746–749. <https://doi.org/10.1126/science.282.5389.746>
- 3508 Buckley, P. B., & Gillman, C. B. (1974). Comparisons of digits and dot patterns. *Journal of*
3509 *Experimental Psychology*, *103*(6), 1131–1136. <https://doi.org/10.1037/h0037361>
- 3510 Bulthé, J., De Smedt, B., & Op de Beeck, H. P. (2014). Format-dependent representations of
3511 symbolic and non-symbolic numbers in the human cortex as revealed by multi-voxel
3512 pattern analyses. *NeuroImage*, *87*, 311–322.
3513 <https://doi.org/10.1016/j.neuroimage.2013.10.049>
- 3514 Bulthé, Jessica, De Smedt, B., & Op de Beeck, H. P. (2015). Visual Number Beats Abstract
3515 Numerical Magnitude: Format-dependent Representation of Arabic Digits and Dot
3516 Patterns in Human Parietal Cortex. *Journal of Cognitive Neuroscience*, *27*(7), 1376–
3517 1387. https://doi.org/10.1162/jocn_a_00787
- 3518 Burr, D. C., Anobile, G., & Arrighi, R. (2018a). Psychophysical evidence for the number
3519 sense. *Philosophical Transactions of the Royal Society B: Biological Sciences*,
3520 *373*(1740). <https://doi.org/10.1098/rstb.2017.0045>
- 3521 Burr, D. C., Anobile, G., & Arrighi, R. (2018b). Psychophysical evidence for the number
3522 sense. *Philosophical Transactions of the Royal Society B: Biological Sciences*,
3523 *373*(1740), 20170045. <https://doi.org/10.1098/rstb.2017.0045>
- 3524 Burr, D. C., Anobile, G., & Turi, M. (2011). Adaptation affects both high and low (Subitized)
3525 numbers under conditions of high attentional load. *Seeing and Perceiving*, *24*(2), 141–
3526 150. <https://doi.org/10.1163/187847511X570097>
- 3527 Burr, D. C., Turi, M., & Anobile, G. (2010). Subitizing but not estimation of numerosity
3528 requires attentional resources. *Journal of Vision*, *10*(6), 1–10.
3529 <https://doi.org/10.1167/10.6.20>
- 3530 Burr, D., & Ross, J. (2008). A Visual Sense of Number. *Current Biology*, *18*(6), 425–428.
3531 <https://doi.org/10.1016/j.cub.2008.02.052>
- 3532 Butterworth, B. (2018). The implications for education of an innate numerosity-processing

- 3533 mechanism. *Philosophical Transactions of the Royal Society B: Biological Sciences*,
3534 373(1740). <https://doi.org/10.1098/rstb.2017.0118>
- 3535 Cai, Y., Hofstetter, S., van der Zwaag, W., Zuiderbaan, W., & Dumoulin, S. O. (2021).
3536 Individualized cognitive neuroscience needs 7T: Comparing numerosity maps at 3T and
3537 7T MRI. *NeuroImage*, 237(December 2020), 118184.
3538 <https://doi.org/10.1016/j.neuroimage.2021.118184>
- 3539 Cai, Y., Hofstetter, S., van Dijk, J., Zuiderbaan, W., van der Zwaag, W., Harvey, B. M., &
3540 Dumoulin, S. O. (2021b). Topographic numerosity maps cover subitizing and estimation
3541 ranges. *Nature Communications*, 12(1), 1–10. [https://doi.org/10.1038/s41467-021-](https://doi.org/10.1038/s41467-021-23785-7)
3542 [23785-7](https://doi.org/10.1038/s41467-021-23785-7)
- 3543 Cantlon, J. F., & Brannon, E. M. (2006). Shared system for ordering small and large numbers
3544 in monkeys and humans. *Psychological Science*, 17(5), 401–406.
3545 <https://doi.org/10.1111/j.1467-9280.2006.01719.x>
- 3546 Cantlon, J. F., Platt, M. L., & Brannon, E. M. (2009). Beyond the number domain. *Trends in*
3547 *Cognitive Sciences*, 13(2), 83–91. <https://doi.org/10.1016/j.tics.2008.11.007>
- 3548 Carey, S. (2001). Cognitive foundations of arithmetic: Evolution and ontogenesis. *Mind and*
3549 *Language*, 16(1), 37–55. <https://doi.org/10.1111/1468-0017.00155>
- 3550 Carrasco, M. (2011). Visual attention: The past 25 years. *Vision Research*, 51(13), 1484–
3551 1525. <https://doi.org/10.1016/j.visres.2011.04.012>
- 3552 Castaldi, E., Piazza, M., Dehaene, S., Vignaud, A., & Eger, E. (2019). Attentional
3553 amplification of neural codes for number independent of other quantities along the
3554 dorsal visual stream. *ELife*, 8, 1–26. <https://doi.org/10.7554/eLife.45160>
- 3555 Chesney, D. L., & Haladjian, H. H. (2011). Evidence for a shared mechanism used in
3556 multiple-object tracking and subitizing. *Attention, Perception, and Psychophysics*, 73(8),
3557 2457–2480. <https://doi.org/10.3758/s13414-011-0204-9>
- 3558 Cheyette, S. J., & Piantadosi, S. T. (2020). A unified account of numerosity perception.
3559 *Nature Human Behaviour*, 4(December). <https://doi.org/10.1038/s41562-020-00946-0>
- 3560 Cicchini, G. M., Anobile, G., & Burr, D. C. (2016). Spontaneous perception of numerosity in
3561 humans. *Nature Communications*, 7(1), 12536. <https://doi.org/10.1038/ncomms12536>
- 3562 Clare, S. (1997). *Functional MRI: Methods and Applications*. (October), 155.
- 3563 Clifford, C. W. G., Wenderoth, P., & Spehar, B. (2000). A functional angle on some after-
3564 effects in cortical vision. *Proceedings of the Royal Society B: Biological Sciences*,
3565 267(1454), 1705–1710. <https://doi.org/10.1098/rspb.2000.1198>
- 3566 Cohen Kadosh, R., Cohen Kadosh, K., Kaas, A., Henik, A., & Goebel, R. (2007). Notation-
3567 Dependent and -Independent Representations of Numbers in the Parietal Lobes. *Neuron*,
3568 53(2), 307–314. <https://doi.org/10.1016/j.neuron.2006.12.025>
- 3569 Collins, D. L., Neelin, P., Peters, T. M., & Evans, A. C. (1994). Automatic 3D intersubject
3570 registration of MR volumetric data in standardized Talairach space. *Journal of*
3571 *Computer Assisted Tomography*, 18(2), 192–205.
- 3572 Connor, C. E., Preddie, D. C., Gallant, J. L., & Van Essen, D. C. (1997). Spatial attention
3573 effects in macaque area V4. *Journal of Neuroscience*, 17(9), 3201–3214.
3574 <https://doi.org/10.1523/jneurosci.17-09-03201.1997>
- 3575 Corbetta, M., Miezin, F., Dobmeyer, S., Shulman, G., & Petersen, S. (1990). Attentional
3576 modulation of neural processing of shape, color, and velocity in humans. *Science*,
3577 248(4962), 1556–1559. <https://doi.org/10.1126/science.2360050>
- 3578 Corbetta, M., & Shulman, G. L. (2002). Control of goal-directed and stimulus-driven
3579 attention in the brain. *Nature Reviews Neuroscience*, 3(3), 201–215.
3580 <https://doi.org/10.1038/nrn755>
- 3581 Cordes, S., Gelman, R., Gallistel, C. R., & Whalen, J. (2001). Variability signatures
3582 distinguish verbal from nonverbal counting for both large and small numbers.

3583 *Psychonomic Bulletin and Review*, 8(4), 698–707. <https://doi.org/10.3758/BF03196206>

3584 Cox, R. W. (1996). AFNI: Software for analysis and visualization of functional magnetic
3585 resonance neuroimages. *Computers and Biomedical Research*, 29(3), 162–173.
3586 <https://doi.org/10.1006/cbmr.1996.0014>

3587 Cox, R. W., & Hyde, J. S. (1997). Software tools for analysis and visualization of fMRI data.
3588 *NMR in Biomedicine*, 10(4–5), 171–178. [https://doi.org/10.1002/\(SICI\)1099-](https://doi.org/10.1002/(SICI)1099-)
3589 1492(199706/08)10:4/5<171::AID-NBM453>3.0.CO;2-L

3590 Dacke, M., & Srinivasan, M. V. (2008). Evidence for counting in insects. *Animal Cognition*,
3591 11(4), 683–689. <https://doi.org/10.1007/s10071-008-0159-y>

3592 Dakin, S. C., Tibber, M. S., Greenwood, J. A., Kingdom, F. A. A., & Morgan, M. J. (2011).
3593 A common visual metric for approximate number and density. *Proceedings of the*
3594 *National Academy of Sciences*, 108(49), 19552–19557.
3595 <https://doi.org/10.1073/pnas.1113195108>

3596 Dakin, Steven C., Tibber, M. S., Greenwood, J. A., Kingdom, F. A. A., & Morgan, M. J.
3597 (2011). A common visual metric for approximate number and density. *Proceedings of*
3598 *the National Academy of Sciences of the United States of America*, 108(49), 19552–
3599 19557. <https://doi.org/10.1073/pnas.1113195108>

3600 Daniel, B. Y. P. M., Whitteridge, D., Hospital, M., & London, S. E. (1961). *THE*
3601 *REPRESENTATION OF THE VISUAL FIELD ON THE CEREBRAL CORTEX IN*
3602 *MONKEYS From the Department of Neuropathology , Institute of Psychiatry , On the*
3603 *basis of his extensive and elegant anatomical investigations on the visual cortex , Poliak*
3604 *(1932) suggested.* 203–221.

3605 Dayan, P., & Abbott, L. F. (2001). *Theoretical neuroscience: computational and*
3606 *mathematical modeling of neural systems.*

3607 De Martino, F., Yacoub, E., Kemper, V., Moerel, M., Uludag, K., De Weerd, P., ...
3608 Formisano, E. (2018). The impact of ultra-high field MRI on cognitive and
3609 computational neuroimaging. *NeuroImage*, 168(March 2017), 366–382.
3610 <https://doi.org/10.1016/j.neuroimage.2017.03.060>

3611 Defever, E., Sasanguie, D., Gebuis, T., & Reynvoet, B. (2011). Children’s representation of
3612 symbolic and nonsymbolic magnitude examined with the priming paradigm. *Journal of*
3613 *Experimental Child Psychology*, 109(2), 174–186.
3614 <https://doi.org/10.1016/j.jecp.2011.01.002>

3615 Dehaene, A. S., Spelke, E., Pined, P., Stanescu, R., Tsivkin, S., Dehaene, S., ... Tsivkin, S.
3616 (2016). *Sources of Mathematical Thinking : Behavioral and Brain-Imaging Evidence*
3617 *Published by : American Association for the Advancement of Science Stable URL :*
3618 *http://www.jstor.org/stable/2899209 REFERENCES Linked references are available on*
3619 *JSTOR for this artic.* 284(5416), 970–974.

3620 Dehaene, S. (1992). Varieties of numerical abilities. *Cognition*, 44(1–2), 1–42.
3621 [https://doi.org/10.1016/0010-0277\(92\)90049-N](https://doi.org/10.1016/0010-0277(92)90049-N)

3622 Dehaene, S. (2001). Precise of The Number Sense. *Mind and Language*, 16(1), 16–36.
3623 <https://doi.org/10.1111/1468-0017.00154>

3624 Dehaene, S. (2003). The neural basis of the Weber-Fechner law: A logarithmic mental
3625 number line. *Trends in Cognitive Sciences*, 7(4), 145–147.
3626 [https://doi.org/10.1016/S1364-6613\(03\)00055-X](https://doi.org/10.1016/S1364-6613(03)00055-X)

3627 Dehaene, S., & Changeux, J. P. (1993). Development of elementary numerical abilities: A
3628 neuronal model. *Journal of Cognitive Neuroscience*, 5(4), 390–407.
3629 <https://doi.org/10.1162/jocn.1993.5.4.390>

3630 Dehaene, S., & Cohen, L. (1995).
3631 DehaeneCohen_TripleCodeModelNumberProcessing_MathCognition1995.pdf.
3632 *Mathematical Cognition*, Vol. 1, pp. 83–120.

- 3633 Dehaene, S., & Cohen, L. (2007). Cultural recycling of cortical maps. *Neuron*, *56*(2), 384–
3634 398. <https://doi.org/10.1016/j.neuron.2007.10.004>
- 3635 Dehaene, S., Dehaene-Lambertz, G., & Cohen, L. (1998). Abstract representations of
3636 numbers in the animal and human brain. *Trends in Neurosciences*, *21*(8), 355–361.
3637 [https://doi.org/10.1016/S0166-2236\(98\)01263-6](https://doi.org/10.1016/S0166-2236(98)01263-6)
- 3638 Dehaene, S., Molko, N., Cohen, L., & Wilson, A. J. (2004). Arithmetic and the brain. *Current*
3639 *Opinion in Neurobiology*, *14*(2), 218–224. <https://doi.org/10.1016/j.conb.2004.03.008>
- 3640 DeWind, N. K., Adams, G. K., Platt, M. L., & Brannon, E. M. (2015). Modeling the
3641 approximate number system to quantify the contribution of visual stimulus features.
3642 *Cognition*, *142*, 247–265. <https://doi.org/10.1016/j.cognition.2015.05.016>
- 3643 DeWind, N. K., Park, J., Woldorff, M. G., & Brannon, E. M. (2019). Numerical encoding in
3644 early visual cortex. *Cortex*, *114*, 76–89. <https://doi.org/10.1016/j.cortex.2018.03.027>
- 3645 Deyoe, E. A., Carman, G. J., Bandettini, P., Glickman, S., Wieser, J., Cox, R., ... Neitz, J.
3646 (1996). Mapping striate and extrastriate visual areas in human cerebral cortex.
3647 *Proceedings of the National Academy of Sciences of the United States of America*, *93*(6),
3648 2382–2386. <https://doi.org/10.1073/pnas.93.6.2382>
- 3649 Ditz, H. M., & Nieder, A. (2015). Neurons selective to the number of visual items in the
3650 corvid songbird endbrain. *Proceedings of the National Academy of Sciences*, *112*(25),
3651 7827–7832. <https://doi.org/10.1073/pnas.1504245112>
- 3652 Ditz, H. M., & Nieder, A. (2016a). Numerosity representations in crows obey the Weber–
3653 Fechner law. *Proceedings of the Royal Society B: Biological Sciences*, *283*(1827),
3654 20160083. <https://doi.org/10.1098/rspb.2016.0083>
- 3655 Ditz, H. M., & Nieder, A. (2016b). Sensory and Working Memory Representations of Small
3656 and Large Numerosities in the Crow Endbrain. *The Journal of Neuroscience*, *36*(47),
3657 12044–12052. <https://doi.org/10.1523/jneurosci.1521-16.2016>
- 3658 Dumoulin, S. O., Bittar, R. G., Kabani, N. J., Baker, C. L., Le Goualher, G., Pike, G. B., &
3659 Evans, A. C. (2000). A new anatomical landmark for reliable identification of human
3660 area V5/MT: A quantitative analysis of sulcal patterning. *Cerebral Cortex*, *10*(5), 454–
3661 463. <https://doi.org/10.1093/cercor/10.5.454>
- 3662 Dumoulin, S. O., Fracasso, A., van der Zwaag, W., Siero, J. C. W., & Petridou, N. (2018).
3663 Ultra-high field MRI: Advancing systems neuroscience towards mesoscopic human
3664 brain function. *NeuroImage*, *168*(September 2016), 345–357.
3665 <https://doi.org/10.1016/j.neuroimage.2017.01.028>
- 3666 Dumoulin, S. O., & Knapen, T. (2018). How visual cortical organization is altered by
3667 ophthalmologic and neurologic disorders. *Annual Review of Vision Science*, *4*, 357–379.
3668 <https://doi.org/10.1146/annurev-vision-091517-033948>
- 3669 Dumoulin, S. O., & Wandell, B. A. (2008). Population receptive field estimates in human
3670 visual cortex. *NeuroImage*, *39*(2), 647–660.
3671 <https://doi.org/10.1016/j.neuroimage.2007.09.034>
- 3672 Duong, T. Q., Yacoub, E., Adriany, G., Hu, X., Ugurbil, K., & Kim, S. G. (2003).
3673 Microvascular BOLD contribution at 4 and 7 T in the human brain: Gradient-echo and
3674 spin-echo fMRI with suppression of blood effects. *Magnetic Resonance in Medicine*,
3675 *49*(6), 1019–1027. <https://doi.org/10.1002/mrm.10472>
- 3676 Durgin, F. H. (2008). Texture density adaptation and visual number revisited. *Current*
3677 *Biology*, *18*(18), 855–856. <https://doi.org/10.1016/j.cub.2008.07.053>
- 3678 Eger, E., Michel, V., Thirion, B., Amadon, A., Dehaene, S., & Kleinschmidt, A. (2009).
3679 Deciphering Cortical Number Coding from Human Brain Activity Patterns. *Current*
3680 *Biology*, *19*(19), 1608–1615. <https://doi.org/10.1016/j.cub.2009.08.047>
- 3681 Eger, E., Sterzer, P., Russ, M. O., Giraud, A.-L., & Kleinschmidt, A. (2003). A Supramodal
3682 Number Representation in Human Intraparietal Cortex. *Neuron*, *37*(4), 719–726.

3683 [https://doi.org/10.1016/S0896-6273\(03\)00036-9](https://doi.org/10.1016/S0896-6273(03)00036-9)

3684 Emmerton, J., Lohmann, A., & Niemann, J. (1997). Pigeons' serial ordering of numerosity
3685 with visual arrays. *Animal Learning and Behavior*, 25(2), 234–244.
3686 <https://doi.org/10.3758/BF03199062>

3687 Feigenson, L., Dehaene, S., & Spelke, E. (2004). Core systems of number. *Trends in*
3688 *Cognitive Sciences*, 8(7), 307–314. <https://doi.org/10.1016/j.tics.2004.05.002>

3689 Fornaciai, M., Brannon, E. M., Woldorff, M. G., & Park, J. (2017). Numerosity processing in
3690 early visual cortex. *NeuroImage*, 157(May), 429–438.
3691 <https://doi.org/10.1016/j.neuroimage.2017.05.069>

3692 Fracasso, A., Petridou, N., & Dumoulin, S. O. (2016). Systematic variation of population
3693 receptive field properties across cortical depth in human visual cortex. *NeuroImage*,
3694 139. <https://doi.org/10.1016/j.neuroimage.2016.06.048>

3695 Gallistel, C. R., & Gelman, R. (1992). Preverbal and verbal counting and computation.
3696 *Cognition*, 44(1–2), 43–74. [https://doi.org/10.1016/0010-0277\(92\)90050-R](https://doi.org/10.1016/0010-0277(92)90050-R)

3697 Gati, J. S., Menon, R. S., U?urbil, K., & Rutt, B. K. (1997). Experimental determination of
3698 the BOLD field strength dependence in vessels and tissue. *Magnetic Resonance in*
3699 *Medicine*, 38(2), 296–302. <https://doi.org/10.1002/mrm.1910380220>

3700 Gebuis, T., Gevers, W., & Cohen Kadosh, R. (2014). Topographic representation of high-
3701 level cognition: Numerosity or sensory processing? *Trends in Cognitive Sciences*, 18(1),
3702 1–3. <https://doi.org/10.1016/j.tics.2013.10.002>

3703 Gebuis, T., & Reynvoet, B. (2012). The role of visual information in numerosity estimation.
3704 *PLoS ONE*, 7(5). <https://doi.org/10.1371/journal.pone.0037426>

3705 Geißler, A., Matt, E., Fischmeister, F., Wurnig, M., Dymerska, B., Knosp, E., ... Beisteiner,
3706 R. (2014). Differential functional benefits of ultra highfield MR systems within the
3707 language network. *NeuroImage*, 103, 163–170.
3708 <https://doi.org/10.1016/j.neuroimage.2014.09.036>

3709 Geißler, Alexander, Fischmeister, F. S. P., Grabner, G., Wurnig, M., Rath, J., Foki, T., ...
3710 Robinson, S. D. (2013). Comparing the microvascular specificity of the 3- and 7-T
3711 BOLD response using ICA and susceptibility-weighted imaging. *Frontiers in Human*
3712 *Neuroscience*, 7(JUL), 1–7. <https://doi.org/10.3389/fnhum.2013.00474>

3713 Gilmore, C. K., McCarthy, S. E., & Spelke, E. S. (2010). Non-symbolic arithmetic abilities
3714 and mathematics achievement in the first year of formal schooling. *Cognition*, 115(3),
3715 394–406. <https://doi.org/10.1016/j.cognition.2010.02.002>

3716 Giurfa, M. (2019). An Insect's Sense of Number. *Trends in Cognitive Sciences*, 23(9), 720–
3717 722. <https://doi.org/10.1016/j.tics.2019.06.010>

3718 Glover, G. H. (1999). Deconvolution of impulse response in event-related BOLD fMRI.
3719 *NeuroImage*, 9(4), 416–429. <https://doi.org/10.1006/nimg.1998.0419>

3720 Gonzalez-Castillo, J., Hoy, C. W., Handwerker, D. A., Roopchansingh, V., Inati, S. J., Saad,
3721 Z. S., ... Bandettini, P. A. (2015). Task dependence, tissue specificity, and spatial
3722 distribution of widespread activations in large single-subject functional MRI datasets at
3723 7T. *Cerebral Cortex*, 25(12), 4667–4677. <https://doi.org/10.1093/cercor/bhu148>

3724 Gonzalez-Castillo, J., Saad, Z. S., Handwerker, D. A., Inati, S. J., Brenowitz, N., &
3725 Bandettini, P. A. (2012). Whole-brain, time-locked activation with simple tasks revealed
3726 using massive averaging and model-free analysis. *Proceedings of the National Academy*
3727 *of Sciences of the United States of America*, 109(14), 5487–5492.
3728 <https://doi.org/10.1073/pnas.1121049109>

3729 Gourtzelidis, P., Tzagarakis, C., Lewis, S. M., Crowe, D. A., Auerbach, E., Jerde, T. A., ...
3730 Georgopoulos, A. P. (2005). Mental maze solving: directional fMRI tuning and
3731 population coding in the superior parietal lobule. *Experimental Brain Research*, 165(3),
3732 273–282.

- 3733 Green, D. M., & Swets, J. A. (1966). *Signal Detection Theory and Psychophysics* (Vol. 1).
3734 New York: Wiley.
- 3735 Grotheer, M., Herrmann, K. H., & Kovács, G. (2016). Neuroimaging evidence of a bilateral
3736 representation for visually presented numbers. *Journal of Neuroscience*, *36*(1), 88–97.
3737 <https://doi.org/10.1523/JNEUROSCI.2129-15.2016>
- 3738 Haast, R. A. M., Ivanov, D., & Uludağ, K. (2018). The impact of B1+ correction on
3739 MP2RAGE cortical T 1 and apparent cortical thickness at 7T. *Human Brain Mapping*,
3740 *39*(6), 2412–2425. <https://doi.org/10.1002/hbm.24011>
- 3741 Halberda, J., & Feigenson, L. (2008). Developmental Change in the Acuity of the “Number
3742 Sense”: The Approximate Number System in 3-, 4-, 5-, and 6-Year-Olds and Adults.
3743 *Developmental Psychology*, *44*(5), 1457–1465. <https://doi.org/10.1037/a0012682>
- 3744 Halberda, J., Mazocco, M. M. M., & Feigenson, L. (2008). Individual differences in non-
3745 verbal number acuity correlate with maths achievement. *Nature*, *455*(7213), 665–668.
3746 <https://doi.org/10.1038/nature07246>
- 3747 Hannagan, T., Amedi, A., Cohen, L., Dehaene-Lambertz, G., & Dehaene, S. (2015). Origins
3748 of the specialization for letters and numbers in ventral occipitotemporal cortex. *Trends*
3749 *in Cognitive Sciences*, *19*(7), 374–382. <https://doi.org/10.1016/j.tics.2015.05.006>
- 3750 Harvey, B. M., Klein, B. P., Petridou, N., & Dumoulin, S. O. (2013). Topographic
3751 Representation of Numerosity in the Human Parietal Cortex. *Science*, *341*(6150), 1123–
3752 1126. <https://doi.org/10.1126/science.1239052>
- 3753 Harvey, Ben M., & Dumoulin, S. O. (2011). The relationship between cortical magnification
3754 factor and population receptive field size in human visual cortex: Constancies in cortical
3755 architecture. *Journal of Neuroscience*, *31*(38), 13604–13612.
3756 <https://doi.org/10.1523/JNEUROSCI.2572-11.2011>
- 3757 Harvey, Ben M., & Dumoulin, S. O. (2017a). A network of topographic numerosity maps in
3758 human association cortex. *Nature Human Behaviour*, *1*(2), 0036.
3759 <https://doi.org/10.1038/s41562-016-0036>
- 3760 Harvey, Ben M., & Dumoulin, S. O. (2017b). Can responses to basic non-numerical visual
3761 features explain neural numerosity responses? *NeuroImage*, *149*(February), 200–209.
3762 <https://doi.org/10.1016/j.neuroimage.2017.02.012>
- 3763 Harvey, Ben M., & Dumoulin, S. O. (2018). Data describing the accuracy of non-numerical
3764 visual features in predicting fMRI responses to numerosity. *Data in Brief*, *16*, 193–205.
3765 <https://doi.org/10.1016/j.dib.2017.11.022>
- 3766 Harvey, Ben M., Dumoulin, S. O., Fracasso, A., & Paul, J. M. (2020). A Network of
3767 Topographic Maps in Human Association Cortex Hierarchically Transforms Visual
3768 Timing-Selective Responses. *Current Biology*, *30*(8), 1424-1434.e6.
3769 <https://doi.org/10.1016/j.cub.2020.01.090>
- 3770 Harvey, Ben M., Fracasso, A., Petridou, N., & Dumoulin, S. O. (2015). Topographic
3771 representations of object size and relationships with numerosity reveal generalized
3772 quantity processing in human parietal cortex. *Proceedings of the National Academy of*
3773 *Sciences*, *112*(44), 13525–13530. <https://doi.org/10.1073/pnas.1515414112>
- 3774 He, L., Zhou, K., Zhou, T., He, S., & Chen, L. (2015). *Topology-defined units in numerosity*
3775 *perception*. 2015. <https://doi.org/10.1073/pnas.1512408112>
- 3776 He, X., Guo, P., Li, S., Shen, X., & Zhou, X. (2021). Non-symbolic and symbolic number
3777 lines are dissociated. *Cognitive Processing*, *22*(3), 475–486.
3778 <https://doi.org/10.1007/s10339-021-01019-4>
- 3779 Hermes, D., Rangarajan, V., Foster, B. L., King, J. R., Kasikci, I., Miller, K. J., & Parvizi, J.
3780 (2017). Electrophysiological responses in the ventral temporal cortex during reading of
3781 numerals and calculation. *Cerebral Cortex*, *27*(1), 567–575.
3782 <https://doi.org/10.1093/cercor/bhv250>

3783 Hesse, P. N., Schmitt, C., Klingenhoefer, S., & Bremmer, F. (2017). Preattentive Processing
3784 of Numerical Visual Information. *Frontiers in Human Neuroscience*, *11*(February), 1–
3785 14. <https://doi.org/10.3389/fnhum.2017.00070>

3786 Hofstetter, S., Cai, Y., Harvey, B. M., & Dumoulin, S. O. (2021). Topographic maps
3787 representing haptic numerosity reveals distinct sensory representations in supramodal
3788 networks. *Nature Communications*, *12*(1), 1–13. <https://doi.org/10.1038/s41467-020-20567-5>

3790 Hofstetter, S., & Dumoulin, S. O. (2021). Tuned neural responses to haptic numerosity in the
3791 putamen. *NeuroImage*, *238*(February), 118178.
3792 <https://doi.org/10.1016/j.neuroimage.2021.118178>

3793 Hopfinger, J. B., Buonocore, M. H., & Mangun, G. R. (2000). The neural mechanisms of top-
3794 down attentional control. *Nature Neuroscience*, *3*(3), 284–291.
3795 <https://doi.org/10.1038/72999>

3796 Huntenburg, J. M., Steele, C. J., & Bazin, P. L. (2018). Nighres: processing tools for high-
3797 resolution neuroimaging. *GigaScience*, *7*(7), 1–9.
3798 <https://doi.org/10.1093/gigascience/giy082>

3799 Hutton, C., Josephs, O., Stadler, J., Featherstone, E., Reid, A., Speck, O., ... Weiskopf, N.
3800 (2011). The impact of physiological noise correction on fMRI at 7T. *NeuroImage*, *57*(1),
3801 101–112. <https://doi.org/10.1016/j.neuroimage.2011.04.018>

3802 Hyde, D. C., & Spelke, E. S. (2011). Neural signatures of number processing in human
3803 infants: Evidence for two core systems underlying numerical cognition. *Developmental*
3804 *Science*, *14*(2), 360–371. <https://doi.org/10.1111/j.1467-7687.2010.00987.x>

3805 Izard, V. R., Sann, C., Spelke, E. S., & Streri, A. (2009). Newborn infants perceive abstract
3806 numbers. *Proceedings of the National Academy of Sciences of the United States of*
3807 *America*, *106*(25), 10382–10385. <https://doi.org/10.1073/pnas.0812142106>

3808 JASP Team. (2020). JASP (Version 0.14.1)[Computer software]. Retrieved from [https://jasp-](https://jasp-stats.org/)
3809 [stats.org/](https://jasp-stats.org/)

3810 Jerde, T. A., Lewis, S. M., Goerke, U., Gourtzelidis, P., Tzagarakis, C., Lynch, J., ...
3811 Georgopoulos, A. P. (2008). Ultra-high field parallel imaging of the superior parietal
3812 lobule during mental maze solving. *Experimental Brain Research*, *187*(4), 551–561.
3813 <https://doi.org/10.1007/s00221-008-1318-8>

3814 Kaufman, E. L., & Lord, M. W. (1949). The discrimination of visual number. *The American*
3815 *Journal of Psychology*, *62*(4), 498–525. <https://doi.org/10.2307/1418556>

3816 Kay, K. N., Naselaris, T., Prenger, R. J., & Gallant, J. L. (2008). Identifying natural images
3817 from human brain activity. *Nature*, *452*(7185), 352–355.
3818 <https://doi.org/10.1038/nature06713>

3819 Kay, K. N., Winawer, J., Mezer, A., & Wandell, B. A. (2013). Compressive spatial
3820 summation in human visual cortex. *Journal of Neurophysiology*, *110*(2), 481–494.
3821 <https://doi.org/10.1152/jn.00105.2013>

3822 Kim, G., Jang, J., Baek, S., Song, M., & Paik, S. B. (2021). Visual number sense in untrained
3823 deep neural networks. *Science Advances*, *7*(1), 1–10.
3824 <https://doi.org/10.1126/sciadv.abd6127>

3825 Kirjakovski, A., & Matsumoto, E. (2016). Numerosity underestimation in sets with illusory
3826 contours. *Vision Research*, *122*, 34–42. <https://doi.org/10.1016/j.visres.2016.03.005>

3827 Klein, B. P., Harvey, B. M., & Dumoulin, S. O. (2014). Attraction of position preference by
3828 spatial attention throughout human visual cortex. *Neuron*, *84*(1), 227–237.
3829 <https://doi.org/10.1016/j.neuron.2014.08.047>

3830 Kleiner, M., Brainard, D., & Pelli, D. (2007). *What 's new in Psychtoolbox-3 ?*

3831 Krasnow, B., Tamm, L., Greicius, M. D., Yang, T. T., Glover, G. H., Reiss, A. L., & Menon,
3832 V. (2003). Comparison of fMRI activation at 3 and 1.5 T during perceptual, cognitive,

3833 and affective processing. *NeuroImage*, 18(4), 813–826. [https://doi.org/10.1016/S1053-8119\(03\)00002-8](https://doi.org/10.1016/S1053-8119(03)00002-8)

3834

3835 Krüger, G., & Glover, G. H. (2001). Physiological noise in oxygenation-sensitive magnetic
3836 resonance imaging. *Magnetic Resonance in Medicine*, 46(4), 631–637.
3837 <https://doi.org/10.1002/mrm.1240.abs>

3838 Kutter, E. F., Bostroem, J., Elger, C. E., Mormann, F., & Nieder, A. (2018). Single Neurons
3839 in the Human Brain Encode Numbers. *Neuron*, 100(3), 753–761.e4.
3840 <https://doi.org/10.1016/j.neuron.2018.08.036>

3841 Lage-Castellanos, A., Valente, G., Formisano, E., & De Martino, F. (2019). Methods for
3842 computing the maximum performance of computational models of fMRI responses.
3843 *PLOS Computational Biology*, 15(3), e1006397.
3844 <https://doi.org/10.1371/journal.pcbi.1006397>

3845 Lasne, G., Piazza, M., Dehaene, S., Kleinschmidt, A., & Eger, E. (2019). Discriminability of
3846 numerosity-evoked fMRI activity patterns in human intra-parietal cortex reflects
3847 behavioral numerical acuity. *Cortex*, 114, 90–101.
3848 <https://doi.org/10.1016/j.cortex.2018.03.008>

3849 Lerma-Usabiaga, G., Benson, N., Winawer, J., & Wandell, B. A. (2020). A validation
3850 framework for neuroimaging software: The case of population receptive fields. *PLoS
3851 Computational Biology*, 16(6), 1–18. <https://doi.org/10.1371/journal.pcbi.1007924>

3852 Li, Y. (2013). T1 and T2 Metabolite Relaxation Times in Normal Brain at 3T and 7T.
3853 *Journal of Molecular Imaging & Dynamics*, 02(02), 1–5. <https://doi.org/10.4172/2155-9937.s1-002>

3854

3855 Libertus, M. E., Feigenson, L., & Halberda, J. (2011). Preschool acuity of the approximate
3856 number system correlates with school math ability. *Developmental Science*, 14(6),
3857 1292–1300. <https://doi.org/10.1111/j.1467-7687.2011.01080.x>

3858 Logothetis, N. K. (2002). The neural basis of the blood-oxygen-level-dependent functional
3859 magnetic resonance imaging signal. *Philosophical Transactions of the Royal Society B:
3860 Biological Sciences*, 357(1424), 1003–1037. <https://doi.org/10.1098/rstb.2002.1114>

3861 Logothetis, N. K., & Wandell, B. A. (2004). Interpreting the BOLD Signal. *Annual Review of
3862 Physiology*, 66(1), 735–769. <https://doi.org/10.1146/annurev.physiol.66.082602.092845>

3863 Machens, C. K., Wehr, M. S., & Zador, A. M. (2004). Linearity of Cortical Receptive Fields
3864 Measured with Natural Sounds. *Journal of Neuroscience*, 24(5), 1089–1100.
3865 <https://doi.org/10.1523/JNEUROSCI.4445-03.2004>

3866 Maldonado Moscoso, P. A., Castaldi, E., Burr, D. C., Arrighi, R., & Anobile, G. (2020).
3867 Grouping strategies in number estimation extend the subitizing range. *Scientific Reports*,
3868 10(1), 1–10. <https://doi.org/10.1038/s41598-020-71871-5>

3869 Mandler, G., & Shebo, B. J. (1982). Subitizing: An analysis of its component processes.
3870 *Journal of Experimental Psychology: General*, 111(1), 1–22.
3871 <https://doi.org/10.1037//0096-3445.111.1.1>

3872 Mante, V., Frazor, R. A., Bonin, V., Geisler, W. S., & Carandini, M. (2005). Independence of
3873 luminance and contrast in natural scenes and in the early visual system. *Nature
3874 Neuroscience*, 8(12), 1690–1697. <https://doi.org/10.1038/nn1556>

3875 Marinova, M., Sasanguie, D., & Reynvoet, B. (2021). Numerals do not need numerosities:
3876 robust evidence for distinct numerical representations for symbolic and non-symbolic
3877 numbers. *Psychological Research*, 85(2), 764–776. <https://doi.org/10.1007/s00426-019-01286-z>

3878

3879 Marques, J. P., Kober, T., Krueger, G., van der Zwaag, W., Van de Moortele, P. F., &
3880 Gruetter, R. (2010). MP2RAGE, a self bias-field corrected sequence for improved
3881 segmentation and T1-mapping at high field. *NeuroImage*, 49(2), 1271–1281.
3882 <https://doi.org/10.1016/j.neuroimage.2009.10.002>

3883 Martinez-Trujillo, J. C., & Treue, S. (2004). Feature-Based Attention Increases the
3884 Selectivity of Population Responses in Primate Visual Cortex. *Current Biology*, *14*(9),
3885 744–751. <https://doi.org/10.1016/j.cub.2004.04.028>

3886 Maunsell, J. H. R., & Treue, S. (2006). Feature-based attention in visual cortex. *Trends in*
3887 *Neurosciences*, *29*(6), 317–322. <https://doi.org/10.1016/j.tins.2006.04.001>

3888 McAdams, C. J., & Maunsell, J. H. R. (1999a). Effects of attention on orientation-tuning
3889 functions of single neurons in macaque cortical area V4. *Journal of Neuroscience*, *19*(1),
3890 431–441. <https://doi.org/10.1523/jneurosci.19-01-00431.1999>

3891 McAdams, C. J., & Maunsell, J. H. R. (1999b). Effects of Attention on the Reliability of
3892 Individual Neurons in Monkey Visual Cortex. *Neuron*, *23*(4), 765–773.
3893 [https://doi.org/10.1016/S0896-6273\(01\)80034-9](https://doi.org/10.1016/S0896-6273(01)80034-9)

3894 Meck, W. H., & Church, R. M. (1983). A mode control model of counting and timing
3895 processes. *Journal of Experimental Psychology: Animal Behavior Processes*, *9*(3), 320.

3896 Merten, K., & Nieder, A. (2009). Compressed scaling of abstract numerosity representations
3897 in adult humans and monkeys. *Journal of Cognitive Neuroscience*, *21*(2), 333–346.
3898 <https://doi.org/10.1162/jocn.2008.21032>

3899 Moran, J., & Desimone, R. (1985). Selective attention gates visual processing in the
3900 extrastriate cortex. *Science*, *229*(4715), 782–784.
3901 <https://doi.org/10.1126/science.4023713>

3902 Moyer, R. S., & Landauer, T. K. (1967). Time required for judgements of numerical
3903 inequality. *Nature*, *215*(5109), 1519–1520.

3904 Murphy, K., Bodurka, J., & Bandettini, P. A. (2007). How long to scan? The relationship
3905 between fMRI temporal signal to noise ratio and necessary scan duration. *NeuroImage*,
3906 *34*(2), 565–574. <https://doi.org/10.1016/j.neuroimage.2006.09.032>

3907 Naccache, L., Dehaene, S., Inselem, U., Hospitalier, S., & Joliot, F. (2001).
3908 *NaccacheDehaene_ParietalPriming_CerebralCortex2001*. 966–974.

3909 Naselaris, T., Kay, K. N., Nishimoto, S., & Gallant, J. L. (2011). Encoding and decoding in
3910 fMRI. *NeuroImage*, *56*(2), 400–410. <https://doi.org/10.1016/j.neuroimage.2010.07.073>

3911 Nasr, K., & Nieder, A. (2021). Spontaneous representation of numerosity zero in a deep
3912 neural network for visual object recognition. *iScience*, *24*(11).
3913 <https://doi.org/10.1016/j.isci.2021.103301>

3914 Nasr, K., Viswanathan, P., & Nieder, A. (2019). Number detectors spontaneously emerge in a
3915 deep neural network designed for visual object recognition. *Science Advances*, *5*(5), 1–
3916 11. <https://doi.org/10.1126/sciadv.aav7903>

3917 Nieder, A. (2012). Supramodal numerosity selectivity of neurons in primate prefrontal and
3918 posterior parietal cortices. *Proceedings of the National Academy of Sciences*, *109*(29),
3919 11860–11865. <https://doi.org/10.1073/pnas.1204580109>

3920 Nieder, A., & Merten, K. (2007). A Labeled-Line Code for Small and Large Numerosities in
3921 the Monkey Prefrontal Cortex. *Journal of Neuroscience*, *27*(22), 5986–5993.
3922 <https://doi.org/10.1523/jneurosci.1056-07.2007>

3923 Nieder, A., & Miller, E. K. (2004). A parieto-frontal network for visual numerical
3924 information in the monkey. *Proceedings of the National Academy of Sciences*, *101*(19),
3925 7457–7462. <https://doi.org/10.1073/pnas.0402239101>

3926 Nieder, Andreas. (2004). The number domain - Can we count on parietal cortex? *Neuron*,
3927 *44*(3), 407–409. <https://doi.org/10.1016/j.neuron.2004.10.020>

3928 Nieder, Andreas. (2012). Supramodal numerosity selectivity of neurons in primate prefrontal
3929 and posterior parietal cortices. *Proceedings of the National Academy of Sciences of the*
3930 *United States of America*, *109*(29), 11860–11865.
3931 <https://doi.org/10.1073/pnas.1204580109>

3932 Nieder, Andreas. (2016). The neuronal code for number. *Nature Reviews Neuroscience*,

3933 17(6), 366–382. <https://doi.org/10.1038/nrn.2016.40>

3934 Nieder, Andreas. (2020a). Neural constraints on human number concepts. *Current Opinion in*
3935 *Neurobiology*, 60, 28–36. <https://doi.org/10.1016/j.conb.2019.10.003>

3936 Nieder, Andreas. (2020b). The Adaptive Value of Numerical Competence. *Trends in Ecology*
3937 *& Evolution*, 1–13. <https://doi.org/10.1016/j.tree.2020.02.009>

3938 Nieder, Andreas. (2021). The Evolutionary History of Brains for Numbers. *Trends in*
3939 *Cognitive Sciences*, 25(7), 608–621. <https://doi.org/10.1016/j.tics.2021.03.012>

3940 Nieder, Andreas, & Dehaene, S. (2009). Representation of Number in the Brain. *Annual*
3941 *Review of Neuroscience*, 32(1), 185–208.
3942 <https://doi.org/10.1146/annurev.neuro.051508.135550>

3943 Nieder, Andreas, Freedman, D. J., & Miller, E. K. (2002a). Representation of the quantity of
3944 visual items in the primate prefrontal cortex. *Science*, 297(5587), 1708–1711.
3945 <https://doi.org/10.1126/science.1072493>

3946 Nieder, Andreas, Freedman, D. J., & Miller, E. K. (2002b). Representation of the quantity of
3947 visual items in the primate prefrontal cortex. *Science*, 297(5587), 1708–1711.
3948 <https://doi.org/10.1126/science.1072493>

3949 Nieder, Andreas, & Miller, E. K. (2003). Coding of Cognitive Magnitude. *Neuron*, 37(1),
3950 149–157. [https://doi.org/10.1016/s0896-6273\(02\)01144-3](https://doi.org/10.1016/s0896-6273(02)01144-3)

3951 Nieder, Andreas, & Miller, E. K. (2004a). A parieto-frontal network for visual numerical
3952 information in the monkey. *Proceedings of the National Academy of Sciences*, 101(19),
3953 7457–7462. <https://doi.org/10.1073/pnas.0402239101>

3954 Nieder, Andreas, & Miller, E. K. (2004b). Analog numerical representations in rhesus
3955 monkeys: Evidence for parallel processing. *Journal of Cognitive Neuroscience*, 16(5),
3956 889–901. <https://doi.org/10.1162/089892904970807>

3957 O’Craven, K. M., Rosen, B. R., Kwong, K. K., Treisman, A., & Savoy, R. L. (1997).
3958 Voluntary attention modulates fMRI activity in human MT-MST. *Neuron*, 18(4), 591–
3959 598. [https://doi.org/10.1016/S0896-6273\(00\)80300-1](https://doi.org/10.1016/S0896-6273(00)80300-1)

3960 Oliveira, Í. A. F., Cai, Y., Hofstetter, S., Siero, J. C. W., van der Zwaag, W., & Dumoulin, S.
3961 O. (2022). Comparing BOLD and VASO-CBV population receptive field estimates in
3962 human visual cortex. *NeuroImage*, 248(December 2021).
3963 <https://doi.org/10.1016/j.neuroimage.2021.118868>

3964 Op de Beeck, H. P., Pillet, I., & Ritchie, J. B. (2019). Factors Determining Where Category-
3965 Selective Areas Emerge in Visual Cortex. *Trends in Cognitive Sciences*, 23(9), 784–797.
3966 <https://doi.org/10.1016/j.tics.2019.06.006>

3967 Pan, Y., Yang, H., Li, M., Zhang, J., & Cui, L. (2021). Grouping strategies in numerosity
3968 perception between intrinsic and extrinsic grouping cues. *Scientific Reports*, 1–10.
3969 <https://doi.org/10.1038/s41598-021-96944-x>

3970 Park, J., Bermudez, V., Roberts, R. C., & Brannon, E. M. (2016). Non-symbolic approximate
3971 arithmetic training improves math performance in preschoolers. *Journal of Experimental*
3972 *Child Psychology*, 152, 278–293. <https://doi.org/10.1016/j.jecp.2016.07.011>

3973 Park, J., Dewind, N. K., Woldorff, M. G., & Brannon, E. M. (2016). Rapid and Direct
3974 Encoding of Numerosity in the Visual Stream. *Cerebral Cortex*, 26(2), 748–763.
3975 <https://doi.org/10.1093/cercor/bhv017>

3976 Park, J., Hebrank, A., Polk, T. A., & Park, D. C. (2012). Neural Dissociation of Number from
3977 Letter Recognition and Its Relationship to Parietal Numerical Processing. *Journal of*
3978 *Cognitive Neuroscience*, 24(1), 39–50. https://doi.org/10.1162/jocn_a_00085

3979 Paul, J. M., van Ackooij, M., ten Cate, T. C., & Harvey, B. M. (2021). Transformation from
3980 local image contrast to location-independent numerosity tuning in human extrastriate
3981 cortex. *BioRxiv*, 2021.03.28.437364. Retrieved from
3982 <http://biorxiv.org/content/early/2021/04/05/2021.03.28.437364.abstract>

3983 Pelli, D G. (1997). The VideoToolbox software for visual psychophysics: transforming
3984 numbers into movies. *Spatial Vision*, 10(4), 437–442.

3985 Pelli, Denis G. (1997). The VideoToolbox software for visual psychophysics: transforming
3986 numbers into movies. *Spatial Vision*, 10(4), 437–442.
3987 <https://doi.org/10.1163/156856897X00366>

3988 Peters, A. M., Brookes, M. J., Hoogenraad, F. G., Gowland, P. A., Francis, S. T., Morris, P.
3989 G., & Bowtell, R. (2007). T2* measurements in human brain at 1.5, 3 and 7 T. *Magnetic
3990 Resonance Imaging*, 25(6), 748–753. <https://doi.org/10.1016/j.mri.2007.02.014>

3991 Piazza, M. (2010). Neurocognitive start-up tools for symbolic number representations.
3992 *Trends in Cognitive Sciences*, 14(12), 542–551.
3993 <https://doi.org/10.1016/j.tics.2010.09.008>

3994 Piazza, M., Izard, V., Pinel, P., Le Bihan, D., & Dehaene, S. (2004). Tuning curves for
3995 approximate numerosity in the human intraparietal sulcus. *Neuron*, 44(3), 547–555.
3996 <https://doi.org/10.1016/j.neuron.2004.10.014>

3997 Piazza, M., Pinel, P., Le Bihan, D., & Dehaene, S. (2007). A Magnitude Code Common to
3998 Numerosities and Number Symbols in Human Intraparietal Cortex. *Neuron*, 53(2), 293–
3999 305. <https://doi.org/10.1016/j.neuron.2006.11.022>

4000 Pohmann, R., Speck, O., & Scheffler, K. (2016). Signal-to-noise ratio and MR tissue
4001 parameters in human brain imaging at 3, 7, and 9.4 tesla using current receive coil
4002 arrays. *Magnetic Resonance in Medicine*, 75(2), 801–809.
4003 <https://doi.org/10.1002/mrm.25677>

4004 Pomè, A., Anobile, G., Cicchini, G. M., & Burr, D. C. (2019). Different reaction-times for
4005 subitizing, estimation, and texture. *Journal of Vision*, 19(6), 1–9.
4006 <https://doi.org/10.1167/19.6.14>

4007 Pomè, A., Anobile, G., Cicchini, G. M., Scabia, A., & Burr, D. C. (2019). Higher attentional
4008 costs for numerosity estimation at high densities. *Attention, Perception, and
4009 Psychophysics*, 81(8), 2604–2611. <https://doi.org/10.3758/s13414-019-01831-3>

4010 Protopapa, F., Hayashi, M. J., Kulashkhar, S., Van Der Zwaag, W., Battistella, G., Murray,
4011 M. M., ... Bueti, D. (2019). Research article chronotopic maps in human supplementary
4012 motor area. In *PLoS Biology* (Vol. 17). <https://doi.org/10.1371/journal.pbio.3000026>

4013 Puckett, A. M., & Deyoe, E. A. (2015). The attentional field revealed by single-voxel
4014 modeling of fMRI time courses. *Journal of Neuroscience*, 35(12), 5030–5042.
4015 <https://doi.org/10.1523/JNEUROSCI.3754-14.2015>

4016 Railo, H., Koivisto, M., Revonsuo, A., & Hannula, M. M. (2008). The role of attention in
4017 subitizing. *Cognition*, 107(1), 82–104. <https://doi.org/10.1016/j.cognition.2007.08.004>

4018 Ress, D., Glover, G. H., Liu, J., & Wandell, B. (2007). Laminar profiles of functional activity
4019 in the human brain. *NeuroImage*, 34(1), 74–84.
4020 <https://doi.org/10.1016/j.neuroimage.2006.08.020>

4021 Revkin, S. K., Piazza, M., Izard, V., Cohen, L., & Dehaene, S. (2008). Does subitizing reflect
4022 numerical estimation? *Psychological Science*, 19(6), 607–614.
4023 <https://doi.org/10.1111/j.1467-9280.2008.02130.x>

4024 Reynolds, J. H., & Chelazzi, L. (2004). Attentional modulation of visual processing. *Annual
4025 Review of Neuroscience*, 27, 611–647.
4026 <https://doi.org/10.1146/annurev.neuro.26.041002.131039>

4027 Reynolds, J. H., & Heeger, D. J. (2009). The Normalization Model of Attention. *Neuron*,
4028 61(2), 168–185. <https://doi.org/10.1016/j.neuron.2009.01.002>

4029 Sasanguie, D., De Smedt, B., & Reynvoet, B. (2017). Evidence for distinct magnitude
4030 systems for symbolic and non-symbolic number. *Psychological Research*, 81(1), 231–
4031 242. <https://doi.org/10.1007/s00426-015-0734-1>

4032 Sawamura, H., Shima, K., & Tanji, J. (2002). Numerical representation for action in the

4033 parietal cortex of the monkey. *Nature*, 415(6874), 918–922.
4034 <https://doi.org/10.1038/415918a>

4035 Schäfer, A., Van Der Zwaag, W., Francis, S. T., Head, K. E., Gowland, P. A., & Bowtell, R.
4036 W. (2008). High resolution SE-fMRI in humans at 3 and 7 T using a motor task.
4037 *Magnetic Resonance Materials in Physics, Biology and Medicine*, 21(1–2), 113–120.
4038 <https://doi.org/10.1007/s10334-007-0099-6>

4039 Sereno, M. I., Dale, A. M., Reppas, J. B., Kwong, K. K., Belliveau, J. W., Brady, T. J., ...
4040 Tootell, R. B. H. (1995). Borders of multiple visual areas in humans revealed by
4041 functional magnetic resonance imaging. *Science*, 268(5212), 889–893.
4042 <https://doi.org/10.1126/science.7754376>

4043 Shum, J., Hermes, D., Foster, B. L., Dastjerdi, M., Rangarajan, V., Winawer, J., ... Parvizi, J.
4044 (2013). A brain area for visual numerals. *Journal of Neuroscience*, 33(16), 6709–6715.
4045 <https://doi.org/10.1523/JNEUROSCI.4558-12.2013>

4046 Sokolowski, H. M., Fias, W., Mousa, A., & Ansari, D. (2017). Common and distinct brain
4047 regions in both parietal and frontal cortex support symbolic and nonsymbolic number
4048 processing in humans: A functional neuroimaging meta-analysis. *NeuroImage*, 146,
4049 376–394. <https://doi.org/10.1016/j.neuroimage.2016.10.028>

4050 Stoianov, I., & Zorzi, M. (2012). Emergence of a “visual number sense” in hierarchical
4051 generative models. *Nature Neuroscience*, 15(2), 194–196.
4052 <https://doi.org/10.1038/nn.2996>

4053 Storm, R. W., & Pylyshyn, Z. W. (1988). Tracking multiple independent targets: Evidence
4054 for a parallel tracking mechanism. *Spatial Vision*, 3(3), 179–197.

4055 Strauss, M. S., & Curtis, L. E. (1981). Infant perception of numerosity. *Child Development*,
4056 52(4), 1146–1152. <https://doi.org/10.1111/j.1467-8624.1981.tb03160.x>

4057 Szkudlarek, E., & Brannon, E. M. (2017). Does the Approximate Number System Serve as a
4058 Foundation for Symbolic Mathematics? *Language Learning and Development*, 13(2),
4059 171–190. <https://doi.org/10.1080/15475441.2016.1263573>

4060 Torrisi, S., Chen, G., Glen, D., Bandettini, P. A., Baker, C. I., Reynolds, R., ... Ernst, M.
4061 (2018). Statistical power comparisons at 3T and 7T with a GO / NOGO task.
4062 *NeuroImage*, 175, 100–110. <https://doi.org/10.1016/j.neuroimage.2018.03.071>

4063 Treue, S., & Martínez Trujillo, J. C. (1999). Feature-based attention influences motion
4064 processing gain in macaque visual cortex. *Nature*, 399(6736), 575–579.
4065 <https://doi.org/10.1038/21176>

4066 Treue, S., & Maunsell, J. H. R. (1996). Attentional modulation of visual motion processing in
4067 cortical areas MT and MST. *Nature*, 382(6591), 539–541.
4068 <https://doi.org/10.1038/382539a0>

4069 Triantafyllou, C., Hoge, R. D., Krueger, G., Wiggins, C. J., Potthast, A., Wiggins, G. C., &
4070 Wald, L. L. (2005). Comparison of physiological noise at 1.5 T, 3 T and 7 T and
4071 optimization of fMRI acquisition parameters. *NeuroImage*, 26(1), 243–250.
4072 <https://doi.org/10.1016/j.neuroimage.2005.01.007>

4073 Trick, L. M., & Pylyshyn, Z. W. (1993). What Enumeration Studies Can Show Us About
4074 Spatial Attention: Evidence for Limited Capacity Preattentive Processing. *Journal of*
4075 *Experimental Psychology: Human Perception and Performance*, 19(2), 331–351.
4076 <https://doi.org/10.1037/0096-1523.19.2.331>

4077 Trick, L. M., & Pylyshyn, Z. W. (1994). Why are small and large numbers enumerated
4078 differently? A limited-capacity preattentive stage in vision. *Psychological Review*,
4079 101(1), 80–102. <https://doi.org/10.1037/0033-295X.101.1.80>

4080 Tsouli, A., Cai, Y., van Ackooij, M., Hofstetter, S., Harvey, B. M., te Pas, S. F., ...
4081 Dumoulin, S. O. (2021). Adaptation to visual numerosity changes neural numerosity
4082 selectivity. *NeuroImage*, 229(11), 117794.

4083 <https://doi.org/10.1016/j.neuroimage.2021.117794>

4084 Tsouli, A., Dumoulin, S. O., te Pas, S. F., & van der Smagt, M. J. (2019). Adaptation reveals
4085 unbalanced interaction between numerosity and time. *Cortex*, *114*, 5–16.
4086 <https://doi.org/10.1016/j.cortex.2018.02.013>

4087 Tsouli, A., Harvey, B. M., Hofstetter, S., Cai, Y., van der Smagt, M. J., te Pas, S. F., &
4088 Dumoulin, S. O. (2021). The Role of Neural Tuning in Quantity Perception. *Trends in*
4089 *Cognitive Sciences*, *xx(xx)*, 1–14. <https://doi.org/10.1016/j.tics.2021.10.004>

4090 Ungerleider, S. K. and L. G. (2000). Mechanisms of Visual Attention in the Human Cortex.
4091 *Annual Review of Neuroscience*, *23*(1), 315–341.
4092 <https://doi.org/10.1146/annurev.neuro.23.1.315>

4093 van der Zwaag, W., Francis, S., Head, K., Peters, A., Gowland, P., Morris, P., & Bowtell, R.
4094 (2009). fMRI at 1.5, 3 and 7 T: Characterising BOLD signal changes. *NeuroImage*,
4095 *47*(4), 1425–1434. <https://doi.org/10.1016/j.neuroimage.2009.05.015>

4096 van der Zwaag, W., Schäfer, A., Marques, J. P., Turner, R., & Trampel, R. (2016). Recent
4097 applications of UHF-MRI in the study of human brain function and structure: a review.
4098 *NMR in Biomedicine*, *29*(9), 1274–1288. <https://doi.org/10.1002/nbm.3275>

4099 van Dijk, J. A., Fracasso, A., Petridou, N., & Dumoulin, S. O. (2020). Linear systems
4100 analysis for laminar fMRI: Evaluating BOLD amplitude scaling for luminance contrast
4101 manipulations. *Scientific Reports*, *10*(1), 1–15. [https://doi.org/10.1038/s41598-020-](https://doi.org/10.1038/s41598-020-62165-x)
4102 [62165-x](https://doi.org/10.1038/s41598-020-62165-x)

4103 van Dijk, J. A., Fracasso, A., Petridou, N., & Dumoulin, S. O. (2021). Laminar processing of
4104 numerosity supports a canonical cortical microcircuit in human parietal cortex. *Current*
4105 *Biology*, *31*(20), 4635-4640.e4. <https://doi.org/10.1016/j.cub.2021.07.082>

4106 Vaughan, J. T., Garwood, M., Collins, C. M., Liu, W., Delabarre, L., Adriany, G., ...
4107 Ugurbil, K. (2001). 7T vs. 4T: RF power, homogeneity, and signal-to-noise comparison
4108 in head images. *Magnetic Resonance in Medicine*, *46*(1), 24–30.
4109 <https://doi.org/10.1002/mrm.1156>

4110 Venkatraman, V., Ansari, D., & Chee, M. W. L. (2005). Neural correlates of symbolic and
4111 non-symbolic arithmetic. *Neuropsychologia*, *43*(5), 744–753.
4112 <https://doi.org/10.1016/j.neuropsychologia.2004.08.005>

4113 Verguts, T., & Fias, W. (2004). Representation of number in animals and humans: A neural
4114 model. *Journal of Cognitive Neuroscience*, Vol. 16, pp. 1493–1504.
4115 <https://doi.org/10.1162/0898929042568497>

4116 Vetter, P., Butterworth, B., & Bahrami, B. (2008). Modulating attentional load affects
4117 numerosity estimation: Evidence against a pre-attentive subitizing mechanism. *PLoS*
4118 *ONE*, *3*(9), 1–6. <https://doi.org/10.1371/journal.pone.0003269>

4119 Viessmann, O., & Polimeni, J. R. (2021). High-resolution fMRI at 7 Tesla: challenges,
4120 promises and recent developments for individual-focused fMRI studies. *Current*
4121 *Opinion in Behavioral Sciences*, *40*, 96–104.
4122 <https://doi.org/10.1016/j.cobeha.2021.01.011>

4123 Viswanathan, P., & Nieder, A. (2013). Neuronal correlates of a visual “sense of number” in
4124 primate parietal and prefrontal cortices. *Proceedings of the National Academy of*
4125 *Sciences*, *110*(27), 11187–11192. <https://doi.org/10.1073/pnas.1308141110>

4126 Volz, S., Callaghan, M. F., Josephs, O., & Weiskopf, N. (2019). Maximising BOLD
4127 sensitivity through automated EPI protocol optimisation. *NeuroImage*, *189*(December
4128 2018), 159–170. <https://doi.org/10.1016/j.neuroimage.2018.12.052>

4129 Wandell, B. A. (1999). Computational neuroimaging of human visual cortex. *Annual Review*
4130 *of Neuroscience*, *22*, 145–173. <https://doi.org/10.1146/annurev.neuro.22.1.145>

4131 Wandell, B. A., Dumoulin, S. O., & Brewer, A. A. (2007). Visual field maps in human
4132 cortex. *Neuron*, *56*(2), 366–383. <https://doi.org/10.1016/j.neuron.2007.10.012>

4133 Wandell, B. A., & Winawer, J. (2015). Computational neuroimaging and population
4134 receptive fields. *Trends in Cognitive Sciences*, *19*(6), 349–357.
4135 <https://doi.org/10.1016/j.tics.2015.03.009>

4136 Whalen, J., Gallistel, C. R., & Gelman, R. (1999). Nonverbal Counting in Humans: The
4137 Psychophysics of Number Representation. *Psychological Science*, *10*(2), 130–137.
4138 <https://doi.org/10.1111/1467-9280.00120>

4139 Xu, F. (2003). Numerosity discrimination in infants: Evidence for two systems of
4140 representations. *Cognition*, *89*(1), 15–25. [https://doi.org/10.1016/S0010-0277\(03\)00050-](https://doi.org/10.1016/S0010-0277(03)00050-7)
4141 [7](https://doi.org/10.1016/S0010-0277(03)00050-7)

4142 Yacoub, E., Shmuel, A., Pfeuffer, J., Van De Moortele, P. F., Adriany, G., Andersen, P., ...
4143 Hu, X. (2001). Imaging brain function in humans at 7 Tesla. *Magnetic Resonance in*
4144 *Medicine*, *45*(4), 588–594. <https://doi.org/10.1002/mrm.1080>

4145 Yeo, D. J., Wilkey, E. D., & Price, G. R. (2017). The search for the number form area: A
4146 functional neuroimaging meta-analysis. *Neuroscience and Biobehavioral Reviews*,
4147 *78*(January), 145–160. <https://doi.org/10.1016/j.neubiorev.2017.04.027>

4148 Yushkevich, P. A., Piven, J., Hazlett, H. C., Smith, R. G., Ho, S., Gee, J. C., & Gerig, G.
4149 (2006). User-guided 3D active contour segmentation of anatomical structures:
4150 Significantly improved efficiency and reliability. *NeuroImage*, *31*(3), 1116–1128.
4151 <https://doi.org/10.1016/j.neuroimage.2006.01.015>

4152 Zhao, J., & Yu, R. Q. (2016). Statistical regularities reduce perceived numerosity. *Cognition*,
4153 *146*, 217–222. <https://doi.org/10.1016/j.cognition.2015.09.018>

4154 Zorzi, M., & Testolin, A. (2018). An emergentist perspective on the origin of number sense.
4155 *Philosophical Transactions of the Royal Society B: Biological Sciences*, *373*(1740).
4156 <https://doi.org/10.1098/rstb.2017.0043>

4157 Zuiderbaan, W., Harvey, B. M., & Dumoulin, S. O. (2012). Modeling center-surround
4158 configurations in population receptive fields using fMRI. *Journal of Vision*, *12*(3), 10–
4159 10. <https://doi.org/10.1167/12.3.10>

4160
4161
4162
4163
4164
4165
4166
4167
4168
4169
4170
4171
4172
4173
4174
4175
4176
4177
4178
4179
4180

Summary in Dutch

4181
4182
4183
4184
4185
4186
4187
4188
4189
4190
4191
4192
4193
4194
4195
4196
4197
4198
4199
4200
4201
4202
4203
4204
4205
4206
4207
4208
4209
4210
4211
4212
4213

Curriculum Vitae

4214
4215
4216
4217
4218
4219
4220
4221
4222
4223
4224
4225
4226
4227
4228
4229
4230
4231
4232
4233
4234
4235
4236
4237
4238
4239
4240
4241
4242
4243
4244
4245
4246
4247

Yuxuan Cai was born on 30th August, 1990 in Shantou, China. In 2013 she attained her Bachelor's degree of Arts at Guangzhou University of Chinese Medicine, with the major of English. In 2017 she completed the postgraduate program with the major of Basic Psychology for Master's degree in South China Normal University. During her master she was awarded a scholarship to pursue her study in the University of New South Wales as a joint Master student. The awardee was selected through a rigid academia evaluation process organized by South China Normal University in 2016. Between 2017-2021 she was awarded a scholarship under the State Scholarship Fund to pursue her study in the Vrije Universiteit Amsterdam as a PhD student, under supervision of prof. dr. S. O. Dumoulin and dr. S. Hofstetter. The awardee was selected through a rigid academia evaluation process organized by the China Scholarship Council (CSC) in 2017.

List of publications

4248
4249
4250
4251
4252
4253
4254
4255
4256
4257
4258
4259
4260
4261
4262
4263
4264
4265
4266
4267
4268
4269
4270
4271
4272
4273
4274
4275
4276
4277
4278
4279
4280

Journal articles

Cai, Y., Hofstetter, S., van Dijk, J., Zuiderbaan, W., van der Zwaag, W., Harvey, B. M., & Dumoulin, S. O. (2021). Topographic numerosity maps cover subitizing and estimation ranges. *Nature communications*, 12(1), 1-10.

Cai, Y., Hofstetter, S., van der Zwaag, W., Zuiderbaan, W., & Dumoulin, S. O. (2021). Individualized cognitive neuroscience needs 7T: Comparing numerosity maps at 3T and 7T MRI. *Neuroimage*, 237, 118184.

Cai, Y., Hofstetter, S., Harvey, B. M., & Dumoulin, S. O. (under review). Attention drives human numerosity selective responses.

Cai, Y., Hofstetter, S., & Dumoulin, S. O. (under review). Are numerosity maps involved in symbolic numeral processing?

Hofstetter, S., **Cai, Y.**, Harvey, B. M., & Dumoulin, S. O. (2021). Topographic maps representing haptic numerosity reveals distinct sensory representations in supramodal networks. *Nature communications*, 12(1), 1-13.

Tsouli, A., **Cai, Y.**, van Ackooij, M., Hofstetter, S., Harvey, B. M., Te Pas, S. F., ... & Dumoulin, S. O. (2021). Adaptation to visual numerosity changes neural numerosity selectivity. *Neuroimage*, 229, 117794.

Tsouli, A., Harvey, B. M., Hofstetter, S., **Cai, Y.**, van der Smagt, M. J., Te Pas, S. F., & Dumoulin, S. O. (2022). The role of neural tuning in quantity perception. *Trends in cognitive sciences*, 26(1), 11-24.

Oliveira, Í. A., **Cai, Y.**, Hofstetter, S., Siero, J. C., van der Zwaag, W., & Dumoulin, S. O. (2022). Comparing BOLD and VASO-CBV population receptive field estimates in human visual cortex. *Neuroimage*, 248, 118868.

Academic conference

4281

4282

4283 **Cai, Y.**, Hofstetter, S., Harvey, B. M., & Dumoulin, S. O. (2022). Attention drives numerosity
4284 selective neural responses. *Vision Science Society*. (online talk)

4285

4286 **Cai, Y.**, Hofstetter, S., & Dumoulin, S. O. (2022). Are numerosity maps involved in symbolic
4287 numeral processing? *Annual Meeting of the Organization for Human Brain Mapping* (poster)

4288

4289 **Cai, Y.**, Hofstetter, S., Harvey, B. M., & Dumoulin, S. O. (2020). Attention modulates
4290 numerosity responses in human parietal cortex. *Journal of Vision*, 20(11), 690-690. *Vision*
4291 *Science Society*. (online poster)

4292

4293 **Cai, Y.**, Hofstetter, S., Harvey, B. M., & Dumoulin, S. O. (2019). Attention modulates
4294 numerosity responses in human parietal cortex. *17th NVP Winter Conference on Brain &*
4295 *Cognition*. Egmond aan Zee (poster)

4296

4297 **Cai, Y.**, Zuiderbaan, W., Van der Zwaag, W., Hofstetter, S., & Dumoulin, S. O. (2019).
4298 Individualized cognitive neuroscience needs 7T: comparing numerosity maps at 3T and 7T
4299 MRI. *Annual Meeting of the Organization for Human Brain Mapping*. No. 3410. Rome, Italy
4300 (poster)

4301

4302 **Cai, Y.**, van Dijk, J., Zuiderbaan, W., van der Zwaag, W., Harvey, B., & Dumoulin, S. (2019,
4303 April). Topographic numerosity maps dynamically adjust to the presented numerosity range.
4304 In PERCEPTION (Vol. 48, pp. 18-18). *European Conference on Visual Perception*, Trieste,
4305 Italy. (poster)

4306

4307 **Cai, Y.**, Van Dijk, J. A., Zuiderbaan, W., Van Der Zwaag, W., Harvey, B. M., & Dumoulin, S.
4308 O. (2018) Topographic numerosity maps dynamically adjust to the presented numerosity range.
4309 *Society for Neuroscience*. Abstract 719.04 San Diego. (talk)

4310

4311

4312

4313

4314

Acknowledgements

4315
4316
4317
4318
4319
4320
4321
4322
4323
4324
4325
4326
4327
4328
4329
4330
4331
4332
4333
4334
4335
4336
4337
4338
4339
4340
4341
4342
4343
4344
4345
4346
4347
4348

The last four-and-half-years of studying and living in the Netherlands is a precious adventure in my life. A lot had happened during these years, including many joyful and unforgettable moments but also some rough time, especially since the COVID-19 outbreak. Fortunately, I has been and still being surrounded by many lovely people whom supported me to overcome all the difficulties and completed my PhD. I would like to express my gratitude to these wonderful people for their sincere kindness and great support to me. I cannot possibly thank everyone here personally, but I am very grateful to everyone who has been there for me all the same.

Serge, thank you so much for being an amazing supervisor and a nice friend to me. You are always very patient and gentle when helping me to deal with scientific problems, from coding to writing academic papers. In addition, you are very generous to give me some insightful advices whenever I was confused with my future of being a scientist. Your intelligence and the sense of responsibility of being a PhD supervisor and the director of Spinoza Center inspires me to be a diligent and responsible researcher, and promoter to my students in the future.

Shir, I am so grateful to having you as my co-promotor during my PhD. To me, you are more like a good friend than a supervisor. I will miss a lot the time when we were wandering in the parks of Amsterdam, talking and laughing along the canals, and enjoying the fabulous Light Festival. Moreover, you are always very patient and helpful whenever I turn to you for help, which I always appreciate.

Wietske (Zuiderbaan), thank you for being very nice and kind to me, especially at the first year when I started new life in the Netherlands. I enjoyed discussing with you and you are also very generous to help. I will never forget the wonderful bicycle trip we had for the deers at De Hoge Veluwe National Park, together with Shir, Ernst and lovely Famke.

Ben, thank you for being a very motivated and intelligent colleague. I enjoy collaborating with you and I was always happy to get your input on some new data or ideas. I also appreciate the communications and discussion with other colleagues in your lab, including Jacob, Martijn and Elly.

4349 *Wietske (van der Zwaag)*, you are generous to help me with your expertise, especially on our
4350 3T & 7T comparison project. *Suzan, Maarten*, thanks for your pleasant collaboration. I enjoyed
4351 working with you. *Tomas*, I like your enthusiasm in neuroscience and your humour that usually
4352 makes us laugh loudly at lunch time.

4353

4354 *Maartje*, I am always impressed by your hard-working and intelligence. *Nikos, Jelle, Antoine*
4355 and *Johan*, thanks for your generous help of scanning or participating for my studies.

4356

4357 *Akhil*, thanks for your support and help and I like the Indian food you once cooked for us. *Icaro*,
4358 you are always kind and gentle to everyone. I appreciate for your help during my PhD and wish
4359 you have a great time in Belgium of your postdoc. *Luisa*, you are a sweet heart and I like
4360 playing foosball with you. Thanks for your kindness to me. I wish you much luck with the rest
4361 of your PhD.

4362

4363 *Ada, Carlien, Ineke*, I enjoyed working with you and having fun at NVP. *Marco, Kathi, Sumiya*,
4364 thanks for your help and I enjoyed the discussion at our lab meetings. *Jurjen, Emma, Marcus*,
4365 it was so nice to have you joining us and I enjoyed our little chat at the PhD meeting and I
4366 enjoyed playing foosball with you. I wish we could play ping-pong at spinoza in the near future.
4367 *Gianfranco, Innes*, I am grateful of meeting you in the Netherlands and I wish you all the best.

4368

4369 *Diederick, Minni, Thomas, Trijntje, Jutta, Leonie, Michele, Niklas*, thanks for all your help. I
4370 enjoyed working at Spinoza Centre with all of you.

4371

4372 *Gisele, Shulin*, I am always grateful of meeting you and having you as friends forever. Thanks
4373 your kindness and support during my PhD.

4374

4375 爸妈，公婆，哥嫂，老弟，感谢你们一直以来的支持和鼓励，家人永远是最珍惜和
4376 牵挂的，我永远爱你们。

4377

4378 老公（标哥），对你的感谢早已不能言表，所有的感情都在这些年的点点滴滴和相濡
4379 以沫的生活里，但我还是要特别感谢你的默默付出、理解和支持，让我在异国他乡的
4380 求学路多了一份安心和笃定，你永远是我坚强的后盾和避风的港湾，爱你。